Testing the Standard Model in Heavy Quark Decays

Leljak, Domagoj

University of Zagreb

FACULTY OF SCIENCE

DEPARTMENT OF PHYSICS

Domagoj Leljak

Testing the Standard Model in Heavy Quark Decays

DOCTORAL DISSERTATION

Zagreb, 2021.

University of Zagreb

FACULTY OF SCIENCE

DEPARTMENT OF PHYSICS

Domagoj Leljak

Testing the Standard Model in Heavy Quark Decays

DOCTORAL DISSERTATION

Supervisor:

dr.rer.nat. Blaženka Melić

Zagreb, 2021.

Sveučilište u Zagrebu

PRIRODOSLOVNO–MATEMATIČKI FAKULTET
FIZIČKI ODSJEK

Domagoj Leljak

Testiranje standardnoga modela u raspadima teških kvarkova

DOKTORSKI RAD

Mentor:

dr.rer.nat. Blaženka Melić

Zagreb, 2021.

Information on supervisor

Blaženka Melić obtained her master's degree at the Department of Physics of the University of Zagreb in 1991, and her PhD degree at the Institute for Theoretical Particle Physics, University of Karlsruhe, in Germany in 1994. Today, she holds the Tenure Senior Scientist position on the Ruđer Bošković Institute, where she heads both the Theoretical Particle Division (since 2016) and the Particle Physics and Cosmology Group (since 2013), and is an active member of the Scientific Council (since 2013). Since 2015 she also holds the title of Full Professor at the University of Rijeka, and since 2020 the title of Associate Professor at the University of Zagreb, and has been teaching for many years on both universities. She is an awardee of the Alexander von Humboldt (2001-2002, Universität Mainz) and Fulbright (2012-2013, University of California Riverside) foundation fellowships. She is currently the principal investigator on the Croatian Science Foundation research project "Heavy hadron decays and lifetimes", but has participated in, and led, many more competitive projects.

The main topics of her research include flavour physics, quantum chromodynamics (using both perturbative and non-perturbative methods), and the interplay of the two inside the Standard Model, and beyond, which are often investigated in the decays of heavy ($b-$ or $c-$ flavoured) hadrons.

She is the author/coauthor of 47 published research papers (cited more then 1500 times), with many international collaborators, and has held countless invited talks.

Acknowledgements

The writing of this thesis would not have been possible without the mentorship and guidance of Dr. Blaženka Melić, for which I am deeply thankful. Her watchful eye, clear perspectives and inexhaustible patience made my research work very straightforward.

Heartfelt thanks go to Dr. Danny van Dyk, for many hours of bountiful conversations, his enormously generous help, and lastly his warm welcome during my visit at the Technical University of Munich. I am very grateful for a fruitful collaboration with Dr. Monalisa Patra. Dr. Goran Duplančić was of immense help on many occasions, both in terms of support and deep scientific insight and advice, and has my sincere gratitude. To Dr. Damir Bečirević I am indebted for his hospitality and lessons during my visit at the Laboratory of Theoretical Physics in Orsay.

I am lucky to have shared a deep experience during my doctoral years on the Ruđer Bošković Institute with such wonderful colleagues and friends - Mihovil, Clay, Ana, Marija, Goran, Grga, Vanja, and Andrea. Very special thanks to all of you.

I would like to thank all the other departmental colleagues for many happy hours, smoking breaks, and most of all helpful advice. Biserka Kečkeš deserves an especially great appreciation for all the aid she provided in times of urgency.

A big thank you goes to my parents and brothers, who helped me on a daily basis, even if I didn't deserve it. Little Eva Borna, thank you for making me smile.

Last, but not least, I would like to thank Dunja for her emotional support and love. No amount of monkeying around seems to divert you from being a wonderful companion. I hope that never changes, because the monkey in me seems relentless.

Summary

A matter of utmost focus in experimental and theoretical research in high energy physics today is testing the Standard Model through searches of deviations from its predictions. The determination of Cabibbo–Kobayashi–Maskawa quark mixing matrix is one of the key testing grounds in particle physics phenomenology. This is especially the case for the $|V_{ub}|$ matrix element, where a tension has been noticed between the values obtained in inclusive and exclusive determinations. In recent years, a deviation of measurements of several observables in semileptonic decays of heavy mesons from their expected Standard Model values has sparked a renewed interest in theoretical research of what is known as lepton flavour universality, or the universality of weak coupling constant among lepton flavours.

Since the study of quark flavour transitions necessarily deals with hadronic physics involving strong, non-perturbative interactions which introduce large uncertainties, a large effort has been made to put these uncertainties under control. At the moment, there are several theoretical tools at disposal used to extract the values of desired hadronic parameters: lattice quantum chromodynamics, effective theories and various types of sum rules based on quark-hadron duality.

In this thesis, sum rules will be used in a computation of B_c and B_u meson transition form factors. Extracting non-perturbative quantities will enable scrutinizing SM predictions of important semileptonic B_c and B_u decays. In particular, an extraction of the $|V_{ub}|$ CKM matrix element from $\bar{B} \to \pi \ell \bar{\nu}_\ell$ and $B_c \to D^{(*)} \ell \bar{\nu}_\ell$ decays is performed, alongside a test of lepton flavour universality in the SM. In the $B_c \to (J/\psi, \eta_c) \ell \bar{\nu}_\ell$ decays new physics effects are additionally explored.

Sažetak

Testiranje Standardnog modela (SM) kroz potrage za odstupanjima od predviđanja je u primarnom fokusu eksperimentalnih i teorijskih istraživanja u fizici visokih energija danas. Pri tome je precizno određivanje elemenata Cabibbo–Kobayashi–Maskawa matrice kvarkovskog miješanja jedno od ključnih poligona. To je posebno istina u slučaju $|V_{ub}|$ matričnog elementa, gdje je niz godina prisutna tenzija između vrijednosti dobivenih u ekskluzivnim i inkluzivnim raspadima. Također je neobičan skup mjerenja opservabli povezanih sa poluleptonskim raspadima teških mezona. Ona indiciraju odstupanja od vrijednosti koje imaju u Standardnom modelu, što je potaklo nova teorijska razmatranja mogućnosti narušenja univezalnosti leptonskog okusa, odnosno univerzalnosti slabe konstante vezanja među okusima leptona.

Kako su proučavanja slabih kvarkovskih prijelaza direktno povezana sa hadronskom fizikom, koja opisuje neperturbativne učinke jake sile, neodređenosti predviđanja su velike, te se izuzetan trud ulaže u sustavno kontroliranje tih neodređenosti. Trenutno postoje nekoliko teorijskih alata pogodnih za određivanje vrijednosti hadronskih parametara, od kojih su neki: kvantna kromodinamika na rešetci, efektivne teorije, te razni oblici pravila zboja, u kojima se pod pretpostavkom dualnosti kvarkova i hadrona relevantne korelacijske funkcije računaju koristeći disperzijske relacije te Wilsonov razvoj umnožaka operatora.

U ovoj tezi istražene su mogućnosti pravila zbroja (SR) pri računu strukturnih funkcija u slabim poluleptonskim raspadima teških mezona. Računi neperturbativnih veličina će omogućiti produbljivanje uvida u Standardni model kroz portal B_u i B_c mezona. Specifično, istražena je perspekivnost mjerenja $|V_{ub}|$ matričnog elementa u $\bar{B} \to \pi \ell \bar{\nu}_\ell$ i $B_c \to D^{(*)} \ell \bar{\nu}_\ell$ raspadima, te su predočene neke opservable koje testiraju univerzalnost leptonskog okusa. U $B_c \to (J/\psi, \eta_c) \ell \bar{\nu}_\ell$ raspadima predočen

je test univerzalnosti leptonskog okusa, te su istraženi neki efekti koje operatori izvan Standardnog modela mogu imati.

Hadronski dio amplitude slabih poluleptonskih raspada mezona koji sadrže jedan kvark b okusa shematski se može napisati kao

$$\langle M_f(p_f)|\, \bar{q}_2(0)\Gamma_{[\mu\ldots]}b(0)\,|B_{q_1}(p_i)\rangle = \sum_i \Pi_{[\mu\ldots]}\mathcal{F}_i(q^2), \tag{1}$$

gdje je $b \to q_2$ relevantan kvarkovski prijelaz, i $q = p_i - p_f$. Korelacijske funkcije koje opisuju strukturne funkcije $\mathcal{F}_i(q^2)$ se u pravilima zbroja računaju koristeći njihova disperzivna te analitička svojstva. Primjećuje se da se u domeni u kojoj je q^2 dovoljno daleko od skale jakih interakcija Λ_{QCD} korelacijske funkcije mogu računati u perturbativnom računu. Perturbativnom dijelu se, koristeći OPE, dodaju "mekani" doprinosi, ili u obliku usrednjenih interakcija sa vakuumom (kondenzati) u trotočkastim pravilima zbroja kvantne kromodimanike (3ptQCDSR, ili samo QCDSR), ili u obliku distribucijskih amplituda u pravilima zbroja na svjetlosnom stošču (LCSR). Ključna razlika je da se u 3ptQCDSR pristupu generički operatori $\hat{\mathcal{O}}(x,y)$ razvijaju za $x-y \approx 0$, dok se u LCSR oni razvijaju za $(x-y)^2 \approx 0$. Drugim riječima, operatori su u prvom slučaju razvijeni po malim udaljenostima, a u drugom po malim udaljenostima na svjetlosnom stošcu. U oba pristupa se primjećuje da je analitička struktura u domeni u kojoj se hadoni formiraju određena polovima te rezovima uz realnu os. Polovi i rezovi predstavljaju jednočestične i višečestične hadronske rezonance, kojima je lako analitički manipulirati. Tako se analitičnost korelacijske funkcije u područjima u kojima rezonanci nema lako može iskoristiti - nakon što se primjeni Cauchyev teorem za korelacijsku funkciju, doprinose polova i rezova krivuljnom integralu je lako kompenzirati. To definira pravilo zbroja, i shematski

$$\mathcal{F}_i^{\mathrm{OPE}}(\text{male udaljenosti}) \overset{q^2\to-\infty}{=} \mathcal{F}_i^{\mathrm{res}}. \tag{2}$$

Koristeći form faktore koji su dobiveni u ova dva pristupa, različiti fenomenološki izračuni su predstavljeni za nekoliko poluleptonskih raspada B i B_c mezona. Struktura teze je sljedeća:

1. U poglavlju 1 predstavljen je sažetak temeljnih svojstava Standardnog mod-

ela, bitnih za slabe mezonse. Elektroslabi i jaki sektor su ukratko uvedeni, uključujući motivaciju za istraživanja predočena kasnije u disertaciji. Neki nedostatci Standardnog modela su navedeni, usključujući trenutne tenzije u sektoru kvarkovskih okusa.

2. Poglavlje 2 sadrži pregled metoda najčešće primjenjenih na račune neperturbativnih hadronskih veličina. Dva odvojena odjeljka su posvećena metodama primjenjenim na računima strukturnih funkcija u ovoj disertaciji, odnosno sumacijskim pravilima, QCDSR-u i LCSR-u.

3. Poglavlje 3 je posvećeno definiranju baze matričnih elemenata relevantnih za fenomenološka istraživanja interesantnih raspada. Neki daljni detalji pristupa pravila zbroja specifični za račune strukturnih funkcija su raspravljeni.

4. Poglavlje 4 temelji se na istraživanju objavljenom u ref. [1]. Istražena je fenomenologija poluleptonskog kanala raspada B_c mezona u šarmantne mezone. Potrebni form faktori su izračunati u okviru koji udružuje razvoj korelacijskih funkcija na svjetosnom stošcu sa gausijanskom valnom funkcijom J/ψ mezona inspiriranom nerelativističkom kvantnom kromodinamikom. Strukturne funkcije zadovoljavaju relacije koje dolaze iz spinskih simetrija teških kvarkova i nerelativističkog limesa kvantne kromodinamike. Neke kutne opservable su predložene kao test univerzalnosti leptonskog okusa, i po prvi put su predstavljeni izrazi za diferencijalnu kutnu distribuciju u tri kuta za $B_c \to J/\psi(\to \mu^+\mu^-)\ell\bar{\nu}_\ell$ proces,

$$\begin{aligned}\frac{\mathrm{d}\Gamma(B_c \to (J/\psi \to \mu_R^+\mu_L^-)\ell\bar{\nu}_\ell)}{\mathrm{d}q^2\mathrm{d}\cos\theta_\ell\mathrm{d}\cos\theta_V\mathrm{d}\chi} &= \frac{3G_F^2|V_{cb}|^2|\vec{p}_2|q^2}{8(4\pi)^4 m_{B_c}^2}\left(1-\frac{m_\ell^2}{q^2}\right)^2 \times \\ &\times \Big[|1+V_L|^2\mathcal{T}_{V_L} + |V_R|^2\mathcal{T}_{|V_R|^2} + \mathcal{T}_{V_R^{int}} + 2|P|^2(H_S^V)^2\sin^2\theta_V \\ &+ \mathcal{T}_{P^{int}} + |T_L|^2\mathcal{T}_{|T_L|^2} + \mathcal{T}_{T_L^{int}}\Big]\mathcal{B}(J/\psi \to \mu_L^-\mu_R^+),\end{aligned} \tag{3}$$

gdje amplitude $\mathcal{T}_i$ ovise o strukturnim funkcijama i kinematičkim varijablama. Istražen je učinak kojeg ima uvođenje nekih operatora izvan SM-a na opservale. Nađeno je da, iako neki operatori mogu imati relativno snažan utjecaj na neke opservable, nijedan ne može u isto vrijeme objasniti postojeće tenzije primjećene u $B \to D^{(*)}\ell\bar{\nu}_\ell$ procesu, što je istina i za omjer koji mjeri lepton-

sku univerzalnost okusa, za koji je dobiveno da u standardnom modelu ima vrijednosti

$$R_{\eta_c}|_{\rm SM} \equiv \frac{\Gamma(B_c\to\eta_c\tau\bar{\nu}_\tau)}{\Gamma(B_c\to\eta_c\mu\bar{\nu}_\mu)} = 0.32\pm0.02\,, \tag{4}$$

$$R_{J/\psi}|_{\rm SM} \equiv \frac{\Gamma(B_c\to J/\psi\tau\bar{\nu}_\tau)}{\Gamma(B_c\to J/\psi\mu\bar{\nu}_\mu)} = 0.24\pm0.02. \tag{5}$$

5. Poglavlje 5 temelji se na istraživanju objavljenom u ref. [2]. Predložen je način mjerenja $|V_{ub}|$ matričnog elementa u $B_c \to D^{(*)}\ell\bar{\nu}_\ell$ raspadu. Strukturne funkcije unutar Standardnog modela izračunate su koristeći 3ptQCDSR, i koristeći ih testirane su relacije koje dolaze od spinskih simetrija teških kvarkova. Kondenzatski nelokalni doprinosi strukturnim funkcijama su ispitani, i nađeno je da nemaju značajnog utjecaja na numeričke vrijednosti. Predikcije nekoliko kutnih opservabli prezentirane su unutar Standardnog modela, a za omjer koji mjeri leptonsku univerzalnost okusa dobiveno je

$$\begin{aligned} R_c(D^0) &\equiv \frac{\mathcal{B}(B_c\to D^0\tau\bar{\nu}_\tau)}{\mathcal{B}(B_c\to D^0\mu\bar{\nu}_\mu)} = 0.64\pm0.05, \\ R_c(D^*) &\equiv \frac{\mathcal{B}(B_c\to D^*\tau\bar{\nu}_\tau)}{\mathcal{B}(B_c\to D^*\mu\bar{\nu}_\mu)} = 0.55\pm0.05, \end{aligned} \tag{6}$$

6. Poglavlje 6 temelji se na istraživanju objavljenom u ref. [3]. LCSR $\bar{B}\to\pi$ strukturne funkcije ažurirane su u bayesianskoj analizi koristeći najrecentnije hadronske parametre. Nakon toga one su kombinirane sa postojećim dostupnim podatcima sa rešetke u svrhu povećanja preciznosti u cijeloj fizikalnoj kinematskoj domeni. Precizno određivanje $|V_{ub}|$ matričnog elementa predstavljeno je u prilagodbi koja koristi posljednje usrednjenje eksperimentalnih podataka $\bar{B}\to\pi\ell\bar{\nu}_\ell$ raspada, te je dobiveno

$$|V_{ub}|^{\bar{B}\to\pi}_{\rm LCSR+LQCD} = (3.77\pm0.15)\cdot10^{-3}. \tag{7}$$

Time je tenzija sa posljednjim inkulzivnim određivanjem $|V_{ub}|$ ublažena. Neke

kutne opservable koje mjere leptonsku univerzalnost okusa su također izračunate

$$R_\pi = \frac{\Gamma(\bar{B} \to \pi\tau^-\bar{\nu}_\tau)}{\Gamma(\bar{B} \to \pi\ell^-\bar{\nu}_\ell)} = 0.699^{+0.022}_{-0.020}. \tag{8}$$

Ključne riječi: standardni model, slabi raspadi, Cabibbo-Kobayashi-Maskawa matrica, fizika hadrona, fizika kvarkova, strukturne funkcije, pravila zbroja

Contents

Information on supervisor **i**

Introduction **1**

1 The Standard Model **4**

1.1 The strong sector 7

1.2 The electroweak sector 13

1.3 Some shortcomings of the SM 20

1.4 Tensions in the flavor sector 22

1.4.1 Inclusive and exclusive $|V_{ub}|$ determination 22

1.4.2 Lepton flavour universality 24

2 Treatment of non-perturbative phenomena **28**

2.1 QCD sum rules (QCDSR) 35

2.1.1 Two-point correlation functions 35

2.1.2 Three-point correlation functions 40

2.1.3 Wilson's OPE and quark-hadron duality 42

2.2 Light-cone sum rules (LCSR) 46

3 Form factors in weak decays **50**

3.1 Form factor definitions 51

3.1.1 $P \to P$ form factors 52

3.1.2 $P \to V$ form factors 53

3.2 Form factors in QCDSR 56

3.3 Form factor kinematical extrapolation 61

4 Probing LFU and NP effects in the $B_c^+ \to [J/\psi, \eta_c]\, \ell^+ \nu_\ell$ decay 67

4.1 LCSR/NRQCD form factors . . . 70

4.1.1 Leading twist contributions . . . 73

4.1.2 Higher twist corrections . . . 75

4.1.3 Extrapolation to high q^2 . . . 78

4.1.4 HQSS/NRQCD symmetry relations at the zero recoil . . . 81

4.2 Phenomenology . . . 85

4.2.1 Two-fold differential decay widths . . . 87

4.2.2 Lepton flavour universality ratios . . . 90

4.2.3 Forward-backward asymmetry, convexity parameter and the τ polarization . . . 92

4.2.4 Four-fold differential decay widths . . . 97

4.3 Conclusion . . . 105

5 $|V_{ub}|$ determination from the $B_c^+ \to D^{(*)}\, \ell^+ \nu_\ell$ decay 107

5.1 QCDSR form factors . . . 109

5.1.1 Setting the sum rule parameters . . . 111

5.1.2 Extrapolation to high q^2 . . . 115

5.1.3 A comment on correlations between pseudo data points . . . 120

5.2 Phenomenology . . . 123

5.2.1 Lepton flavor universality ratios . . . 126

5.2.2 Angular observables in $B_c \to D^{(*)} \ell \bar{\nu}_\ell$ . . . 127

5.3 Exclusive $|V_{ub}|$ determination and the $|V_{ub}|/|V_{cb}|$ ratio . . . 131

5.3.1 The $|V_{ub}|/|V_{cb}|$ ratio . . . 133

5.3.2 The $|V_{ub}|/|V_{cs}|$ ratio and the HQSS compatibility . . . 137

5.4 Conclusion . . . 140

6 $|V_{ub}|$ determination from the $\bar{B} \to \pi\, \ell \bar{\nu}_\ell$ decay 142

6.1 LCSR form factors . . . 144

6.1.1 Input parameters . . . 145

6.1.2 Setting the duality thresholds and Borel parameters . . . 148

6.1.3 Numerical results for the form factors . . . 152

6.1.4 Extrapolation to high q^2 . . . 154
6.2 Interpolation between LCSR and lattice QCD form factors . . . 160
6.3 Phenomenology . . . 168
6.3.1 Exclusive $|V_{ub}|$ determination . . . 168
6.3.2 Lepton flavour universality ratio . . . 171
6.3.3 Angular observables and polarizations in $\bar{B} \to \pi \ell^- \bar{\nu}_\ell$ . . . 174
6.4 Conclusion . . . 176

Conclusions **178**

Appendices **181**

A QCDSR expressions **182**
A.1 Correlation function calculation . . . 182
A.1.1 Perturbative terms . . . 182
A.1.2 Nonlocal quark and quark-gluon condensate terms . . . 185
A.1.3 Gluon condensate terms . . . 190
A.2 Master integrals . . . 193
A.2.1 Perturbative master integrals . . . 194
A.2.2 Non-perturbative master integrals . . . 197

B LCSR higher-twist expressions **199**

C Effective theory of weak interactions **201**

D Angular observables **202**
D.1 Helicity form factors . . . 202
D.2 Angular observables . . . 205

E Bayesian analysis using `EOS` **209**

Curriculum Vitae **213**

Bibliography **215**

Introduction

The Standard Model faces an increasing number of challenges in the quark flavor sector. A sophisticated interplay between electroweak and strong interactions takes place in decays of heavy mesons - the knowledge of hadronic parameters plays a crucial role in accurately predicting their weak decay rates. Due to this entanglement, the inherent non-perturbativity of the hadronic matrix elements poses a serious obstacle in testing the Standard Model's flavour sector. Distinguishing between potential effects of new physics and the Standard Model is impossible without a firm grasp on the hadronic uncertainties.

This is especially important in light of the tension present in the $b \to u$ semileptonic decays, where the exclusive and inclusive determinations of $|V_{ub}|$ seem to give mutually exclusive values with statistical significance of $\approx 3\sigma$. This surely calls for a detailed analysis of hadronic contributions relevant for the transition, being the largest source of theoretical uncertainty.

The same need for a precise determination of hadronic observables reflects on an another tension persisting for years now. The Standard Model lepton flavour universality implies that the widths of mesonic decays to leptons of different flavour should be the same up to a phase space factor. However, in $B \to D^{(*)}\ell\bar{\nu}_\ell$, $B_c \to J/\psi\ell\bar{\nu}_\ell$ and the rare $B \to K\ell^+\ell^-$ decays this seems not to be the case at $\approx 2-3\sigma$ statistical significance, depending on the process. Again, in order to conclude if this tension can be alleviated in the Standard Model, more precise calculations of hadronic matrix elements are of crucial importance.

For these reasons, in this thesis several b-flavored meson exclusive decay channels are investigated in hopes of further scrutinizing the Standard Model phenomenology. The chapters contained within are structured as the following:

1. In Chapter 1 a recap of elementary Standard Model properties relevant for the weak decays of mesons is presented. Electroweak and strong sectors are briefly introduced, with a motivation for the studies presented further in the thesis. Some shortages of the Standard Model are listed, together with present tensions in the quark flavour sector.

2. Chapter 2 contains an overview of methods most commonly applied to calculations of non-perturbative hadronic quantities. Two separate sections are further dedicated to methods applied to form factors computations in this thesis, namely the sum rules of quantum chromodynamics and the light-cone sum rules.

3. Chapter 3 is dedicated to defining the basis of matrix elements relevant for phenomenological decay studies of interest. Some details of the sum rule approach specific to the form factor calculations are also discussed.

4. Chapter 4 is based on research published in ref. [1]. The phenomenology of semileptonic decay channels of B_c meson to charmonia is investigated. Required form factors are calculated in a framework that combines light-cone expansion of correlation functions with a gaussian wave function used for J/ψ, inspired by non-relativistic quantum chromodynamics. Angular observables are proposed as a test of lepton flavour universality, where for the first time expressions are presented for four-fold decay distributions of the $B_c \to J/\psi(\to \mu^+\mu^-)\ell\bar{\nu}_\ell$ process. The effect some new physics operators have on these observables is computed.

5. Chapter 5 is based on research published in ref. [2]. A proposal is made for the measurement of $|V_{ub}|$ matrix element through the $B_c \to D^{(*)}\ell\bar{\nu}_\ell$ decay. The Standard Model form factors are calculated using three-point sum rules of quantum chromodynamics, and the heavy quark spin symmetry relations are probed using the results. A prediction of several angular observables is presented inside the Standard Model.

6. Chapter 6 is based on research published in ref. [3]. Light-cone sum rule

$\bar{B} \to \pi$ form factors are updated in a Bayesian analysis using the most recent hadronic parameters. They are then combined with the available lattice data in order to increase precision in the entire physical kinematical domain. A precise extraction of the $|V_{ub}|$ matrix element is presented in a fit that uses the most recent experimental average of the $\bar{B} \to \pi \ell \bar{\nu}_\ell$ decay. This nullifies the tension with the most recent inclusive determination of $|V_{ub}|$. Some lepton flavour universality angular observables are also computed.

1. The Standard Model

The Standard Model (SM) is an experimentally very well tested [4] quantum field theory (QFT) widely accepted as the best model of the elementary particle content and its interactions in existence. The theory is based on a gauge symmetry group product of three groups

$$SU(3)_c \times SU(2)_L \times U(1)_Y, \tag{1.1}$$

where $SU(3)_c$ corresponds to the gauge sector of quantum chromodynamics (QCD), and $SU(2)_L \times U(1)_Y$ to the electroweak (EW) sector. Consequently, whole of the particle content carries quantum numbers that testify to the transformations under rotations in those groups. They are usually classified as in table 1.1. The left-handed fields are organized in three generations of $SU(2)_L$ doublets both for quarks

Table 1.1: Standard Model field content classified according to the representations of $SU(3)_c \times SU(2)_L \times U(1)_Y$

Symbol	Nomenclature	Representation
	Gauge fields	
B_μ	$U(1)_Y$ hypercharge boson	(**1**, **1**, 0)
W_μ	$SU(2)_L$ bosons	(**1**, **3**, 0)
G_μ	$SU(3)_c$ gluons	(**8**, **1**, 0)
	Matter fields	
Q_L	left-handed quarks	(**3**, **2**, 1/3)
U_R	right-handed up-type quarks	(**3**, **1**, 4/3)
D_R	right-handed down-type quarks	(**3**, **1**, -2/3)
ℓ_L	left-handed leptons (including neutrinos)	(**1**, **2**, -1)
ℓ_R	right-handed leptons	(**1**, **1**, -2)
	Higgs field	
ϕ	the Higgs boson	(**1**, **2**, 1)

and leptons, while the right-handed ones are singlets

$$\begin{aligned} Q_L \sim \begin{bmatrix} u_L \\ d_L \end{bmatrix}, \begin{bmatrix} c_L \\ s_L \end{bmatrix}, \begin{bmatrix} t_L \\ b_L \end{bmatrix}, \qquad \text{and} \quad L_L \sim \begin{bmatrix} \nu_e \\ e_L \end{bmatrix}, \begin{bmatrix} \nu_\mu \\ \mu_L \end{bmatrix}, \begin{bmatrix} \nu_\tau \\ \tau_L \end{bmatrix}, \\ u'_R \sim u_R, c_R, t_R, \quad d'_R \sim d_R, s_R, b_R, \quad \text{and} \qquad \ell_R \sim e_R, \mu_R, \tau_R. \end{aligned} \tag{1.2}$$

Each fermion generation has, when formulated like this, two different flavors associated with it. In section 1.2 it will become obvious that one important aspect of the EW Lagrangian is the appearance of a flavor-changing mechanism. However, it turns out that quarks from the upper components of the $SU(2)_L$ doublets can only exchange flavor with the ones from the lower components. For this reason, the left-handed doublets can be symbolically organized such that the upper and lower components are incorporated into 3-component vectors in flavor space for quarks and leptons separately, so that

$$\begin{aligned} Q_L = \begin{bmatrix} u'_L \\ d'_L \end{bmatrix} \quad \text{with} \quad u'_L = \begin{bmatrix} u_L \\ c_L \\ t_L \end{bmatrix}, \quad \text{and} \quad d'_L = \begin{bmatrix} d_L \\ s_L \\ b_L \end{bmatrix}, \\ L_L = \begin{bmatrix} \nu_L \\ \ell_L \end{bmatrix} \quad \text{with} \quad \nu_L = \begin{bmatrix} \nu_e \\ \nu_\mu \\ \nu_\tau \end{bmatrix}, \quad \text{and} \quad \ell_L = \begin{bmatrix} e_L \\ \mu_L \\ \tau_L \end{bmatrix}, \end{aligned} \tag{1.3}$$

whereas the singlet right-handed states are combined in their own 3-component flavor vectors. This simplifies unifying expressions, since flavor changing currents will occur through a 3×3 flavor mixing matrix (here denoted symbolically V), and then interact with vector potentials W_μ in the form

$$W_\mu [\bar{u}'_L]_i \gamma^\mu V_{ij} [d'_L]_j + \text{leptons} + \text{h.c.} \tag{1.4}$$

where the indices i and j concern flavor, and repeated indices (both Lorenz and otherwise) will always imply summation unless explicitly stated otherwise. Quarks and leptons are fermions, but spinor (as well as flavor) degrees of freedom will gen-

erally be left implicit (or implied in matrix form). In gauge theories in general all the elementary fields are massless by definition, but can acquire mass through the breaking down of internal symmetries. In the SM, this is achieved by the spontaneous symmetry breaking (SSB) of the EW $SU(2)_L \times U(1)_Y$ symmetry to the $U(1)_{\mathrm{EM}}$ of electromagnetism by coupling the Higgs field to the fermions, and expanding it around the minimum of its potential. This minimum is actually the point in which the symmetry of the Lagrangian gets broken, more on which will be said in section 1.2.

Quarks and gluons are peculiar among elementary particles due to the property of color confinement. That is, they are never observed as free particles in nature, but are rather confined in QCD bound states, hadrons. This makes phenomenology involving QCD extremely challenging, due to the breakdown of traditional perturbative aspects of QFT. In the Large Hadron Collider (LHC) era, this challenge is an unavoidable one. Understanding proton collisions, and resulting particle production and decays is inherently impossible without a firm and detailed grasp of QCD phenomenology. A nonperturbativity inherent to it is explored more in section 1.1 and methods encountered in treating it in section 2.

The SM is in principle completely determined by 18 parameters (aside from several ones which either haven't been implemented in the SM as of yet, such as neutrino masses and mixing parameters, or are disputed to have measurable effect, or even exist, such as the QCD charge conjugation parity (CP) violating parameter) - 10 particle masses, 3 coupling constants, 4 weak mixing parameters and the Higgs vacuum expectation values. The entirety of particle phenomenology (with the exception of gravity, and its impact) should in principle be derivable using QFT tools from the SM. However, there is an immense ongoing effort in understanding all the peculiar idiosyncrasies concerning SM dynamics, its implications, and the phenomenology in general together with the theoretical tools used to extract it.

In summary, priori to the EW SSB the entire SM Lagrangian can be decomposed as

$$\mathcal{L}_{\mathrm{SM}} = \mathcal{L}_{\mathrm{QCD}} + \mathcal{L}_{\mathrm{EW}}, \tag{1.5}$$

and it contains all the particles and interactions from Tab. (1.1). QCD is historically

referred to as the strong sector, because the magnitude of its coupling constant is several orders of magnitude that of the EW one at energies of order $Q^2 \sim 1 - 100$ GeV^2. Any shortcomings and/or new physics contributions, due to the extreme scrutiny under which the SM has been placed in the last several decades, will be reflected on the level of the Lagrangian.

1.1. The strong sector

After the realization that the properties of hadronic particles discovered in the bubble and spark chambers of the 1950's cannot be classified only according only to their charge and spin, Kazuhiko Nishijima [5] and Murray Gell-Mann [6] independently postulated that an additional degree of freedom must exist, unknown at the time. The quantum number assigned to these "strange" particles was aptly named strangeness, and in 1961 a particle spectrum was structured and classified by Gell-Mann, who named it the *eightfold way* [7], according to the 8 mesons arising from the 8 generators of the SU(3) symmetry group, called the flavor symmetry group after it was postulated that the hadronic particles are in fact composite, and that they consisted of three different quark flavors (up, down and strange) bound in mesons (integer spin) or baryons (half-integer spin). The model seemed problematic, since one of the features of the eightfold way was an appearance of a $S = 3$ baryon Ω^-, a particle consisted of 3 strange quarks, and the Δ^{++} baryon, consisted of 3 up quarks. Quarks are fermionic particles, and are subject to the Pauli principle, which means such a particle shouldn't exist, unless there is an another degree of freedom yet unaccounted for. This degree of freedom was suggested independently both in a paper by Greenberg [8] and in one by Han and Nambu [9] to account for the discrepancies, and the picture was completed by incorporating gluons as gauge bosons in a field-theoretical sense [10], assigning the term color to the newly postulated degree of freedom.

The underlying theory of hadrons was therefore formulated as what we know as QCD today, the theory of interacting quarks and gluons. Quarks are massive, but their masses are generated through the interaction with the Higgs boson, a

feature generally associated with the EW part of the Lagrangian, not being explicitly included into the QCD one, while gluons are massless. In the language of QFT, the quark-gluon interaction properties are encoded in the $SU(3)_c$-symmetric (c stands for color) Lagrangian

$$\mathcal{L}_{\mathrm{QCD}} = -\frac{1}{4} G^a_{\mu\nu} G^{a\,\mu\nu} + \sum_{i=1}^{6} \bar{q}_i (\mathrm{i}\not{D}) q_i, \tag{1.6}$$

where explicit coordinate dependence has been suppressed, as have the color and spinor indices, the sum goes over all quark flavors, q_i are the quark fields of i-th flavor, D_μ is the covariant derivative

$$D_\mu = \partial_\mu - \mathrm{i} g_s t^a G^a_\mu, \tag{1.7}$$

with t^a being the 8 Gell-Mann matrices [11] generating the $SU(3)_C$ gauge symmetry group, and $G^a_{\mu\nu}$ is the non-abelian gluonic field strength tensor

$$G^a_{\mu\nu} = \partial_\mu G^a_\nu - \partial_\nu G^a_\mu + g_s f^{abc} G^b_\mu G^c_\nu, \tag{1.8}$$

with the appropriate group structure constants f^{abc}

$$[\frac{\lambda^a}{2}, \frac{\lambda^b}{2}] = \mathrm{i} f^{abc} \frac{\lambda^c}{2}. \tag{1.9}$$

Obviously, unlike photons, gluons interact with themselves on the elementary level. Interaction diagrams involving gluon loops enter the renormalization procedure and one finds that quarks are asymptotically free [12, 13], that is

$$\lim_{\mu^2 \to +\infty} \alpha_s(\mu^2) = 0, \tag{1.10}$$

where $\alpha_s = g_s/4\pi$ by examining the sign of the QCD beta function describing the running of the coupling constant

$$\beta(\alpha_s(\mu^2)) \equiv \mu^2 \frac{\partial \alpha_s^2(\mu^2)}{\partial \mu^2} = -\alpha_s(\mu^2)[b_0 + b_1 \alpha_s(\mu^2) + b_2 \alpha_s^2(\mu^2) + \dots] < 0. \tag{1.11}$$

Running the coupling constant towards lower energies, a natural scale emerges, as is made obvious in the leading order (LO) expression for the coupling constant in the modified minimal subtraction ($\overline{\text{MS}}$) renormalization scheme

$$\alpha_s(\mu^2) = \frac{\alpha_s(\mu_0^2)}{1 + b_0 \alpha_s(\mu_0^2) \ln \frac{\mu^2}{\mu_0^2}} \equiv \frac{1}{b_0 \ln \frac{\mu^2}{\Lambda^2_{\text{QCD}}}} \quad \text{with} \quad b_0 = \frac{11 C_A - 2 N_f}{12\pi}, \tag{1.12}$$

where $C_A = N_c = 3$ is the color factor, and N_f takes into account number of quark flavors involved on the scale in question. In the $\overline{\text{MS}}$ renormalizaton scheme the loop integral divergences are regularized dimensionally by substituting the 4-momentum integrated over by a D-dimensional one, which scales the integral measure according to substitution

$$p^\mu \to p^{\mu_D} \Rightarrow \mathrm{d}^4 p \to \mu^{4-D} \mathrm{d}^D p, \tag{1.13}$$

and the renormalization scale is shifed as compared to the minimal substracton (MS) scheme by a multiplicative Euler–Mascheroni constant γ_{E}, $\mu^2 \to \frac{\mathrm{e}^{\gamma_{\text{E}}}}{4\pi} \mu^2$. The QCD Landau pole (i.e. the scale at which the strong constant from eq. (1.11) diverges) appears at a scale dependent on the renormalization scheme and the order of the expansion, but is roughly at the order of $\sim 200 - 300$ MeV^2 [14]. As a consequence, at energies high enough, the standard perturbative approach describes the particle phenomena sufficiently accurately, but at the same time a more troubling result occurs - at low energies the coupling constant, as calculated perturbatively, starts to rise uncontrollably, and already at the scale of the proton mass it becomes comparable to unity

$$\alpha_s(\mu^2 \lesssim m_p^2) \sim 1, \tag{1.14}$$

essentially deeming perturbative approach obsolete on the scales comparable to the mass of the proton.

Even though QCD can be treated perturbatively at ultraviolet (UV) energy scales, at low energies the confinement phenomena dominates - quarks cannot be isolated from the bound states they appear in, but this effect does not arise out of the low-energy behaviour of the perturbative coupling constant running. Perturbative calculations can not be trusted at $\mu^2 \sim \Lambda^2_{QCD}$ by definition, since there the theory

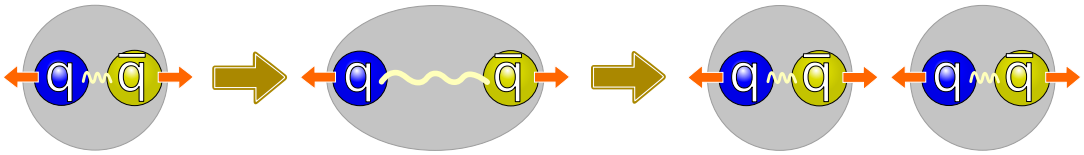

Figure 1.1: A depiction of the effect of the linear part of the confining QCD potential

stops being perturbative. The existence of confinement phenomena is an empirical conclusion supported also by lattice [15] - no free quark has ever been detected in an experiment. Typically, confinement is explained in terms of the classical potential that would emulate the QCD interaction between quarks. Today, e.g. it is known that quark-antiquark interaction in heavy quarkonium states [16] can be very well described by the Cornell potential

$$V(r) = V_0 - \frac{A(\alpha_s)}{r} + \sigma r, \tag{1.15}$$

which, aside from the short-distance $1/r$ behaviour, also contains a linear term that dominates at comparatively larger values of r (usually V_0 is set at the scale at which the linear term starts dominating, that is the radius of the bound state in question). This means that the amount of energy one needs to put into taking the quark-antiquark pair apart grows with distance, and at a certain threshold a quark-antiquark pair gets produced, as in figure 1.1, resulting in confinement, or the inability to separate quarks from bound states. The appearance of light quark-antiquark pairs can be incorporated into the QCD potential by smearing the linear part with a gaussian or an exponential test function. A further hint of the QCD confinement was found in the scaling of the hadron angular momentum J with its mass

$$J \propto M^2, \tag{1.16}$$

a picture emerging from considering bound states as quark-antiquark pairs tied by a gluon flux tube, or considering hadrons as Regge particles, poles moving along a so called Regge trajectory [17, 18], a finding later suppported by the anti-de Sitter (AdS)/QCD duality approach [19].

As a specific example of the interplay of the perturbative and nonperturbative physics, one might consider a decay of a heavy $\bar{B}_d$ meson to a lepton-neutrino pair and a charged meson P^+ (e.g. $\pi^+, \rho^+, D^+ ...$), characterized by the amplitude

$$\mathrm{i}\mathcal{M} = \left\langle P^+ \ell^- \bar{\nu}_\ell \right| \hat{\mathcal{H}}_{\text{eff}} \left| \bar{B}_d \right\rangle \propto L_\mu \left\langle P^+ \right| \hat{J}^\mu \left| \bar{B}_d \right\rangle , \tag{1.17}$$

where the effective Hamiltonian $\mathcal{H}_{\text{eff}}$ contains the relevant operator (or operators, generally) composed of free fields, L_μ is the leptonic tensor (easily calculated using standard perturbation techniques) factorised from the hadronic matrix element, which squeezes the quark transition current operator. This type of hadron-to-hadron transition amplitude is usually called a form factor. The decay is mediated by the charged $W^\pm$ current, which changes the quark flavor from $b \to q$ (with $q = u, c$), and then produces the leptonic pair characterized by an invariant mass q^2. When one tries to perturbatively calculate the form factor, a problem arises. To illustrate it, one might focus on a pseudoscalar hadronic final state of momentum k, and write its two-quark Fock component in terms of light-cone coordinates (a basis in which the nontrivial QCD vacuum simplifies drastically [20], i.e. it is equal to the free vacuum, up to the gauge zero modes problem), which looks like [21]

$$\begin{aligned} \left| P^+(k) \right\rangle = \int_0^1 \frac{\mathrm{d}u}{\sqrt{u(1-u)}} \frac{\mathrm{d}^2 l_\perp}{16\pi^3} \frac{1}{\sqrt{2N_c}} \psi(u, \vec{l}_\perp) \times \\ \times \left[a^\dagger_{q\uparrow}(uk_+, \vec{l}_\perp) b^\dagger_{\bar{q}\downarrow}((1-u)k_+, -\vec{l}_\perp) - a^\dagger_{q\downarrow}(uk_+, \vec{l}_\perp) b^\dagger_{\bar{q}\uparrow}((1-u)k_+, -\vec{l}_\perp) \right] |0\rangle , \end{aligned} \tag{1.18}$$

depending on the state in question, where the light-cone coordinates are

$$k_\pm = \frac{k^0 \pm k^3}{\sqrt{2}}, \quad \text{where} \quad k = (k^0, k^1, k^2, k^3) \to (k_+, k_-, k^1, k^2). \tag{1.19}$$

One quark carries uk_+ portion of longitudinal momentum and the other $(1-u)k_+$. Transverse momentum is given by $\vec{l}_\perp$, while the $|\vec{l}_\perp|^2$ contributions have been neglected due to an assumption that kinematically $u \approx 1 - u$ (for pions at LO this assumpion is valid). The wave function $\psi(u, l_\perp)$ is connected with the so called light-cone wavefunction, on which a more detailed discussion follows in section 2.2.

When considering higher Fock states, one must also consider an appropriate number of wave functions. After Wick contracting the creation operators from the final state ket with the interaction current one obtains, schematically

$$\left\langle P^{+}\right| \hat{J}^{\mu} \left|\bar{B}_{d}\right\rangle \propto \left[(\text{Perturbative}) \otimes (\text{Nonperturbative})\right]^{\mu}, \tag{1.20}$$

where a convolution is implied. The perturbative part is easily loop-expanded, but the nonperturbative one is a consequence of the fundamental inability to account for confined state interactions, and is inscribed in the wavefunction. The specific outlook of the convolution in question depends on the factorization assumptions made, and the relevant scales in question, but the point remains - one must somehow account for the deeply nonperturbative contributions to the form factors.

1.2. The electroweak sector

A crucial feature of the SM is the EW spontaneous symmetry breaking (SSB). Today the unification of QED and weak field theories at $v \sim (G_F\sqrt{2})^{-1/2} \approx 246\,\text{GeV}$ is inscribed in the SM, and below the theory's $SU(2)_L \times U(1)_Y$ symmetry spontanously breaks through the Higgs-Kibble mechanism [22–24], and the remaining symmetry (that keeps the photon massless) is the one of the electromagnetic $U(1)_{EM}$, i.e.

$$SU(2)_L \times U(1)_Y \overset{\text{SSB}}{\to} U(1)_{EM}. \tag{1.21}$$

The EW SSB generates both the $W^{\pm}$ and Z^0 bosons' masses in the process, as well as the masses of all the other elementary particles in the SM, which is fortunate considering no explicit mass terms are allowed in gauge theories in general, since they render the theory unrenormalizable. To depict this in short, the gauge part of a $SU(2)_L \times U(1)_Y$-symmetric theory with 4 massless gauge bosons, $W_\mu^{1,2,3}$ and B_μ is given by

$$\mathcal{L}_{\text{gauge}} = -\frac{1}{4}W^a_{\mu\nu}W^{a\,\mu\nu} - \frac{1}{4}B_{\mu\nu}B^{\mu\nu}, \tag{1.22}$$

where

$$W^a_{\mu\nu} = \partial_\mu W^a_\nu - \partial_\nu W^a_\mu + g_W f^{abc} W^b_\mu W^c_\nu \quad \text{and} \quad B_{\mu\nu} = \partial_\mu B_\nu - \partial_\nu B_\mu, \tag{1.23}$$

with the $SU(2)_L$ structure constants defined through the commutators of 3 Pauli matrices

$$[\frac{\sigma^a}{2}, \frac{\sigma^b}{2}] = \mathrm{i} f^{abc}\frac{\sigma^c}{2}. \tag{1.24}$$

To break the symmetry, a scalar term including an $SU(2)_L$ complex Higgs doublet is added to the Lagrangian

$$\mathcal{L}_h = (D_\mu\phi)^\dagger D^\mu\phi - \mu^2\phi^\dagger\phi - \lambda(\phi^\dagger\phi)^2, \quad \text{with} \quad \phi(x) = \begin{bmatrix}\phi^{(+)}(x)\\ \phi^{(0)}(x)\end{bmatrix}, \tag{1.25}$$

where the $SU(2)_L \times U(1)_Y$ covariant derivative is now

$$D_\mu \phi = (\partial_\mu - \mathrm{i} g_W \frac{1}{2} \sigma^a W_\mu^a - \mathrm{i} g' \frac{Y}{2} B_\mu)\phi, \tag{1.26}$$

and Y is called hypercharge, and is conserved under $U(1)_Y$ rotations. If the Higgs parameters are chosen such that $\mu^2 < 0$ and $\lambda > 0$, the Lagrangian in the ground states of the theory's potential does not share the symmetry that the Lagrangian with all other field configurations exhibits. The expectation value of the Higgs field is in this convention parametrized as

$$\langle 0|\phi^{(0)}|0\rangle = \sqrt{\frac{-\mu^2}{2\lambda}} = \frac{v}{\sqrt{2}}. \tag{1.27}$$

The most important consequence of the SSB is made obvious if the scalar field is reparametrized as a real fied with four degrees of freedom expanded around the vaccum expectation, i.e.

$$\phi(x) \to \phi'(x) = \mathrm{e}^{\mathrm{i}\frac{\sigma^a}{2}\theta^a(x)} \frac{1}{\sqrt{2}} \begin{bmatrix} 0 \\ v + H(x) \end{bmatrix}, \tag{1.28}$$

where one can now choose (due to gauge invariance), the unitary gauge $\theta^a(x) = 0$, and notice that the first term in the Lagrangian from eq. (1.25) now generates terms quadratic in gauge fields proportional to $\sim v^2$. This effectively generates the masses of the physical $W^\pm$ and Z^0 bosons, while keeping the SM renormalizable, and they become

$$m_{W^\pm} = \frac{1}{2} v g_W, \quad \text{and} \quad m_{Z^0} = \frac{1}{2} v \sqrt{g_W^2 + g'^2}, \tag{1.29}$$

while the boson states after the SSB are written in the basis of gauge fields as

$$\begin{bmatrix} A_\mu \\ Z_\mu^0 \end{bmatrix} = \frac{1}{\sqrt{g_W^2 + g'^2}} \begin{bmatrix} g' & g_W \\ g_W & -g' \end{bmatrix} \begin{bmatrix} W_\mu^3 \\ B_\mu \end{bmatrix}, \quad \text{and} \quad W_\mu^\pm = \frac{1}{\sqrt{2}} \big(W_\mu^1 \mp \mathrm{i} W_\mu^2\big), \tag{1.30}$$

including the photon, here designated as A_μ, which remains massless since $U(1)_{\mathrm{EM}}$ is the residual symmetry after the SSB. The unphysical Goldstone bosons, which appear when a non-symmetrical Higgs field configuration is considered (as above),

have been "gauged away" effectively by choosing the unitary gauge, and one can compare the number of degrees of freedom before SSB and after it

$$3 \cdot 2_{[W^1_\mu, W^2_\mu, W^3_\mu]} + 2_{[B_\mu]} + 4_{[\phi]} = 3 \cdot 3_{[W^+_\mu, W^-_\mu, Z^0_\mu]} + 2_{[A_\mu]} + 1_{[H]}, \tag{1.31}$$

where one has to keep in mind that the massless vector bosons have 2 degrees of freedom, while the massive ones have 3. The Goldsone bosons can be explicitly included in calculations (i.e. by not setting them to zero), but the physical result would stay the same, albeit including more diagrams. Almost generally [25], one can count the number of massive bosons that aquire mass by "eating" the Goldstone bosons by looking at the dimension of the coset G/H, where the generic initial symmetry group G is broken to a generic subgroup H.

The fermionic masses are included through the Yukawa couplings with the Higgs doublet, in a gauge invariant way

$$\mathcal{L}_Y = -\big[(\bar{Q}_L Y_u) u_R\big]\phi - \big[(\bar{Q}_L Y_d) d_R\big]\tilde{\phi} - \big[(\bar{\ell}_L Y_e) e_R\big]\tilde{\phi} + \text{h.c.}, \tag{1.32}$$

where a helpful notation $\tilde{\phi} = \mathrm{i}\sigma^2\phi^*$ has been introduced. The coupling matrices Y_u, Y_d and Y_l in effect generate the fermion masses in the SM, which is made obvious in the unitary gauge after the SSB

$$\begin{aligned} -\big[(\bar{Q}_L Y_u) u'_R\big]\phi &\overset{\text{SSB}}{\to} -\frac{v}{\sqrt{2}}(\bar{u}'_L Y_u u'_R), \\ -\big[(\bar{Q}_L Y_d) d'_R\big]\tilde{\phi} &\overset{\text{SSB}}{\to} -\frac{v}{\sqrt{2}}(\bar{d}'_L Y_d d'_R), \\ -\big[(\bar{L}_L Y_\ell) \ell_R\big]\tilde{\phi} &\overset{\text{SSB}}{\to} -\frac{v}{\sqrt{2}}(\bar{\ell}_L Y_\ell \ell_R), \end{aligned} \tag{1.33}$$

where one has to keep in mind that these 3×3 matrices in flavor space are in general not diagonal. They can be diagonalized by simultaneously transforming the fermion fields and the Yukawa matrices

$$f_{(L,R)} \to V_{f(L,R)} f_{(L,R)} \equiv \tilde{f}_{(L,R)}, \quad \text{and} \quad Y_f \to V_{fL} Y_f V^\dagger_{fR} \equiv \frac{\sqrt{2}}{v} M_f, \tag{1.34}$$

where $f = (u, d, \ell)$ are the SM fields in weak-eigenstate basis, $\tilde{f} = (\tilde{u}, \tilde{d}, \tilde{\ell})$ are the

SM fields in mass-eigenstate basis, and M_f is now a diagonal mass matrix containing the elementary particle mass terms. The newly introduced vectors $V_{f(L,R)}$ must be determined by an experiment in the quark sector, whereas they are unit vectors in the lepton sector since the right-handed neutrinos do not exist in the SM. In another words, neutrinos remain massless in the SM. So for quarks one can define a complex unitary matrix

$$V_{uL}V_{dL}^{\dagger} \equiv V_{\mathrm{CKM}} = \begin{bmatrix} V_{ud} & V_{us} & V_{ub} \\ V_{cd} & V_{cs} & V_{cb} \\ V_{td} & V_{ts} & V_{tb} \end{bmatrix}, \tag{1.35}$$

which allows casting weak-eigenstate basis interaction to fermion mass-eigenstate basis. The matrix is called the Cabbibo-Kobayashi-Maskawa (CKM) matrix [26, 27], and its elements are not independent, due to unitarity constraints, and can in fact be completely determined by only 4 parameters. While a few different parametrizations are popular, the most commonly used one is the so called Wolfenstein parametrization [28], defined by the parameters

$$\lambda = \frac{|V_{us}|}{\sqrt{|V_{ud}|^2 + |V_{us}|^2}}, \quad A = |V_{cb}|\frac{\sqrt{|V_{ud}|^2 + |V_{us}|^2}}{|V_{us}|^2}, \quad \text{and} \quad \bar{\rho} + \mathrm{i}\bar{\eta} = -\frac{V_{ud}V_{ub}^*}{V_{cd}V_{cb}^*}. \tag{1.36}$$

The unitarity relations imply a graphical representation in the form of a triangle in the complex plane. The parameters determining the triangle are determined by several collaborations, of which the result depicted here is by the CKMfitter[1] group in the form of a global fit, and is shown in figure 1.2, together with various experimental constraints that enter the fit. One might notice an impressive agreement on the physical $(\bar{\rho}, \bar{\eta})$ point measurements from a wide variety of different experiments (nuclear $0^+ \to 0^+$ transitions, leptonic, semileptonic and hadronic decays of mesons etc.), pointing to incredible strength of SM prediction power. Any deviation from the unitarity of the CKM matrix would imply the existence of some unknown particles and interactions.

The CKM matrix elements enter the interaction part of the Lagrangian as couplings of quarks of differents generations through an interaction with the charged

[1] http://ckmfitter.in2p3.fr/

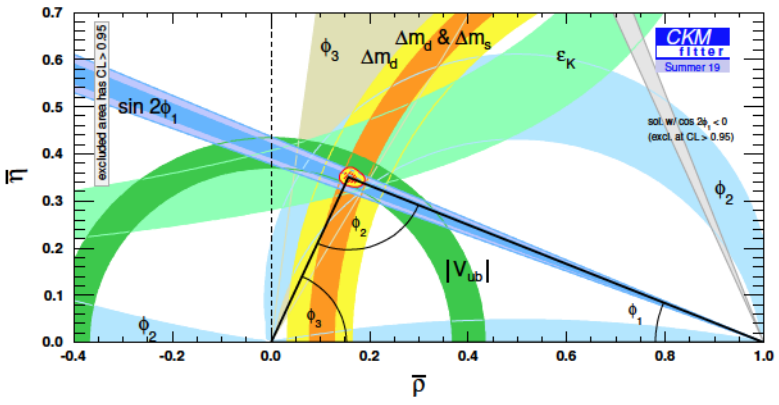

Figure 1.2: The unitarity triangle in the $\bar{\rho} - \bar{\eta}$ plane, the topmost angle is fount at the physical $(\bar{\rho}, \bar{\eta})$ point, by the CKMfitter group

$W^{\pm}$ bosons, which after SSB in unitary gauge looks like

$$\mathcal{L}_f \supset -\frac{g_W}{\sqrt{2}}\left(\bar{\tilde{u}}_L \gamma^\mu W_\mu^+ V_{\mathrm{CKM}} \tilde{d}_L\right) + \mathrm{h.c.}, \tag{1.37}$$

and it is now obvious, since $V_{\mathrm{CKM}}^* \neq V_{\mathrm{CKM}}$, that charge-parity (CP) violation is one of the consequences of this SM formulation. In fact, the only way to violate CP in the SM is through the electroweak sector, aside from a hypotethical (and, from a gauge-symmetry perspective, allowed) QCD antisymmetric term proportional to a near-zero (or possibly, zero) parameter $\theta_{\mathrm{QCD}} \simeq 0$ [29] hypothesized to contribute to CP violation through the Lagrangian

$$\mathcal{L}_{\mathrm{QCD}}^{\theta} = -n_f g_s^2 \frac{\theta_{\mathrm{QCD}}}{32\pi^2} G_{\mu\nu} \tilde{G}^{\mu\nu}. \tag{1.38}$$

To be more specific, CP violation can only occur through the parameter $\eta \neq 0$, which can be incorporated in the V_{CKM} through an introduction of a complex phase factor δ_{13}, as

$$\begin{aligned} s_{12} &= \lambda, \\ s_{23} &= A\lambda^2, \\ s_{13} e^{\mathrm{i}\delta_{13}} &= A\lambda^3(\rho - \mathrm{i}\eta). \end{aligned} \tag{1.39}$$

A more convenient way to parametrize the CP violation in the SM is through the

so called Jarlskog invariant [30]

$$J = \mathrm{Im}(V_{us}V_{cb}V_{ub}^{*}V_{cs}^{*}) = (3.18 \pm 0.15) \times 10^{-5}, \tag{1.40}$$

which vanishes if and only if CP is exactly conserved in the SM. Although measured to be very small, CP violation has been confirmed indirectly [31, 32], and directly, in K [33], D [34] and B [35] meson decays. Aside from the charged current that changes quark flavors from the up-type to the down-type and vice versa, a neutral quark current is generated mediated by the Z^0 boson

$$\mathcal{L}_f \supset -\sqrt{g_W^2 + g'^2}\big(c_L^u \bar{\tilde{u}}_L \gamma^\mu Z_\mu^0 \tilde{u}_L + c_R^u \bar{\tilde{u}}_R \gamma^\mu Z_\mu^0 \tilde{u}_R + (u \to d)\big), \tag{1.41}$$

through which the flavor changes cannot occur in the SM at tree level. This is what is known as the non-existence of flavour-changing neutral currents (FCNCs) in the SM. However, they can occur as suppressed higher-order quantum corrections, e.g. through the so-called electroweak penguin diagrams, which helped to predict the large t quark mass through the sensitivity of the ϵ'/ϵ parameter to it [36], or the box diagrams, which involve $W^\pm$ in the loop exchange, and relate to the mixing of meson states.

An important comment is in order. When measuring hadronic and semileptonic decay rates involving flavor-changing charged currents, such as the one in eq. (1.17), the SM tests inevitably depend both on the form factors and the CKM matrix elements relevant for the quark transition in question, since

$$\frac{\mathrm{d}\Gamma(\bar{B}_d \to \pi^+ \ell^- \bar{\nu}_\ell)}{\mathrm{d}q^2} \propto |V_{ub}|^2 \big|f_+(q^2)\big|^2 \Bigg(+ \mathcal{O}\ \frac{m_\ell^2}{q^2}\big|f_0(q^2)\big|^2 \Bigg), \tag{1.42}$$

where with $f_+(q^2)$ a common notation for the pseudoscalar $\to$ pseudoscalar mesonic transition form factors has been introduced, and will be elaborated upon in section 3. In mature stages of the LHC precision era, this means that every uncertainty associated with CKM matrix elements that were extracted from these types of decays has inscribed in itself the uncertainties stemming from the inherently nonperturbative aspects of QCD, since in experiments the differential or full decay rate is measured.

Precision determination of decay-specific form factors was one of the motivations for the topic of this thesis, as will be further elaborated in section 2, where methods of determining nonperturbative QCD elements are listed and compared.

1.3. Some shortcomings of the SM

Despite an amazing amount of success the SM has enjoyed in the LHC era, there are several shortcomings which will need to be ameliorated in the years to come.

The most obviously glaring one is the absence of inscription of gravity into the theory. Gravity is considered to be the fourth elementary force (along the electromagnetic, weak and strong forces) in the universe, but is phenomenologically experienced only on a macroscopical, classical level. The language of gravity is today widely considered to be that of Einstein's general theory of relativity, a classical theory plagued by the divergence of solutions around the centre of mass of a black hole, i.e. a very densely distributed mass. At this scale, it is expected that the spacetime quantum fluctuations play an important role. As the source of gravitation is the stress-energy tensor (a rank-2 tensor), the graviton is expected to be a spin-2 massless (due to gravity's long range) particle. This in turn deems quantum gravity perturbatively unrenormalizable. Two modern allevations are the string theory approach, and the loop quantum gravity approach. The former is a unifying one, in which gravity is treated on the same level as other forces, and has problems with compactifications (one needs a lot of extra dimensions) and additional degrees of freedom (such as supersymmetry), while the former treats gravity on its own.

Two additional problems somewhat connected to the one of gravity are the ones of dark matter and dark energy. Decades of astrophysical observations have led researchers to conclude that our universe might be inhabited by an as of yet undiscovered type of matter. This is most obviously witnessed when measuring the velocity of stars (or gas) in spiral galaxies at different distances from the galaxy's centre [37]. It becomes clear that, at given distance, the velocity of matter is often several times larger than the expectation involving ordinary matter. Similarly, rotation velocities do not decrease with distance from the center [38], as would be expected. Since the matter hypothesized to exist in the halos of galaxies, and account for this phenomenon, is electromagnetically neutral, and is only observed to interact gravitationally, it is commonly called dark. Similarly, a constant energy density source term, named dark energy, can be added to Einstein's field equation

that would drive the universe's accelerating expansion. This energy density can also be realized in a more dynamical way, e.g. through the so called quintessence models. Today, majority of estimates agree that a total of $\approx 95\%$ of matter-energy density is comprised of these two dark modes, while ordinary matter constitues only $\approx 5\%$.

Concerning the EW sector, it is an experimentally confirmed fact that neutrinos have masses, which is a necessary consequence of the detection of neutrino oscillations [39]. However, in the SM there are no right-handed neutrinos, i.e. the neutrinos do not interact with the Higgs field through Yukawa couplings. Since the exact way these masses are to be implemented in the SM has heavy implications for the future experimental phenomenology, this is a bountiful area of research [40]. As an example one might consider the seesaw models, in which the smallness of neutrino masses is explained by the existence of heavier degrees of freedom that dynamically determine the mass generation, or scotogenic models, which explore the possibility of inducing the mass through higher-order loop corrections involving new physics.

The baryon asymmetry refers to the fact that, even though the CP violation in the SM is very small, very little antimatter is detected in comparison to ordinary matter [41]. In fact, as mentioned in the chapter above, the only way CP is violated in the SM is through the complex phase inscribed in the CKM matrix, of which a measure is the Jarlskog invariant, which is of order $\mathcal{O}(10^{-5})$, not nearly enough to explain the currently observed baryon-antibaryon asymmetry in the universe. Often, scenarios of new physics are invoked to explain the baryon-antibaryon asymmetry.

1.4. Tensions in the flavor sector

Aside from the problems SM is facing on a very direct level, a significant number of measurements of various observables in the flavor sector has stubbornly been defying their SM predictions in the last decade. Among these, the most prominent are the determinations of the $|V_{ub}|$ CKM matrix element, and a set of observables based on ratios of decay widths of heavy hadrons which test the universality of EW lepton coupling across flavours.

1.4.1. Inclusive and exclusive $|V_{ub}|$ determination

The unitarity triangle reflects a robust SM test. The left side of the unitarity triangle in figure 1.2 is of length

$$R_b = (1 - \frac{\lambda^2}{2})\frac{1}{\lambda}\frac{|V_{ub}|}{|V_{cb}|}. \tag{1.43}$$

This means that measuring the Wolfenstein parameter λ, and both CKM matrix elements $|V_{ub}|$ and $|V_{cb}|$ determines a ring (green color in figure 1.2) on which the side of the triangle lies. At the moment, λ is measured to a sub-percent level, while $|V_{cb}|$ and $|V_{ub}|$ have an experimental uncertainty of $\approx 2\%$ and $\approx 8\%$ respectively [4], that is, $|V_{ub}|$ is comparatively imprecise. Although the measurements seem compatible with the triangle being unitary, a more scrutinized look at experimental data reveals a somewhat troubling fact.

Determinations of a CKM matrix element can be classified as being either inclusive or exclusive. In the case of $|V_{ub}|$, these two terms are reserved for semileptonic processes in which the initial state is always a B meson and the final state always contains a lepton-neutrino pair (sometimes other $b \to u$ type decays of b-flavored hadrons are also classified under exclusive decays), as shown in figure 1.3. However, the exclusive channels only contain one final state meson ($\pi, \rho, \omega ...$), while the inclusive channel implies a summation over hadronic final states. To date, the most precise exclusive channel for determining $|V_{ub}|$ is the decay $\bar{B} \to \pi \ell \bar{\nu}_\ell$. Surprisingly, a direct comparison of the exclusive and inclusive results of the $|V_{ub}|$ determinations yields a discrepancy with a statistical significance of $\approx 2.7\sigma$ [42], assuming no

correlations between determinations and normally distributed results.

Theoretically, inclusive $\bar{B} \to X_u \ell \bar{\nu}_\ell$ (where X_u denotes hadronic states involving a u quark) processes are explored using either factorization tools or Wilson's Operator Product Expansion (OPE), where often the Heavy-Quark Effective Theory (HQET) is used (for a brief introduction of both terms see section 2). In the specific case of $b \to u$ transitions a problem emerges of large $b \to c$ background contamination, requiring the employment of hadronic phase space cuts in order to separate the two channels. Additionally, shape functions appear describing the structure functions relevant for the decay, which are always modeled to an extent using conservative constraints and fitted to reproduce e.g. the available $\bar{B} \to X_s \gamma$ data. Multiple scales separating the kinematical regions additionally complicate the issue. These are among the reasons theoretical uncertainties still dominate the $|V_{ub}|$ value determined from the inclusive channel.

On the other hand, the largest source of uncertainty in the exclusive $\bar{B} \to \pi \ell \bar{\nu}_\ell$ decay are the weak transition form factors (see section 3). These have to be evaluated by use of one of the methods described in section 2. Additionally, from the experimental side one has to always choose between pure and efficient modes of detection, resulting in limited precision. In this way, the untagged decays are highly efficient, but rather impure, whereas disentangling hadronically tagged decays turns out to be very inefficient. Somewhere halfway is the semileptonically tagged method, resulting in mediocre purity and efficiency.

The tension between the exclusively and inclusively determined $|V_{ub}|$ is depicted

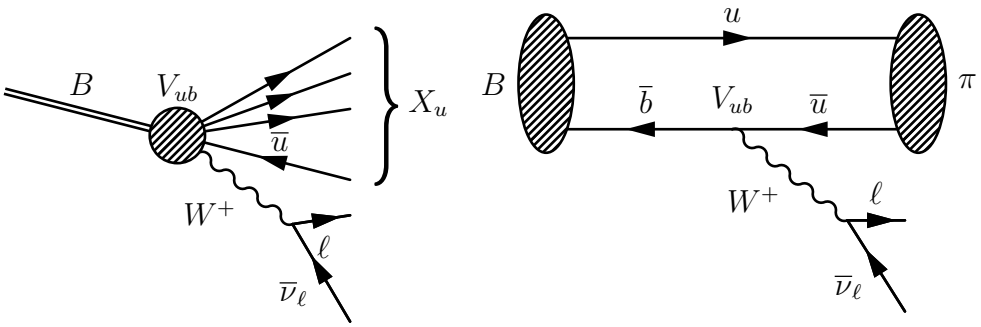

Figure 1.3: Feynman diagrams describing inclusive (left) and exclusive (right) channels of $|V_{ub}|$ determination

in figure 1.4, where the values quoted by the Particle Data Group (PDG) collaboration [4] is shown by the year of the publication. If the tension persists with increasing precision of the calculation of hadronic contributions, new physics effects would have to be introduced to alleviate it. This puzzle is a showcase of the need to precisely determine hadronic matrix elements inside the SM in order to be able to say something about the more fundamental parameters. The precise $|V_{ub}|$ determination hinges crucially on the ability to determine the QCD matrix elements with as little model dependency as possible.

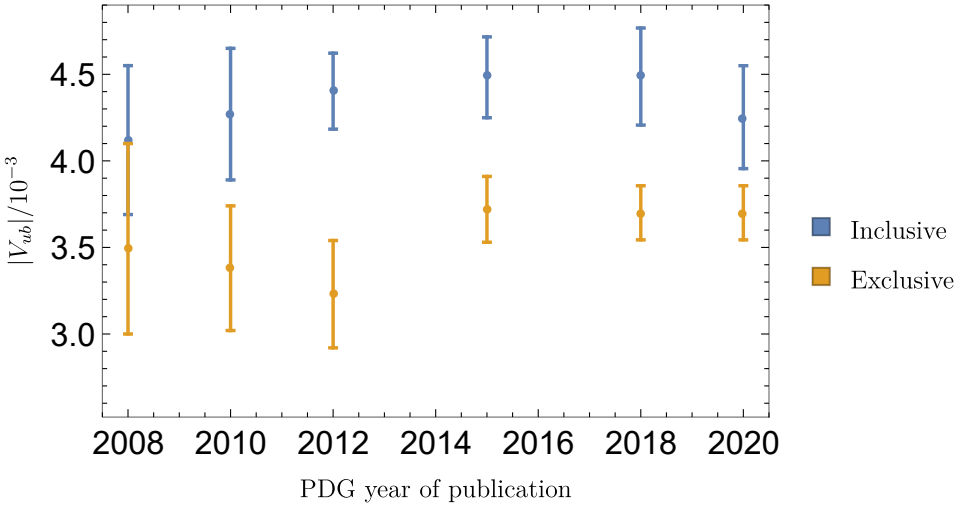

Figure 1.4: PDG quoted values of inclusive versus exclusive $|V_{ub}|$ from different publication years. The latest result can be found in [4]

1.4.2. Lepton flavour universality

In the SM, the EW interaction is described by a single coupling between leptons of all flavours and the $W^{\pm}$ boson, as

$$\mathcal{L}_f \supset -\frac{g_W}{2\sqrt{2}} \sum_f \bar{\nu}_{l_f} \gamma^\mu (1-\gamma^5) l_f W_\mu^+ + \text{h.c.}, \tag{1.44}$$

and equivallently, to the neutral Z^0 boson, as

$$\mathcal{L}_f \supset \frac{g_W}{2\cos\theta_W} \sum_f \bar{l}_f \left[T_{3f} \gamma^\mu (1-\gamma^5) - Q_f \sin^2\theta_W \gamma^\mu \right] l_f Z_\mu. \tag{1.45}$$

This property is called Lepton Flavour Universality (LFU), and as a SM test one might imagine a universe in which LFU does not hold, and consider the consequences. As already mentioned, measuring the semileptonic decay widths of mesons directly would be inadequate due to the lack of precision in determination of both CKM and hadronic matrix elements. However, glancing at eq. (1.42) inspires observables defined as ratios

$$R_{if}^{\mathrm{CC}} = \frac{\Gamma(H_i \to M_f \ell_A \bar{\nu}_{\ell_A})}{\Gamma(H_i \to M_f \ell_B \bar{\nu}_{\ell_B})}, \qquad \text{and} \qquad R_{if}^{\mathrm{NC}} = \frac{\Gamma(H_i \to M_f \ell_A \bar{\ell}_A)}{\Gamma(H_i \to M_f \ell_B \bar{\ell}_B)}, \tag{1.46}$$

testing the lepton flavour universality between generations A and B for the charged current and neutral current decays respectively. Since flavour can only change through charged currents at tree level, the electromagnetically neutral transitions are loop suppressed. These so called LFU ratios are especially sensitive to LFU violation (hence the name), since the CKM matrix element dependence cancels out entirely, while the form factor dependence cancels only partially, since the decay width is actually an integral of functions involving form factors over the leptonic pair invariant mass squared. Numerically, the uncertainties turn out to drastically decrease due to this partial cancellation, which is very convenient for testing the SM.

Interestingly, a series of channels has shown persistent tension between the measurements of LFU ratios and their SM values, as is the case for instance for the ratio

$$R_{D^{(*)}} = \frac{\Gamma(\bar{B} \to D^{(*)} \tau \bar{\nu}_\tau)}{\Gamma(\bar{B} \to D^{(*)} \mu \bar{\nu}_\mu)}. \tag{1.47}$$

This tree level decay occurs through the $W^\pm$ boson, and its difference from unity is almost entirely an effect of the difference in lepton masses. Generally, the corrections to unity are of order $\sim \frac{\Delta m_\ell^2}{(m_{H_i} - m_{M_f})^2}$. For the aforementioned case the current world averages [42–52] are

$$\begin{aligned} R_D^{\mathrm{SM}} &= 0.299 \pm 0.003 < R_D^{\mathrm{exp}} = 0.340 \pm 0.030, \\ R_{D^*}^{\mathrm{SM}} &= 0.258 \pm 0.005 < R_{D^*}^{\mathrm{exp}} = 0.295 \pm 0.014, \end{aligned} \tag{1.48}$$

with a combined tension of $\approx 3\sigma$, as shown in figure 1.5, taken from the HFLAV collaboration[2]. Again, in order to make a conclusive statement, hadronic uncertainties need to be put under better control.

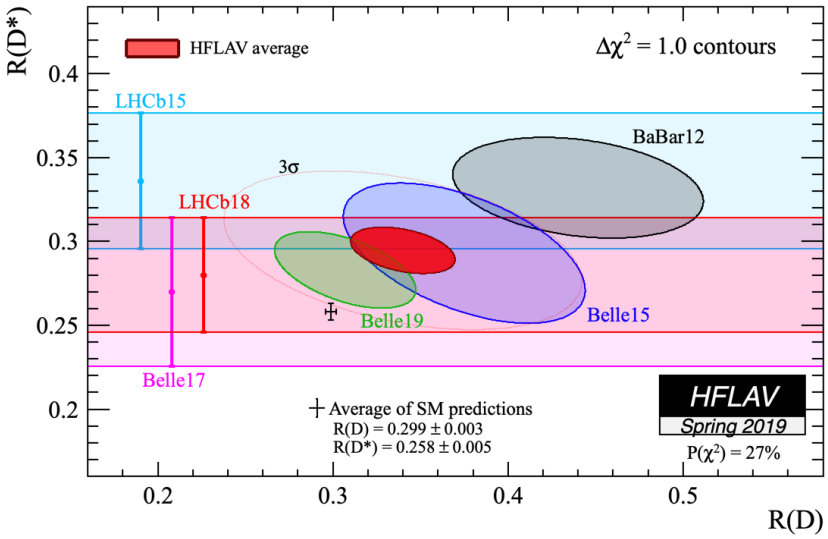

Figure 1.5: The measurements of $R_D - R_{D^*}$ as of spring 2019, taken from the HFLAV collaboration

Another such ratio with a measurement deviating about $\approx 2\sigma$ from its SM value was found in a semileptonic decays of B_c meson [53–55], where the quark transition also occurs at tree level, defined as

$$R^{\text{SM}}_{J/\psi} = \frac{\Gamma(B_c^- \to J/\psi \tau \bar{\nu}_\tau)}{\Gamma(B_c^- \to J/\psi \mu \bar{\nu}_\mu)} \approx 0.25 \pm 0.02 < R^{\text{exp}}_{J/\psi} = 0.71 \pm 0.025. \tag{1.49}$$

The experimental measurement uncertainties are still quite large, but what is surprising is the fact that the central value is almost three times higher than the SM expectation.

Perhaps most strikingly, recently an old tension was reaffirmed and strengthened in the loop suppressed process ratios

$$R_{K^{(*)}} = \frac{\Gamma(B \to K^{(*)} \mu^+ \mu^-)_{[1.1\,\text{GeV}^2, 6.0\,\text{GeV}^2]}}{\Gamma(B \to K^{(*)} e^+ e^-)_{[1.1\,\text{GeV}^2, 6.0\,\text{GeV}^2]}}, \tag{1.50}$$

[2] https://hflav-eos.web.cern.ch/hflav-eos/semi/spring19/main.shtml

where the integration of the differential decay width in both numerator and denominator has been performed in the range where the square of the invariant mass of the leptonic pair is $1.1\,\mathrm{GeV}^2 < q^2 < 6.0\,\mathrm{GeV}^2$. Measurements are presented in figure 1.6. Now tension exceeds 3σ for the R_K, whereas the tension is smaller for R_{K^*}, as [56–59]

$$\begin{aligned} R_K^{\mathrm{SM}} &= 1 \pm 0.01 > R_K^{\mathrm{exp}} = 0.846^{+0.044}_{-0.041}, \\ R_{K^*}^{\mathrm{SM}} &= 1 \pm 0.01 > R_{K^*}^{\mathrm{exp}} = 0.69^{+0.12}_{-0.09}. \end{aligned} \tag{1.51}$$

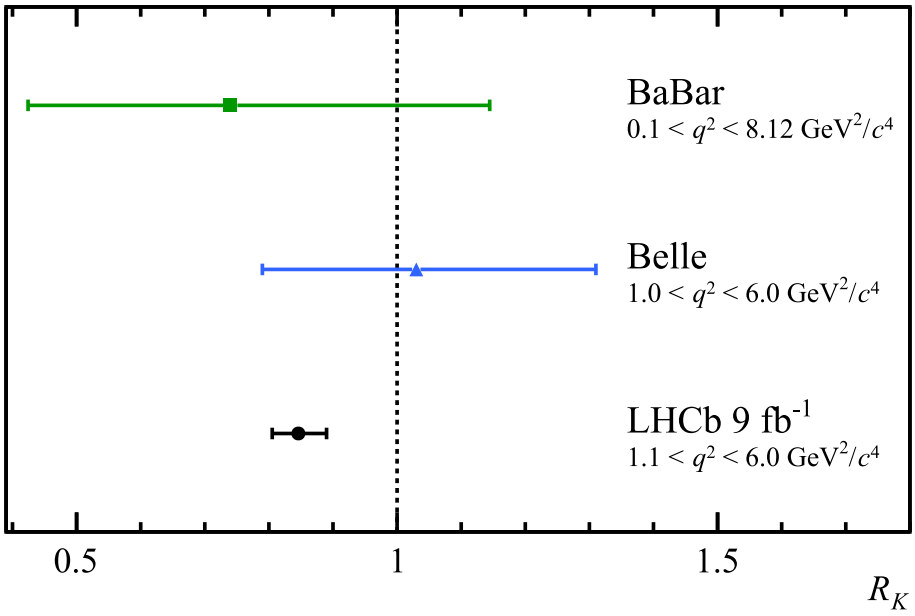

Figure 1.6: The measurements of R_K presented in ref. [58], with a $\approx 3\sigma$ deviation from unity. In the plot older BaBar [60] and Belle [61] measurements are also depicted.

Taken at face value, these measurements at the very least seem to imply hadronic uncertainties are still not under competitive control. A more radical resolution would lead to hints towards new physics prospects.

2. Treatment of non-perturbative phenomena

Since hadronic physics exhibits many fundamentally nonperturbative features, one has to resort to approaches alternative to standard perturbation techniques in order to extract the particular phenomenology including them. The mantra in contemporary particle phenomenology is to avoid introducing any model-dependence as much as possible, making two options rather obvious: effective field theories and numerical lattice calculations, both however still plagued by some idiosyncrasies of their own.

On the front of the effective field theories containing heavy quarks, it was realised early on in the 90's independently by Georgi [62] and Eichten & Hill [63] that a proper effective field theory can be formulated based on the separation of scales of the heavy quark mass m_Q and the scale of QCD dynamics of the bound system Λ_{QCD},

$$\frac{\Lambda_{\mathrm{QCD}}}{m_Q} \ll 1. \tag{2.1}$$

Here, after employing the "velocity superselection" rule, the heavy quark is treated as static, and the Lagrangian of the theory actually contains a heavy degree of freedom for each velocity. This is in a way redundant after requiring that the kinematical transformation of the low-energy (heavy quark) field of velocity v^μ

$$H_w(x) = \mathrm{e}^{\mathrm{i}(q\cdot x)} H_v(x), \quad \text{with} \quad w^\mu = v^\mu + \frac{q^\mu}{m_Q}, \quad \text{and} \quad \frac{q^2}{m_Q^2} \ll 1 \tag{2.2}$$

leaves the effective Lagrangian invariant, a property named reparametrisation invariance [64] (which must hold to all orders in perturbation theory). The field in question is therefore the reparameterisation covariant spinor field, whereas the or-

dinary spinor fields must also be properly boosted. Reparametrization invariance is usually interpreted as a remnant of the obvious loss of Lorentz symmetry in the nonrelativistic limit - an effective field theory is expected to respect all the relevant symmetries of the original field theory, in this case QCD. The theory was aptly named the Heavy Quark Effective Theory (HQET), and has subsequently shown incredible success in the description of bound systems involving both heavy and light degrees of freedom. This of course implies that the expansion is at least ambiguous when considering for example the B_c mesons, since here the bound state contains only heavy degrees of freedom (b- and c-flavored quarks), and the heavy flavor symmetry is broken by the kinetic terms proportional to $1/m_Q$, which regulate the infrared (IR) divergences involving two heavy quarks of the same velocity. Fortunately, the heavy quark spin symmetry (HQSS), i.e. the invariance of the effective Lagrangian under the spin rotations of heavy quarks, is unbroken here, on which a few words are to be spent in the later parts of the thesis.

The appropriate effective field theory required to deal with heavy-heavy bound systems is actually the Nonrelativistic QCD (NRQCD) [65, 66], originally designed to be treated on the lattice. The NRQCD Lagrangian is in principe the same as the one for HQET (aside from the four-fermion operators which only show up in NRQCD), but exhibits a different power counting scheme, that's to say it results in different interaction, and different physics. In NRQCD there are multiple relevant scales, usually expressed in terms of the average quark velocity. Velocity becomes the expansion parameter, as opposed to $\Lambda_{\mathrm{QCD}}/m_Q$ in the case of HQET. In the literature, the new kinematic domains are respectively named *hard*, *soft* and *ultrasoft*, where the adjective refers to the "hardness" of the gluons exchanged between the heavy quarks. Since the theory is nonrelativistic, the time and space components of the gluon propagator are separated. Later, extensions of NRQCD were also developed, named potential NRQCD (pNRQCD) and velocity NRQCD (vNRQCD).

An effort has been made to unify the HQET with the Chiral Perturbation Theory [11, 67–69], characterized by an expansion in the expansion parameter involving a

characteristic low momentum p

$$\frac{1}{(4\pi)^2}\frac{p^2}{F_\pi^2} \ll 1, \tag{2.3}$$

where F_π is the chiral pionic decay constant, resulting in the Heavy Meson Chiral Perturbation Theory (HMχPT) [70, 71], which, aside from direct phenomenological extractions involving both heavy and light hadrons, allows for some useful relations to be derived, e.g. the vector form factor in the decay of D meson to a pion and a pair of electrons at low pionic recoil can be written in HMχPT as

$$f_+(q^2) \approx \frac{f_D}{f_\pi}\frac{g_{D^*D\pi}}{1-\frac{q^2}{M_{D^*}^2}}, \tag{2.4}$$

where $g_{D^*D\pi}$ is the strong coupling constant of mesons. However, this equation also contains corrections stemming from the mass of the final state meson, which become relevant for instance if one decides to substitute $\pi \to K$. A reminder is in order - the heavy hadrons whose behaviour is well-described by HMχPT always contain a light quark.

On the lattice QCD (LQCD) front, there has been an incredible influx of information on heavy hadrons in the past few decades. In LQCD, physics is studied on the level of correlation functions directly, where (in path-integral formulation) the expectation value of an operator (after integrating out the fermionic, Grossman fields) can be written as

$$\langle \mathcal{O} \rangle = \frac{\int \prod_{\alpha=0}^{4} \left[\mathcal{D}A_\alpha(x)\right] \mathcal{O}\, \mathrm{e}^{-S[A_\alpha(x)]}}{\int \prod_{\alpha=0}^{4} \left[\mathcal{D}A_\alpha(x)\right] \mathrm{e}^{-S[A_\alpha(x)]}}, \tag{2.5}$$

where the continuum QCD action is replaced by the discretized action on a spatial lattice of dimension a, i.e.

$$\int \mathrm{d}^4x \to a^4 \sum_{x\epsilon V} \quad and \quad \mathcal{D}_\mu\psi(x) \to \Delta_\mu\psi(x) \equiv \frac{U_\mu(x)\psi(x+a\hat{\mu}) + U_\mu^\dagger(x)\psi(x-a\hat{\mu})}{2a}, \tag{2.6}$$

where $\hat{\mu}$ is a unit vector in the μ-th direction, and with $U_\mu(x) \equiv \mathcal{P}\mathrm{e}^{\mathrm{i}g\int_x^{x+\hat{\mu}} \mathrm{d}x^\mu A_\mu(x)}$ being the path-ordered link field operator that transports the fermion field from a point x to a point $x + a\hat{\mu}$. The discretization process is not uniquely defined and different discretizations have different properties on finite lattice spacing size, albeit all of them reproducing the correct QCD continuum behaviour. Evaluating the correlation functions amounts to producing ensembles of gauge fields with the probability distribution

$$\mathcal{P} \propto \mathrm{e}^{-S[A_\alpha(x)]}, \tag{2.7}$$

calculating the fermionic propagator, and lastly, evaluating the operator value for every configuration of the ensemble and averaging it out by

$$\langle \mathcal{O} \rangle \approx \frac{1}{N}\sum_{i=1}^{N} \mathcal{O}(i\text{−th configuration}) + \text{order}(\frac{1}{\sqrt{N}}).$$

Ranging from the basic meson properties such as masses, lifetimes and decay constants, all the way to the more specific observables, such as the decay form factors and mixing angles, the lattice community has proven to be an endless well of the heavy quark physics input. In the last decade, an especially useful type of calculation has emerged, one using a new discretization type called Highly-Improved Staggered Quarks (HISQ) [72], exploiting a "doubling" symmetry of the lattice action, and then improving on it by specific smearing and reunitarization of the lattice operators to reduce the errors. Recently, using the HISQ action combined with NRQCD, the HPQCD collaboration has been successful in extracting the form factors of $B_c \to B_{d,s}$ [73] and $B_c \to J/\psi$ [55] weak decays to a very high precision, i.e. a degree now competitive with experimental one. For a while now, the $B \to D$ [74, 75], $B \to D^*$ [76, 77] and $B \to \pi$ [78–80] decay form factors have been determined to an admirable precision on the lattice.

The LQCD approach has some theoretical ambiguities, but the main downsides of it are certainly the computational power needed to evaluate the correlation functions on huge ensembles (typically, the simulations are run on either one of the very few super-computers in the world), and lack of a dynamical interpretation of the results. Prior to the development of modern LQCD, the standard for calculating hadronic,

low-energy quantities from the QCD principles was a method retroactively called the Shifman-Vainshtein-Zakharov sum rules (SVZSR) after the authors or, more simply QCD sum rules (QCDSR) [81–83]. The method is based on the Kenneth G. Wilson's OPE [84], where the expectation value of the nonlocal product of multiple operators is expanded in a series of long-distance local operators weighted by short-distance coefficients

$$\langle\alpha|\,\mathcal{T}[\hat{A}(x)\hat{B}(y)]\,|\beta\rangle = \sum_i C_i(x-y;\mu)\,\langle\alpha|\,\hat{\mathcal{O}}_i(x;\mu)\,|\beta\rangle\,, \tag{2.8}$$

where the dimension of the local operators increases with i, provided that $x-y$ is small compared to the dimensions of interaction, and μ is the factorization scale. The short distance coefficients are calculable in perturbation theory since QCD is asymptotically free, and in QCDSR the expectation values $\langle\alpha|\,\hat{\mathcal{O}}_i(x;\mu)\,|\beta\rangle$ are usually taken as parameters either measured experimentally, or extracted from a phenomenological consideration or a lattice calculation. Next, a unitarity relation is utilized by inserting a complete sum of states which couple to the operators $\hat{A}(x)$ and $\hat{B}(y)$ (have the same quantum numbers) in a vacuum-to-vacuum correlation function so that

$$\text{Disc}\,\langle\Omega|\,\mathcal{T}[\hat{A}(x)\hat{B}(y)]\,|\Omega\rangle \propto \sum_n \langle\Omega|\,\hat{A}(x)\,|n\rangle\,\langle n|\,\hat{B}(y)\,|\Omega\rangle\,. \tag{2.9}$$

where $|\Omega\rangle$ is the interacting vacuum, in order to extract various hadronic properties. E.g. if one is interested in the leptonic decay constants, $\hat{A}(x)$ and $\hat{B}(y)$ would represent quark currents. It is important to notice that the $|n\rangle$ states are hadronic particles in the case of QCD, which means that one is in position to relate hadronic parameters to the expectation values of operators involving free quark fields by means of OPE. Compared to LQCD this method is less time-consuming, and provides a relatively clear insight into how the quark degrees of freedom impact the physics on the hadronic level, and was historically very important in calculating quark masses [85, 86], meson [87] and baryon masses [88, 89], and a wide plethora of other QCD features, stemming from lifetimes, to decay constants and form factors.

However, it is at the moment significantly less precise for most problems it is applied on, mostly due to the introduction of some additional parameters and some other concerns involving unitarity and convergence of the three-point sum rules, the topic on which more will be said in the following subchapter.

To ameliorate these problems the light-cone sum rules (LCSR) were developed [90–92] a decade later. In LCSR bilocal operators are introduced in terms of power corrections for large spacelike momenta, and hadron-to-vacuum correlation functions (in eq. (2.8) this would mean $\beta \to 0$, and α representing a hadronic state) are written in terms of integrals over multiparticle distribution amplitudes (DA) of increasing twist, i.e. the difference between spin and dimension of the corresponding operators. When considering a form factor for a decay of the type $A \to B + X$, where X is some other factorizable contribution, relevant operators begin to emerge as

$$\begin{aligned} \langle B(p)|\, \hat{\mathcal{O}}_2(x,y)\, |0\rangle &\propto \int \mathrm{d}u\, \varphi_B^{\mathrm{tw}_i}(u) f_B^{\mathrm{tw}_i}(u;x,y) \qquad \forall i \geq 2 \\ \langle B(p)|\, \hat{\mathcal{O}}_3(x,y)\, |0\rangle &\propto \int \mathrm{d}u\, \Phi_{3B}^{\mathrm{tw}_i}(u) f_{3B}^{\mathrm{tw}_i}(u;x,y) \qquad \forall i \geq 3 \\ &\dots, \end{aligned} \tag{2.10}$$

where the first line symbolizes the two-particle contribution, the second line the three-particle one, and so on, and so on. Each of the operators contains contributions of increasing twist (denoted by i). Twist is defined as the dimension of the operator minus its spin. This is very convenient, since higher twist contributions are heavily suppressed. The $f_{nB}^{\mathrm{tw}_i}(u;x,y)$ functions are calculable perturbatively, while $\varphi_B^{\mathrm{tw}_i}(u)$ and $\Phi_{3B}^{\mathrm{tw}_i}(u)$ encode the nonperturbative contribution. This is especially useful in heavy-to-light type of decays, e.g. decays involving a heavy b quark [93–97], and one encounters virtualities of the type

$$m_b^2 - p_B^2 \geq \mathcal{O}(\Lambda_{\mathrm{QCD}} m_b) \quad \& \quad m_b^2 - q^2 \geq \mathcal{O}(\Lambda_{\mathrm{QCD}} m_b), \tag{2.11}$$

where p_B is the four-momentum of the B meson, and q is the difference in momenta of initial state and final state hadron, so that the zero-recoil point is defined by the maximum q^2. This allows for a reliable expansion around the light-cone, so that

the only relevant degrees of freedom are the longitudinal momenta of the partons. The method has historically been incredibly fruitful at describing B decays to light mesons [98, 99], rare B decays [100], radiative decays [91], and a vast number of other phenomenological applications.

There is a class of models usually referred to as quark models [101–105] which have historically been very fertile in producing phenomenological predictions in heavy quark decays. Though the specific technicalities vary from model to model, most of them construct dressed correlation functions (propagators and vertices) according to some symmetry property or renormalization considerations by fitting model parameters to experimental data, and then calculate the desired properties in a diagrammatic approach. The most troubling aspect of this approach is an unclear connection to QCD, which makes it rather difficult to estimate systematic uncertainties.

On the phenomenological side, through various assumptions as well as truncations and approximations to Dyson-Schwinger equations of QCD (such as the ladder approximation) one can qualitatively explain various phenomenologically successful quark models. While the truncation of exact equations remains a problem also on the side of ab initio Dyson-Schwinger approach to QCD, improved consistent truncations (e.g., beyond the ladder approximation) gradually reduce modeling [106–111].

To summarize, when dealing with non-perturbative phenomena involving heavy degrees of freedom typically the methodology can be assigned to one of the following categories:

1. effective field theories (HQET, NRQCD, HMχPT...),
2. lattice QCD,
3. sum rules,
4. Dyson-Schwinger equations of QCD and various quark models.

This thesis will mainly focus on utilizing various sum rules, together with some experimental, HQET and NRQCD considerations in order to extract the phenomenology of some exclusive decays of heavy mesons. The following two chapters are

therefore dedicated to expanding on the methodology of those two techniques.

2.1. QCD sum rules (QCDSR)

The ultimate goal of the QCDSR method is to estimate the contribution of QCD degrees of freedom to amplitudes describing various particle processes. The central premise underlying the principle is the quark-hadron duality. Generally, quark-hadron duality is a synthesis of the experimental fact that only color-singlet states propagate, and the notion that they are built up from colored states - quarks and gluons. Therefore, calculation of a cross section or a decay width using well established perturbative techniques including partons in an appropriate kinematical domain should, up to a certain precision, describe the hadronic process measured experimentally. Applying this notion using QCDSR in practice turns out to be very convoluted, which can be demonstrated on the example of two- and three-point correlation functions most often encountered in hadronic processes. Often, one also encounters four-point correlation functions, e.g. when considering purely hadronic decays with multiple final state hadrons, or processes involving tetraquarks, but these applications are beyond the scope of this thesis and therefore omitted.

2.1.1. Two-point correlation functions

In order to understand QCDSR on a more technical level, it is demonstrative to inspect the first order EM correction to the electron-electron scattering, which contains a quark-antiquark loop describing a virtual pair creation [112]. Imagining that the electrons carry momenta k_1 and k_2, the momentum transfer carried by the photon is defined as $q = k_1 - k_2$. The vacuum-to-vacuum correlation function describing this loop correction is then

$$\Pi_{\mu\nu}(q) = \mathrm{i} \int \mathrm{d}^4x \, \mathrm{e}^{\mathrm{i}q\cdot x} \langle \Omega | \, \mathcal{T}[\hat{j}_\mu(x)\hat{j}_\nu^\dagger(0)] \, | \Omega \rangle = (q_\mu q_\nu - q^2 g_{\mu\nu})\Pi(q^2), \tag{2.12}$$

where the Lorentz decomposition hinges crucially on the conservation of the EM quark current $\hat{j}_\mu(x)$. Here one can anticipate the OPE by comparing with the

expression in eq. (2.8). Two kinematical regions are of interest here:

1. a highly virtual photon is exchanged so that $-q^2 \gg \Lambda_{\mathrm{QCD}}$;

2. a photon is exchanged so that $q^2 > 0$.

In the first case, for massless quarks, the integral is dominated by $|\vec{x}| \sim x_0 \sim 1/\sqrt{-q^2} \ll R_{\mathrm{had.}} \sim 1/\Lambda_{\mathrm{QCD}}$, and a perturbative expansion is justified. In the case of heavy quarks, symbolically denoted Q, the situation is even simpler due to the appearance of heavy quark mass scale - virtual quark and gluons mostly carry momenta of order m_Q. In other words - they propagate predominantly at short distances and during short time intervals, and quark-gluon interactions are suppressed even at $q^2 = 0$.

In the second case, however, the average distance $|x - 0|$ grows, and quarks start forming hadrons observed as resonances in the $e^-e^- \to e^-e^-$ spectrum. Referring to eq. (2.9), now a unitarity relation holds so that

$$\mathrm{Disc}\,\langle\Omega|\,\mathcal{T}[\hat{j}_\mu(x)\hat{j}^\dagger_\nu(0)]\,|\Omega\rangle \propto \sum_n \langle\Omega|\,\hat{j}_\mu(x)\,|n\rangle\,\langle n|\,\hat{j}^\dagger_\nu(0)\,|\Omega\rangle\,, \tag{2.13}$$

where states $|n\rangle$ represent both single meson states, or multi-particle ones. Turning to momentum representation, in the former case, the correlation function has a pole, while for an n-particle state it experiences a branch cut for $q^2 > (\sum_i^n m_i)^2$. The order at which poles and branch cuts appear on the real axis depends on the system, a mass of a certain radial excitation might be higher than an invariant mass of a multiparticle resonance, and vice versa. An effective energy threshold parameter denoting the lowest of the residues is defined as $s_{min} = m^2_{\mathrm{res}}$. These conclusions are important, since they affect the way quark-hadron duality is imposed on the correlation function.

A very convenient way to bridge the perturbative region and the hadronic region of the correlation function is by analytically continuing it in a complex variable z, and focusing on the Cauchy relation at a point on the negative part of the real axis, $z = q^2 < 0$. In this region the function is analytic, and the Cauchy representation

is valid, so that

$$\Pi(q^2) = \frac{1}{2\pi \mathrm{i}} \oint_C \mathrm{d}z \frac{\Pi(z)}{z - q^2} = \frac{1}{2\pi \mathrm{i}} \oint\limits_{|z|=R} \mathrm{d}z \frac{\Pi(z)}{z - q^2} + \frac{1}{2\pi \mathrm{i}} \int_0^R \mathrm{d}z \left[\frac{\Pi(z + \mathrm{i}\epsilon)}{z + \mathrm{i}\epsilon - q^2} - \frac{\Pi(z - \mathrm{i}\epsilon)}{z - \mathrm{i}\epsilon - q^2} \right], \tag{2.14}$$

where the chosen integration curve has been symbolically denoted by C, and depicted in figure 2.1. The correlation function $\Pi(z)$ often tends to zero as $R \to +\infty$, but can be otherwise renormalized by subtracting the value at $q^2 = 0$, so that $\Pi(q^2) \to \Pi(q^2) - \Pi(q^2 = 0)$. In case this doesn't ameliorate the divergence, one might have to resort to multiple subtractions. Supposing the integral over the circle vanishes, now

$$\Pi(q^2) = \frac{1}{2\pi \mathrm{i}} \oint_C \mathrm{d}z \frac{\Pi(z)}{z - q^2} = \frac{1}{\pi} \int_{s_{\min}}^{+\infty} \mathrm{d}s \frac{\operatorname{Im} \Pi(s + \mathrm{i}\epsilon)}{s - q^2}, \tag{2.15}$$

where the only contributions to the rightmost integral in eq. (2.14) are at the points where residues exist, i.e. at $q^2 > s_{\min}$. The reflection principle $\Pi(z - \mathrm{i}\epsilon) = \Pi^*(z + \mathrm{i}\epsilon)$ has also been implemented. This is very informative - the correlation function at $q^2 < 0$, where a perturbative expansion is justified if $-q^2 \gg \Lambda_{\mathrm{QCD}}$, relates directly to hadronic properties also measurable experimentally at $q^2 > s_{\min}$.

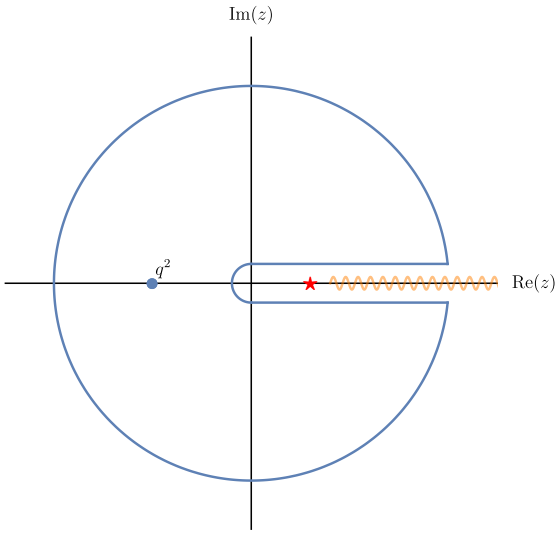

Figure 2.1: The integration curve C, along which the correlation function is integrated. Depicted by the red star is the lowest lying resonance, while the wavy line represents the multiparticle states (branch cuts).

The point of latter discussion becomes more obvious when focusing on the momentum representation of eq. (2.14), where, and focusing on the single particle resonances, we have (for the positive time ordered term in the T-product)

$$\begin{aligned}
&\mathrm{i}\int \mathrm{d}^4x\, \mathrm{e}^{\mathrm{i}(q\cdot x)}\, \langle\Omega|\, \hat{j}_\mu(x)\hat{j}^\dagger_\nu(0)\, |\Omega\rangle\, \theta(x) \\
&\qquad = \mathrm{i}\sum_n \int \mathrm{d}^4x \frac{\mathrm{d}^3p_n}{(2\pi)^3}\, \mathrm{e}^{\mathrm{i}(q-p_n)\cdot x}\theta(x)\, \langle\Omega|\, \hat{j}_\mu(0) \frac{|n;\vec{p}_n\rangle\, \langle n;\vec{p}_n|}{2E_n} \hat{j}^\dagger_\nu(0)\, |\Omega\rangle \\
&\qquad + \text{multiparticle states},
\end{aligned} \tag{2.16}$$

and for the negative time ordered term

$$\begin{aligned}
&\mathrm{i}\int \mathrm{d}^4x\, \mathrm{e}^{\mathrm{i}(q\cdot x)}\, \langle\Omega|\, \hat{j}^\dagger_\nu(0)\hat{j}_\mu(x)\, |\Omega\rangle\, \theta(-x) \\
&\qquad = \mathrm{i}\sum_n \int \mathrm{d}^4x \frac{\mathrm{d}^3p_n}{(2\pi)^3}\, \mathrm{e}^{\mathrm{i}(q+p_n)\cdot x}\theta(x)\, \langle\Omega|\, \hat{j}^\dagger_\nu(0) \frac{|n;\vec{p}_n\rangle\, \langle n;\vec{p}_n|}{2E_n} \hat{j}_\mu(0)\, |\Omega\rangle \\
&\qquad + \text{multiparticle states}.
\end{aligned} \tag{2.17}$$

The expectation values on the right-hand side of the equation define the vector meson weak decay constant, denoted f_n for the state n

$$\langle n;\vec{q}|\, \hat{j}_\nu(0)\, |\Omega\rangle = f_n m_n \epsilon^*_\nu\, (n;\vec{q})\,. \tag{2.18}$$

Writing the Heaviside θ function in the integral representation as

$$\theta(x) = \frac{1}{2\pi\mathrm{i}} \int_{-\infty}^{+\infty} \mathrm{d}w \frac{\mathrm{e}^{\mathrm{i}(w\cdot x)}}{w - \mathrm{i}\epsilon}, \tag{2.19}$$

allows for the evaluation of delta functions in the correlator. Turning back to the Cauchy representation from eq. (2.15), and keeping in mind that the sum over n also implies a sum over polarizations, here the the $n = 1$ state is singled out and

symbolically denoted V (for the vector state)

$$\Pi(q^2) = f_V^2 \int\limits_{s_{\min}}^{+\infty} \mathrm{d}s \frac{\delta(s - m_V^2)}{s - q^2} + \int\limits_{s_{\min}}^{+\infty} \mathrm{d}s \frac{\rho^{\mathrm{res}}(s)}{s - q^2} = \frac{f_V^2}{m_V^2 - q^2} + \int\limits_{s_{\min}}^{+\infty} \mathrm{d}s \frac{\rho^{\mathrm{res}}(s)}{s - q^2}, \quad (2.20)$$

where ρ^{res} gathers all the information about higher radial excitations and the continuum of multiparticle states. As stated before, sometimes it turns out that the dispersion relation needs subtracting one or more divergent terms at $q^2 = 0$. At $q^2 < 0$ the correlation function is calculable by use of Wilson's OPE using quark and gluon fields, which are then related through the dispersive properties to the hadronic parameters, as is obvious in eq. (2.20) for the case of the leptonic decay constant of a vector meson, f_V. The exact way OPE is appropriated is demonstrated in section 2.1.3, as is the determination of ρ^{res}, after a brief discussion on the three-point correlation functions inside the QCDSR paradigm.

Considering interpolating currents with adequate quantum numbers composed of alternative Dirac structures results in description of various mesonic states. A common choice of currents, especially for mesons with at least one heavy degree of freedom, is

$$\begin{aligned} j(0) &\propto \bar{q}_1(0)\mathbb{1}q_2(0) \rightarrow \text{scalar mesons}, \\ j_5(0) &\propto \bar{q}_1(0)\gamma_5 q_2(0) \rightarrow \text{pseudoscalar mesons}, \\ j_\mu(0) &\propto \bar{q}_1(0)\gamma_\mu q_2(0) \rightarrow \text{vector mesons}, \\ j_{5\mu}(0) &\propto \bar{q}_1(0)\gamma_\mu\gamma_5 q_2(0) \rightarrow \text{axial vector mesons}. \end{aligned} \quad (2.21)$$

The choice of interpolating current is somewhat arbitrary, but in the mesonic case doesn't present a large source of uncertainty. However, in the case of baryons, the choice can be quite ambiguous.

Weak leptonic decays of flavorful pseudoscalar mesons, as depicted in figure 2.2, are an especially explicit example of the importance of leptonic decay constant determination. In this special case, the decay width at leading order is

$$\Gamma(P \rightarrow \ell\bar{\nu}) \propto f_P^2 |V_{q_1 q_2}|^2. \quad (2.22)$$

Decay width is an experimentally determinable observable proportional to a product of squares of a CKM matrix element and a leptonic decay constant. This means that a precise determination of the fundamental SM parameter is impossible without prior knowledge of the hadronic parameter. A similar case of semileptonic decays was discussed above, where hadronic matrix elements are not determined by a single parameter, but are rather functions of the square of invariant mass of the lepton pair, which reflects on the decay width as presented in eq. (1.42).

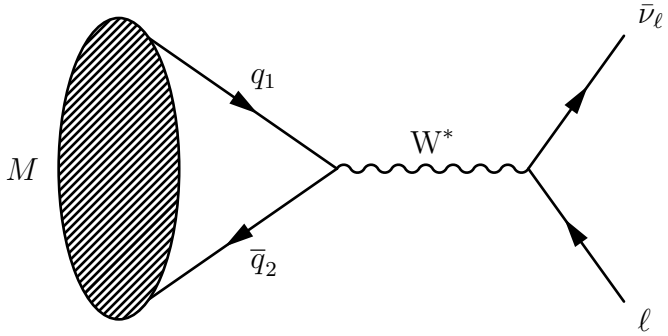

Figure 2.2: Feynman diagram describing a leptonic decay of a meson M.

2.1.2. Three-point correlation functions

When considering weak hadronic transitions, matrix elements emerge such as

$$H_\mu = \langle M_f(p_f)| \left(\mathrm{V}-\mathrm{A}\right)_\mu |M_i(p_i)\rangle \,. \tag{2.23}$$

Here, the mesonic transition that occurs is $M_i \to M_f$, and $\left(\mathrm{V}-\mathrm{A}\right)_\mu$ denotes the vector-axial vector weak transition current from the SM Lagrangian. This invites exploring a correlation function of type

$$\Pi_{\mu[\alpha\beta]}(p_i,p_f,q) = \mathrm{i}^2 \int \mathrm{d}^4x\mathrm{d}^4y\, \mathrm{e}^{\mathrm{i}(p_i\cdot y - p_f\cdot x)} \langle\Omega|\, \mathcal{T}[\hat{j}_{[\alpha]}(x)(\mathrm{V}-\mathrm{A})_\mu \hat{j}^\dagger_{[\beta]}(y)]\,|\Omega\rangle \,, \tag{2.24}$$

where $\hat{j}_{[\alpha],[\beta]}(x)$ are interpolating currents describing initial and final state mesons, and the Lorentz indices $[\alpha]$ and $[\beta]$ exist if, respectively, final or initial meson state is a vector particle, and $q = p_i - p_f$ is the momentum transfer. By complete analogy with the two-point correlation function, now two completeness relations are applied

resulting in

$$\Pi_{\mu[\alpha\beta]}(p_i, p_f, q) = \mathrm{i}^2 \sum_{n,m} \int \mathrm{d}^4x \mathrm{d}^4y \frac{\mathrm{d}^3p_n}{2E_n(2\pi)^3} \frac{\mathrm{d}^3p_m}{2E_m(2\pi)^3} \mathrm{e}^{\mathrm{i}(p_f \cdot x - p_i \cdot y)} \times \\ \times \langle \Omega | \hat{j}_{[\alpha]}(x) | n; \vec{p}_n \rangle \langle n; \vec{p}_n | (\mathrm{V} - \mathrm{A})_\mu | m; \vec{p}_m \rangle \langle m; \vec{p}_m | \hat{j}^\dagger_{[\beta]}(y) | \Omega \rangle . \tag{2.25}$$

In this way, and sticking to the OPE framework from previous section, the hadronic matrix element in question can be extracted at $q^2 < 0$, with a few important and rather problematic caveats. These are discussed at the end of section 2.1.3. The number of independent functions that determine the Lorentz structure of the correlation function depends on the initial- and final-state meson spin properties. For the case of pseudoscalar to pseudoscalar ($P \to P$) transition, two form factors are adequate for the description (one for each pseudoscalar), while for the pseudoscalar to vector ($P \to V$) transition one needs four form factors - one for the pseudoscalar, and three for the massive vector spin degrees of freedom. Focusing on an arbitrary Lorentz structure

$$\Pi_{\mu[\alpha\beta]}(p_i, p_f) \supset \tilde{g}(p_i^2, p_f^2, q^2) \tilde{\Gamma}_{\mu[\alpha\beta]}(p_i, p_f), \tag{2.26}$$

and singling out the $\langle n = M_i | (\mathrm{V} - \mathrm{A})_\mu | m = M_f \rangle$ contribution, the Cauchy representation for the function $\tilde{g}(q^2)$ is

$$\tilde{g}(p_i^2, p_f^2, q^2) = \frac{f_{M_i} f_{M_f}}{(p_i^2 - m_i^2)(p_f^2 - m_f^2)} \tilde{f}(q^2) + \int\limits_{s^i_{\min}}^{\infty} \int\limits_{s^f_{\min}}^{\infty} \mathrm{d}s_i \mathrm{d}s_f \frac{\tilde{\rho}^{\mathrm{res}}(s_i, s_f, q^2)}{(p_i^2 - s_i)(p_f^2 - s_f)} + \ldots , \tag{2.27}$$

where $\tilde{f}(q^2)$ is the form factor multiplying the appropriate Lorentz structure inside H_μ. Again, discussion on subtractions is omitted, and they need to be accounted for if divergences are present. These are also nullified by the use of Borel transformations, which serve a more important purpose of suppressing the impact of soft degrees of freedom at $q^2 < 0$, which is explained in detail in section 2.1.3.

There is several novelties and subtleties here when compared to the two-point correlation function example. First, the non-perturbative hadronic properties are

now encoded in a function - the form factor, instead of a simple parameter. Since the mesons produced are on shell, form factors only depend on one kinematic parameter, the momentum transfer squared, q^2. Second, the dispersive integral over higher resonant states is now a double integral. This, as will be demonstrated in section 3.2, creates further ambiguities related to the continuum threshold and introduces uncertainties hard to estimate. Additionally, when analytically continuing the expression in p_i^2 and p_f^2 a careful approach is in order, since now the analytic structure is much more complicated [113, 114]. On the OPE side, as mentioned before, there are now multiple scales present, and $-q^2 \gg \Lambda_{\mathrm{QCD}}$ is not a sufficient condition to justify the perturbative expansion any more. In fact, the expansion is justified only if $\left|p_i^2\right|, \left|p_f^2\right| \gg \Lambda_{\mathrm{QCD}}$ for light quarks, and involves the heavy quark mass scale for heavy quarks, which will be further elaborated upon, again in following sections.

2.1.3. Wilson's OPE and quark-hadron duality

In summary of previous sections, in order to evaluate hadronic quantities of interest in this thesis two OPE's are encountered (here in momentum space):

1. the two-point OPE,

$$\bar{\Pi}^{\mathrm{2pt.}}(q^2) = \mathrm{i}\int \mathrm{d}^4x\, \mathrm{e}^{\mathrm{i}(q\cdot x)} \left\langle\Omega\right| \mathcal{T}[\hat{j}(x)\hat{j}^\dagger(0)] \left|\Omega\right\rangle = \sum_i C_i(q^2;\mu) \left\langle\Omega\right| \hat{\mathcal{O}}_i(\mu) \left|\Omega\right\rangle , \tag{2.28}$$

   where the expansion is valid for

   - $q^2 \ll -\Lambda_{\mathrm{QCD}}$ for light quark currents, or
   - $q^2 \ll m_Q$ for currents with at least one heavy degree of freedom,

2. the three-point OPE,

$$\bar{\Pi}^{\mathrm{3pt.}}(q^2, p_i^2, p_f^2) = \mathrm{i}^2 \int \mathrm{d}^4x \mathrm{d}^4y\, \mathrm{e}^{\mathrm{i}(p_i\cdot y - p_f\cdot x)} \left\langle\Omega\right| \mathcal{T}[\hat{j}(x) j(0) \hat{j}^\dagger(y)] \left|\Omega\right\rangle = \sum_i \tilde{C}_i(q^2, p_i^2, p_f^2;\mu) \left\langle\Omega\right| \hat{\mathcal{O}}_i(\mu) \left|\Omega\right\rangle , \tag{2.29}$$

   where the expansion is valid for

- $q^2, p_i^2, p_f^2 \ll -\Lambda_{\mathrm{QCD}}$ for light quark currents, or
- $q^2, p_i^2, p_f^2 \ll m_Q$ for currents with at least one heavy degree of freedom.

The Lorentz indices and the flavor content of the currents has been left implicit for simplicity. A scale μ naturally emerges separating the soft contributions from the hard ones. In principle, both the coefficients and the operators contain soft and hard contributions, but this is often simplified for calculations purposes, and can be disregarded if the scale is chosen appropriately in a specific kinematical domain. The operators on the right hand side can be classified according to their dimension and are suppressed by powers of q^2 (or p_i^2 and p_f^2), and are, (up to dimension 5)

$$\begin{aligned} d = 0 \quad &\Rightarrow \quad \hat{\mathcal{O}}_0 = \mathbb{1}, \\ d = 3 \quad &\Rightarrow \quad \hat{\mathcal{O}}_3 = \bar{q}(0)q(0), \\ d = 4 \quad &\Rightarrow \quad \hat{\mathcal{O}}_4 = \frac{\alpha_s}{\pi} G^a_{\mu\nu}(0) G^{a\,\mu\nu}(0), \\ d = 5 \quad &\Rightarrow \quad \hat{\mathcal{O}}_5 = \mathrm{i} g_s \bar{q}(0) \sigma^{\mu\nu} t^a G^a_{\mu\nu}(0) q(0). \end{aligned} \tag{2.30}$$

The short-distance coefficient in front of the $d = 0$ operator is just the perturbative term, while the other coefficients contain the contributions from the quark condensate, the gluon condensate, and the mixed quark-gluon condensate. These so called condensates are actually averages of the virtual quarks' interactions with the QCD vacuum over larger times and distances, and are power suppressed with q^2. As such, their contributions vanish as $q^2 \to -\infty$, i.e. in the deep Euclidean region, which means that

$$\begin{aligned} \left(\lim_{q^2 \to -\infty} \tilde{\Pi}^{\mathrm{2pt.}} \right) &= C_0(q^2; \mu), \quad \text{and} \\ \left(\lim_{q^2 \to -\infty} \tilde{\Pi}^{\mathrm{3pt.}} \right) &= \tilde{C}_0(q^2, p_i^2, p_f^2; \mu). \end{aligned} \tag{2.31}$$

Considering the dispersive relations from eq. (2.20) and eq. (2.27), this has a far reaching consequence inspiring the quark-hadron duality. Namely, this means that the resonant continuum contributions to the spectral function can, at large enough

q^2 be modeled using the perturbative spectral function so that

$$\begin{aligned}
\int\limits_{s_{\min}}^{+\infty} \mathrm{d}s \frac{\rho^{\mathrm{res}}(s)}{s-q^2} &\overset{q^2\to-\infty}{=} \frac{1}{\pi}\int\limits_{s_{\mathrm{eff}}}^{+\infty} \mathrm{d}s \frac{\mathrm{Im}\, C_0(s;\mu)}{s-q^2}, \\
\int\limits_{s^i_{\min}}^{\infty}\int\limits_{s^f_{\min}}^{\infty} \mathrm{d}s_i \mathrm{d}s_f \frac{\tilde{\rho}^{\mathrm{res}}(s_i,s_f,q^2)}{(p_i^2-s_i)(p_f^2-s_f)} &\overset{q^2\to-\infty}{=} \frac{1}{\pi^2}\int\limits_{s^i_{\mathrm{eff}}}^{\infty}\int\limits_{s^f_{\mathrm{eff}}}^{\infty} \mathrm{d}s_i \mathrm{d}s_f \frac{\mathrm{Im}\, \tilde{C}_0(s_i,s_f,q^2;\mu)}{(p_i^2-s_i)(p_f^2-s_f)},
\end{aligned} \tag{2.32}$$

respectively for the two- and three-point correlation functions. The thresholds s_{eff} and $s^{i,f}_{\mathrm{eff}}$ are exactly the square of sums of current quark masses at $q^2 \to -\infty$, but have to be modified for finite q^2, so are named effective thresholds. This modification is necessary due to the contributions of radial excitations to the spectral function, whose magnitude depend on the system in question. Generally, this parameter is fitted to such that the sum rules converge properly, and has to be deduced from experimental information, but is empirically always close to the square of the mass of the first radial excitation. This finally allows for a sum rule to be evaluated, which can schematically be written as

$$\Pi^{\mathrm{OPE}}(\text{small distances}) \overset{\text{disp.}}{=} \Pi^{\mathrm{had}}. \tag{2.33}$$

The exact way this is implemented is shown in section 3.2. Practically, this allows for determination of hadronic quantities from the QCD Lagrangian *ab initio*.

Commonly, in order to suppress the contribution of non-diagonal states and to improve the convergence of the power series, either a Borel transformation is applied, or the correlation is differentiated n times and a moment sum rule is established for the n-moment. Moment sum rules are not employed in this thesis. Borel transform of a function is defined as

$$\hat{\mathcal{B}}_{q^2\to M^2} f(q^2) = \lim_{\substack{-q^2,n\to+\infty \\ -q^2/n\to M^2}} \frac{(-q^2)^{n+1}}{n!}\frac{\mathrm{d}^n}{\mathrm{d}(q^2)^n} f(q^2). \tag{2.34}$$

In other words the function's derivative is taken n times with respect to q^2, and a limit is sought for $-q^2, n \to +\infty$, while the ratio $-q^2/n$ is kept fixed and equal to

M^2. In this way, parameter M^2, called the Borel mass, or the Borel parameter is introduced. Most commonly, the amplitudes will contain propagator terms multiplied by powers of a kinematical variable squared. Since

$$\frac{\mathrm{d}^n}{\mathrm{d}(q^2)^n}\left[\frac{1}{(q^2-m^2)^k}\right] = \frac{(-1)^n}{(q^2-m^2)^{k+n}}\frac{\Gamma(k+n)}{\Gamma(k-1)}, \tag{2.35}$$

as can be checked by induction, the Borel transform is

$$\mathcal{B}_{q^2\to M^2}\left[\frac{1}{(q^2-m^2)^k}\right] = (-1)^k\frac{1}{M^{2(k-1)}}\frac{\mathrm{e}^{-\frac{m^2}{M^2}}}{(k-1)!}. \tag{2.36}$$

The exponent is of order ~ 1, but the suppression is now both power-wise and factorial-wise. Since M^2 is not really a physical parameter, it can be assesed such that at chosen values

1. the correlation function reproduces a certain known hadronic parameter,
2. the soft contributions do not overwhelm the perturbative contribution,
3. the continuum contribution to the correlation function is adequately controlled.

If powers of q^2 appear in the numerator, one can always complete the square such that one power of the denominator is canceled. The Borel transformation is applied both to the partonic (left) and the hadronic (right) side of eq. (2.33). The application of three point QCDSR is shown in section 3.2, and appendix A.

2.2. Light-cone sum rules (LCSR)

Reliance on three-point sum rules historically led to some troubling conclusions [115].

1. Unexpected non suppressed condensate terms appear in the expansion of the electormagnetic pion form factor$F_\pi(q^2)$ [116] and the $A_1(q^2 = 0)$ form factor in the semileptonic $B \to \rho$ decay. In the first case, condensate terms present wrong asymptotics failing to vanish as $q^2 \to -\infty$, while in the second the amplitude blows up in the limit of infinitely heavy b-quark mass.

2. Off-diagonal transition contributions vanish if a Borel transformation is applied [115,117], which opens a whole new set of problems. Namely, the double dispersion relation can be contaminated with non-Landauian singularities [99], which may be hard to determine. Also, the effect of the suppression with respect to the so called Borel parameter might be too weak.

In LCSR these problematic points were ameliorated by considering an expansion in operators of increasing twist rather than dimension, which occur when the two-point correlation function is expanded around the light-cone. Twist is defined by subtracting the canonical spin of the operator from its mass dimension, as

$$\tau = d - j. \tag{2.37}$$

Allowing for a possibillity that the degree of singularity is not determined by the mass dimensions of the composite operators, the authors of [118] investigate the operator product expansion in increasing twist, where the commutator of two operators is expanded around the light cone $(x-y)^2 \approx 0$ is

$$\langle\alpha|\,\mathcal{T}[\hat{A}(x)\hat{B}(y)]\,|\alpha\rangle = \sum_\tau C_\tau\left(\frac{1}{2}(x-y);\mu\right)\langle\alpha|\,\hat{\mathcal{O}}_\tau\left(\frac{1}{2}(x-y),\frac{1}{2}(x+y);\mu\right)|\beta\rangle\,, \tag{2.38}$$

and on the right hand side all of the local operators of the same twist have been

summed in a single bilocal operator such that

$$\left(\hat{\mathcal{O}}_\tau \quad \frac{1}{2}(x-y), \frac{1}{2}(x+y); \mu \right) = \sum_{i \,|\, d(\mathcal{O}_i)=\tau+j_i} \left(\frac{1}{2} \right)^{j_i} (x-y)_{\mu_1} \cdots (x-y)_{\mu_{j_i}} \hat{\mathcal{O}}_i^{\mu_1 \ldots \mu_{j_i}} \left(\quad \frac{1}{2}(x+y); \mu \right) . \tag{2.39}$$

Now, not all four components of vector $(x-y)^\mu$ need to vanish, as long as $(x-y)^2 \approx 0$. The most singular contributions near the light cone come from the bilocal operators with smallest τ, when

$$\left(C_\tau \quad \frac{1}{2}(x-y); \mu \right) \sim \left[\frac{2}{(x-y)^2} \right]^{(d[A]+d[B]-\tau)/2} . \tag{2.40}$$

In practice, to obtain the light-cone sum rule in weak heavy-to-light decays, a two point vacuum-to-meson function of type

$$\Pi_{\mu[\alpha]} = \mathrm{i} \int \mathrm{d}^4 x \, \mathrm{e}^{\mathrm{i}(q \cdot x)} \, \langle M_f(p_f) | \, \mathcal{T} \left[(\mathrm{V}-\mathrm{A})_\mu j_{[\alpha]}(x) \right] | \Omega \rangle \, , \tag{2.41}$$

is investigated, where $(\mathrm{V}-\mathrm{A})_\mu$ is the weak quark transition current with quantum numbers corresponding to M_f, and $j_{[\alpha]}(x)$ is the interpolating current with Lorentz structure symbolically denoted $[\alpha]$. The operator squezeed between the vacuum and the final state meson is expanded in twist around the light cone $(x-0)^2 \approx 0$. The operators contributing to final state light meson wave functions of increasing twist are [119]

$$\begin{aligned}
\tau = 2 \quad &\Rightarrow \quad [\hat{\mathcal{O}}_2]_\mu = \bar{q}_1(z) \gamma_\mu \gamma_5 \, [z,-z] \, q_2(-z), \\
\tau = 3 \quad &\Rightarrow \quad [\hat{\mathcal{O}}_{3p}] = \bar{q}_1(z) \mathrm{i} \gamma_5 q_2(-z), \\
&\Rightarrow \quad [\hat{\mathcal{O}}_{3\sigma}]_{\mu\nu} = \bar{q}_1(z) \sigma_{\mu\nu} \gamma_5 q_2(-z), \\
&\Rightarrow \quad [\hat{\mathcal{O}}_3]_{\mu\nu\alpha\beta} = \bar{q}_1(z) \sigma_{\mu\nu} \gamma_5 g_s G_{\alpha\beta}(vz) q_2(-z), \\
\tau = 4 \quad &\Rightarrow \quad [\hat{\mathcal{O}}_4]_{\mu\alpha\beta} = \bar{q}_1(z) \gamma_\mu \gamma_5 g_s G_{\alpha\beta}(vz) q_2(-z), \\
&\Rightarrow \quad [\hat{\tilde{\mathcal{O}}}_4]_{\mu\alpha\beta} = \bar{q}_1(z) \gamma_\mu \mathrm{i} g_s \tilde{G}_{\alpha\beta}(vz) q_2(-z),
\end{aligned} \tag{2.42}$$

where $[z,-z]$ is the path-ordered gauge factor

$$[z,-z] = P\left[\exp\left\{\mathrm{i}g_s\int_0^1 \mathrm{d}t\,(x-y)_\mu A^\mu\left(tx+(1-t)y\right)\right\}\right]. \tag{2.43}$$

Their contributions to decay amplitudes are incorporated through wave functions $\phi_{i;M_f}, \Phi_{i;M_f}$ and $\Psi_{i;M_f}$, defined up to $\tau = 4$ as

$$\begin{aligned}
\langle\Omega|\,\bar{q}_1(z)\not{z}\gamma_5\,[z,-z]\,q_2(-z)\,|M_f(p_f)\rangle &= \mathrm{i}f_{M_f}(p\cdot z)\int_0^1 \mathrm{d}u\,\mathrm{e}^{\mathrm{i}(2u-1)(p\cdot z)}\phi_{2;M_f}(u;\mu^2),\\
\langle\Omega|\,\bar{q}_1(z)\mathrm{i}\gamma_5 q_2(-z)\,|M_f(p_f)\rangle &= \frac{f_{M_f}m_{M_f}^2}{m_{q_1}+m_{q_2}}\int_0^1 \mathrm{d}u\,\mathrm{e}^{\mathrm{i}(2u-1)(p\cdot z)}\phi^p_{3;M_f}(u;\mu^2),\\
\langle\Omega|\,\bar{q}_1(z)\sigma_{\mu\nu}\gamma_5 q_2(-z)\,|M_f(p_f)\rangle &= -\frac{\mathrm{i}}{3}\frac{f_{M_f}m_{M_f}^2}{m_{q_1}+m_{q_2}}(p_{f\alpha}z_\beta - p_{f\beta}z_\alpha)\times\\
&\qquad\times\int_0^1 \mathrm{d}u\,\mathrm{e}^{\mathrm{i}(2u-1)(p\cdot z)}\phi^\sigma_{3;M_f}(u;\mu^2),\\
\langle\Omega|\,\bar{q}_1(z)\sigma_{\mu\nu}\gamma_5 g_s G_{\alpha\beta}(vz)q_2(-z)\,|M_f(p_f)\rangle &= \mathrm{i}f_{3M_f}\left(p_\alpha p_\mu g^\perp_{\nu\beta} - p_\alpha p_\nu g^\perp_{\mu\beta} - (\alpha\to\beta)\right)\times\\
&\qquad\times\int \mathcal{D}\bar{\alpha}\,\mathrm{e}^{\mathrm{i}(p\cdot z)(\alpha_1-\alpha_2-v\alpha_3)}\Phi_{3;M_f}(\alpha_1,\alpha_2,\alpha_3;\mu^2),\\
\langle\Omega|\,\bar{q}_1(z)\gamma_\mu\gamma_5 g_s G_{\alpha\beta}(vz)q_2(-z)\,|M_f(p_f)\rangle &=\\
&\quad p_\mu\left(p_\alpha z_\beta - p_\beta z_\alpha\right)\frac{1}{p\cdot z}f_{M_f}\int \mathcal{D}\bar{\alpha}\,\mathrm{e}^{\mathrm{i}(p\cdot z)(\alpha_1-\alpha_2-v\alpha_3)}\Phi_{4;M_f}(\alpha_1,\alpha_2,\alpha_3;\mu^2)\\
&\quad + \left(p_\beta g^\perp_{\alpha\mu} - p_\alpha g^\perp_{\beta\mu}\right)f_{M_f}\int \mathcal{D}\bar{\alpha}\,\mathrm{e}^{\mathrm{i}(p\cdot z)(\alpha_1-\alpha_2-v\alpha_3)}\Psi_{4;M_f}(\alpha_1,\alpha_2,\alpha_3;\mu^2),\\
\langle\Omega|\,\bar{q}_1(z)\gamma_\mu\mathrm{i}g_s\tilde{G}_{\alpha\beta}(vz)q_2(-z)\,|M_f(p_f)\rangle &=\\
&\quad p_\mu\left(p_\alpha z_\beta - p_\beta z\alpha\right)\frac{1}{p\cdot z}f_{M_f}\int \mathcal{D}\bar{\alpha}\,\mathrm{e}^{\mathrm{i}(p\cdot z)(\alpha_1-\alpha_2-v\alpha_3)}\tilde{\Phi}_{4;M_f}(\alpha_1,\alpha_2,\alpha_3;\mu^2)\\
&\quad + \left(p_\beta g^\perp_{\alpha\mu} - p_\alpha g^\perp_{\beta\mu}\right)f_{M_f}\int \mathcal{D}\bar{\alpha}\,\mathrm{e}^{\mathrm{i}(p\cdot z)(\alpha_1-\alpha_2-v\alpha_3)}\tilde{\Psi}_{4;M_f}(\alpha_1,\alpha_2,\alpha_3;\mu^2),
\end{aligned} \tag{2.44}$$

for pseudoscalar mesons, where, for simplicity, light-like vectors p_μ and z_μ have been introduced as

$$p_\mu = p_{f\mu} - \frac{1}{2}z_\mu\frac{m_{M_f}^2}{p\cdot z}, \tag{2.45}$$

and, additionally, a projector on a plane perpendicular to both p_μ and z_μ has been

introduced as

$$g_{\mu\nu}^{\perp} = g_{\mu\nu} - \frac{1}{p \cdot z}(p_\mu z_\nu + p_\nu z_\mu). \tag{2.46}$$

Usually, $\phi_{2;M_f}$ is called the twist-two wave function, $\phi_{3;M_f}^{\{p,\sigma\}}$ and $\Phi_{3;M_f}$ are classified as twist-three wave functions, while $\Phi_{4;M_f}$, $\Psi_{4;M_f}$, $\tilde{\Phi}_{4;M_f}$ and $\tilde{\Psi}_{4;M_f}$ are classified as twist-four wave functions. Expressions for vector states are available as well [120, 121], but are not listed in this thesis. The integration measure of the three-particle wave-function integrals is defined as

$$\int \mathcal{D}\bar{\alpha} = \int_0^1 \mathrm{d}\alpha_1 \mathrm{d}\alpha_2 \mathrm{d}\alpha_3 \delta(1 - \alpha_1 - \alpha_2 - \alpha_3), \tag{2.47}$$

and the integral is performed over the momentum fractions of two quarks and a single gluon, respectively. The twist-three three-particle contribution introduces a new non-perturbative parameter f_{3M_f}, defined in appendix B, along with the non-perturbative parameters entering twist-four wave function definitions. Not going into the construction of the collinear conformal group algebra, it suffices to note that the twist-two wave function can be expanded in Gegenbauer polynomials $C_n^{3/2}$

$$\phi_{2;M_f}(u;\mu^2) = 6u(1-u)\left(1 + \sum_{n=1}^{\infty} a_n^{M_f}(\mu^2) C_n^{3/2}(2u-1)\right), \tag{2.48}$$

where the scale dependence of the wave function is inscribed in the non-perturbative Gegenbauer coefficients $a_n^{M_f}(\mu^2)$, which renormalize multiplicatively at LO in $\alpha_s(\mu^2)$, as described also for higher twist wave-function parameters in appendix B. The asymptotic form of eq. (2.48) is given by

$$\phi_{2;M_f}^{\mathrm{as}}(u) = \phi_{2;M_f}(u;\mu^2 \to +\infty) = 6u(1-u). \tag{2.49}$$

Since twist contributions with $\tau > 4$ are usually very suppressed (cf. [122] for the $B \to \pi$ decay), in this thesis only the contributions up to twist-four are considered.

3. Form factors in weak decays

The main channel of testing the SM in this thesis is the one of semileptonic meson decays which occur through a charged weak current. In all of the decays investigated the initial state meson contains one b quark, and another one, say q_1. The transition amplitude can then be written as

$$\mathrm{i}\mathcal{M} = \langle M_f(p_f)\ell\bar{\nu}_\ell|\,\hat{\mathcal{H}}_{\text{eff}}(0)\,|B_{q_1}(p_i)\rangle\,, \tag{3.1}$$

where $\hat{\mathcal{H}}_{\text{eff}}$ symbolically denotes part of the Weak Effective Theory (WET) Hamiltonian relevant for the specific transition. In this thesis, $b \to q_2 = c$ and $b \to q_2 = u$ transitions are considered, and the construction of relevant four-Fermi operators is described in appendix C. Obviously, this implies that the quark flavour content of the final meson in this naming scheme is $\bar{q}_1 q_2$. An advantage in considering semileptonic decays as SM probes as compared to the fully hadronic modes is the factorization of the amplitude on the hadronic and the leptonic part. There is no final state interaction to a great approximation. This means that, depending on the relevant operator, as announced in eq. (1.17)

$$\mathrm{i}\mathcal{M} = \frac{G_F}{\sqrt{2}} V_{bq_2} L^{[\mu\dots]}(0)\,\langle M_f(p_f)|\,\hat{j}^{b\to q_2}_{[\mu\dots]}(0)\,|B_{q_1}(p_i)\rangle\,, \tag{3.2}$$

where the Lorentz structure of the effective operators is determined by the nature of the effective Hamiltonian. The leptonic current for a generic Dirac structure $\Gamma^{[\mu\dots]}$ is always

$$L^{[\mu\dots]}(0) = \langle \ell\bar{\nu}_\ell|\,\bar{\ell}(0)\Gamma^{[\mu\dots]}\nu_\ell(0)\,|0\rangle\,, \tag{3.3}$$

where $\bar{\ell}(0)$ and $\nu_\ell(0)$ are the leptonic and neutrino fermion fields, while the hadronic matrix element is defined through the decay form factors. Since the quark transition underlying the process in question is of the type $b \to q_2$, the hadronic current operator is

$$\hat{j}^{b\to q_2}_{[\mu\dots]}(0) = \bar{q}_2(0)\Gamma_{[\mu\dots]}b(0), \tag{3.4}$$

where, again, $b(0)$ and $\bar{q}_2(0)$ represent the quark fields.

As explained in section 1.2, in the SM, weak charged current quark transitions occur only through vector−axial Dirac structure

$$\Gamma^\mu = (\mathrm{V}-\mathrm{A})^\mu = \gamma^\mu(1-\gamma_5). \tag{3.5}$$

However, when considering possible new physics contributions, the effective Hamiltonian is complemented with scalar, vector and tensor operators. The inclusion of these new operators implies in turn the necessity to introduce new form factors. Sometimes (as in the case of the scalar form factor, see section 3.1.1) these form factors can be reduced to the usual SM form factors by an appropriate use of equations of motion. However, in most cases, the correlation functions describing the form factors are linearly independent, and require an additional calculation, as will become clear in the following sections.

In this thesis only decays of b-flavored pseudoscalar mesons are considered. This is due to the experimental availability of such decays - a large number of $b-$flavoured pseudoscalar meson states is produced on both the hadronic (LHC) and leptonic (KEK) colliders. However, in the final state, both pseudoscalar and vector meson states are experimentally distinguished.

3.1. Form factor definitions

In this section, form factors required for the description of both pseudoscalar→pseudoscalar (symbolically denoted $P \to P$) and pseudoscalar→vector (symbolically denoted $P \to V$) mesonic transition matrix elements are listed and explored. Here, they are classified by the Dirac structure of the effective operators responsible for

the decay. Since the exact definitions can vary depending on the Lorenz structures chosen as the basis, here the so called Wirbel-Stech (WS) basis [123] is utilized.

3.1.1. $P \to P$ form factors

Starting with the SM form factors, the Dirac structure defining the hadronic matrix element is

- $\Gamma^\mu = \gamma^\mu(1-\gamma_5)$,

and there are two independent form factors, since the transition occurs through the $(\mathrm{V}-\mathrm{A})_\mu$ current. The form factors are

$$\begin{aligned}\langle P_f(p_2)|\,\bar{q}_2(0)\gamma^\mu(1-\gamma_5)b(0)\,|B_{q_1}(p_1)\rangle = \\ f_+(q^2)\big[P^\mu - \frac{m^2_{B_{q_1}}-m^2_{P_f}}{q^2}q^\mu\big] + f_0(q^2)\frac{m^2_{B_{q_1}}-m^2_{P_f}}{q^2}q^\mu\,,\end{aligned} \tag{3.6}$$

where $P_\mu \equiv p_1^\mu + p_2^\mu$ and $q_\mu \equiv p_1^\mu - p_2^\mu$. The substitution $M_f \to P_f$ has been made in order to symbolically distinguish from the processes in which a vector state is produced in the final state. Furthermore, to better systematize the calculations, now initial and final momenta have been indexed with p_1 for the initial meson state momentum and p_2 for the final meson state momentum. Due to the momentum conservation, q^2 is exactly the squared invariant mass of the lepton-neutrino pair. Kinematical behaviour of weak decay form factors is entirely determined by q^2. In order for the matrix element to be finite in at the maximum hadronic recoil point $q^2 = 0$, the form factor relation at $q^2 = 0$

$$f_+(0) = f_0(0) \tag{3.7}$$

needs to hold. For light leptons, i.e. when $\frac{m_\ell^2}{m^2_{B_{q_1}}-m^2_{M_f}} \ll \mathcal{O}(1)$ the hadronic matrix element contribution to decay width is entirely determined by $f_+(q^2)$.

The first operator not present in SM listed here is defined by the unit Dirac structure

- $\Gamma = \mathbb{1}$,

which in turn defines the scalar form factor

$$\langle P_f(p_2)|\,\bar{q}_2(0)b(0)\,|B_{q_1}(p_1)\rangle = f_S(q^2) = \frac{m^2_{B_{q_1}} - m^2_{P_f}}{m_b(\mu) - m_{q_2}(\mu)} f_0(q^2). \tag{3.8}$$

Here the introduction of a new scalar form factor is unnecessary due to the vector current conservation, which connects the vector operator matrix element with the scalar one. A direct consequence of this is that, unlike the SM form factors, the scalar matrix element has a renormalization scale dependence defined by the quark mass running.

The last operator relevant for the $P \to P$ transition not present in SM is

- $\Gamma^{\mu\nu} = \sigma^{\mu\nu}$,

which results in the tensor form factor defined as

$$\langle P_f(p_2)|\,\bar{q}_2(0)\sigma^{\mu\nu}q_\nu b(0)\,|B_{q_1}(p_1)\rangle = \frac{\mathrm{i}}{m_{B_{q_1}} + m_{P_f}} \left[q^2 P^\mu - (m^2_{B_{q_1}} - m^2_{P_f})q^\mu\right] f_T(q^2). \tag{3.9}$$

For the tensor operator the equality

$$\sigma_{\mu\nu}\gamma_5 = -\frac{\mathrm{i}}{2}\varepsilon_{\mu\nu\alpha\beta}\sigma^{\alpha\beta} \tag{3.10}$$

is valid, so no additional form factors need to be introduced for the $\sigma_{\mu\nu}\gamma_5$ structure.

For $\Gamma = \gamma_5$ the matrix element is exactly zero.

3.1.2. $P \to V$ form factors

In a completely analogous way, the form factors relevant for the $P \to V$ transition are listed below, starting with the SM contribution, when

- $\Gamma^\mu = \gamma^\mu(1 - \gamma_5)$.

Now, however, there are four form factors (one for the pseudoscalar degree of freedom, and three accounting for the polarizations of the massive vector meson)

$$\begin{aligned}\langle V_f(p_2)|\,\bar{q}_2(0)\gamma^\mu(1-\gamma_5)b(0)\,|B_{q_1}(p_1)\rangle = &-\frac{2V(q^2)}{m_{B_{q_1}}+m_{V_f}}\varepsilon_{\mu\nu\alpha\beta}\epsilon^{*\nu}p_2^\alpha p_1^\beta \\ &-\mathrm{i}(m_{B_{q_1}}+m_{V_f})A_1(q^2)\epsilon^*_\mu+\mathrm{i}\frac{A_2(q^2)}{m_{B_{q_1}}+m_{V_f}}(\epsilon^*\cdot q)(p_1+p_2)_\mu \\ &+\mathrm{i}\frac{2m_{V_f}}{q^2}(A_3(q^2)-A_0(q^2))(\epsilon^*\cdot q)q_\mu.\end{aligned} \tag{3.11}$$

Again, in order for the matrix element to be finite, the relation $A_0(0) = A_3(0)$ must hold. Additionally, as the pseudoscalar current matrix element is defined with a single function, the relation follows,

$$A_3(q^2) = \frac{m_{B_{q_1}}+m_{V_f}}{2m_{V_f}}A_1(q^2) - \frac{m_{B_{q_1}}-m_{V_f}}{2m_{V_f}}A_2(q^2), \tag{3.12}$$

confirming that there are exactly four independent form factors.

As mentioned above, the pseudoscalar Dirac structure

- $\Gamma = \gamma_5$

defines a single form factor, which is again through a Ward identity connected to one used to describe the $(\mathrm{V}-\mathrm{A})_\mu$ transition

$$\langle V_f(p_2)|\,\bar{q}_2(0)\gamma_5 b(0)\,|B_{q_1}(p_1)\rangle = -(\epsilon^*\cdot q)\frac{2m_{V_f}}{m_b(\mu)+m_{q_2}(\mu)}A_0(q^2). \tag{3.13}$$

This matrix element again has a renormalization scale dependence defined by the quark mass running.

Finally, outside the SM the $P \to V$ transition also receives contributions from the tensor Dirac structure

- $\Gamma_{\mu\nu} = \sigma_{\mu\nu}(1+\gamma_5)$,

which defines the tensor form factors

$$\begin{aligned}\langle V_f(p_2)|\,\bar{q}_2(0)\sigma_{\mu\nu}q^\nu(1+\gamma_5)b(0)\,|B_{q_1}(p_1)\rangle &= 2\mathrm{i}\varepsilon_{\mu\nu\rho\sigma}\epsilon^{*\nu}p_1^\rho p_2^\sigma T_1(q^2)\\ &+ T_2(q^2)\left[\epsilon_\mu^*(m_{B_{q_1}}^2-m_{V_f}^2)-(\epsilon^*\cdot q)P_\mu\right]\\ &+ T_3(q^2)(\epsilon^*\cdot q)\left[q_\mu-\frac{q^2}{m_{B_{q_1}}^2-m_{V_f}^2}P_\mu\right],\end{aligned} \tag{3.14}$$

where, in order for the matrix element to be finite the relation $T_1(0)=T_2(0)$ must hold. A note is in order. The arbitrariness of the form factor basis is commonly utilized in the correlation function calculations. Since in QCDSR and LCSR one has to consider off-shell meson momenta ($p_1^2\neq m_{B_{q_1}}^2$), in order to avoid any ambiguity in the interpretation of the initial momentum squared, often the following basis is employed

$$\begin{aligned}\langle V_f(p_2)|\,\bar{q}_2(0)\sigma_{\mu\nu}\gamma_5 b(0)\,|B_{q_1}(p_1)\rangle &= A(q^2)\left(\epsilon_\mu^*P_\nu-P_\mu\epsilon_\nu^*\right)-B(q^2)\left(\epsilon_\mu^*q_\nu-q_\mu\epsilon_\nu^*\right)\\ &- 2C(q^2)\frac{(\epsilon^*\cdot q)}{m_{B_{q_1}}^2-m_{V_f}^2}\left(p_{2\mu}q_\nu-q_\mu p_{2\nu}\right).\end{aligned} \tag{3.15}$$

Even though the operators squeezed between the mesonic states are different, they are not independent, and

$$T_1(q^2)=A(q^2),\quad T_2(q^2)=A(q^2)-\frac{q^2}{m_{B_{q_1}}^2-m_{V_f}^2}B(q^2),\quad T_3(q^2)=B(q^2)+C(q^2). \tag{3.16}$$

3.2. Form factors in QCDSR

In the QCDSR paradigm applied on the calculation of $B_{q_1} \to M_f$ weak decay form factors, the definition of the correlation functions of interest (respectively for the decays to vector and pseudoscalar mesons) is

$$\begin{aligned}\Pi_V^{\mu\nu}(p_{\mathrm{B}_{q_1}}, p_V) &\equiv \mathrm{i}^2 \iint \mathrm{d}^4x\, \mathrm{d}^4y\, \mathrm{e}^{-i(p_{\mathrm{B}_{q_1}} x - p_V y)} \langle\Omega|\mathcal{T}\{:j_V^\nu(y)::j^\mu(0)::j_{\mathrm{B}_{q_1}}^\dagger(x):\}|\Omega\rangle \\ \Pi_P^{\mu}(p_{\mathrm{B}_{q_1}}, p_P) &\equiv \mathrm{i}^2 \iint \mathrm{d}^4x\, \mathrm{d}^4y\, \mathrm{e}^{-i(p_{\mathrm{B}_{q_1}} x - p_P y)} \langle\Omega|\mathcal{T}\{:j_P(y)::j^\mu(0)::j_{\mathrm{B}_{q_1}}^\dagger(x):\}|\Omega\rangle\end{aligned} \tag{3.17}$$

where the colon represents normal ordering with respect to the free vacuum

$$:\hat{\mathcal{O}}(x):\equiv \hat{\mathcal{O}}(x) - \langle 0|\hat{\mathcal{O}}(x)|0\rangle \tag{3.18}$$

and $|\Omega\rangle$ is the interacting vacuum state. Normally ordered Hamiltonians are considered in order not to have to consider contractions between quark fields inside normally ordered currents (not relevant for the physics). The $j^\mu(0)$ current represents the weak quark transition current. Hadronic currents are defined as

$$\begin{aligned} j_{B_{q_1}}(x) &= \bar{q}_1(x)\mathrm{i}\gamma_5 b(x), \\ j_P(x) &= \bar{q}_1(x)\mathrm{i}\gamma_5 q_2(x), \\ j_V^\nu(x) &= \bar{q}_1(x)\gamma^\nu q_2(x). \end{aligned} \tag{3.19}$$

According to Wick's theorem, one can decompose the time ordered operator product to a sum of products of normally ordered operators and propagators, which, in the

case of $B_c \to D^0$ looks like

$$\begin{aligned}
\mathcal{F}^{\mu}_{xy} \equiv & - : \overbrace{\bar{c}_i^y \big(\gamma_5\big)_{ij} u_j^y \bar{u}_k^0 \big(\gamma^\mu\big)_{kl} \big(1-\gamma_5\big)_{lm} b_m^0 \bar{b}_n^x \big(\gamma_5\big)_{np} c_p^x}^{} : \\
& - : \overbrace{\bar{c}_i^y \big(\gamma_5\big)_{ij} u_j^y \bar{u}_k^0}^{} \big(\gamma^\mu\big)_{kl} \big(1-\gamma_5\big)_{lm} \overbrace{b_m^0 \bar{b}_n^x}^{} \big(\gamma_5\big)_{np} c_p^x : \\
& - : \overbrace{\bar{c}_i^y \big(\gamma_5\big)_{ij} u_j^y \bar{u}_k^0 \big(\gamma^\mu\big)_{kl} \big(1-\gamma_5\big)_{lm} b_m^0 \bar{b}_n^x \big(\gamma_5\big)_{np} c_p^x}^{} : \\
& - : \overbrace{\bar{c}_i^y \big(\gamma_5\big)_{ij} u_j^y \bar{u}_k^0}^{} \big(\gamma^\mu\big)_{kl} \big(1-\gamma_5\big)_{lm} b_m^0 \bar{b}_n^x \big(\gamma_5\big)_{np} c_p^x : \\
& - : \overbrace{\bar{c}_i^y \big(\gamma_5\big)_{ij} u_j^y \bar{u}_k^0 \big(\gamma^\mu\big)_{kl} \big(1-\gamma_5\big)_{lm} b_m^0 \bar{b}_n^x \big(\gamma_5\big)_{np} c_p^x}^{} : \\
& - : \bar{c}_i^y \big(\gamma_5\big)_{ij} \overbrace{u_j^y \bar{u}_k^0}^{} \big(\gamma^\mu\big)_{kl} \big(1-\gamma_5\big)_{lm} b_m^0 \bar{b}_n^x \big(\gamma_5\big)_{np} c_p^x : \\
& - : \bar{c}_i^y \big(\gamma_5\big)_{ij} u_j^y \bar{u}_k^0 \big(\gamma^\mu\big)_{kl} \big(1-\gamma_5\big)_{lm} \overbrace{b_m^0 \bar{b}_n^x}^{} \big(\gamma_5\big)_{np} c_p^x :
\end{aligned} \tag{3.20}$$

where, for brevity, the coordinate dependence was made obvious through the index. Here, the more general quark flavor considerations have been substituted, as $q_1 \to c$ and $q_2 \to u$, again for brevity. However, the flavor structure can be also be exchanged in order to represent other b-flavored mesons transition, e.g. for the $B_c \to B_s$ weak decay $q_1 \to c$ and $q_2 \to s$. Contractions are implied by the lines above the field operators, and they indicate quark propagators immersed in external (classical) gluon fields. Quark field (in the formalism of background field theory) then satisfies the equation of motion

$$\big(\mathrm{i}\gamma_\mu \frac{\partial}{\partial x_\mu} + g\not{A}^{\mathrm{cl}}(x) - m\big)\psi(x) = 0 \tag{3.21}$$

which means that the propagator satisfies

$$\big(\mathrm{i}\gamma_\mu \frac{\partial}{\partial x_\mu} + g\not{A}^{\mathrm{cl}}(x) - m\big)S(x,y) = \delta(x-y) \tag{3.22}$$

where the propagator expressed through the means of contraction is

$$\mathrm{i}[S_q(x,y)]_{ij} = \overbrace{q_i^x \bar{q}_j^y}. \tag{3.23}$$

In the Fock-Schwinger gauge [83] (technically only a gauge for quantities that are otherwise gauge-invariant, due to translational non-invariance), defined by

$$(x - x_0)^\mu A^{\mathrm{a}}_\mu = 0, \tag{3.24}$$

the quark propagator can be expanded for $x - y \approx 0$ in terms of the external (classical) gluon field

$$\begin{aligned} \mathrm{i}S(x,y) &= \mathrm{i}S^{(0)}(x-y) + g\int \mathrm{d}^4 z \mathrm{i}S^{(0)}(x-z)\mathrm{i}\not{A}^{\mathrm{cl}}(z)\mathrm{i}S^{(0)}(z-y) \\ &+ g^4 \int \mathrm{d}^4 z \int \mathrm{d}^4 z' \mathrm{i}S^{(0)}(x-z')\mathrm{i}\not{A}^{\mathrm{cl}}(z')\mathrm{i}S^{(0)}(z'-z)\mathrm{i}\not{A}^{\mathrm{cl}}(z)\mathrm{i}S^{(0)}(z-y) + \dots \end{aligned} \tag{3.25}$$

where $S^{(0)}(x-y)$ is the free quark propagator in coordinate space,

$$S^{(0)}(x-y) = \frac{1}{2\pi^2}\frac{\not{x} - \not{y}}{(x-y)^4}, \tag{3.26}$$

with color and Dirac indices suppressed. In the aforementioned gauge, the gluon field can be expressed through its field strength (going up to linear term) as

$$A_\mu(x) \approx \frac{1}{2} x^\rho G_{\rho\mu}(0) \tag{3.27}$$

which is, in principle, all that is needed to write out the correlation function in terms of expectation values of operators, beside a technical reminder that fermion fields can be expanded around the origin using (again, in this gauge) covariant derivatives instead of the ordinary ones

$$q(x) = q(0) + \left[x^\alpha D_\alpha q(x)\right]_{x=0} + \dots \tag{3.28}$$

A more detailed derivation of the diagrammatic evaluation can be found in appendix A.

If the correlation functions from eq. (3.17) are decomposed as

$$\begin{aligned}\Pi_P^{\mu}(p_1,p_2) &= \Pi_{P,1}p_1^{\mu} + \Pi_{P,2}p_2^{\mu},\\ \Pi_V^{\mu\nu}(p_1,p_2) &= g^{\mu\nu}\,\Pi_{V,0} + p_2^{\mu}p_1^{\nu}\,\Pi_{V,1} + p_1^{\mu}p_1^{\nu}\,\Pi_{V,2}\\ &\quad + p_2^{\mu}p_2^{\nu}\,\Pi_{V,3} + p_1^{\mu}p_2^{\nu}\,\Pi_{V,4} + \mathrm{i}\epsilon^{\mu\nu\alpha\beta}p_{2\alpha}p_{1\beta}\,\Pi_{V,v},\end{aligned} \tag{3.29}$$

after the Borel transforming them one gets the final expressions for the pseudoscalar form factors

$$\begin{aligned}f_+(q^2) &= \frac{(m_b+m_c)m_c}{2m_{B_c}^2 m_{D^*}^2 f_{B_c} f_{D^0}}\mathrm{e}^{\frac{m_{B_c}^2}{M_1^2}+\frac{m_{D^*}^2}{M_2^2}} M_1^2M_2^2\Big[\mathcal{B}_{-p_1^2}(M_1^2)\mathcal{B}_{-p_2^2}\Big(M_2^2\Big)\ \Pi_{P,1}(q^2)+\Pi_{P,2}(q^2)\Big)\Big],\\ f_0(q^2) &= \frac{(m_b+m_c)m_c}{2m_{B_c}^2 m_{D^*}^2 f_{B_c} f_{D^0}}\mathrm{e}^{\frac{m_{B_c}^2}{M_1^2}+\frac{m_{D^*}^2}{M_2^2}} M_1^2M_2^2\times\\ &\quad\times\Big[\mathcal{B}_{-p_1^2}(M_1^2)\mathcal{B}_{-p_2^2}\Big(M_2^2\Big)\ \frac{\Pi_{P,1}(q^2)-\Pi_{P,2}(q^2)}{m_{B_c}^2-m_{D^*}^2}q^2+\Pi_{P,1}(q^2)+\Pi_{P,2}(q^2)\Big)\Big],\end{aligned} \tag{3.30}$$

and with complete analogy for the vector case

$$\begin{aligned}V(q^2) &= -\frac{(m_{B_c}+m_{D^*})(m_b+m_c)}{2f_{B_c}f_{D^*}m_{B_c}^2m_{D^*}}\exp\Big\{\frac{m_{B_c}^2}{M_1^2}+\frac{m_{D^*}^2}{M_2^2}\Big\}M_1^2M_2^2\Big[\mathcal{B}_{-p_1^2}(M_1^2)\mathcal{B}_{-p_2^2}(M_2^2)\Pi_{V,v}\Big],\\ A_1(q^2) &= -\frac{m_b+m_c}{(m_{B_c}+m_{D^*})f_{B_c}f_{D^*}m_{B_c}^2m_{D^*}}\exp\Big\{\frac{m_{B_c}^2}{M_1^2}+\frac{m_{D^*}^2}{M_2^2}\Big\}M_1^2M_2^2\times\\ &\qquad\times\Big[\mathcal{B}_{-p_1^2}(M_1^2)\mathcal{B}_{-p_2^2}(M_2^2)\Pi_{V,0}\Big],\\ A_2(q^2) &= +\frac{(m_{B_c}+m_{D^*})(m_b+m_c)}{2f_{B_c}f_{D^*}m_{B_c}^2m_{D^*}}\exp\Big\{\frac{m_{B_c}^2}{M_1^2}+\frac{m_{D^*}^2}{M_2^2}\Big\}M_1^2M_2^2\times\\ &\qquad\times\Big[\mathcal{B}_{-p_1^2}(M_1^2)\mathcal{B}_{-p_2^2}(M_2^2)\big(\Pi_{V,1}+\Pi_{V,2}\big)\Big],\\ A_0(q^2) &= -\frac{m_b+m_c}{2f_{B_c}f_{D^*}m_{B_c}^2m_{D^*}^2}\exp\Big\{\frac{m_{B_c}^2}{M_1^2}+\frac{m_{D^*}^2}{M_2^2}\Big\}M_1^2M_2^2\times\\ &\quad\times\Big[\mathcal{B}_{-p_1^2}(M_1^2)\mathcal{B}_{-p_2^2}\Big(M_2^2\Big)\ \Pi_{V,0}+(m_{B_c}^2-m_{D^*}^2)\frac{\Pi_{V,1}+\Pi_{V,2}}{2}-q^2\frac{\Pi_{V,1}-\Pi_{V,2}}{2}\Big)\Big],\end{aligned} \tag{3.31}$$

with the expressions given explicitly for $B_c \to D$ and $B_c \to D^*$ respectively, and M_1^2, M_2^2 are the Borel parameters in the B_c and $D^{(*)}$ channels, respectively. All the

semileptonic decays follow the similar convention, up to substituting appropriate masses in the expressions.

3.3. Form factor kinematical extrapolation

Since QCD-based sum rules are valid only in a very limited kinematical range (in $b \to q$ transitions, resonances do not contribute to the correlation function when $(m_b + m_q)\Lambda_{\rm QCD} \ll (m_b + m_q)^2 - q^2$), a large effort has been put into determining model-independent bounds on the form factors in the entire kinematically allowed semileptonic phase space. This is succesfully achieved by considering an expansion in a conformal variable [124–126]

$$z(q^2; t_*, t_0) = \frac{\sqrt{t_* - q^2} - \sqrt{t_* - t_0}}{\sqrt{t_* - q^2} + \sqrt{t_* - t_0}}, \tag{3.32}$$

which maps the q^2 line for $q^2 > t_*$ onto a unit circle C in the complex plane. The q^2 region below t_* is mapped along the real axis inside the unit circle C. Obviously $z(t_*; t_*, t_0) = -1$, and $z(t_0; t_*, t_0) = 0$. Therefore, t_0 defines the q^2 point that maps to the unit circle origin, and can be chosen relatively free, as long as $t_0 < t_*$. Hadronic correlation functions, described by form factors and expanded in $z(q^2) \equiv z(q^2; t_*, t_0)$ have a known analytic structure, which is in principle easily exploited. To illustrate this, here a general two-point correlation function of type

$$\Pi_j^{[\mu\nu]} = \mathrm{i} \int \mathrm{d}^4x \, \mathrm{e}^{\mathrm{i}(q\cdot x)} \, \langle \Omega | \, \mathcal{T} \left[j^{[\mu]}(x) j^{\dagger[\nu]}(0) \right] | \Omega \rangle = \sum_i^{N_j} \Gamma_i^{[\mu\nu]} \Pi^i(q^2), \tag{3.33}$$

is explored where, again, Lorentz indices have been put in square brackets to denote generality (the procedure applies equally well to correlation functions defined by currents with different Lorentz structures), and N_j is the number of independent Lorentz structures $\Gamma_i^{[\mu\nu]}$ in the decomposition multplied by functions $\Pi_i(q^2)$. The imaginary part of the independent functions $\Pi_i(q^2)$ can be written as a sum over complete hadronic states as

$$\mathrm{Im}\, \Pi^i(q^2) = \frac{1}{2} \sum_i (2\pi)^4 \delta^4(q - p_{H_i}) \left| \langle \Omega | \, j^{[\mu]} \, | H_i \rangle \right|^2. \tag{3.34}$$

Taking a look at the (properly subtracted) integral representation of the functions $\Pi_i(q^2)$

$$\chi_j^i(q^2) = \frac{1}{n!}\frac{\partial^n \Pi^i(q^2)}{\partial (q^2)^n} = \frac{1}{\pi}\int_0^\infty \mathrm{d}t \frac{\mathrm{Im}\,\Pi^i(t)}{(t-q^2)^{n+1}}, \tag{3.35}$$

it becomes obvious that by substituting q^2 for $z(q^2)$, if there are no discontinuities below t_*, the integral deforms to a contour integral over the unit circle with the origin at $z = 0$. This is why t_* is commonly chosen as the lowest threshold of multiparticle production $t_* = t_+ \equiv m_{bq}^2$ relevant for the $b \to u$ transition, since they would contribute a branch cut hard to account for inside the unit circle. In that case, the only discontinuities the correlation function experiences are the pole contributions which are easily accounted for.

The shape of the extrapolation function with bounded expansion coefficients is introduced by noticing that all of the terms on the right-hand side of eq. (3.34) are positive-definite, so that the sum is always positive, and larger then any of the individual terms. This is true for both the single-particle and multi-particle states. Focusing for example on a generic $|M_1 M_2\rangle$ state consisting of two (pseudo)scalar mesons, the inequality results in

$$\begin{aligned}&\mathrm{Im}\,\Pi^i(q^2)\\ &\geq \frac{n_f}{2}\int_\Omega \frac{\mathrm{d}\Omega}{16\pi^2}\sqrt{\frac{k^2}{q^2}}\theta(q^2-(m_{M_1}+m_{M_2})^2)\left|\langle\Omega|\, j^{[\mu]}\left|M_1(\frac{q}{2}-k)M_2(\frac{q}{2}+k)\right\rangle\right|^2.\end{aligned} \tag{3.36}$$

The variable k^2 relates to the final meson state of the decay, in the rest frame of the initial meson state, so if a semileptonic decay $B_{q_1} \to M_f \ell \bar{\nu}_\ell$ is considered

$$k^2 = \frac{m_{B_{q_1}}^2}{q^2}\vec{p}_{M_f}^{\,2} = \frac{1}{4q^2}\left[q^2-(m_{B_{q_1}}+m_{M_f})^2\right]\left[q^2-(m_{B_{q_1}}-m_{M_f})^2\right]. \tag{3.37}$$

Inserting eq. (3.36) into eq. (3.35) a model independent bound presents itself. Since this discussion is reserved for initial states containing one b-quark, eq. (3.35) is perturbatively calculable at the point of maximum hadronic recoil (with soft power corrections), since $(m_b+m_q)\Lambda_{\mathrm{QCD}} \ll (m_b+m_q)^2$. Written explicitly in terms of the

complex variable $z \equiv z(q^2)$, the inequality for the i-th form factor $F_i(z)$ is

$$\frac{1}{2\pi \mathrm{i}} \oint_C \frac{\mathrm{d}z}{z} |\phi_i(z) F_i(z)|^2 \leq 1; \quad \forall i, \tag{3.38}$$

where the outer weighing functions $\phi_i(z)$ have been introduced which by construction depend on the specific form factor, always include $\chi^i_j(q^2 = 0)$, and are analytic on the unit circle.

If a form factor $F_i(z)$ contains pole behaviour below t_* (for $-1 < z < 0$), they can be canceled out by the Blaschke factors defined as

$$P(z) = \prod_i^N \frac{z - z_i}{1 - \bar{z}_i z}, \tag{3.39}$$

where the numer of subthreshold poles is N, and for the i-th pole $z_i = z(m_i^2)$. For a $b \to q$ transition, ground states and radial exitations of bq bound states represent relevant poles. The spin-parity properties of poles to be accounted for are determined by the spin-parity properties of the initial- and final-meson states as well as the transition current. Since Blaschke factors are unimodular on the unit circle, substituting $F_i(z) \to P_i(z)F_i(z)$ will not spoil the inequality from eq. (3.36). Both $P_i(z)F_i(z)$ and $\phi_i(z)$ are now analytic on the unit disk, and their product can be Taylor-expanded, and

$$F_i(z) = \frac{1}{P_i(z)\phi_i(z)} \sum_{n=0}^{\infty} a_n z^n. \tag{3.40}$$

Substituting this in eq. (3.36) generates model-independent bounds on the form factors as

$$\sum_{n=0}^{\infty} |a_n|^2 \leq 1. \tag{3.41}$$

It can be shown that truncating the expression at the K-th term in the sum (resulting in the form factor approximation $F_i^K(z)$) implies that the maximum relative truncation error is defined by the inequality

$$\max \left| F_i(z) - F_i^K(z) \right| < \frac{1}{P(z_{\max})\phi(z_{\max})} \frac{z_{\max}^{K+1}}{\sqrt{1 - z_{\max}^2}}. \tag{3.42}$$

The parametrization from eq. (3.40) is named the Boyd-Grinstein-Lebed (BGL) parametrization after the authors [127, 128].

For the $f_+(q^2)$ form factor of the $\bar{B} \to \pi$ decay, an another parametrization, more simple in form, can be deduced from the same principles, named the Bourrely-Caprini-Lellouch (BCL) parametrization, again after the authors [129]. The authors propose a simpler form

$$f_+(q^2; t_+, t_0) = \frac{1}{1 - q^2/m_{B^*}} \sum_{n=0}^{K} b_n(t_+, t_0) z^n(q^2; t_+, t_0), \tag{3.43}$$

where $t_+ = (m_B + m_\pi)^2$ is the $\bar{B}\pi$ pair production threshold, the lowest multi-particle threshold relevant for the $b \to u$ transition, and it replaces the more general threshold t_* from eq. (3.32). Since the only pole below the threshold t_+ relevant for the decay is the vector state B^*, the divergece of the form factor is made explicit by the simple pole factor. This also reproduces the correct perturbative QCD scaling - as $q^2 \to +\infty$ the form factor scales as $f_+(q^2) \sim 1/q^2$. The z-expansion under the sum is thus analytic on the entire unit disk in the complex plane.

Since angular momentum is conserved in the process, the behaviour of the form factor around the $\bar{B}\pi$ threshold is

$$\operatorname{Im} f_+(q^2 \approx t_+) \sim (q^2 - t_+)^{3/2}, \tag{3.44}$$

and analyticity implies that

$$\operatorname{Re} f_+(q^2 \approx t_+) \sim c_1 + c_2(q^2 - t_+). \tag{3.45}$$

Recalling that $q^2 = t_+$ maps onto $z(t_+) = -1$, it is obvious that $z(q^2 \approx t_+) + 1 \sim \sqrt{q^2 - t_+}$. Taken together with eq. (3.44) and eq. (3.45), this means that

$$\left[\frac{\mathrm{d}f_+(z)}{\mathrm{d}z}\right]_{z=-1} = 0, \tag{3.46}$$

allowing for a further constraint on the expansion coefficients, i.e.

$$b_K = -\frac{(-1)^K}{K}\sum_{n=0}^{K-1}(-1)^n n\, b_n. \tag{3.47}$$

This condition reduces the number of free parameters by one, and the final BCL form is given by

$$f_+(q^2) = \frac{1}{1-q^2/m_{B^*}}\sum_{n=0}^{K-1} b_n\left(z_n - (-1)^{n-K}\frac{n}{K}z^K\right). \tag{3.48}$$

The simplification hinges on the fact that below $t_* = t_+$ the form factor exhibits no discontinuities besides the one made explicit in the pole factor. If the form factor contains branch cuts below t_*, i.e. t_* does not represent the lowest pair production threshold, the condition eq. (3.46) can not be applied.

Since the BCL parametrization is based on similar dispersive properties as the ones the BGL parametrization is based on, the coefficients also satisfy bounds, albeit in a more involved way then those in eq. (3.41). Equating the two parametrizations one arrives at the equality

$$\sum_{n=0}^{\infty} a_n z^n = \frac{m_{B^*}^2}{4(t_+ - t_0)}\phi_+(z)\frac{(1-z)^2(1-z_*)^2}{(1-zz_*)^2}\sum_{n=0}^{K} b_n z^n \equiv \Psi(z)\sum_{n=0}^{K} b_n z^n, \tag{3.49}$$

where $\phi_+(z)$ is the outer function introduced in eq. (3.38) complementary to the $f_+(z)$ form factor, and $z_* = z(q^2 = m_{B^*})$ is the value of the conformal variable z at the position of the B^* pole. Since the function $\Psi(z)$ is analytic on the $|z| < 1$ disk, it can be expanded around $z = 0$

$$\Psi(z) = \sum_{n=0}^{\infty}\eta_n z^n, \tag{3.50}$$

which, when inserted in eq. (3.49) results in

$$\sum_{j,k=0}^{K} B_{jk} b_j b_k \leq 1, \tag{3.51}$$

with

$$B_{jk} = \sum_{n=0}^{\infty} \eta_n \eta_{n+|j-k|}. \tag{3.52}$$

Since the sum of squares of the BGL coefficients at leading order recieve contributions proportional to $a_n^2 \sim (\frac{\bar{\Lambda}}{m_b})^3$ [130], $\bar{\Lambda}$ being the hadronic scale in the large-m_b expansion, it is realistic to expect this bound is a very conservative one.

4. Probing LFU and NP effects in the $B_c^+ \to [J/\psi, \eta_c]\, \ell^+ \nu_\ell$ decay

*This chapter is based on research published in D. Leljak, B. Melic and M. Patra, JHEP **05** (2019), 094 [arXiv:1901.08368 [hep-ph]] [1].*

A few years ago the LHCb collaboration announced the first LFU test using charmed-beauty meson semileptonic decays to $J/\psi\tau^+\nu_\mu$ and $J/\psi\mu^+\nu_\mu$ [53]. A measurement of the ratio of muonic and tauoinc semileptonic branching fractions was performed, resulting in

$$R_{J/\psi}|_{\rm exp} = \frac{\mathcal{B}(B_c^+ \to J/\psi\tau^+\nu_\tau)}{\mathcal{B}(B_c^+ \to J/\psi\mu^+\nu_\mu)} = 0.71 \pm 0.17 \pm 0.18, \tag{4.1}$$

which is more than 2σ away from the Standard model (SM) prediction. Currently there are many model-dependent calculations of $R_{J/\psi}$ [102, 104, 105, 131–139] within the SM, predicting results in the range (without including model uncertainties)

$$R_{J/\psi}|_{\rm SM} \in [0.24, 0.30]\,, \tag{4.2}$$

However, the $R_{J/\psi}$ measurement is challenging. The detection of both muonic and tauonic decay channels occurs only by identifying the three final-state leptons, two of them coming from $c\bar{c}$ muonic annihilation and being perfectly identified. The third lepton enables distinguishing the two semileptonic B_c^+ decay channels from the background, and is a large source of uncertainty of the measurement. Three other large sources of experimental uncertainty are an inadequate size of simulation

samples, the q^2 binning strategy and the bias of the fitting procedure. Reducing the experimental uncertainties is, therefore, a matter of great priority in distinguishing any new physics prospects in semileptonic B_c^+ decays. However, having in mind the anomalies listed in section 1.4.2 noticed in processes with similar quark transitions, it is interesting to entertain the possibilities. As mentioned, combining the R_D and R_{D^*} measurements the deviation slightly exceeds 3σ, which is similarly observed for the R_K and R_{K^*} ratios.

The theoretical uncertainties are associated to a large extent with the inability to determine precisely the hadronic transition form factors, which is in part ameliorated by defining observables in which such uncertainties cancel.

Calculations of $B_c \to$ charmonia form factors are theoretically demanding. A variety of model calculations are available, all of which include large uncertainties in their predictions. Summarizing the values of B_c into S-wave charmonia form factors at $q^2 = 0$ calculated in different models (perturbative QCD (pQCD) [131], three-point QCD sum rules (3ptQCDSR) [132], light cone sum rules (LCSR) [133], relativistic quark model (RQM) [104, 105, 134, 135], nonrelativistic quark models (NRQM) [136, 137], light-font quark model (LFQM) [138], constituent quark model (CQM) [139], relativistic quark model (RCQM) [102]) in the literature a range of results at $q^2 = 0$ can be found,

$$f_+(0) = f_0(0) \in [0.20, 1.43]\,, \tag{4.3}$$

for the $B_c \to \eta_c$ transition form factors, and

$$\begin{aligned} V(0) &\in [0.17, 1.63]\,, \\ A_1(0) &\in [0.21, 1.19]\,, \\ A_2(0) &\in [0.23, 1.27]\,, \\ A_0(0) &\in [0.12, 1.09]\,, \end{aligned} \tag{4.4}$$

for the $B_c \to J/\psi$ transition form factors. No reliable prediction for the R_{η_c} and $R_{J/\psi}$ LFU ratios can be made until the theoretical systematic uncertainties are put under scrutiny. To illustrate this, by including uncertainties in the estimations of

the publications that provide them [140–145], the range of the SM predictions from eq. (4.2) widens even more, as

$$R_{J/\psi}|_{\rm SM} \in [0.17, 0.41]\,. \tag{4.5}$$

In this thesis a calculation of the form factors for $B_c \to S$-wave charmonia in the full q^2 range was addressed using a LCSR-inspired approach. The LCSR method was proven to be a reliable method for calculating transition form factors of many heavy-to light decays, such as $B_{(s)}, D_{(s)} \to \pi, \rho, K, K^*, \eta, \eta'$ [94–97, 99] and even for $\Lambda_b \to \Lambda_c$ decays [146,147]. A comparison of the results with the previously published QCD lattice points for $f_+(q^2)$ and $f_0(q^2)$ from $B_c \to \eta_c$ and $V(q^2)$ and $A_1(q^2)$ from $B_c \to J/\psi$ is presented and shows a nice agreement, especially comparing to the preliminary results available at the time the publication this section is based on was published. Following [142, 143] here a 20% uncertainty to the lattice QCD results is assigned.

At the time of publication of the paper this section is based on, the lattice QCD pseudo data for $B_c \to J/\psi$ form factors $V(q^2)$ and $A_1(q^2)$ were published in preliminary form by the HPQCD collaboration at several q^2 points for $V(q^2)$ and $A_1(q^2)$ [148]. Earlier, the same collaboration had also produced a preliminary set of results for $B_c \to \eta_c$ form factors, which were reported on in the same proceedings. Since, a complete set of form factors was published by the HPQCD collaboration [54, 55]. While the result for the $R_{J/\psi}$ in the LCSR-inspired method presented here shows a very good agreement with the lattice results, some of the form factors show slight devations.

Possible deviations from the SM $R_{J/\psi}$ predictions inspires many scenarios of possible new physics (NP) effects in the semileptonic $B_c \to \eta_c(J/\psi)\ell\bar{\nu}_\ell$ decays. These usually appear either in the context of specific models, for instance models containing leptoquarks [149], left-right symmetric models, R-parity violating supersymmetric models, etc. [150–152] or in a model independent approach based on the general weak interaction effective Hamiltonian [140, 141, 145, 153–155]. To account for possible NP effects in $B_c \to \eta_c$ and $B_c \to J/\psi$ semileptonic decays here the effective

Hamiltonian approach consisting of all possible four-Fermi operators was employed. The constraints on NP operator contributions and the corresponding Wilson coefficients are obtained from the available experimental data pertaining R_D, R_{D^*}, τ and D^* polarizations in $B \to D^{(*)}\ell\bar{\nu}_\ell$ decays, as well as the B_c lifetime. There are various studies [156–161] performing a global fit on the relevant NP operators considering the presence of only one or two NP operators simultaneously. Here, the latest constraints on the Wilson coefficients [158] are utilized, and an analysis of the effects of the NP operators on various observables is performed, including the branching fractions ratio, the forward-backward asymmetry, the convexity parameter and the longitudinal as well as the transverse polarization components of τ in the final state. For the first time, the study of the full four-fold differential decay rate $B_c \to J/\psi\,(\to \mu^+\mu^-, e^+e^-)\ell\bar{\nu}_\ell$ is performed, where the leptons from the J/ψ decay are of opposite helicities. The four-fold decay distribution in this case is proportional to three angles and the momentum transfer q^2. Existence of three independent decay angles gives the freedom to construct additional asymmetries which are sensitive to the real as well as the imaginary part of the new physics couplings.

4.1. LCSR/NRQCD FORM FACTORS

The form factors are extracted from the correlation function of the $\mathcal{T}$-product of the weak current j_Γ, where $\Gamma = V, A, S, P, T$ represents the vector, axial-vector, scalar, pseudoscalar, or tensor structure, respectively, and an interpolating current of the B_c meson $j_{B_c}(0) = m_b\bar{c}(0)\mathrm{i}\gamma_5 b(0)$ among the vacuum and the external on-shell meson M_f ($M_f = J/\psi, \eta_c$),

$$\Pi(q^2, p_{B_c}^2) \;=\; \mathrm{i}\int \mathrm{d}^4x\, \mathrm{e}^{\mathrm{i}(q\cdot x)} \left\langle M_f(p) \left| \mathcal{T}\left\{ j_\Gamma(x) j_{B_c}^\dagger(0) \right\} \right| 0 \right\rangle \tag{4.6}$$

Both $B_c \to M_f$ decays proceed through b-quark decays and here an assumption is made, that in the region of the large $m_b^2 - q^2 \leq \mathcal{O}(m_b\Lambda_{QCD})$ and $m_b^2 - p_{B_c}^2 \leq \mathcal{O}(m_b\Lambda_{QCD})$ virtualities, the correlation function Eq. (4.6) are dominated by the light-like distances and the description in terms of the products of perturbatively

calculable hard-scattering kernels with non-perturbative and universal light-cone distribution amplitude (LCDA), ordered by increasing twist, is appropriate.

The LCSR method was extensively used for determining the heavy-to-light transition form factors. Here the situation is far more involved since the final-state meson is a quarkonium state - η_c or J/ψ. Therefore, to properly account for the non-negligible $\mathcal{O}(2m_c)$ mass corrections in the correlator, a systematic expansion of the correlator near the light cone including latter corrections should be performed. This is a highly nontrivial task and to this date has not been achieved. In the future, to improve the whole picture, a revised consideration of the charmonia LCDA's is expected, similar to what was done in the case of heavy hadrons (B-mesons and Λ_b). Proving the factorization theorems and deriving the RG evolution kernels of LCDA while considering full mass corrections would amount to a respectable task. However, in the case of charmonia, this task proves to be far more involved - neither HQET nor heavy-quark symmetries can be applied. Also, heavy-mass expansion convergence is less obviously stable. Such a calculation, if consistently doable for charmonia, is far beyond the scope of this study. Here it is assumed that potentially large intrinsic mass effects can be effectively absorbed by using DA models that reproduce the charmonia phenomenology. Here, a simplified sum rule model was used, where the final-state charmonia in B_c-decays are treated as light particles in the correlator expansion near the light-cone and will closely follow the approach of the standard LCSR. On the other hand, to describe non perturbative properties of charmonia NRQCD-inspired DAs were used, which exactly reproduces leading charmonia NR moments at $\sim 1\,\text{GeV}$ energies. To resolve the right DA structure at the $\sim m_b$ energies of the decay, the DAs are Gegenbauer-expanded and evolved accordingly. A twist-expansion is performed as a correction to the leading approximation, and large m_c mass corrections in twist-3 and twist-4 DAs are taken into account. The genuine $\mathcal{O}(4m_c^2/m_b\Lambda_{QCD})$ corrections are not included as the collinearity of the wave functions is assumed. Moreover, since the model constraints in describing charmonia particles are obvious, the stability of the model on the variation of parameters of the model is explored. The results seem consistent with the QCDSR calculations of the same form factors, and obey HQSS/NRQCD symmetry relations

among form factors.

By inserting the sum over states with B_c quantum numbers and by using

$$\langle 0|j_{B_c}(0)|B_c(p_B)\rangle = \frac{f_{B_c} m_{B_c}^2}{m_b(\mu) + m_c(\mu)} \tag{4.7}$$

for the ground state, employing the hadronic dispersion relation in the virtuality $p_{B_c}^2$ of the B_c channel, the correlation function Eq. (4.6) can be related to the $B_c \to M_f$ matrix elements and the form factors defined in section 3. As usual, the quark-hadron duality is employed to approximate the contribution of higher resonances by introducing the effective threshold parameter $s_0^{B_c}$ and the ground state contribution of the B_c meson is enhanced by the Borel transformation in the variable $p_{B_c}^2 \to \sigma^2$.

The strategy of fixing the sum rule parameters, in particular the continuum threshold parameter $s_0^{B_c}$, is to use the lattice results for the decay constant of B_c, and fix the continuum threshold parameters by requiring that the 2-point functions calculated in the LCSR numerically match the lattice value. This is done by using the NLO expression and the pole m_b, m_c masses. The $\overline{\text{MS}}$ masses used in the study are taken as $m_b(\overline{m_b}) = 4.18$ GeV and $m_c(\overline{m_c}) = 1.27$ GeV. Taken this way, sum rules exhibit stable behaviour, i.e. the continuum and higher-order corrections are suppressed and the B_c mass is correctly reproduced for $\mu = 3.9 \pm 0.3\,\text{GeV}$ by the daughter sum rules. With the estimated $s_0^{B_c} = 46.8 \pm 0.8\ \text{GeV}^2$ we have also checked the stability of the sum rules for $B_c \to M_f$ transitions. In both cases, the results are very stable on the variation of the Borel parameter, allowing σ^2 to vary between $70 - 90\,\text{GeV}^2$ with almost no change. Other parameters used in the study are provided by various lattice collaborations or are taken from NRQCD-inspired determinations, as described below.

4.1.1. Leading twist contributions

The leading twist-2 DA of a η_c meson is defined as in eq. (2.44) [162] for $M_f = \eta_c$ and $q_{1,2} = c$, while for the J/ψ the expressions are

$$\begin{aligned}\langle 0|\bar{c}(z)\gamma_\mu[z,-z]c(-z)|J/\psi(p,\epsilon^{(\lambda=0)})\rangle &= f_{J/\psi}m_{J/\psi}p_\mu\int_{-1}^{1}\mathrm{d}\xi\,\mathrm{e}^{\mathrm{i}\xi(p\cdot x)}\phi_{||}(\xi,\mu),\\ \langle 0|\bar{c}(z)\sigma_{\mu\nu}[z,-z]c(-z)|J/\psi(p,\epsilon^{(\lambda=\pm1)})\rangle &= \mathrm{i}f^{\perp}_{J/\psi}(\epsilon_\mu p_\nu-\epsilon_\nu p_\mu)\int_{-1}^{1}\mathrm{d}\xi\,\mathrm{e}^{\mathrm{i}\xi(p\cdot x)}\phi_{\perp}(\xi,\mu),\end{aligned} \tag{4.8}$$

where $\xi = u - (1-u)$, and u is the fraction of longitudinal momentum of the $M_f = J/\psi$ meson carried by c-quark and $(1-u)$ is the fraction of momentum carried by $\bar{c}$-quark. DAs experience a scale dependence, and are evaluated at a scale μ, up to which the transverse momenta are integrated out. Non perturbative DAs $\phi(\xi,\mu)$ contain contributions from momenta below μ. The higher-twist amplitudes and higher-order corrections are not listed here, but are available in the literature [121]. The vector and tensor decay constants $f_{J/\psi}$ and $f^T_{J/\psi}$ are defined as

$$\begin{aligned}\langle 0|\bar{c}(0)\gamma_\mu c(0)|J/\psi(p,e^{(\lambda)})\rangle &= f_{J/\psi}m_{J/\psi}e^{(\lambda)}_\mu,\\ \langle 0|\bar{c}(0)\sigma_{\mu\nu}c(0)|J/\psi(p,e^{(\lambda)})\rangle &= if^T_{J/\psi}(\mu)(e^{(\lambda)}_\mu p_\nu - e^{(\lambda)}_\nu p_\mu),\end{aligned} \tag{4.9}$$

where $f^T_{J/\psi}$ is renormalization scale dependent, and at LO it renormalizes multiplicatively, as

$$f^T_{J/\psi}(\mu'^2) = \big(\alpha_s(\mu'^2)/\alpha_s(\mu^2)\big)^{C_f/\beta_0}\, f^T_{J/\psi}(\mu), \tag{4.10}$$

with $\beta_0 = 11 - 2/3n_f$, $C_F = 4/3$ is the usual group factor, and n_f is the number of flavors involved. The η_c decay constant is defined correspondingly as

$$\langle 0|\bar{c}\gamma_\mu\gamma_5 c|\eta_c(p)\rangle = -\mathrm{i}f_{\eta_c}p_\mu. \tag{4.11}$$

For the decay constants the following lattice results are used

$$\begin{aligned} f_{B_c} &= 0.427(6)(2)\,\text{GeV} \quad [163, 164], \\ f_{J/\psi} &= 0.405(6)(2)\,\text{GeV} \quad [165], \\ f_{\eta_c} &= 0.3947(24)\,\text{GeV} \quad [166], \end{aligned} \tag{4.12}$$

while for $f_{J/\psi}^T$, a precisely determined ratio of decay constants is employed

$$R_{J/\psi}^T = \frac{f_{J/\psi}^T(\mu = 2\ \text{GeV})}{f_{J/\psi}} = 0.975 \pm 0.010, \tag{4.13}$$

derived by considering combined QCDSR and lattice results [167]. The predictions for charmonia decay constants in [167] also nicely agree with the lattice results above.

The leading twist-2 DAs are expanded in terms of Gegenbauer polynomials, as in eq. (2.48), and the expression can be inverted so that

$$a_n^{M_f}(\mu^2) = \frac{2(2n+3)}{3(n+1)(n+2)} \int_0^1 \mathrm{d}u\, C_n^{(3/2)}(2u-1)\phi_{2;M_f}(u,\mu^2). \tag{4.14}$$

For light mesons, the coefficients are explicitly calculated at a scale μ_0 on the lattice, or are phenomenologically extracted. However, no such data exists for charmonium. Thus, representing the wave function in DA moments is more useful. The latter are defined at a scale μ as

$$\langle \xi^n(\mu) \rangle = \int_{-1}^1 \mathrm{d}\xi \xi^n \phi(\xi,\mu). \tag{4.15}$$

Due to the flavor symmetric quark content of charmonium, the wave function is symmetric around $u = \frac{1}{2}$, and the first relevant moment is the second one. It can be extracted from NRQCD [168–170] as

$$\langle \xi^n(\mu_0) \rangle = \frac{1}{3}\langle v^2 \rangle_{M_f} + \mathcal{O}(v^4), \tag{4.16}$$

where v is the non-relativistic velocity of a quark confined in the meson state. As-

suming a gaussian model at a scale μ_0 [171] for the LCDA

$$\phi(u,\mu_0) = N_\sigma \frac{4u(1-u)}{\sqrt{2\pi}\sigma} \exp\left[-\frac{(u-\frac{1}{2})^2}{2\sigma^2}\right]; \qquad \sigma^2 = \frac{\langle v^2\rangle_{M_f}}{12}, \tag{4.17}$$

where $N_\sigma \approx 1$ is the normalization constant defined by

$$\int_{-1}^{1} \mathrm{d}\xi \phi(\xi,\mu) = 1, \tag{4.18}$$

the evolution is easily performed to an arbitrary perturbative scale μ.

In NRQCD the average square velocities are extracted at the NLO order in α_s from the rates $\Gamma(\eta_c \to \gamma\gamma)$ and $\Gamma(J/\psi \to e^+e^-)$. These vary across determinations, $\langle v^2\rangle_{J/\psi} = 0.225^{+0.106}_{-0.088}$ [172], $\langle v^2\rangle_{\eta_c} = 0.226^{+0.123}_{-0.098}$ [172], $\langle v^2\rangle_{J/\psi} = \langle v^2\rangle_{\eta_c} = 0.21 \pm 0.02$ [169, 170]. Also in existence is the matching of charmonium (and B_c) leading-twist LCDAs to NRQCD with relativistic corrections [173, 174]. The higher order α_s corrections are thought to possibly be large [175–177]. Here, the latest improved value is used [172, 178, 179] for both charmonia, since at leading order there is no difference of quark relative velocities between J/ψ and η_c

$$\langle v^2\rangle = 0.201 \pm 0.064. \quad [21] \tag{4.19}$$

4.1.2. Higher twist corrections

Concerning higher twist corrections, the Wandzura-Wilczek approximation (WWA) is used, where the three-particle contributions are entirely neglected. For η_c this means sticking to the asymptotic form with the inclusion of m_c corrections [119]

$$\begin{aligned} \phi^p_{3;M_f}(u;\mu^2)\big|_{\mathrm{WWA}} &= 1 + \rho_+(\mu^2)\phi_{p,+}(u,\mu^2), \\ \phi^\sigma_{3;M_f}(u;\mu^2)\big|_{\mathrm{WWA}} &= 6u(1-u) + \rho_+(\mu^2)\phi_{\sigma,+}(u,\mu^2), \end{aligned} \tag{4.20}$$

where $\rho_+(\mu^2) = 4m_c^2(\mu^2)/m_{\eta_c}^2$ and

$$\begin{aligned}\phi_{p,+}(u,\mu^2) &= \frac{1}{4}\left[\int_0^u dv\,\frac{\phi'(v,\mu^2)}{1-v} - \int_u^1 dv\,\frac{\phi'(v,\mu^2)}{v}\right],\\ \phi_{\sigma,+}(u,\mu^2) &= -\frac{3}{2}u(1-u)\left[\int_0^u dv\,\frac{\phi(v,\mu^2)}{(1-v)^2} + \int_u^1 dv\,\frac{\phi(v,\mu^2)}{v^2}\right]. \end{aligned} \tag{4.21}$$

For the J/ψ meson a more involved elaboration is in order. Neglecting the three particle contributions in the WWA, equations of motion are used to express the twist-three DAs in terms of the leading twist-two DAs $\phi_{\parallel,\perp}$ with the corrections stemming from the non-negligible valence quark mass

$$\delta_+(\mu) = \frac{2m_c(\mu)}{m_{J/\psi}}\frac{1}{R^T_{J\psi}}, \quad \tilde{\delta}_+(\mu) = \frac{2m_c(\mu)}{m_{J/\psi}}R^T_{J\psi}, \tag{4.22}$$

as [120, 180–182]:

$$\tilde{h}_\parallel^{(s)} = (1-\delta_+(\mu))h_\parallel^{(s)}, \qquad \tilde{g}_\perp^{(a)} = (1-\tilde{\delta}_+(\mu))g_\perp^{(a)},$$

and

$$g_\perp^{(v)}(x,\mu)\big|_{\rm WWA} = \frac{1}{4}\left[\int_0^u dv\,\frac{\Phi_\parallel(y,\mu)}{1-v} + \int_u^1 dv\,\frac{\Phi_\parallel(v,\mu)}{v}\right] + \tilde{\delta}_+(\mu)\phi_\perp(u,\mu), \tag{4.23}$$

$$\tilde{g}_\perp^{(a)}(x,\mu)\big|_{\rm WWA} = (1-u)\int_0^u dv\,\frac{\Phi_\parallel(v,\mu)}{1-v} + u\int_u^1 dv\,\frac{\Phi_\parallel(v,\mu)}{v}, \tag{4.24}$$

$$h_\parallel^{(t)}(u,\mu)\big|_{\rm WWA} = \frac{1}{2}\xi\left[\int_0^u dv\,\frac{\Phi_\perp(y,\mu)}{1-v} - \int_u^1 dv\,\frac{\Phi_\perp(v,\mu)}{v}\right] + \delta_+(\mu)\phi_\parallel(u,\mu), \tag{4.25}$$

$$\tilde{h}_\parallel^{(s)}(u,\mu)\big|_{\rm WWA} = (1-u)\int_0^u dv\,\frac{\Phi_\perp(v,\mu)}{1-v} + u\int_u^1 dv\,\frac{\Phi_\perp(v,\mu)}{v}, \tag{4.26}$$

with

$$\begin{aligned}\Phi_\parallel(u) &= 2\phi_\parallel(u) + \tilde{\delta}_+\xi\phi'_\perp(u),\\ \Phi_\perp(u) &= 2\phi_\perp(u)\left(+\delta_+\right)\phi_\parallel(u) - \frac{\xi}{2}\phi'_\parallel(u)\Big). \end{aligned} \tag{4.27}$$

The J/ψ twist-four DAs are assumed to take their asymptotic form:

$$\begin{aligned} h_{\perp,3} &= 6u(1-u)\,, \quad g_{\parallel,3} = 6u(1-u)\,, \\ A_{||} &= 24u^2(1-u)^2\,, \quad A_\perp = 12u^2(1-u)^2\,. \end{aligned} \tag{4.28}$$

While the light-cone paradigm works rather well in the case of mesons containing light degrees of freedom, it is possible that the twist-four contributions are large in the case of η_c, due to the existence of m_c corrections. Moreover, in this case the required hadronic parameters are not yet available so the twist-four contribution is disregarded.

Also, since the J/ψ DAs defined above do not correspond to matrix elements of operators with definite twist [94]: $\phi_{\perp,\parallel}$ are of twist-two, $h_\parallel^{(s,t)}$ and $g_\perp^{(v,a)}$ contain a mixture of twist-two and twist-three contributions and $\mathbb{A}_{\perp,\parallel}$, h_3, g_3 are a mixture of twist-two, twist-three and twist-four contributions. Therefore it is usual to refer to $g_\perp^{(v,a)}, h_\parallel^{(s,t)}$ as twist-three LCDAs and to $h_3, g_3, \mathbb{A}_{\perp,\parallel}$ as twist-four LCDAs.

Finally, the sum rules can be constructed as in section 2.2. The expression for the calculation of the form factors can be given in a closed form as

$$F_{B_c\to M}(q^2) = \frac{m_b + m_c}{m_{B_c}^2 f_{B_c}} e^{m_b^2/\sigma^2} \int_{u_0^{B_c}}^1 \frac{du}{u} \exp\left[-\frac{m_b^2 - \bar{u}q^2 - u\bar{u}m_M^2}{u\sigma^2}\right] F(u,\mu,q^2), \tag{4.29}$$

where

$$u_0^{B_c} = \frac{1}{2m_M^2}\sqrt{(s_0^{B_c} - q^2 - m_M^2)^2 + 4m_M^2(m_b^2 - q^2)} - (s_0^{B_c} - q^2 - m_M^2), \tag{4.30}$$

σ is a Borel parameter and $\bar{u} = 1 - u$. The functions $F(u,\mu,q^2)$ contain all twist contributions listed above. It suffices to further comment that the higher-twist contributions are suppressed by the Borel parameter. A list of results at $q^2 = 0$ is presented in table 4.1.

The definitions of form factors are as in section 3.1.1 and 3.1.2. A rough agreement can be seen between the modified LSCR approach utilized in this study and the results provided in other publications. The only exception is the form factor $A_2(q^2)$, where the LCSRs produce a rather low value. However, the cited errors

Table 4.1: Form factor predictions at $q^2 = 0$. Recent relevant lattice results are given by the HPQCD collaboration [148], reported here without the systematical error.

Form Factor	this work	QCDSR [183]	QCDSR [132]	SR [133]	pQCD [131]	CCQM [145, 184]	RQM [104]	RQM [105]	LFQM [138]	latt. [148]
$f_{+,0}^{\eta_c}(0)$	0.62 ± 0.05	0.41 ± 0.04	0.66	0.87	0.48(7)	0.75	0.47	0.54	0.61(5)	0.59
$V^{J/\psi}(0)$	0.73 ± 0.06	0.70 ± 0.06	1.03	1.69	0.42(2)	0.78	0.49	0.73	0.74(4)	0.70
$A_1^{J/\psi}(0)$	0.55 ± 0.04	0.50 ± 0.05	0.63	0.75	0.46(3)	0.56	0.50	0.52	0.50(3)	0.48
$A_2^{J/\psi}(0)$	0.35 ± 0.03	0.43 ± 0.05	0.69	1.69	0.64(3)	0.55	0.73	0.51	0.44(5)	-
$A_0^{J/\psi}(0)$	0.54 ± 0.04	0.53 ± 0.04	0.60	0.27	0.59(3)	0.56	0.40	0.53	0.53(3)	-
$f_T^{\eta_c}(0)$	0.93 ± 0.07	-	-	-	-	0.93	-	-	-	-
$T_{1,2}^{J/\psi}(0)$	0.47 ± 0.04	0.48 ± 0.03	-	-	-	0.56	-	-	-	-
$T_3^{J/\psi}(0)$	0.19 ± 0.01	0.27 ± 0.03	-	-	-	0.20	-	-	-	-

are obtained just by varying the model parameters, and do not include the relevant uncertainties coming from the lack of $4m_c^2/(m_b\Lambda_{\rm QCD})$ corrections. It is possible that these could potentially significantly influence the form factor values.

4.1.3. Extrapolation to high q^2

To extrapolate the form factors to the q^2 values that LCSR is not applicable at, a slightly modified BCL parametrization from section 3.3 is employed. For each form factor, five equally spaced points are produced including their parametric uncertainties using the LCSR method in the range $q^2 \in \left[-5\,\text{GeV}^2, 5\,\text{GeV}^2\right]$, which are a posteriori fitted to the BCL shape function. The $B_c M_f$ pair production threshold is chosen for t_*

$$t_* = t_+ = (m_{B_c} + m_{M_f})^2, \tag{4.31}$$

while the choice has been made for the free parameter $t_0 = t_{\rm opt} = t_+(1 - \sqrt{1 - \frac{q^2_{\rm max}}{t_+}})$, which optimizes the truncation error and maps the semileptonic domain symmetrically in z. This choice numerically doesn't impact the extrapolation. The pole structure has been approximated with a single pole for each form factor. Even though in principle there are more poles for each transition below the pair-production threshold, the semileptonic range is far enough from the lowest $b \to c$ resonance for higher

multipole contributions to be safely disregarded. The shift in the pole due to the existence of other resonances is absorbed by the BCL expansion coefficients, i.e.

$$\frac{1}{1-\frac{q^2}{m^2_{\text{Res}_1}}}\frac{1}{1-\frac{q^2}{m^2_{\text{Res}_2}}}\sum_n a_n z^n \overset{q^2\ll\text{Res}}{\approx} \frac{1}{1-\frac{q^2}{m^2_{\text{Res}_1}}}\sum_n \bar{a}_n z^n. \tag{4.32}$$

Furthermore, it has been shown in previous studies that branch cuts below t_* do not contribute significantly to the form factors in the semileptonic region [127]. Their contributions to the BCL bounds are not considered in this study. Thus, the modified BCL parametrization for the i-th form factor used here is

$$F^i(q^2) \;=\; P(q^2)\left[b_0^i + b_1^i z(q^2)\right], \tag{4.33}$$

where $P(q^2) = (1-q^2/m^2_{\text{Res}})^{-1}$ is the pole factor. Including more resonances beneath t_+ empirically does not change the shape of the form factor in the semileptonic region.

Specific form factor properties rigorously determine and select resonances relevant for the transition in question. Form factors $V(q^2)$ and $T_1(q^2)$ correspond to the vector components of the transition currents, and, as the B_c meson is a pseudoscalar, the transition occurs through a negative parity resonance. $A_{1,2}(q^2)$, as well as $T_{2,3}(q^2)$, correspond to the axial vector component of the $V-A$, while the form factor $A_0(q^2)$ corresponds to the pseudoscalar current and only contributes in

Table 4.2: Summary of the BCL fit for $B_c \to \eta_c$ and $B_c \to J/\psi$ form factors. The masses of the low-laying B_c resonances are taken from [185–188]

Form factor	J^P	m_R (GeV)	b_0	b_1
f_+	1^-	6.34	0.62	-6.13
f_0	0^+	6.71	0.63	-4.86
f_T	1^-	6.34	0.93	-9.36
V	1^-	6.34	0.74	-8.66
A_1	1^+	6.75	0.55	-4.67
A_2	1^+	6.75	0.35	-1.78
A_0	0^-	6.28	0.54	-6.80
T_1	1^-	6.34	0.48	-4.88
T_2	1^+	6.75	0.48	-2.93
T_3	1^+	6.75	0.19	-1.69

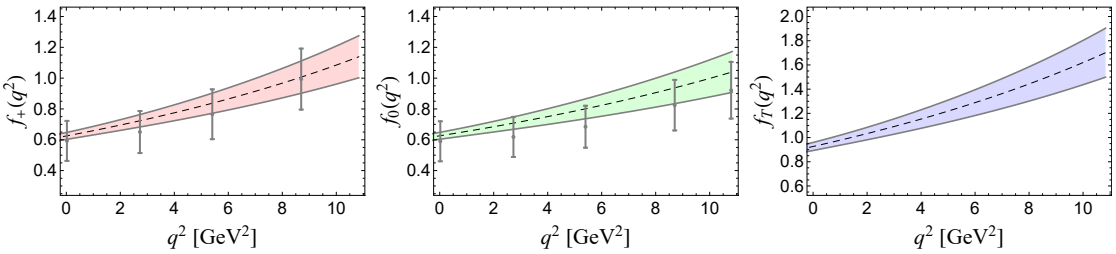

Figure 4.1: $B_c \to \eta_c$ form factors calculated in this study, including the lattice points from [148] with added 20% systematical error.

the decays with the non-vanishing lepton masses (in the semileptonic B_c decays with the τ lepton). All relevant resonance masses are given in table 4.2, together with the fitted parameters b_0^i and b_1^i from eq. (4.33).

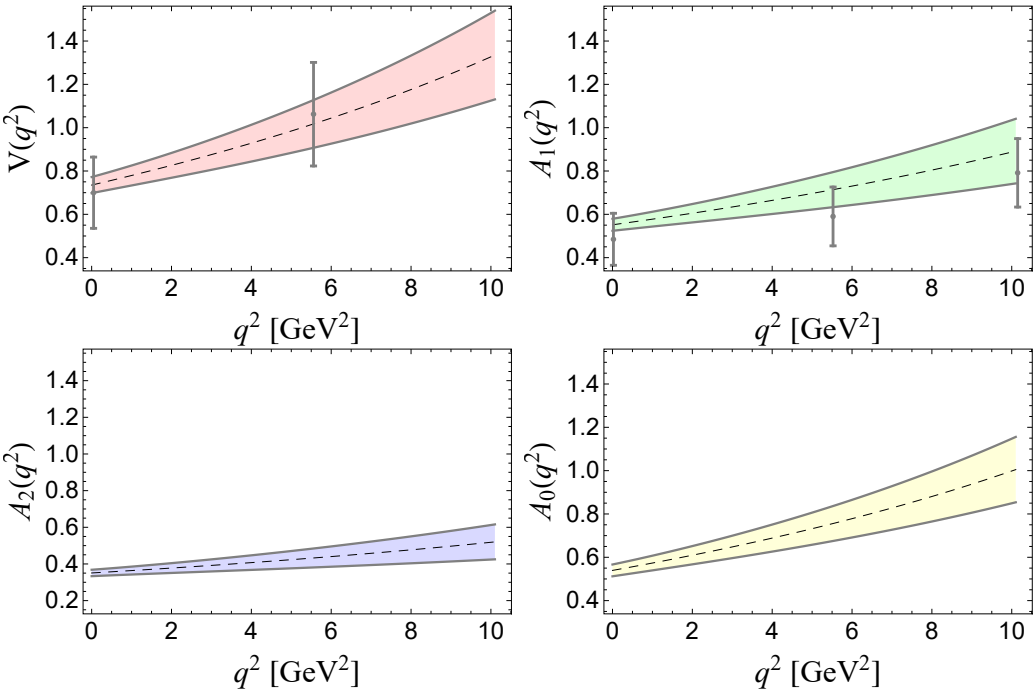

Figure 4.2: $B_c \to J/\psi$ SM form factors calculated in this study, including the lattice points from [148] with added 20% systematical error.

Fits to both SM and NP $B_c \to \eta_c$ form factors are presented in figure 4.1, together with the projected uncertainties. No correlations between the form factor pseudo data points are taken into account. Pseudo data is indeed very correlated, but including the correlations would in a sense underestimate the total uncertainty, since no systematics errors due to the $4m_c^2/(m_b\Lambda_{\rm QCD})$ can be estimated or included. Also, since under the pair production threshold there are several branch cuts and

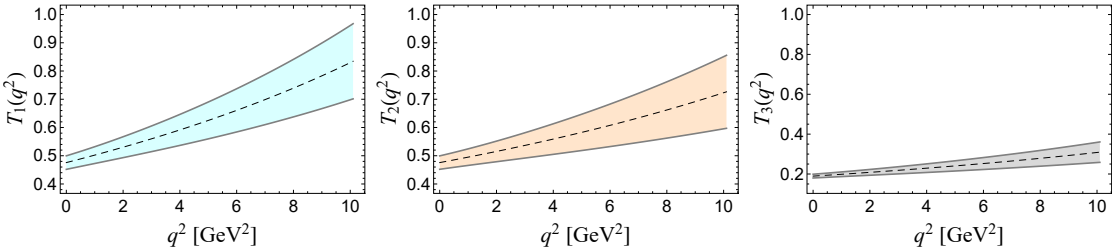

Figure 4.3: $B_c \to J/\psi$ NP form factors calculated in this study.

poles not included explicitly in the fit, no unitarity constraints are applied.

4.1.4. HQSS/NRQCD symmetry relations at the zero recoil

Inside the HQSS and NRQCD paradigm a set of model-independent limits for the form factors for $B_c \to \eta_c$ and $B_c \to J/\psi$ decays can be derived. Although the aforementioned decays bear a resemblance with heavy-to-heavy transitions and in fact do produce interesting symmetries in a heavy-quark limit [189], the c-quark is significantly lighter than the b-quark which causes the produced c-quark to be quite energetic, which in turn spoils exact heavy-flavor symmetries. On the other hand, the c-quark is in fact heavy enough that non-relativistic limits can be exploited at the point of zero hadronic recoil - symmetry relations for maximal momentum transfer $q^2_{\rm max} = (m_{B_c} - m_{J/\psi,\eta_c})^2$ still hold, and the form factors can be related to a single function Δ [189–191], with an unknown normalization. Following [189] near zero recoil ($q' \ll m_c$) the form factors can be approximated

$$\langle \eta_c(v,q')|\, V_\mu(q^2)\, |B_c(v)\rangle = 2\sqrt{m_{B_c} m_{\eta_c}}\, \Delta(a_0 q')\, v_\mu, \tag{4.34}$$

$$\langle J/\psi(v,q')|\, A_\mu(q^2)\, |B_c(v)\rangle = 2\sqrt{m_{B_c} m_{J/\psi}}\, \Delta(a_0 q')\, \epsilon^*_\mu, \tag{4.35}$$

where $V_\mu = \bar{b}\gamma_\mu c$ and $A_\mu = \bar{b}\gamma_\mu\gamma_5 c$ and ϵ_μ is a polarization vector of J/ψ. Here v is the velocity of the B_c meson with $v^2 = 1$, and q' is a small residual velocity carried by the final state meson (not to be confused by q, the momentum carried by the lepton pair system), so that

$$p^\mu_{B_c} = m_{B_c} v^\mu; \quad (p_{\eta_c,J/\psi})^\mu = m_{\eta_c,J/\psi} v^\mu + q'^\mu. \tag{4.36}$$

The parameter a_0 is connected to the Bohr radius of the B_c meson, it value is not important for the further discussion and will not be discussed here.

The $\Delta(a_0 q')$ function can now be related to the $B_c \to \eta_c$ form factor $f_+(q^2)$ at the zero recoil as

$$\Delta(a_0 q') \approx \sqrt{\frac{m_{B_c}}{m_{\eta_c}}} f_+(q^2_{\rm max}), \tag{4.37}$$

which amounts, using the predicted $f_+(q^2_{\rm max})$ from the calculation above, to

$$\Delta(a_0 q')_{\rm our} \approx 0.79 \pm 0.09. \tag{4.38}$$

This value can be compared with the value obtained in the QCD relativistic potential model in [191].

In [190] it was shown that in the NRQCD approximation one can derive a generalized set of relations using the HQSS, so that the transition form factors of $B_c \to \eta_c$ and $B_c \to J/\psi$ decays can be given in terms of a single form factor, even for the case of non-equal four-velocities $v_1 \neq v_2$, of the initial and the final state heavy mesons. To show this the $B_c \to J/\psi$ form factors are defined in the helicity basis as

$$\begin{aligned}
g(q^2) &\equiv (H_{++} - H_{--})/\sqrt{\lambda(m_{B_c}, m_{J/\psi}, q^2)} = \frac{2}{m_{B_c} + m_{J/\psi}} V(q^2), \\
f(q^2) &\equiv -(H_{++} + H_{--})/2 = (m_{B_c} + m_{J/\psi}) A_1(q^2), \\
\mathcal{F}_1(q^2) &\equiv -\sqrt{q^2} H_{00} \\
&= \frac{1}{m_{J/\psi}} \Big[-\frac{\lambda(m_{B_c}, m_{J/\psi}, q^2)}{2(m_{B_c} + m_{J/\psi})} A_2(q^2) \\
&\qquad - \frac{1}{2}(q^2 - m^2_{B_c} + m^2_{J/\psi})(m_{B_c} + m_{J/\psi}) A_1(q^2) \Big], \\
\mathcal{F}_2(q^2) &\equiv -2 \frac{\sqrt{q^2}}{\sqrt{\lambda(m^2_{B_c}, m^2_{J/\psi}, q^2)}} H_{t0} = 2A_0(q^2),
\end{aligned} \tag{4.39}$$

and the triangle function is defined as

$$\lambda(m_{B_c}, m_{J/\psi}, q^2) \equiv (q^2 + m^2_{B_c} - m^2_{J/\psi})^2 - 4 m_{B_c} q^2. \tag{4.40}$$

Using the expressions from [190], stemming from considering NRQCD and HQSS,

and relating different decay form factors at the point of zero recoil $q^2_{\rm max}$, the $\bar{Q}q \to \bar{Q}'q$ helicity form factors can be expressed as [142]:

$$\begin{aligned} g(q^2_{\rm max}) &= \frac{3+r_Q}{4m^2_{B_c} r_{J/\psi}} f(q^2_{\rm max}), \\ \mathcal{F}_1(q^2_{\rm max}) &= m_{B_c}(1-r_{J/\psi}) f(q^2_{\rm max}), \\ \mathcal{F}_2(q^2_{\rm max}) &= \frac{2(1+r_{J/\psi})+(1-r_{J/\psi})(1-r_Q)}{4m_{B_c} r_{J/\psi}} f(q^2_{\rm max}), \end{aligned} \tag{4.41}$$

for the $B_c \to J/\psi$ decay, and

$$f_0(q^2_{\rm max}) = \frac{1}{m^2_{B_c} - m^2_{\eta_c}} \frac{8m^2_{B_c}(1-r_{\eta_c}) r_{\eta_c}}{2(1+r_{\eta_c})+(1-r_{\eta_c})(1-r_Q)} f_+(q^2_{\rm max}), \tag{4.42}$$

for the $B_c \to \eta_c$ decay [143], where some shorthand notation has been introduced: $r_M = m_M/m_{B_c}$ (with $m_M = [m_{J/\psi}, m_{\eta_c}]$), $r_Q = m_{Q'}/m_Q = m_c/m_b$ and $r_q = m_q/m_Q = r_Q$. Additionally, the vector decay form factors can be related to the pseudoscalar ones as [144]

$$\begin{aligned} f(q^2_{\rm max}) &= \frac{8m_{B_c} r_{\eta_c}}{3+r_{\eta_c}-(1-r_{\eta_c})r_Q} f_+(q^2_{\rm max}), \\ g(q^2_{\rm max}) &= \frac{1+r_Q}{m_{B_c} r_{J/\psi}} \frac{4r_{\eta_c}}{3+r_{\eta_c}-(1-r_{\eta_c})r_Q} f_+(q^2_{\rm max}), \\ \mathcal{F}_1(q^2_{\rm max}) &= m^2_{B_c}(1-r_{J/\psi}) \frac{8r_{\eta_c}}{3+r_{\eta_c}-(1-r_{\eta_c})r_Q} f_+(q^2_{\rm max}), \\ \mathcal{F}_2(q^2_{\rm max}) &= \frac{1+r_{J/\psi}}{r_{J/\psi}} \frac{4r_{\eta_c}}{3+r_{\eta_c}-(1-r_{\eta_c})r_Q} f_+(q^2_{\rm max}), \end{aligned} \tag{4.43}$$

where $r_q = r_Q$ for $B_c \to \eta_c, J/\psi$ was used, which simplified the relations. It is expected that these relations are broken by terms of order $\mathcal{O}(m_c/m_b, \Lambda_{\rm QCD}/m_c) \lesssim 30\%$.

Below the consistency check of the HQSS/NRQCD relations and form factors obtained in the previous section is performed. At the zero-recoil $\mathcal{F}_1(q^2)$ and $f(q^2)$ are the same up to a constant factor, eq. (4.41), which explicitly gives

$$\frac{\mathcal{F}_1(q^2_{\rm max})}{f(q^2_{\rm max})} = m_{B_c}(1-r_{J/\psi}) = 3.18\,, \tag{4.44}$$

whereas

$$\begin{aligned} \frac{g(q^2_{\rm max})|}{g(q^2_{\rm max})|_{\text{eq.(4.41)}}} &\approx 0.81, \\ \frac{\mathcal{F}_2(q^2_{\rm max})|}{\mathcal{F}_2(q^2_{\rm max})|_{\text{eq.(4.41)}}} &\approx 0.89, \end{aligned} \tag{4.45}$$

and

$$\frac{f_0(q^2_{\rm max})|}{f_0(q^2_{\rm max})|_{\text{eq.(4.42)}}} \approx 1.18. \tag{4.46}$$

We see that the HQSS/NRQCD predictions are quite consistent with the modified LCSR predictions for form factors at the zero recoil point and can be safely used as model-independent bounds on R ratios. Such bounds were also used in cf. [142–144]. It should be kept in mind that the accuracy of the predictions cited there is limited to $\mathcal{O}(30\%)$.

Finally, using eq. (4.43) the following numerical values are obtained

$$\begin{aligned} \frac{f(q^2_{\rm max})|}{f(q^2_{\rm max})|_{\text{eq.(4.43)}}} &\approx 1.02, \\ \frac{g(q^2_{\rm max})|}{g(q^2_{\rm max})|_{\text{eq.(4.43)}}} &\approx 1.05, \\ \frac{\mathcal{F}_1(q^2_{\rm max})|}{\mathcal{F}_1(q^2_{\rm max})|_{\text{eq.(4.43)}}} &\approx 1.02, \\ \frac{\mathcal{F}_2(q^2_{\rm max})|}{\mathcal{F}_2(q^2_{\rm max})|_{\text{eq.(4.43)}}} &\approx 1.02, \end{aligned} \tag{4.47}$$

which confirms an excellent agreement among the relations between $B_c \to \eta_c$ and $B_c \to J/\psi$ transition form factors derived from HQSS/NRQCD symmetry relations and the LCSR-inspired results at the point of zero hadronic recoil.

4.2. Phenomenology

Referring now to appendix C for the weak interaction effective Hamiltonian, a phenomenological analysis is presented of a set of observables including NP contributions. The NP degrees of freedom are further assumed to couple only to τ leptons, as an additional contribution to the $\bar{B} \to D^{(*)}\tau\bar{\nu}_\tau$ might account for the discrepancy in $R_{D^{(*)}}$.

Operators containing axial or pseudoscalar hadronic currents do not contribute to the $B_c \to \eta_c$ decay, hence $V_R - V_L = 0.$ and $S_R - S_L = 0$ and therefore $V_R = V_L$, and $S_R = S_L$. The scalar hadronic current does not contribute to the $B_c \to J/\psi$ transition, which leads to $S_L + S_R = 0$. Considering this, a shorthand notation is introduced $S_R + S_L = S$ and $S_R - S_L = P$ further in the text.

Constraints on the Wilson coefficients appearing in WET Lagrangian are obtained from a combined analysis of the BaBar, Belle and LHCb data for the branching fraction ratios $R_{D^{(*)}}$, the τ polarization asymmetry along the longitudinal direction of the τ lepton in $B \to D^*$, as well as the longitudinal D^* polarization in $B_c \to D^*\tau\nu_\tau$ decay [158]. The leptonic branching fraction of the B_c meson $\mathcal{B}(B_c^- \to \tau\bar{\nu}_\tau)$ has not yet been measured, and the possible NP scenarios are constrained by the precise experimental measurements of the B_c lifetime, $\tau_{B_c}^{\text{exp}} = (0.507 \pm 0.009)$ ps [192]. Since B_c lifetime is very sensitive to the value of the charm quark mass, the total B_c decay width still allows for up to 60% contribution from NP [158, 193]. In particular, the best fit point for S_R is dependent on the assumption of the value for the $B_c \to \tau\bar{\nu}_\tau$ decay width.

In the following analysis the limit $\text{BR}(B_c \to \tau\bar{\nu}) < 30\%$ is considered, and the values of the Wilson coefficients are taken from a combined analysis done in cf. [158]. There, all one-dimensional scenarios with only one NP Wilson coefficient considered at a time were studied, as well as two-dimensional scenarios with two NP Wilson coefficients considered simultaneously. The best fit points in the 1D scenarios and

the 2σ ranges cited in the publication at the scale 1 TeV are

$$\begin{aligned} V_L &= 0.11^{+4}_{-5}, \\ S_R &= 0.16^{+7}_{-8}, \\ S_L &= 0.12^{+8}_{-11}, \\ S_L &= 4T_L = -0.07^{+9}_{-8}. \end{aligned} \tag{4.48}$$

The existence of these one-dimensional NP scenarios is motivated by adding a single particle to the SM, as follows:

- $\boldsymbol{V_L \neq 0}$: This operator arises in vector leptoquark (LQ) models. Two examples are $\mathrm{SU}(2)_L$-singlet vector U_1 LQ [194], or the scalar $\mathrm{SU}(2)_L$-triplet [195]. Also interesting are the left handed W' models [196].

- $\boldsymbol{S_R \neq 0}$: This operator is generated in models containing extra charged scalars, and is the dominant operator in models containing two Higgs doublets [197]. It can also be generated by the $\mathrm{SU}(2)_L$-doublet vector V_2 LQ [198].

- $\boldsymbol{S_L \neq 0}$: Similar as $S_R \neq 0$ [199].

- $\boldsymbol{S_L = 4T_L \neq 0}$: This operator constraint derives from the scalar $\mathrm{SU}(2)_L$-doublet S_2 LQ [200] at the new physics scale $\mu^2 \approx \Lambda_{\mathrm{NP}}$. QCD renormalization group effects scale this to $S_L \approx 8.1 T_L$ at $\mu^2 \approx m_b^2$.

Only the real values of the coefficients were considered for the 1D fit.

For the best fit points in the 2D scenarios at the scale 1 TeV the following values are cited in the publication

$$\begin{aligned} (V_L,\ S_L = -4T_L) &= (0.08,\ 0.05), \\ (S_R,\ S_L) &= (-0.30,\ -0.64), \\ (V_L,\ S_R) &= (0.09\ 0.06), \\ (\mathrm{Re}[S_L = 4\,T_L],\, \mathrm{Im}[S_L = 4\,T_L]) &= (-0.06, \pm 0.40). \end{aligned} \tag{4.49}$$

Since the uncertainties are large in the 2D fit, they aren't considered. Similar models are relevant as those in the 1D fits, apart from an additional possibility:

- **Re[$S_L = 4\,T_L$], Im[$S_L = 4\,T_L$]**: In this case complex couplings are considered due to the fact that real parameters do not give a good fit to the experimental data. Complex coefficients were found to give a good explanation for the R_{D^*} data [201].

As already mentioned, in R_2 and S_1 LQ scenarios, the coupling S_L and T_L are connected in the following way

$$\begin{aligned} S_L(m_b) &\simeq 8.1 T_L(m_b) \Rightarrow R_2 \text{ LQ scenario,} \\ S_L(m_b) &\simeq -8.5 T_L(m_b) \Rightarrow S_1 \text{ LQ scenario.} \end{aligned} \tag{4.50}$$

The relations holding at 1 TeV are spoiled by the QCD anomalous dimension, and EW corrections.

4.2.1. Two-fold differential decay widths

The following phenomenological analysis is first performed in the SM (with all of the NP couplings turned off), after which all of the 1D and 2D scenarios from the previous paragraphs are considered. The values the NP couplings assume is, as stated previously, taken from a recent publication [158]. The two-fold differential decay width for both $B_c \to \eta_c$ and $B_c \to J/\psi$ semileptonic decay can be written as

$$\frac{d^2\Gamma(B_c \to M_f \ell \bar{\nu}_\ell)}{dq^2 d\cos\theta_\ell} = \frac{1}{(2\pi)^3} \frac{|\vec{p}_2|}{32 m_{B_c}^2} \left(1 - \frac{m_\ell^2}{q^2}\right) |\mathcal{M}(B_c \to M_f \ell \bar{\nu}_\ell)|^2, \tag{4.51}$$

where $\vec{p_2} = \lambda(m_{B_c}^2, m_{M_f}^2, q^2)/(2m_{B_c})$ is the three-momentum of the $M_f = \eta_c, J/\psi$ in the B_c meson rest frame, and θ_ℓ is the polar angle of the lepton ℓ (the angle between the lepton direction in the W^* boson rest frame and the direction of the W^* boson in the B_c rest frame) and q^2 ($q = p_1 - p_2$) is the momentum transfer to the $\ell\bar{\nu}_\ell$ pair.

1. Two-fold differential decay distribution for $B_c \to \eta_c \ell \bar{\nu}_\ell$

The complete expression for the two-fold differential decay width in the basis of helicity form factors is

$$\begin{aligned}\frac{d^2\Gamma(B_c \to \eta_c \ell \bar{\nu}_\ell)}{dq^2 d\cos\theta_\ell} = \frac{G_F^2 |V_{cb}|^2 |\vec{p}_2| q^2}{(2\pi)^3 16 m_{B_c}^2} \left(1 - \frac{m_\ell^2}{q^2}\right)^2 \times \\ \times \Big\{ |1 + V_L + V_R|^2 \left[|H_0|^2 \sin^2\theta_\ell + 2\delta_\ell |H_t - H_0 \cos\theta_\ell|^2 \right] \\ + |S|^2 |H_P^S|^2 + 16 |T_L|^2 \left[2\delta_\ell + (1 - 2\delta_\ell)\cos^2\theta_\ell \right] |H_T|^2 \\ + 2\sqrt{2\delta_\ell} \Big(\mathrm{Re}S + S\, V_L \Big) H_P^S \left[H_t - H_0 \cos\theta_\ell \right] \\ + 8\sqrt{2\delta_\ell} \Big(\mathrm{Re}T_L + T_L V_L \Big) \left[H_0 - H_t \cos\theta_\ell \right] H_T \\ - 8 H_P^S H_T \cos\theta_\ell \Big(T_L S \Big) \Big\},\end{aligned}$$

with the helicity flip-factor $\delta_\ell = m_\ell^2/2q^2$, $T_L V_L = \mathrm{Re}T_L\ \mathrm{Re}V_L + \mathrm{Im}T_L\ \mathrm{Im}V_L$, $T_L S = \mathrm{Re}T_L\ \mathrm{Re}S + \mathrm{Im}T_L\ \mathrm{Im}S$ and $S\, V_L = \mathrm{Re}S\ \mathrm{Re}V_L + \mathrm{Im}S\ \mathrm{Im}V_L$. The q^2 dependence has been left implicit for the purpose of brevity. The helicity form factors from the equation above are

$$\begin{aligned} H_t(q^2) &= \frac{m_{B_c}^2 - m_{\eta_c}^2}{\sqrt{q^2}} f_0(q^2), & H_0(q^2) &= \frac{2 m_{B_c} |\vec{p}_2|}{\sqrt{q^2}} f_+(q^2), \\ H_P^S(q^2) &= \frac{m_{B_c}^2 - m_{\eta_c}^2}{m_b(\mu) - m_c(\mu)} f_0(q^2), & H_T(q^2) &= \frac{2 m_{B_c} |\vec{p}_2|}{m_{B_c} + m_{\eta_c}} f_T(q^2). \end{aligned} \tag{4.52}$$

A brief discussion on the expressions are given in appendix D.

2. Two-fold differential decay distribution for $B_c \to J/\psi \ell \bar{\nu}_\ell$

Next, the differential distribution of the $\bar{B}_c \to J/\psi \ell^- \bar{\nu}_\ell$ decay is considered with $V_R V_L = \mathrm{Re}V_R\ \mathrm{Re}V_L + \mathrm{Im}V_R\ \mathrm{Im}V_L$, $T_L P = \mathrm{Re}T_L\ \mathrm{Re}P + \mathrm{Im}T_L\ \mathrm{Im}P$ and $P\, V_L =$

$\mathrm{Re}P\ \mathrm{Re}V_L + \mathrm{Im}P\ \mathrm{Im}V_L$, and is given by

$$
\begin{aligned}
\frac{d^2\Gamma(B_c \to J/\psi \ell \bar{\nu}_\ell)}{dq^2 d\cos\theta_\ell} &= \frac{G_F^2 |V_{cb}|^2 |\vec{p}_2| q^2}{32(2\pi)^3 m_{B_c}^2} \quad 1 - \frac{m_\ell^2}{q^2}\Big)^2 \times \\
&\times \Big\{ |1+V_L|^2 \Big[(1-\cos\theta_\ell)^2 |H_{++}|^2 + (1+\cos\theta_\ell)^2 |H_{--}|^2 + 2\sin^2\theta_\ell |H_{00}|^2 \\
&\quad + 2\delta_\ell \Big(\sin^2\theta_\ell (|H_{++}|^2 + |H_{--}|^2) + 2|H_{t0} - H_{00}\cos\theta_\ell|^2 \Big) \Big] \\
&+ |V_R|^2 \Big[(1-\cos\theta_\ell)^2 |H_{--}|^2 + (1+\cos\theta_\ell)^2 |H_{++}|^2 + 2\sin^2\theta_\ell |H_{00}|^2 \\
&\quad + 2\delta_\ell \Big(\sin^2\theta_\ell (|H_{++}|^2 + |H_{--}|^2) + 2|H_{t0} - H_{00}\cos\theta_\ell|^2 \Big) \Big] \\
&- 4\Big(\mathrm{Re}V_R + V_R V_L \Big) \Big[(1+\cos^2\theta_\ell) H_{++} H_{--} + \sin^2\theta_\ell |H_{00}|^2 \\
&\quad + 2\delta_\ell \Big(\sin^2\theta_\ell H_{++} H_{--} + |H_{t0} - H_{00}\cos\theta_\ell|^2 \Big) \Big] + 16\cos\theta_\ell H_V^S H_T^0 T_L P \\
&+ 2|P|^2 |H_V^S|^2 + 4\sqrt{2\delta_\ell} H_V^S (H_{t0} - H_{00}\cos\theta_\ell) \Big(\mathrm{Re}P + P\, V_L \Big) \\
&+ 16|T_L|^2 \Big[|H_T^0|^2 \Big(1 + 2\delta_\ell + (1-2\delta_\ell)\cos 2\theta_\ell \Big) \\
&\quad + 2|H_T^+|^2 \sin^2\frac{\theta_\ell}{2} \Big(1 + 2\delta_\ell + (1-2\delta_\ell)\cos\theta_\ell \Big) \\
&\quad + 2|H_T^-|^2 \cos^2\frac{\theta_\ell}{2} \Big(1 + 2\delta_\ell - (1-2\delta_\ell)\cos\theta_\ell \Big) \Big] \\
&- 16\sqrt{2\delta_\ell} \Big(\mathrm{Re}T_L + T_L V_L \Big) \Big[H_{++} H_T^+ + H_{--} H_T^- + H_{00} H_T^0 \\
&\quad - \Big(H_{++} H_T^+ - H_{--} H_T^- + H_{t0} H_T^0 \Big) \cos\theta_\ell \Big] \Big\}.
\end{aligned}
$$

The hadronic helicity amplitudes are expressed as

$$
\begin{aligned}
H_{\pm\pm}(q^2) &= \frac{-(m_{B_c} + m_{J/\psi})^2 A_1(q^2) \pm 2m_{B_c} |\vec{p}_2| V(q^2)}{m_{B_c} + m_{J/\psi}}, \\
H_V^S(q^2) &= \frac{2m_{B_c}}{m_b(\mu) + m_c(\mu)} |\vec{p}_2| A_0(q^2), \\
H_{00}(q^2) &= \frac{-(m_{B_c}^2 - m_{J/\psi}^2 - q^2)(m_{B_c} + m_{J/\psi})^2 A_1(q^2) + 4m_{B_c}^2 |\vec{p}_2|^2 A_2(q^2)}{2m_{J/\psi}\sqrt{q^2}(m_{B_c} + m_{J/\psi})}, \\
H_{t0}(q^2) &= -\frac{2m_{B_c}|\vec{p}_2|}{\sqrt{q^2}} A_0(q^2) \\
H_T^\pm(q^2) &= -\frac{1}{\sqrt{q^2}} \left[\pm\sqrt{\lambda(m_{B_c}^2, m_{J/\psi}^2, q^2)} T_1(q^2) + (m_{B_c}^2 - m_{J/\psi}^2) T_2(q^2) \right], \\
H_T^0(q^2) &= -\frac{1}{2m_{J/\psi}} \Big[(m_{B_c}^2 + 3m_{J/\psi}^2 - q^2) T_2(q^2) - \frac{\lambda(m_{B_c}^2, m_{J/\psi}^2, q^2)}{m_{B_c}^2 - m_{J/\psi}^2} T_3(q^2) \Big],
\end{aligned}
\tag{4.53}
$$

where again, the q^2 dependence has been left implicit in the expression for the decay distribution.

A comparison of the predictions for branching fractions in the SM for both decays is given in table 4.3 from the available literature, where the branching fraction values have been updated using the latest value for the B_c lifetime, $\tau_{B_c} = (0.507 \pm 0.009)$ ps [192], while in the brackets the original published values of the branching fractions are cited. If there are no brackets the branching fractions have already been calculated using the latest value for τ_{B_c}.

Table 4.3: Branching fractions of $B_c \to J/\psi, \eta_c$ decays calculated in different models and given in %, with ℓ denoting a light lepton, e or μ.

Mode	this work	QCDSR [132]	SR [133]	pQCD [131]	RCQM [102]	CCQM [145, 184]	RQM [104]	RQM [134]	RQM [105]	RQM [135]	LFQM [138]
$B_c \to \eta_c \ell \bar{\nu}_\ell$	$0.82^{+0.12}_{-0.11}$	0.85 (0.75)	1.85 (1.64)	0.50 (0.44)	0.91 (0.81)	0.95	0.47 (0.42)	0.89	0.52 (0.52)	0.85	0.74 (0.67)
$B_c \to \eta_c \tau \bar{\nu}_\tau$	$0.26^{+0.06}_{-0.05}$	0.25 (0.23)	0.55 (0.49)	0.15 (0.14)	0.25 (0.22)	0.24	-	-	-	-	0.21 (0.19)
$B_c \to J/\psi \ell \bar{\nu}_\ell$	$2.24^{+0.57}_{-0.49}$	2.16 (1.9)	2.67 (2.37)	1.13 (1.00)	2.33 (2.07)	1.67	1.39 (1.23)	1.42	1.49 (1.47)	2.33	1.64 (1.49)
$B_c \to J/\psi \tau \bar{\nu}_\tau$	$0.53^{+0.16}_{-0.14}$	0.54 (0.48)	0.73 (0.65)	0.33 (0.29)	0.55 (0.49)	0.40	-	-	-	-	0.41 (0.37)

4.2.2. Lepton flavour universality ratios

The LFU-testing ratios of semileptonic branching fractions using the LCSR form factors fitted to the modified BCL parametrization from eq. (4.33) are

$$R_{\eta_c}|_{\rm SM} \equiv \frac{\Gamma(B_c \to \eta_c \tau \bar{\nu}_\tau)}{\Gamma(B_c \to \eta_c \mu \bar{\nu}_\mu)} = 0.32 \pm 0.02\,, \tag{4.54}$$

$$R_{J/\psi}|_{\rm SM} \equiv \frac{\Gamma(B_c \to J/\psi \tau \bar{\nu}_\tau)}{\Gamma(B_c \to J/\psi \mu \bar{\nu}_\mu)} = 0.24 \pm 0.02. \tag{4.55}$$

Results agree very well with the recent model-independent analysis of $R_{J/\psi}$ [142,144] and R_{η_c} [143, 144], but the tension persists with the experimental value at the level of $\approx 2\sigma$.

The ratios of the branching fractions $R_{J/\psi,\eta_c}$ are computed next in the context of different NP scenarios using the form factors presented in section 4.1. The values of

the NP operators' effective couplings considered in this analysis are discussed above and are listed in eq. (4.48) and eq. (4.49). In figure 4.4 the q^2 dependence of the ratios R_{η_c} and $R_{J/\psi}$ is shown in the presence of only one NP operator (first two figures of both panels). The third figure in both panels shows the ratio in presence of two NP operators. The SM value is always shown by the blue dotted line. The ratio increases for most of NP contributions for both J/ψ and η_c. The $S_L = 4\,T_L$ case with the coupling being purely real or imaginary results in a decrease in the ratio R_{η_c}. This is due to the negative interference between S_L and T_L , eq. (4.52). The shaded region shows the 2σ allowed region for $V_L, S_L = 4T_L, S_{L,R}$ parameters in the 1D fit, with the central value shown by a dashed line. In the case of 2D scenarios the results are presented at the best fit point of NP couplings. As expected, the ratio R_{η_c} is more sensitive to the scalar and the tensor operators, whereas $R_{J/\psi}$ is more sensitive to V_L. Values of $R_{J/\psi}$ and R_{η_c} in presence of different NP scenarios

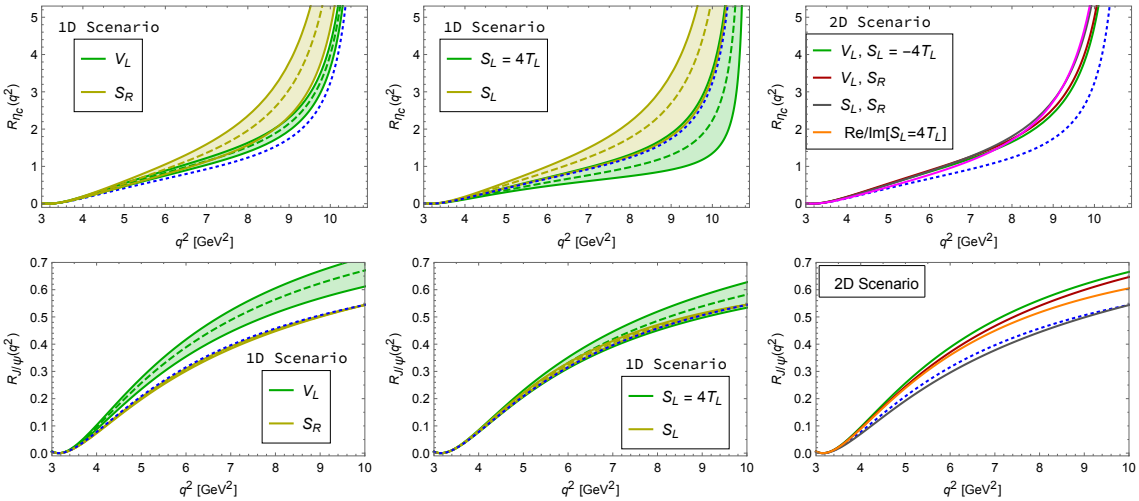

Figure 4.4: Ratios of branching fractions $R_{\eta_c}(q^2)$ (upper panel), $R_{J/\psi}(q^2)$ (lower panel) as a function of q^2. The blue dotted lines are the SM prediction, the green dashed line is for the best fit values of the NP couplings in the 1D scenario as discussed in the text. The green band represents NP effects from the 2σ allowed regions in the 1D scenarios. The third figure in both panels is the result for the best fit points in the 2D scenarios.

are listed in table 4.4. The results are presented for the best fit points, as well as for the 2σ allowed regions in the 1D scenario.

It can be noted that none of the NP scenarios considered here can explain the 2σ

tension in $R_{J/\psi}$ with the experiment, if the values of Wilson coefficients are taken from a recent global fit to experimental data [158].

Table 4.4: The values of R_{η_c} and $R_{J/\psi}$ in presence of different NP scenarios. The subscript and the superscript are the values for the 2σ range of the NP couplings.

	V_L	S_L	S_R	$S_L = 4T_L$
$R^{\rm 1D}_{\eta_c}$	$0.39^{+0.03}_{-0.03}$	$0.44^{+0.11}_{-0.11}$	$0.49^{+0.10}_{-0.09}$	$0.26^{+0.08}_{-0.06}$
$R^{\rm 1D}_{J/\psi}$	$0.29^{+0.02}_{-0.03}$	$0.24^{+0.01}_{-0.01}$	$0.23^{+0.01}_{-0.01}$	$0.25^{+0.01}_{-0.02}$
	$(V_L, S_L = -4T_L)$	(S_R, S_L)	(V_L, S_R)	$\mathrm{Re}, \mathrm{Im}[S_L = 4T_L]$
$R^{\rm 2D}_{\eta_c}$	0.42	0.45	0.44	0.43
$R^{\rm 2D}_{J/\psi}$	0.29	0.22	0.27	0.26

4.2.3. Forward-backward asymmetry, convexity parameter and the τ polarization

Separating the two-fold distribution to terms proportional to powers of $\cos\theta_\ell$, as in appendix D, a set of observables can be defined that test the SM through final-state polarizations/angular kinematics. Since the observables are defined in appendix D, here the definitions are not repeated. Definitions of angles are shown in figure 4.5, and as can be seen, the $\hat{z}$ axis is chosen as the one alone which the J/ψ meson propagates in the B_c rest frame, while the virtual W^* propagates in the $-\hat{z}$ direction. The two planes of leptonic pairs define the angle χ. Definitions of kinematic variables can alter the expressions among publications, so one has to be extra careful when comparing.

1. The backward-forward asymmetry $A_{\rm FB}(q^2)$

Neither the forward-backward asymmetry, nor the convexity parameter are sensitive to the 1D scenario in which only the V_L coupling is turned on. The $B_c \to \eta_c$ transition appears to be more sensitive to the new physics operators as compared to the $B_c \to J/\psi$ transition. In case of the J/ψ decay mode, the presence of the S_L

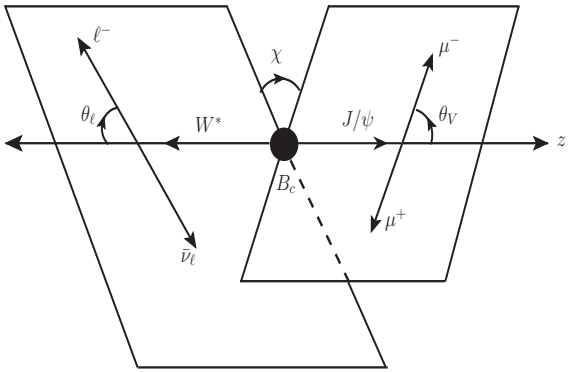

Figure 4.5: Angular conventions for the $B_c \to J/\psi(\to \mu^+\mu^-)\ell\nu_\ell$ decay.

and S_R coefficients in the 2D scenario leads to a significant deviation from $A^{\rm FB}(q^2)$ prediction in the SM (table 4.5). The differential forward-backward asymmetry is shown in figure 4.6.

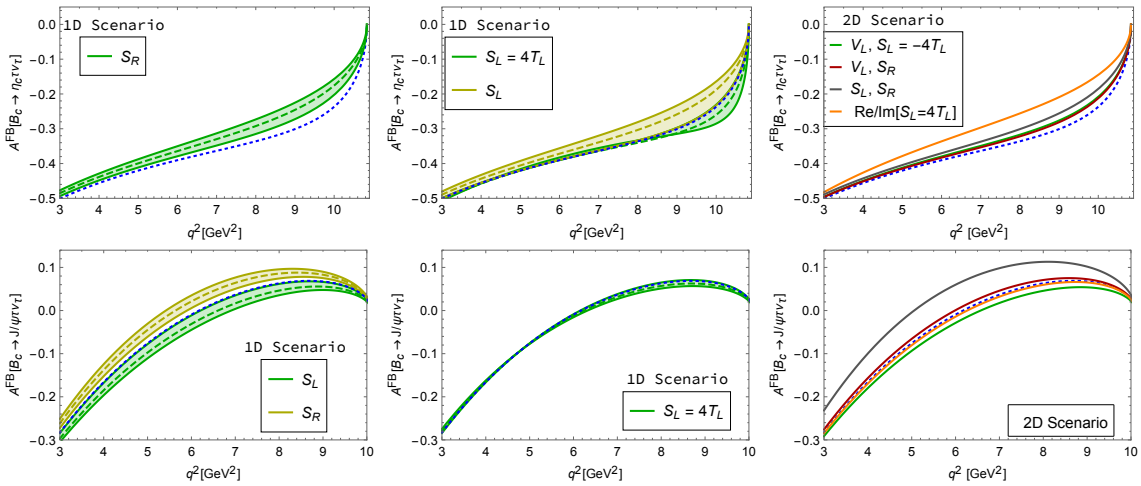

Figure 4.6: Differential forward-backward asymmetry $\mathrm{d}A^{FB}(q^2)/\mathrm{d}q^2$ for η_c (upper panel), and J/ψ (lower panel) as a function of q^2. The blue dotted lines are the SM prediction, the green dashed line is for the best fit values of the NP couplings in the 1D scenario as discussed in the text. The green band represents the NP effects from the 2σ allowed regions. The third figure in both panels is the result for the best fit points in the 2D scenarios.

2. The convexity parameter $C_F^\tau(q^2)$

The present allowed values of the coupling have a very small effect on $C_F^\tau(q^2)$ in case of J/ψ, whereas in case of η_c the $S_L = 4\,T_L$ case enhances $C_F^\tau(q^2)$ only at large

values of q^2 (table 4.5). The differential convexity parameter is shown in figure 4.7.

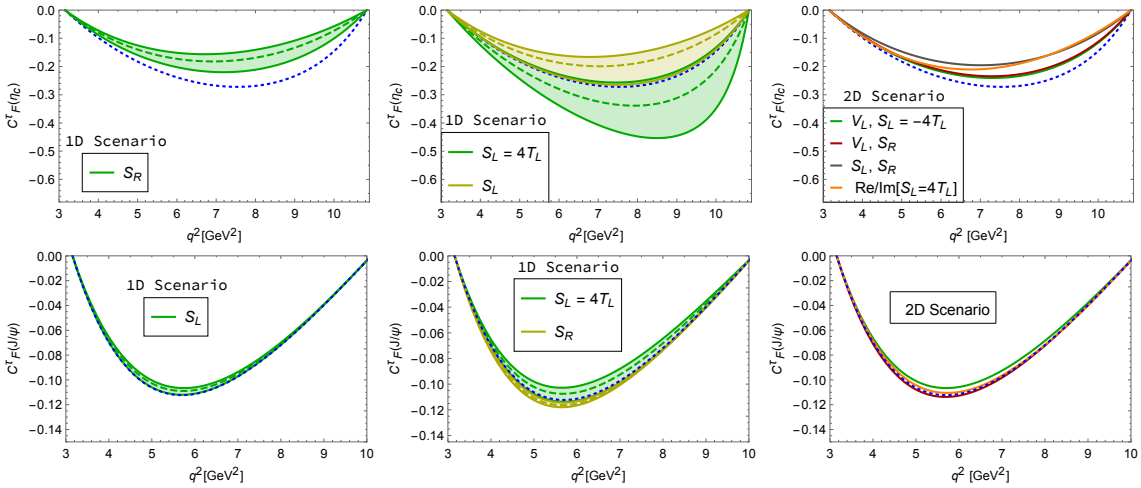

Figure 4.7: Differential convexity parameter $\mathrm{d}C_{\mathrm{F}}^{\tau}(q^2)/\mathrm{d}q^2$ for η_c (upper panel), and J/ψ (lower panel) as a function of q^2. The blue dotted lines are the SM prediction, the green dashed line is for the best fit values of the NP couplings in the 1D scenario as discussed in the text. The green band represents the NP effects from the 2σ allowed regions. The third figure in both panels is the result for the best fit points in the 2D scenarios.

3. The τ lepton polarization $P_{L,T}^{\tau}(q^2)$

Here the polarization of the final-state τ in the W^- rest frame in the presence of the NP operators is discussed. The differential decay rate for a given spin projection in a given direction can be easily obtained with the inclusion of the spin projection operators $(1+\gamma_5 \not{s}_i)/2$ for τ in the calculation, where s_L^μ and s_T^μ are respectively the longitudinal and the transverse sppin projections of τ in the W^- rest frame and are given by [202–204]

$$s_L^\mu = \frac{1}{m_\tau}(|\vec{p}_\tau|, E_\tau \sin\theta_\tau, 0, E_\tau \cos\theta_\tau), \quad s_T^\mu = (0, \cos\theta_\tau, 0, -\sin\theta_\tau). \quad (4.56)$$

The longitudinal and the transverse polarization components of the τ are then defined as:

$$P_i(q^2) = \frac{\mathrm{d}\Gamma(s_i^\mu)/dq^2 - d\Gamma(-s_i^\mu)/dq^2}{d\Gamma(s_i^\mu)/dq^2 + d\Gamma(-s_i^\mu)/dq^2} = \frac{\mathcal{P}_i(q^2)}{2(a_{\theta_\ell}(q^2) + c_{\theta_\ell}(q^2)/3)}, \quad i = L, T, \quad (4.57)$$

where, including the NP effects

$$\begin{aligned}\frac{1}{N(q^2)}\mathcal{P}_L^{\eta_c}(q^2) = \Big\{&|1+V_L+V_R|^2\big[-|H_0|^2+\delta_\tau(|H_0|^2+3|H_t|^2)\big]\\ &+3\sqrt{2\delta_\tau}H_P^S H_t\Big(\mathrm{Re}S+S\,V_L\Big)\\ &+\frac{3}{2}|S|^2|H_P^S|^2+8|T_L|^2(1-4\delta_\tau)|H_T|^2\\ &-4\sqrt{2\delta_\tau}\Big(\mathrm{Re}T_L+T_L V_L\Big)H_0 H_T\Big\},\end{aligned} \tag{4.58}$$

$$\begin{aligned}\frac{1}{N(q^2)}\mathcal{P}_L^{J/\psi}(q^2) = \Big\{&(|1+V_L|^2+|V_R|^2)\big[-\sum_{n=\pm,0}|H_{nn}|^2+\delta_\tau\Big(\sum_{n=\pm,0}|H_{nn}|^2+3|H_{t0}|^2\Big)\big]\\ &+2\mathrm{Re}V_R\big[(1-\delta_\tau)(|H_{00}|^2+2H_{++}H_{--})+3\delta_\tau|H_{t0}|^2\big]\\ &-3\sqrt{2\delta_\tau}\Big(\mathrm{Re}P+P\,V_L\Big)H_V^S H_{t0}\\ &+\frac{3}{2}|P|^2|H_V^S|^2+8|T_L|^2(1-4\delta_\tau)\sum_n|H_T^n|^2\\ &+4\sqrt{2\delta_\tau}\Big(\mathrm{Re}T_L+T_L V_L\Big)\sum_{n=\pm,0}H_{nn}H_T^n\Big\},\end{aligned} \tag{4.59}$$

for the longitudinal polarization, where the differential decay width normalization factor has been defined as

$$N(q^2) = \frac{1}{(2\pi)^3}\frac{|\vec{p}_2|}{32m_{B_c}^2}\left(1-\frac{m_\ell^2}{q^2}\right). \tag{4.60}$$

For the transverse polarization, the functions are

$$\begin{aligned}\frac{1}{N(q^2)}\mathcal{P}_T^{\eta_c}(q^2) = \frac{3\pi\sqrt{\delta_\tau}}{2\sqrt{2}}\Big\{&|1+V_L+V_R|^2H_0H_t+\frac{1}{\sqrt{2\delta_\tau}}\Big(\mathrm{Re}S+S\,V_L\Big)H_P^S H_0\\ &+4\sqrt{2\delta_\tau}\Big(\mathrm{Re}T_L+T_L V_L\Big)H_t H_T+4H_P^S H_T T_L S\Big\},\end{aligned} \tag{4.61}$$

and

$$\frac{1}{N(q^2)}\mathcal{P}_T^{J/\psi}(q^2) = \frac{3\pi\sqrt{\delta_\tau}}{4\sqrt{2}}\Big\{(|1+V_L|^2-|V_R|^2)(|H_{--}|^2-|H_{++}|^2) + 2(|1+V_L|^2+|V_R|^2)H_{t0}H_{00} - 4\mathrm{Re}V_R H_{t0}H_{00} + 8H_S^V H_T^0 T_L P - \frac{2}{\sqrt{2\delta\tau}}\Big(\mathrm{Re}P + P\,V_L\Big)H_V^S H_{00} + 16|T_L|^2(|H_T^-|^2-|H_T^+|^2) + 4\Big(\mathrm{Re}T_L + T_L V_L\Big)\Big[\frac{1+2\delta_\tau}{\sqrt{2\delta_\tau}}(H_{++}H_T^+ - H_{--}H_T^-) - 2\sqrt{2\delta_\tau}H_{t0}H_T^0\Big]\Big\}. \tag{4.62}$$

The transverse polarization of τ, as can be seen from eq. (4.61) and (4.62), has an overall factor of $\sqrt{\delta_\tau}$ and therefore vanishes in the limit of zero lepton mass and the emitted lepton is then fully longitudinally polarized. Consequently, the τ lepton can be largely transversely polarized as compared to the muons or the electrons. The q^2 dependence of the τ polarization in presence of different NP operators is

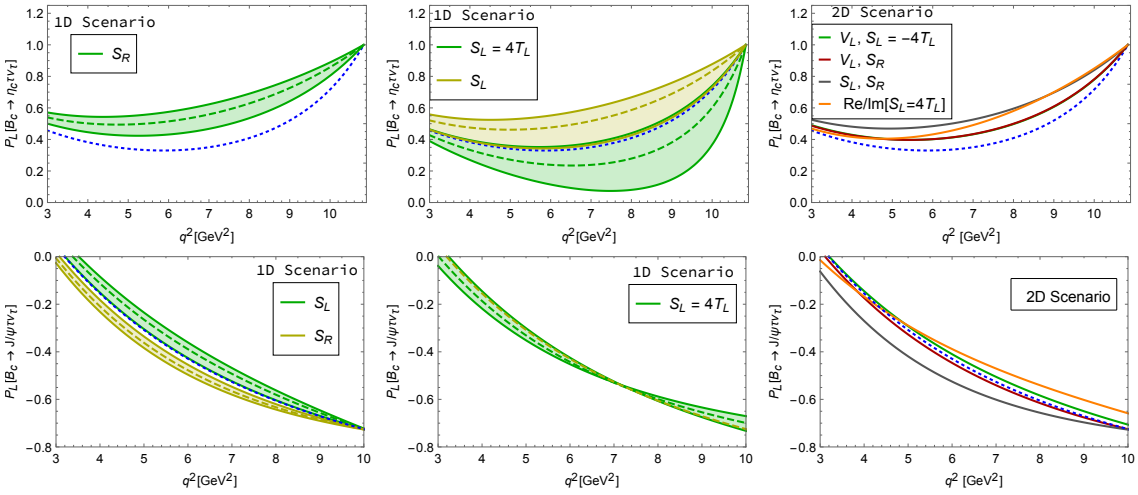

Figure 4.8: Longitudinal polarization of τ ($P_L^{\eta_c, J/\psi}$) in the decay of $B_c \to \eta_c\tau\nu$ (upper panel), and $B_c \to J/\psi\tau\nu_\tau$ (lower panel) as a function of q^2. The blue dotted lines are the SM prediction, the green dashed line is for the best fit values of the NP couplings in the 1D scenario as discussed in the text. The green band represents the NP effects from the 2σ allowed regions. The third figure in both panels is the result for the best fit points in the 2D scenarios.

shown in figure 4.8, and figure 4.9. The following observations can be made from the figures. The longitudinal and transverse polarizations of τ in the η_c decay mode are more sensitive to the NP operators compared to the J/ψ decay mode. The

tau transverse polarization in the J/ψ decay mode is again mostly affected by the NP operator $S_L = 4\,T_L$ at low values of q^2, whereas the S_L, S_R parameters in the 2D scenario lead to a deviation from the SM prediction for both the longitudinal and the transverse τ polarization. The predictions for the mean forward-backward asymmetry, the convexity parameter and the tau polarization in the presence of different NP operators are summarised in table 4.5.

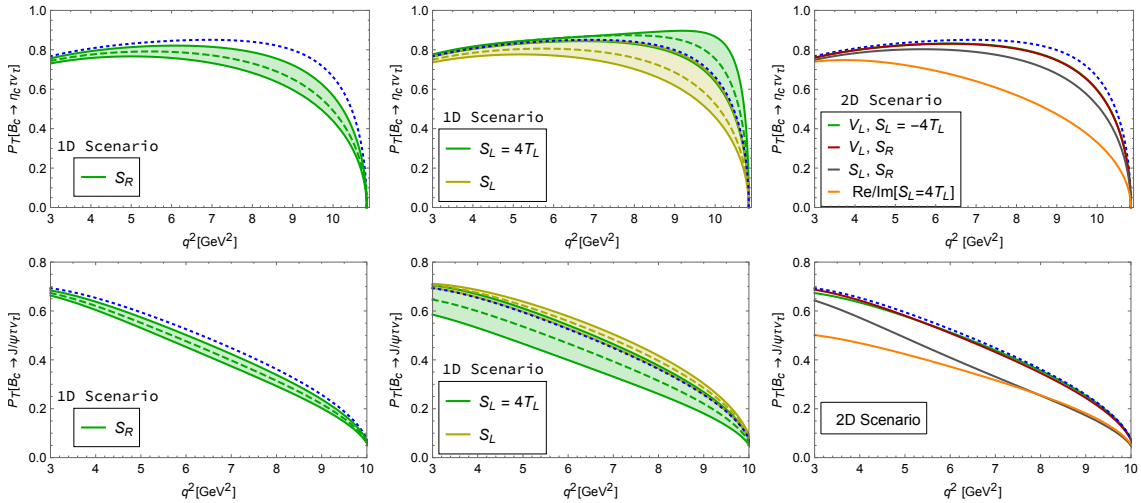

Figure 4.9: Transverse polarization of τ ($P_T^{\eta_c, J/\psi}$) in the decay for $B_c \to \eta_c \tau \nu$ (upper panel), and $B_c \to J/\psi \tau \nu_\tau$ (lower panel) as a function of q^2. The blue dotted lines are the SM prediction, the green dashed line is for the best fit values of the NP couplings in the 1D scenario as discussed in the text. The green band represents the NP effects from the 2σ allowed regions. The third figure in both panels is the result for the best fit points in the 2D scenarios.

4.2.4. Four-fold differential decay widths

In this section for the first time the process $B_c \to J/\psi\,(J/\psi \to \mu^+\mu^-)\,\ell\nu_\ell$ is considered, the 4-fold differential decay rate being dependent on three angles $\theta_V, \theta_\ell, \chi$ and the momentum transfer q^2. The angle θ_ℓ is the same as defined in the previous section, θ_V is the polar angle between the direction of the emitted μ^- in the J/ψ rest frame and the parent J/ψ in the B_c rest frame, and χ is the azimuthal angle between the $W^*\ell\bar{\nu}_\ell$ plane and the $J/\psi\mu^+\mu^-$ plane. The angles are shown in figure 4.5. This offers a possibility to explore numerous asymmetries and an opportunity to constrain future NP searches through multiple observables.

Table 4.5: The integrated values of the forward-backward asymmetry, the convexity parameter and the longitudinal and transverse polarization of τ in the whole q^2 region, in case of different NP scenarios discussed in the text. The subscript and the superscript are the values for the 2σ range of the NP couplings.

	SM	S_L	S_R	$S_L = 4T_L$	$(V_L, S_L = -4T_L)$	(S_R, S_L)	(V_L, S_R)	$\mathrm{Re}, \mathrm{Im}[S_L = 4T_L]$
$A_{FB}^{\eta_c}$	-0.35	$-0.31^{-0.29}_{-0.34}$	$-0.30^{-0.28}_{-0.32}$	$-0.36^{-0.34}_{-0.36}$	-0.33	-0.31	-0.33	-0.27
C_F^{τ,η_c}	-0.22	$-0.16^{-0.13}_{-0.21}$	$-0.14^{-0.12}_{-0.17}$	$-0.27^{-0.21}_{-0.35}$	-0.19	-0.15	-0.19	-0.16
$P_L^{\eta_c}$	0.42	$0.58^{0.66}_{0.43}$	$0.62^{0.68}_{0.53}$	$0.31^{0.45}_{0.14}$	0.50	0.59	0.50	0.57
$P_T^{\eta_c}$	0.81	$0.73^{0.80}_{0.67}$	$0.70^{0.76}_{0.66}$	$0.84^{0.86}_{0.80}$	0.77	0.72	0.77	0.43
$A_{FB}^{J/\psi}$	0.02	$0.005^{0.02}_{-0.01}$	$0.04^{0.05}_{0.03}$	$0.02^{0.02}_{0.01}$	0.006	0.07	0.03	0.02
$C_F^{\tau,J/\psi}$	-0.07	$-0.07^{-0.07}_{-0.07}$	$-0.07^{-0.07}_{-0.07}$	$-0.07^{-0.06}_{-0.07}$	-0.07	-0.08	-0.08	-0.08
$P_L^{J/\psi}$	-0.53	$-0.50^{-0.48}_{-0.53}$	$-0.57^{-0.55}_{-0.58}$	$-0.53^{-0.53}_{-0.53}$	-0.51	-0.60	-0.54	-0.48
$P_T^{J/\psi}$	0.40	$0.43^{0.45}_{0.40}$	$0.35^{0.38}_{0.33}$	$0.35^{0.41}_{0.29}$	0.39	0.29	0.38	0.28

The J/ψ is too light to decay to $\tau^+\tau^-$, therefore the outgoing leptons can be either a pair of muons or of electrons. Masses of leptons originating from the J/ψ decay are ignored, but the leptonic mass from the W^* decay is retained. The total differential decay rate for the $\mu_L^-\mu_R^+$ ($\sigma \sim \lambda_\ell^- - \lambda_\ell^+ = -1$) final state is given by eq. (4.63) below. The corresponding expressions for $\mu_R^-\mu_L^+$ final state can be obtained by setting $\theta_V \to \theta_V + \pi$ in eq. (4.63). Therefore,

$$\begin{aligned}
\mathcal{G}(q^2, \theta_\ell, \theta_V, \chi) &\equiv \frac{\mathrm{d}\Gamma(B_c \to (J/\psi \to \mu_R^+\mu_L^-)\ell\bar{\nu}_\ell)}{\mathrm{d}q^2 \mathrm{d}\cos\theta_\ell \mathrm{d}\cos\theta_V \mathrm{d}\chi} \\
&= \frac{3G_F^2|V_{cb}|^2|\vec{p}_2|q^2}{8(4\pi)^4 m_{B_c}^2}\left(1 - \frac{m_\ell^2}{q^2}\right)^2 \mathcal{B}(J/\psi \to \mu_L^-\mu_R^+)\times \\
&\quad \times \Big[|1+V_L|^2\mathcal{T}_{V_L} + |V_R|^2\mathcal{T}_{|V_R|^2} + \mathcal{T}_{V_R^{int}} + 2|P|^2(H_S^V)^2\sin^2\theta_V \\
&\quad + \mathcal{T}_{P^{int}} + |T_L|^2\mathcal{T}_{|T_L|^2} + \mathcal{T}_{T_L^{int}}\Big],
\end{aligned} \tag{4.63}$$

where the amplitudes $\mathcal{T}_i$ are given in the appendix D. The interference terms with NP operators are contained in the numerical analysis, but are not listed in the

expressions. The 4-fold differential distribution contains various combinations of the θ_ℓ, θ_V and χ angles, with the imaginary couplings being proportional to $\sin\chi$. The constraints on the NP coefficients (V_L, S_L and S_R) in the 1D scenario are obtained using the condition that they are purely real. The global fit results considered here do not include the vector operator V_R, as it does not arise at the dimension-six level in the $SU(2)_L$-invariant effective theory. The application of relation $S_L = 4\,T_L$ in the purely imaginary case is in more agreement with the SM compared to the case with the real Wilson coefficients. However, the effects of the real and the imaginary components of these NP coefficients can be isolated by constructing different angular asymmetries.

First the forward-backward asymmetry in θ_V and both θ_V, θ_ℓ with the angle χ fully integrated over is considered[1]

$$\begin{aligned}
&\tilde{A}_{\rm FB}^{J/\psi} <\theta_V> \\
&\quad= \frac{1}{\Gamma}\int_0^{2\pi} \mathrm{d}\chi \int_{-1}^{1} \mathrm{d}\cos\theta_\ell \left(\int_0^1 - \int_{-1}^0\right) d\cos\theta_V\ \mathcal{G}(q^2,\theta_\ell,\theta_V,\chi) \\
&\quad= \frac{8\pi}{3\Gamma}\Big[|1+V_L|^2(1+\delta_\ell)\Big(H_{--}^2 - H_{++}^2\Big) + 8|T_L|^2(1+4\delta_\ell)(|H_T^-|^2 - |H_T^+|^2) \\
&\quad -12\sqrt{2\delta_\ell}\Big(\mathrm{Re}T_L + T_L V_L\Big)\Big(H_{--}H_T^- - H_{++}H_T^+\Big)\Big]\,,
\end{aligned} \tag{4.64}$$

$$\begin{aligned}
&\tilde{A}_{\rm FB}^{J/\psi} <\theta_V, \theta_\ell> \\
&\quad= \frac{1}{\Gamma}\left(\int_0^{2\pi} \mathrm{d}\chi - \int_{-1}^{1}\right) \mathrm{d}\cos\theta_\ell \left(\int_0^1 - \int_{-1}^0\right) \mathrm{d}\cos\theta_V\ \mathcal{G}(q^2,\theta_\ell,\theta_V,\chi) \\
&\quad= \frac{2\pi}{\Gamma}\Big[|1+V_L|^2\Big(H_{--}^2 + H_{++}^2\Big) + 32|T_L|^2\delta_\ell(|H_T^-|^2 + |H_T^+|^2) \\
&\quad -8\sqrt{2\delta_\ell}\Big(\mathrm{Re}T_L + T_L V_L\Big)\Big(H_{++}H_T^+ + H_{--}H_T^-\Big)\Big]\,,
\end{aligned} \tag{4.65}$$

where Γ in the denominator is the q^2-dependent decay width of $B_c \to \mu^+\mu^-\ell\bar{\nu}_\ell$ normalized to the normalization factor $N(q^2)$, obtained by integrating eq. (4.63)

[1] In the publication, there is a typo in this equation - the q^2 momentum transfer is not integrated over.

over all the angles and is given by

$$\begin{aligned}\Gamma \equiv \frac{1}{N(q^2)}\frac{\mathrm{d}}{\mathrm{d}q^2}\Gamma(B_c \to \mu^+\mu^-\ell\bar{\nu}_\ell) = \\ \frac{16\pi}{9}\Big\{2|1+V_L|^2\Big[(1+\delta_\tau)\Big(H_{00}^2+H_{++}^2+H_{--}^2\Big)+3\delta_\tau H_{t0}^2\Big] \\ +3|H_S^V|^2|P|^2+6\sqrt{2\delta_\tau}H_S^V H_{t0}\Big(\mathrm{Re}P+P\,V_L\Big) \\ +16|T_L|^2(1+4\delta_\tau)\Big(|H_T^0|^2+|H_T^+|^2+|H_T^-|^2\Big) \\ -24\sqrt{2\delta_\tau}\Big(\mathrm{Re}T_L+T_L V_L\Big)\Big(H_{00}H_T^0+H_{++}H_T^+ + H_{--}H_T^-\Big)\Big\},\end{aligned} \tag{4.66}$$

and the $<>$ brackets in eq. (4.66) denote the angle in which the asymmetry is explored. It can be seen from eq. (4.64) that the numerator is not sensitive to the scalar type NP operators. Therefore the sensitivity to the scalar NP comes only from the total decay width in the denominator, eq. (4.66). In figure 4.10

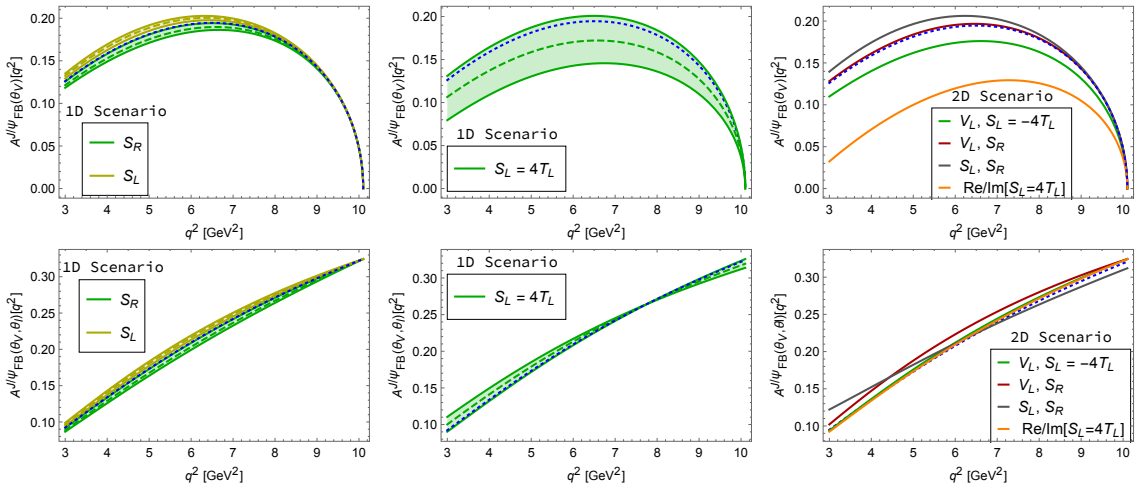

Figure 4.10: Forward-backward asymmetry $A^{FB} <\theta_V>$ [upper-panel] and $A^{FB} <\theta_V, \theta_\ell>$ [lower-panel] as a function of q^2. The blue dotted lines are the SM prediction, the green dashed line is for the best fit values of the NP couplings in the 1D scenario as discussed in the text. The green band represents the NP effects from the 2σ allowed regions. The third figure in both panels is the result for the best fit points in the 2D scenarios.

$A_{FB}^{J/\psi} <\theta_V>$ and $A_{FB}^{J/\psi} <\theta_V, \theta_\ell>$ are shown as a function of q^2 with the values of the new physics couplings as given in eq. (4.48) and eq. (4.49). The current bound on the NP couplings makes the observable $A_{FB}^{J/\psi} <\theta_V>$ sensitive to $S_L = 4\,T_L$ in

the 1D scenario and to the same combination with both the real and the imaginary components present in case of 2D scenario. As for the asymmetry $A_{FB}^{J/\psi} <\theta_V>$, the deviation from the SM in case of 2D scenario for the combination $\mathrm{Re}[S_L = 4\,T_L]$, $\mathrm{Im}[S_L = 4\,T_L]$ can be as large as 50-70% in the region of small q^2. However, the other observable with the asymmetry in both θ_V and θ_ℓ, $A_{FB}^{J/\psi} < \theta_V, \theta_\ell >$ is not a good observable to look for NP scenarios under present constraints on the couplings.

Additional asymmetries can be constructed in the angle χ along with θ_V and θ_ℓ. These asymmetries are proportional to both $\cos\chi$ and $\sin\chi$, and their corresponding expressions are given as

$$
\begin{aligned}
A_{FB}^{J/\psi} &<\chi, \theta_V> \\
&= \frac{1}{\Gamma}\left(\int_{-\pi/2}^{\pi/2} - \int_{\pi/2}^{3\pi/2}\right) \mathrm{d}\chi \int_{-1}^{1} \mathrm{d}\cos\theta_\ell \left(\int_{0}^{1} - \int_{-1}^{0}\right) \mathrm{d}\cos\theta_V \times \\
&\qquad \times \mathcal{G}(q^2, \theta_\ell, \theta_V, \chi) \\
&= \frac{-4\pi}{3\Gamma}\Big\{|1+V_L|^2\left[H_{00}\Big(H_{--} - H_{++}\Big) + 2\delta_\ell H_{t0}\Big(H_{--} + H_{++}\Big)\right] \\
&- 2H_S^V H_T^+ T_L P + \sqrt{2\delta_\ell}\Big(H_{--} + H_{++}\Big) H_S^V \Big(\mathrm{Re}P + P\,V_L\Big) \\
&+ 32\delta_\ell H_T^0\Big(H_T^- - H_T^+\Big)|T_L|^2 - 4\sqrt{2\delta_\ell}\Big(\mathrm{Re}T_L + T_L V_L\Big) \times \\
&\times \Big(H_{00}(H_T^- - H_T^+) + H_T^0(H_{--} - H_{++}) + H_{t0}(H_T^- + H_T^+)\Big)\Big\},
\end{aligned}
\tag{4.67}
$$

and

$$
\begin{aligned}
A_{FB}^{J/\psi} &<\chi, \theta_V, \theta_\ell> \\
&= \frac{1}{\Gamma}\left(\int_{-\pi/2}^{\pi/2} - \int_{\pi/2}^{3\pi/2}\right) \mathrm{d}\chi \left(\int_{0}^{1} - \int_{-1}^{0}\right) \mathrm{d}\cos\theta_\ell \left(\int_{0}^{1} - \int_{-1}^{0}\right) \mathrm{d}\cos\theta_V \times \\
&\qquad \times \mathcal{G}(q^2, \theta_\ell, \theta_V, \chi) \\
&= \frac{16}{9\Gamma}(2\delta_\ell - 1)\left[|1+V_L|^2 H_{00}\Big(H_{--} + H_{++}\Big) - 16|T_L|^2 H_T^0\Big(H_T^- + H_T^+\Big)\right].
\end{aligned}
\tag{4.68}
$$

In figure 4.11, the asymmetries $A_{\mathrm{FB}}^{J/\psi} <\chi, \theta_V>$ [upper-panel] and $A_{\mathrm{FB}}^{J/\psi} <\chi, \theta_V, \theta_\ell>$ [lower-panel] are shown as a function of q^2. They behave similarly to the asymmetries $A_{\mathrm{FB}}^{J/\psi} <\theta_V>$ and $A\mathrm{FB}^{J/\psi} <\theta_V, \theta_\ell>$ discussed above, where χ was integrated over the

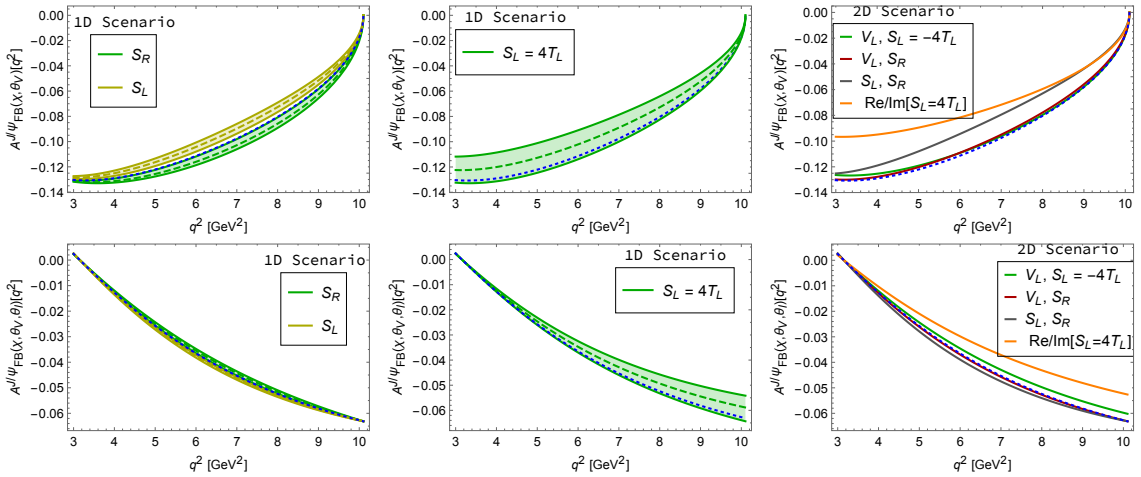

Figure 4.11: Asymmetries $A^{\rm FB} < \chi, \theta_V >$ [upper-panel] and $A^{FB} < \chi, \theta_V, \theta_\ell >$ [lower-panel] as a function of q^2. The blue dotted lines are the SM prediction, the green dashed line is for the best fit values of the NP couplings in the 1D scenario as discussed in the text. The green band represents the NP effects from the 2σ allowed regions. The third figure in both panels is the result for the best fit points in the 2D scenarios.

whole range. These observables do not provide any additional information compared to $A_{\rm FB} < \theta_V >$ and $A_{\rm FB} < \theta_V, \theta_\ell >$ discussed before. The 2D scenario in case of $A_{\rm FB}^{J/\psi} < \chi, \theta_V >$ with Re$[S_L = 4\,T_L]$ and Im$[S_L = 4\,T_L]$ results in about 10-20% deviation from the SM value at low values of q^2.

Finally, observables sensitive only to the imaginary component of the NP operators are considered, which are exactly zero within the SM. There are three possible combinations, (a) asymmetry depending only on χ, (b) asymmetry depending on χ and θ_V, and (c) asymmetry depending on χ, θ_V and θ_ℓ. The relevant expressions are

$$
\begin{aligned}
A_{\rm FB}^{\rm Im} <\chi> & \\
&= \left(\frac{1}{\Gamma}\ \int_0^{\pi} - \int_{\pi}^{2\pi}\right) {\rm d}\chi \int_{-1}^{1} {\rm d}\cos\theta_\ell \int_{-1}^{1} {\rm d}\cos\theta_V\ \mathcal{G}(q^2, \theta_\ell, \theta_V, \chi) \\
&= \frac{\pi^2}{\Gamma}\Big[\sqrt{2\delta_\ell}\Big(4\left\{{\rm Im}T_L + (T_L V_L)^*\right\}\left\{H_{00}(H_T^- - H_T^+) + H_T^0(H_{++} - H_{--})\right. \\
&+ \left. H_{t0}(H_T^+ + H_T^-)\right\} + H_S^V\left\{{\rm Im}P + (P\,V_L)^*\right\}\Big(H_{--} + H_{++}\Big)\Big) + 4H_S^V\,H_T^+(P\,T_L)^*\Big],
\end{aligned}
\tag{4.69}
$$

where $(T_L V_L)^* = \mathrm{Im}T_L \mathrm{Re}V_L - \mathrm{Im}V_L \mathrm{Re}T_L$, $(P\,V_L)^* = \mathrm{Im}P\,\mathrm{Re}V_L - \mathrm{Im}V_L \mathrm{Re}P$ and $(P\,T_L)^* = \mathrm{Im}P\,\mathrm{Re}T_L - \mathrm{Im}T_L \mathrm{Re}P$ shorthand notations have been introduced,

$$
\begin{aligned}
A_{\rm FB}^{\rm Im} <\chi, \theta_V> & \\
&= \left(\frac{1}{\Gamma}\left[\int_0^{\pi} - \int_{\pi}^{2\pi}\right] \mathrm{d}\chi \int_{-1}^{1} \mathrm{d}\cos\theta_\ell \left[\int_0^{1} - \int_{-1}^{0}\right] \mathrm{d}\cos\theta_V\ \mathcal{G}[q^2, \theta_\ell, \theta_V, \chi]\right) \\
&= \frac{4\pi}{3\Gamma}\sqrt{\delta_\ell}\Bigg[4\sqrt{2}\left\{\mathrm{Im}T_L - (T_L V_L)^*\right\} \times \\
&\qquad \times \left\{H_{00}(H_T^- + H_T^+) + H_{t0}(H_T^- - H_T^+) - H_T^0(H_{++} + H_{--})\right\} \\
&\qquad + \sqrt{2} H_S^V \Big(H_{--} - H_{++}\Big)\left\{\mathrm{Im}P - (P\,V_L)^*\right\} + \frac{4}{\sqrt{\delta_\ell}} H_S^V\, H_T^+ (P\,T_L)^*\Bigg],
\end{aligned}
\tag{4.70}
$$

and finally

$$
\begin{aligned}
A_{\rm FB}^{\rm Im} <\chi, \theta_V, \theta_\ell> & \\
&= \left(\frac{1}{\Gamma}\left[\int_0^{\pi} - \int_{\pi}^{2\pi}\right] \mathrm{d}\chi \left[\int_0^{1} - \int_{-1}^{0}\right] \mathrm{d}\cos\theta_\ell \left[\int_0^{1} - \int_{-1}^{0}\right] \mathrm{d}\cos\theta_V\ \mathcal{G}[q^2, \theta_\ell, \theta_V, \chi]\right) \\
&= \frac{16}{9\Gamma}(2\delta_\ell - 1)\left[H_{00}\Big(H_{--} - H_{++}\Big)\Big(2\mathrm{Im}V_R + \mathrm{Im}V_R \mathrm{Re}V_L - \mathrm{Re}V_R \mathrm{Im}V_L\Big)\right].
\end{aligned}
$$

The asymmetry $A_{\rm FB}^{\rm Im} < \chi, \theta_V, \theta_\ell >$ is only sensitive to the NP operator V_R and is therefore not relevant for this case since right-handed vector operators are not considered in the global fits, as discussed before. In figure 4.12 $A_{\rm FB}^{\rm Im} <\chi>$ [upper-panel] and $A_{\rm FB}^{\rm Im} < \chi, \theta_V >$ [lower-panel] are shown as a function of q^2. These observables are only shown for $\mathrm{Im}S_L = 4\,\mathrm{Im}T_L$ in the 1D scenario and $\mathrm{Re}S_L = 4\,\mathrm{Re}T_L$, $\mathrm{Im}S_L = 4\,\mathrm{Im}T_L$ in the 2D scenarios as these were the only cases considered in the global fit in ref. [158]. The forward-backward asymmetry depending only on χ in the light of results from the current global fit shows about 1% deviation from the SM in the 1D scenario and up to 3% deviation in the 2D scenario, in the mid-range of $q^2 = 5 - 9$ GeV^2. The asymmetry $A_{\rm FB}^{\rm Im} <\chi, \theta_V>$ in case of the 2D scenario only deviates around 1% in the low q^2 region, whereas it is insensitive to NP in the 1D scenario. The predictions for the integrated forward-backward asymmetries in the presence of different NP operators is summarised in table 4.6.

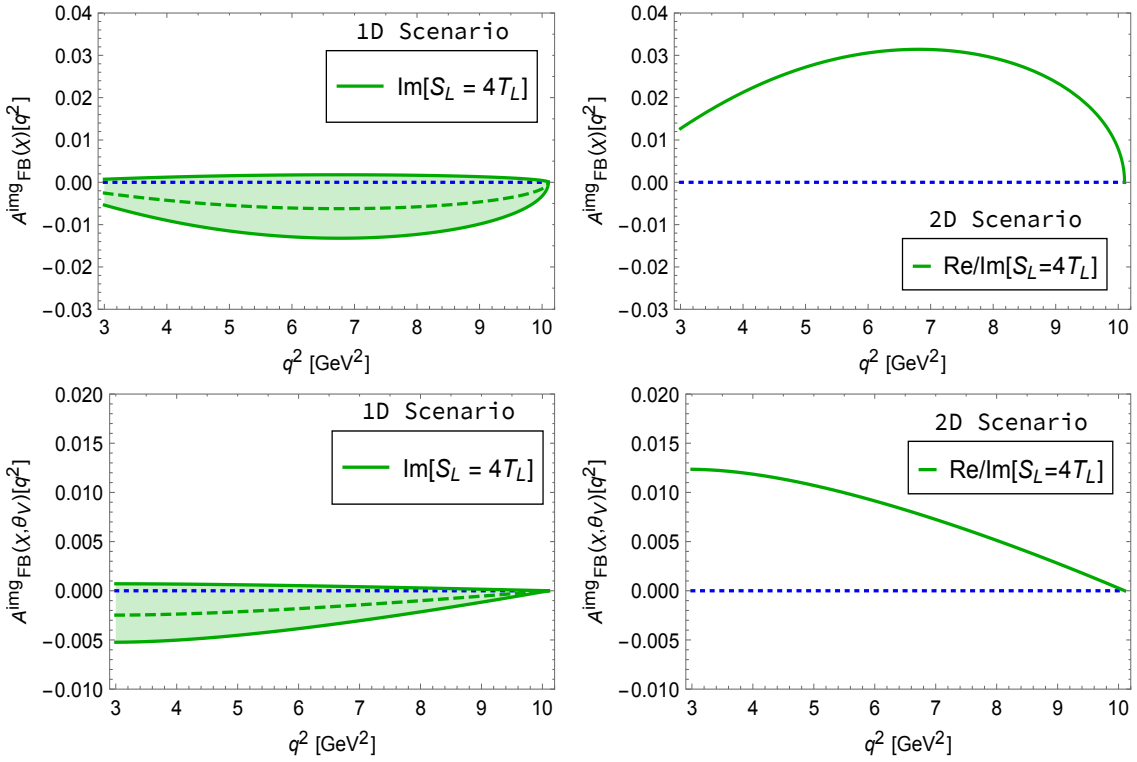

Figure 4.12: Asymmetries $A_{\rm FB}^{\rm Im}(\chi)$ [upper-panel] and $A_{FB}^{img}(\chi,\theta_V)$ [lower-panel] as a function of q^2. The SM value being zero is shown by a blue dotted line, the green dashed line is for the best fit values of the NP couplings in the 1D scenario as discussed in the text. The green band represents the NP effects from the 2σ allowed regions. The second figure is for the relevant 2D scenario.

Table 4.6: The integrated values of the forward-backward asymmetries in the whole q^2 region, in case of different NP scenarios discussed in the text. The subscript and the superscript are the values for the 2σ range of the NP couplings.

	SM	S_L	S_R	$S_L = 4\,T_L$	$(V_L, S_L = -4\,T_L)$	(S_R, S_L)	(V_L, S_R)	Re, Im$[S_L = 4\,T_L]$
$A_{\rm FB}^{J/\psi} <\theta_V>$	0.16	$0.16^{0.16}_{0.15}$	$0.17^{0.17}_{0.16}$	$0.14^{0.17}_{0.12}$	0.15	0.17	0.16	0.09
$A_{\rm FB}^{J/\psi} <\theta_V, \theta_\ell>$	0.21	$0.20^{0.21}_{0.20}$	$0.21^{0.22}_{0.21}$	$0.21^{0.22}_{0.21}$	0.21	0.22	0.21	0.21
$-A_{\rm FB}^{J/\psi} <\chi, \theta_V>$	0.09	$0.10^{0.10}_{0.09}$	$0.09^{0.09}_{0.09}$	$0.09^{0.10}_{0.08}$	0.10	0.08	0.10	0.07
$-A_{\rm FB}^{J/\psi} <\chi, \theta_V, \theta_\ell>$	0.03	$0.03^{0.03}_{0.03}$	$0.03^{0.03}_{0.03}$	$0.03^{0.03}_{0.03}$	0.03	0.03	0.03	0.02
$A_{\rm FB}^{\rm Im} <\chi>$	0.0	0.0	0.0	$-0.004^{0.001}_{-0.01}$	0.0	0.0	0.0	0.02
$A_{\rm FB}^{\rm Im} <\chi, \theta_V>$	0.0	0.0	0.0	$-0.002^{0.0}_{-0.003}$	0.0	0.0	0.0	-0.001

4.3. Conclusion

The sensitivity of all the considered observables in this section to the different NP operators is summarized in table 4.7. Most of the observables in the η_c decay mode are sensitive to the NP coupling S_R. The transverse polarization of τ is mostly affected by the current best fit point of the combination of coefficients $\mathrm{Re}, \mathrm{Im}[S_L = 4\,T_L]$ in the 2D NP scenario. The 2D NP scenario with the presence of both S_R and S_L leads to largest deviation from the SM predictions for most of the observables in the case of J/ψ, apart from $R_{J/\psi}$.

	V_L	S_L	S_R	$S_L = 4\,T_L$	$(V_L, S_L = -4\,T_L)$	(S_R, S_L)	(V_L, S_R)	Re,Im$[S_L = 4\,T_L]$
R_{η_c}			✓					
$A_{FB}^{\eta_c}$		✓*	✓*					✓
C_F^{τ,η_c}		✓	✓	✓*				
$P_L^{\eta_c}$			✓	✓*				
$P_T^{\eta_c}$								✓
$R_{J/\psi}$	✓				✓			
$A_{FB}^{J/\psi}$						✓		
$P_L^{J/\psi}$						✓		
$P_T^{J/\psi}$				✓*		✓		✓

Table 4.7: Summary of the sensitivity of the observables to the NP couplings. The best fit value of the NP coupling which is most sensitive to the observable is marked with ✓. The boxes with ✓* are the ones where 2σ ranges of NP parameters give the largest deviation from the SM value.

In addition, the full 4-fold differential distribution of the decay rate $B_c \to J/\psi\ell\nu_\ell$, with J/ψ decaying to a pair of leptons of opposite helicity is considered for the first time in the presence of new physics operators. We find that the asymmetry in the angle θ_V is mostly sensitive to the NP couplings $\mathrm{Re}, \mathrm{Im}[S_L = 4T_L]$, in the 2D NP scenarios. The asymmetries in the angle χ, which are zero in the SM and are sensitive to the imaginary part of the NP coupling, are also considered and found to be sensitive to $S_L = 4\,T_L$ combination of parameters. Therefore, with the

current allowed parameter space for the $S_L = 4\,T_L$ NP parameters obtained from the global fit to experimental data on semileptonic $B \to D, D^*$ decays, the asymmetries constructed with θ_V, χ and (θ_V, χ) angles lead to significant deviation from the SM prediction.

However, it is important to stress that none of the NP scenarios derived from the recent global fit analysis of the available experimental data on semileptonic $B \to (D, D^*)\ell\bar{\nu}_\ell$ decays [158] can also simultaneously explain the current 2σ tension with the experimental $R_{J/\psi}$ ratio. With the extended experimental LHCb program, future studies with more data will be needed to disentangle the existence of LFU violation in B_c decays.

5. $|V_{ub}|$ DETERMINATION FROM THE $B_c^+ \to D^{(*)}\,\ell^+\nu_\ell$ DECAY

This chapter is based on research published in D. Leljak and B. Melic, JHEP ***02*** *(2020), 171 doi:10.1007/JHEP02(2020)171 [arXiv:1909.01213 [hep-ph]] [2].*

The main source for the extraction of $|V_{ub}|$ from the exclusive decays is the semileptonic $\bar{B} \to \pi\ell\bar{\nu}_\ell$ decay, which is precisely measured and also relatively precisely determined theoretically. Theoretical uncertainties are mainly driven by the lack of precise determinations of hadronic matrix elements, or more specifically - form factors. Nowadays, precise theoretical calculation of $\bar{B} \to \pi$ form factors are available in the framework of the LCSR at $q^2 \leq 12 - 15\,\text{GeV}$ [95, 205, 206] and on the lattice at $q^2 \geq 15\,\text{GeV}$ [78, 80]. Combined and constrained by unitarity and analyticity principles, these two approaches enable a form factor determination in the full q^2 range and, consequently, very precise determination of $|V_{ub}|$ [207]

$$|V_{ub}|^{\bar{B}\to\pi} = (3.53 \pm 0.08_{\text{stat}} \pm 0.06_{\text{syst}}) \cdot 10^{-3}\,. \tag{5.1}$$

Since the work this section is based on was published, two additional, very precise determinations were published [3, 208], in one of which the author of this thesis participated.

With large accumulation of data on Λ_b^0 decays at LHCb, it became possible to study also the semileptonic Λ_b^0 decays, in order to extract the $|V_{ub}|/|V_{cb}|$ ratio [209]

using the QCD lattice results for the form factors [210]:

$$|V_{ub}|/|V_{cb}|^{\Lambda_b\to\Lambda_c} = 0.084 \pm 0.004_{\rm exp} \pm 0.004_{\rm lattice}\,, \tag{5.2}$$

which is again somewhat lower than the most recent averaged inclusive determination of this ratio [42].

With the advancement on the experimental front, more and more hadronic decay channels are becoming available for the exclusive extraction of CKM matrix elements, which is especially beneficial for the $b \to u\ell\bar{\nu}_\ell$ semileptonic transitions [211]. The most promising exclusive decays of this type are $B \to (\eta, \eta', \omega, \rho)\ell\bar{\nu}_\ell$, but also, in the near future, the $B_c \to D^{(*)}\ell\bar{\nu}_\ell$ decay, which is discussed here. LHCb plans to go for rare $B_c \to D^0\ell\bar{\nu}_\ell$ decays in the Upgrade II [212]. As stated for the LHCb Upgrade II, approximately 30,000 reconstructed $B_c \to D^0\ell\bar{\nu}_\ell$ decays can be expected with the 300 fb^{-1} Upgrade II dataset, which could lead to a competitive measurement of $|V_{ub}|$ from these decays too.

In this section the calculation of $B_c \to D^{(*)}$ form factors is addressed and an analysis of the semileptonic $B_c \to D^{(*)}$ decays is performed. For the calculation of the form factors the three-point sum rule (3ptSR) method [81–83, 213] is employed. Although the method itself has some general limitations, for heavy-to-heavy decays of the type considered here the QCDSR seems to be of adequate applicability. This behaviour mainly concerns heavy-to-light transitions, while in $B_c \to D^{(*)}$ decays, considered here, the use of heavy-quark symmetries, and the description of mesons in terms of light-cone distribution amplitudes seem not to be trustworthy approaches. As will be discussed briefly in section 5.1, one can parametrize $B_c \to D^{(*)}$ matrix elements in the heavy quark limit in terms of two form factors which can be further expressed with the help of the heavy-quark symmetry as integrals over the B_c meson wave function, eq. (5.14) and (5.16). However, there are no fully reliable and controllable models for calculating the B_c wave function without further approximations being involved, such as various non-relativistic or heavy-quark approximations at zero-recoil, or the use of constituent quark models related to a quark potential and/or relativistic quark kinematics, as for example the ones used in ref. [191]. Also,

the impact of the deviation from the infinite heavy quark mass limit is then difficult to judge upon and incorporate into systematical uncertainties. On the other hand, the light-cone sum rule method relies on the known description of the final (light) meson or the decaying heavy-meson distribution amplitudes (DAs) of increasing twist, which is hardly applicable for our $B_c \to D^{(*)}$ transitions, since the B_c meson DA's aren't known, nor are the $D^{(*)}$ mesons light enough that their DAs could be systematically expanded near the light-cone. There exists the Brodsky-Huang-Lepage (BHL) prescription [214] on how to (for a relativistic two particle state) approximately connect the wave function with the light-cone functions, used in [133]. But, this approach involves models with constituent quark masses and arbitrary phenomenological parameters which are hardly numerically controllable. There are no available lattice QCD form factor predictions for $B_c \to D^{(*)}$ decays as of this moment, but the HPQCD collaboration has announced some work is in progress. Alternative methods used in the estimation of $B_c \to D^*$ form factors, like various relativistic quark models provide form factors with a precision that cannot be systematically controlled and therefore calculated values for the form factors differ in a wide range, see table 5.3. On the other hand, OPE expansion in the QCDSR is under control, the non-perturbative vacuum condensates are universal and known also from sum rule calculations.

5.1. QCDSR form factors

The form factors are taken in the WS basis, and are defined as in section 3, with $B_{q_1} \to B_c$ and $M_f = D^{(*)}$, which means $q_1 \to c$ and $q_2 \to u$. The required decay constants are defined as

$$\begin{aligned} \langle \Omega |\, \bar{c}(0) i\gamma_5 b(0)\, | B_c \rangle &= f_{B_c} \frac{m_{B_c}^2}{m_c + m_b}\,, \\ \langle \Omega |\, \bar{c}(0) i\gamma_5 u(0)\, \big| D^0 \big\rangle &= f_{D^0} \frac{m_{D^0}^2}{m_u + m_c}\,, \\ \langle \Omega |\, \bar{c}(0) \gamma_\nu c(0)\, | D^* \rangle &= f_{D^*} m_{D^*} \epsilon_\nu\,. \end{aligned} \tag{5.3}$$

The rest of the standard procedure is explained in section 3.2, while the expressions and the details of their derivation are presented in appendix A, so here only the process of sum rule parameter setting is explained, with a comment on the non-local condensate contributions which were published for the first time in a research paper this section is based on. The list of contributions considered is given in figure 5.1, namely the perturbative part and non-perturbative terms up to dimension 5

$$\Pi_i = \Pi_i^{\text{pert}} + \Pi_i^{(3)} + \Pi_i^{(4)} + \Pi_i^{(5)} + \dots\,, \tag{5.4}$$

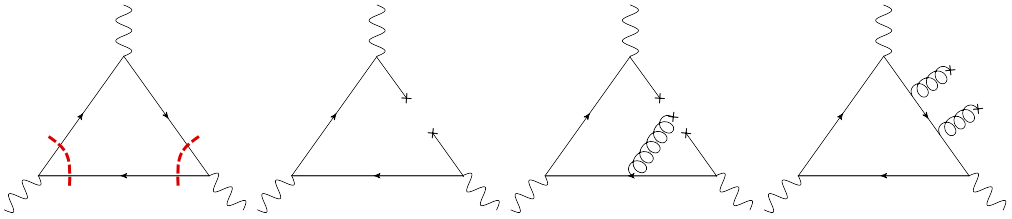

Figure 5.1: Contributions to correlation function from left to right: **(a)** perturbative diagram,**(b)** non local quark condensate diagram, **(c)** an example of a quark-gluon condensate diagram, **(d)** an example of a gluon condensate diagram.

The perturbative part is calculated by standard methods imposing the Cutkosky rules to calculate simultaneously discontinuities in p_1^2 and p_2^2 of amplitudes described by the triagle diagram with quarks in the loop, where for the i-th Lorentz structure $(-4)\text{Im}_{s_1,s_2}\Pi_i^{\text{pert}}(s_1,s_2,q^2) = \rho_i(s_1,s_2,q^2)$, and then by using the double dispersion relation

$$\Pi_i^{\text{pert}}(p_1^2,p_2^2,q^2) = -\frac{1}{(2\pi)^2}\iint \frac{\rho_i(s_1,s_2,q^2)}{(s_1-p_1^2)(s_2-p_2^2)}\text{d}s_1\text{d}s_2\,. \tag{5.5}$$

It is easy to see that the quark- and mixed quark-gluon condensate contributions (figure 5.1) vanish after the Borel transformations in both variables $p_1^2 = p_{B_c}^2$ and $p_2^2 = p_{D^{(*)}}^2$. However, this is only true if one considers local condensates. To improve the picture we examine the influence of non-local quark condensates $\langle\bar{q}(x)[x,0]q(0)\rangle$ [215, 216] in $B_c \to D^{(*)}\ell\bar{\nu}_\ell$ decays. The non-local quark condensates are usually introduced as a function smeared over a gaussian centered around $x = 0$

(since the non-locality is expected to be small)

$$\langle\bar{q}(x)q(0)\rangle = \langle\bar{q}q\rangle \int\limits_0^\infty \mathrm{d}\nu\, \mathrm{e}^{\nu\frac{x^2}{4}} f(\nu) \tag{5.6}$$

with the model-dependent function [217]

$$f(\nu) = \frac{\lambda^{a-2}}{\Gamma(a-2)}\nu^{1-a}e^{-\lambda/\nu}\,, \quad a-3 = \frac{4\lambda}{m_0^2} \tag{5.7}$$

or in the simpler version [218], used in this study

$$f(\nu) = \delta\left(\nu - \frac{m_0^2}{4}\right). \tag{5.8}$$

The first two moments of the model function $f(\nu)$ are fixed by the OPE as

$$\int\limits_0^\infty \mathrm{d}\nu\, f(\nu) = 1, \qquad \int\limits_0^\infty \mathrm{d}\nu\, \nu\, f(\nu) = \frac{m_0^2}{4}\,. \tag{5.9}$$

Here m_0^2 is the standard OPE parameter [219,220] connected with the average quark virtuality, and is defined as a ratio of quark and quark-gluon condensates

$$g\langle\bar{q}(x)(\sigma\cdot G)q(0)\rangle \approx m_0^2\langle\bar{q}(x)q(0)\rangle\,. \tag{5.10}$$

The use of the more sophisticated function $f(\nu)$ given in eq. (5.7) does not change anything in the conclusion. Namely, numerically the non-local quark condensates $\Pi_i^{(3)} = \Pi_i^{\langle\bar{q}q\rangle}$ and the mixed quark-condensate $\Pi_i^{(5)} = \Pi_i^{\langle\bar{q}\sigma.Gq\rangle}$ are contributing just up to 1% to the result.

All of the non-perturbative diagrams are numerically negligible, and can be safely neglected.

5.1.1. Setting the sum rule parameters

To calculate the form factors in QCD sum rules, in which the correlation function is written as a sum of perturbative and non-perturbative contributions as in

eq. (5.4), the perturbative part is calculated by the usual expansion in the coupling constant, while the non-perturbative part is described by the manner of Wilson's operator product expansion as a sum of expectation values of operators of increasing dimension. Since it is known that when using the Borel-transformed sum rules in calculating heavy meson decay constants higher orders of perturbation series can contribute as much as 30-40%, depending on the scheme (heavy-light decay constants are known to NNLO [221]), whereas the QCD 3-point function is only known to LO, here the 3-point function is parametrized with the same threshold parameters s_0^{eff} that at LO in QCDSR reproduce the meson decay constants obtained from the lattice QCD calculations, listed in table 5.1, whereas the 3ptSR Borel mass parameters M^2 are taken in the region where the stability is achieved in the sense of appearance of the so called Borel plateau. In this way, since the form factor in 3ptSRis proportional to the inverse of decay constants, as in eq. (3.30) and (3.31), one may conclude that

$$\begin{aligned} F_i(q^2) \propto \frac{\Pi_i^{\text{3pt.}}(q^2)}{\Pi_i^{\text{2pt.}}} &= \frac{a(q^2)+\alpha_s(\mu^2)b(q^2)}{(c+\alpha_s(\mu^2)d)(e+\alpha_s(\mu^2)f)} \\ &\approx \frac{a(q^2)}{ce} + \mathcal{O}\left[\alpha_s \quad \frac{b(q^2)}{ce} - a(q^2)\left(\frac{d}{c^2e} + \frac{f}{ce^2}\right)\right]. \end{aligned} \tag{5.11}$$

Assuming that form factors also receive positive NLO contributions (this is to be expected from studies resumming ladder corrections [190]), using the leptonic decay

Table 5.1: Decay constants of mesons with 3ptSR parameters.

Meson	lattice [MeV]	our value [MeV]	s_0^{eff} [GeV^2]	M^2 [GeV^2]
f_{B_c}	427 ± 8 [164], 434 ± 5 [222]	425 ± 25	$53 - 55$	$30 - 50$
f_{D^0}	213 ± 2 [223], 207 ± 4 [224]	212 ± 16	$7 - 7.5$	$4 - 6$
f_{D^*}	278 ± 23 [225], 224 ± 9 [226]	258 ± 40	$6 - 8$	$6 - 8$

constants calculated at LO (with the same soft corrections included in the 3 point correlation function) with the parameters that reproduce the lattice value might serve very well to cancel the as-of-yet unknown α_s corrections to the 3 point corre-

lation function.

An approximate relation connecting the Borel mass parameters of different meson decay constants noticed by authors in [99]

$$\frac{M_1^2}{M_2^2} \approx \frac{m_{\mathrm{M}_1}^2 - m_{Q_1}^2}{m_{\mathrm{M}_2}^2 - m_{Q_2}^2} \tag{5.12}$$

where m_{M_i} is mass of the meson, and m_{Q_i} is the mass of its heavier quark, is found to hold here too, and, as will be shown later, in 3-point calculations as well. A reminder is in order - the uncertainties of decay constants arising in the calculation are connected with the specific method of calculation, since the threshold parameters are actually fixed so that they reproduce the lattice values, along with their uncertainties. Venturing into the 3-point calculation, as mentioned above, the same Borel thresholds are used as the ones that reproduce the lattice QCD leptonic decay constants. It is important to notice that, when estimating parametric uncertainties of the 3ptSR calculation, decay constants and thresholds are not varied independently, but are rather always "plugged in" together - the numerical value of the threshold is always used with the numerical value of the QCDSR leptonic decay constant that is reproduced by the latter threshold. The hope is that all the higher order/higher dimension operator contributions are reproduced through the threshold modification in the 3-point calculation as well. Otherwise, for the b quark the so called "potential subtracted" mass [227] is used, which is coincidentally very close to both the $\Upsilon(1S)$ scheme mass [228] and the kinetic scheme mass [229, 230], whereas the c-quark the mass is then given by varying the ratio Z of the two masses given by the QCD lattice calculation [231, 232], keeping in mind that the $\overline{\mathrm{MS}}$ masses are not used, and this ratio for pole masses tends to be lower as higher order corrections are included - which is the choice is made to use a somewhat lower value of Z. The same method described above was already used for calculating $B_c \to \eta_c, J/\psi$ transition form factors in [183]. All parameters used are listed in table 5.2. As for the Borel mass parameters, it is found that stability in the sense of appearance of the Borel plateau is achieved for approximately twice of the values of the Borel mass

Table 5.2: Parameters used in the QCDSR calculation.

$m_b = 4.6^{+0.1}_{-0.1}$ GeV $m_c = Zm_b$, $Z \approx 0.29^{+0.1}_{-0.1}$	$m_{B_c} = 6.275$ GeV $m_{D^0} = 1.865$ GeV $m_{D^*} = 2.007$ GeV	$M^2_{B_c} = 60 - 90$ GeV^2 $M^2_{D^0} = 8 - 12$ GeV^2 $M^2_{D^*} = 12 - 16$ GeV^2
$\left\langle \frac{\alpha_s}{\pi} GG \right\rangle = 0.009 \pm 0.007$ GeV^4 [233]	$m_0 = 0.8 - 1.05$ GeV	$\tau_{B_c} = 0.507 \pm 0.009$ ps

parameters used in the 2-point sum rule, so that

$$\frac{M^2_{\text{2pt.}}}{M^2_{\text{3pt.}}} \approx \frac{1}{2}, \tag{5.13}$$

which is a heuristic finding also confirmed by prior QCDSR studies. Additionally, a demand is set that heavier hadronic states contribute less than 50% of the ground-state B_c meson contribution to 3ptSR in the B_c channel. This condition (and the one arising from the m_{B_c} reproduction) yields an upper limit in ${}^{\uparrow}M^2_{B_c} = 90$ GeV^2, and a lower limit in ${}^{\downarrow}M^2_{D^{(*)}} = 8$ GeV^2. The upper constraint on $M^2_{D^{(*)}}$ is less rigid. This is probably due to a lack of understanding of α_s corrections, which would modify both the 'Borel window' and the threshold values. The sum rules for observables should in principle be independent of the auxiliary Borel parameters M^2. In practice, however, this is only approximately true because of the various approximations made. Therefore it is important to pick the right 'Borel window' where all above requirements are satisfied, by checking the stability of the sum rule against variation of the Borel and other parameters and including the errors into analysis. The form factor uncertainties presented here reflect also these parameter variations, and the form factors do not change by more than ∼5% in the acceptable range of the Borel mass parameters. The estimation of the systematic errors is hard here, due to a lack of higher-order perturbative corrections in the 3ptSR, which could be large and would significantly stabilize the sum rules. The extracted values of sum rule parameters described above are in the acceptable range, expected by some general considerations, such as for example the relation among Borel parameters of two different meson constants in eq. (5.12), as well as among Borel parameters from 2ptSR and 3ptSR calculations, given in eq. (5.13).

With the parameters set by the considerations above, in table 5.3 the prediction

for the form factor values at $q^2 = 0$ are presented together with an extensive list of the earlier results found in literature. The form factors predicted in previous QCDSR calculation [132] are significantly larger then the results presented here and those obtained from other model calculations. The reason can be found in the fact that the authors there renormalize their perturbative spectral densities using Coulomb-like gluon exchange corrections which usually results in multiplying the bare values by a factor of three or more. Another remark is that this kind of renormalization should work at $q^2_{\rm max}$, leaving the scaling with q^2 somewhat ambiguous, especially having in mind that the QCDSR are reliable in the low q^2 region, i.e. at maximum hadronic recoil. The authors thus claim that their results can be considered to represent the upper bounds in the QCDSR approach.

Table 5.3: Form factor predictions at $q^2 = 0$ in various models.

Form Factor	QCDSR this work	QCDSR [132]	LCSR [133]	CCQM [184, 234]	pQCD [235]	RQM [104]	RQM [105]	LFQM [138]	SMD [236]	QCDSR [237]	BSW [238]
$f_{+,0}^{D^0}(q^2=0)$	0.16 ± 0.02	0.32	0.35	0.19	0.19(7)	0.14	0.14	0.16(4)	0.15	0.13(5)	0.08
$V^{D^*}(q^2=0)$	0.27 ± 0.04	1.66	0.57	0.23	0.25(11)	0.18	0.17	0.13(3)	0.22	0.25(8)	0.16
$A_1^{D^*}(q^2=0)$	0.17 ± 0.03	0.43	0.32	0.14	0.18(8)	0.17	0.10	0.08(2)	0.15	0.11(4)	0.10
$A_2^{D^*}(q^2=0)$	0.17 ± 0.03	0.51	0.57	0.15	0.20(8)	0.19	0.11	0.07(2)	0.13	0.17(8)	0.11
$A_0^{D^*}(q^2=0)$	0.17 ± 0.04	0.35	-	0.13	0.17(7)	0.14	0.09	0.09(2)	0.16	-	0.08

5.1.2. Extrapolation to high q^2

Considering the fact that the QCDSR method is reliable only in the low q^2 region, the form factors are calculated at several q^2 values for $0 \leq q^2 \leq 10$ GeV^2, extrapolated to high q^2 region using the BCL approach [129] and then compared to the BGL [127, 128] one. Traditionally, one would choose $t_* = t_+ = (m_{B_c} + m_{D^{(*)}})^2$ and then compensate for all the resonances beneath t_*. Then, one would assume that the two-particle contributions to the form factor (seen as branch cuts beneath t_*) are negligible, even though there might be plenty. In this case, however, it turns

out to be beneficial to use $t_* = (m_{B^{(*)}} + m_\eta)^2$ for $B_c \to D$ semileptonic decays and $t_* = (m_{B^{(*)}} + m_\rho)^2$ for $B_c \to D^*$ semileptonic decays, for then there is a maximum of two resonances contributing to a single form factor which are then removed by the Blaschke factor in the BGL parametrization or by the standard pole dependence of form factors in the BCL parametrization. This strategy was first employed in Ref. [142] for the $B_c \to J/\psi$ decay, where the lowest multiparticle threshold of was chosen for t_*. Here, there are still branch cuts contributing below t_*, e.g. the one starting at $\bar{B}\pi$ pair production threshold. However, this branch cut is closer to $q^2_{\rm max}$, so to be on the safe side, the next two-particle production threshold is used.

The fitting function is then expanded in a power series in z multiplied by a function compensating for the poles, which is for the two cases inspected here given as

$$F_i^{\rm BGL}(z) = \frac{1}{B_i(z)\phi_i(z)} \sum_{k=0}^{\infty} a_k z^k\,, \qquad F_i^{\rm BCL}(z) = \frac{1}{P_i(z)} \sum_{k=0}^{\infty} b_k z^k\,, \tag{5.14}$$

where $F_i^{\rm BGL}(z)$ are the helicity form factors defined as

$$\begin{aligned} g(z) &= \frac{2}{m_{B_c} + m_{D^*}} V(z); \quad f(z) = (m_{B_c} + m_{D^*}) A_1(z); \quad \mathcal{F}_2(z) = 2A_0(z); \\ \mathcal{F}_1(z) &= \frac{1}{m_{D^*}} \Big[- \frac{\lambda(m_{B_c}, m_{D^*}, q^2)}{m_{B_c} + m_{D^*}} A_2(z) - \frac{1}{2}(q^2 - m_{B_c}^2 + m_{D^*}^2)(m_{B_c} + m_{D^*}) A_1(z) \Big] \end{aligned} \tag{5.15}$$

for the vector particle and

$$f_0^{\rm BGL}(q^2) = (M_{B_c}^2 - M_D^2) f_0(q^2) \tag{5.16}$$

for the pseudoscalar one, whereas for $F_i^{\rm BCL}(z)$ the WS form factor basis is used and the functions

$$B_i(z) = \prod_{R=1}^{n} \frac{z - z(m_R^2, t_0)}{1 - z z(m_R^2, t_0)} \quad \text{and} \quad P_i(z) = \prod_{R=1}^{n} \left(1 - \frac{q^2(z)}{m_R^2}\right) \tag{5.17}$$

account for n resonances of masses m_R below the threshold. One can notice that in the original BCL paper authors used the fact that the derivative of the form factor

vanishes at $q^2 = t_+$, which is a consequence of angular momentum conservation, and expression-wise relies on the fact that $z(q^2 = t_+) = -1$, which isn't the case here, since here $t_* \neq t_+$. Therefore, this fact is not utilized and the parametrization is kept in its more simple form. The form factors in the helicity basis are used in the case of fitting to the BGL function, since in this basis unitarity relations are diagonalized and the $\phi_i(z)$ functions are readily available. The latter are calculable perturbatively and have been known for a long time now [128, 142].

A final comment concerns the parameter t_0. Here the value that optimizes the fit in the sense that it reduces the possible error originating from truncating the series in eq. (5.14) was chosen. This is achieved for $z(0, t_0) = -z(q^2_{\rm max}, t_0)$, which lowers the overall maximum value of z, and thus $|z_{\rm max}| \approx 0.106$.

The resonances entering eq. (5.17) are listed in table 5.4. For $m_{B^{(*)}}$ the experimentally well established values were used, while for the other resonances values obtained by a recently updated quark model [239] were used.

Table 5.4: Summary of the fits for $B_c \to D$ and $B_c \to D^*$ form factors.

J^P	threshold	m_R [GeV]	BGL:	a_0	a_1	$\chi^2[10^{-2}]$	BCL:	b_0	b_1	$\chi^2[10^{-2}]$
1^-	$B\eta$	5.32	f_+	0.0087	-0.032	0.1	f_+	0.23	-0.7	4
0^+	$B\eta$	5.76	$f_0^{\rm BGL}$	0.019	-0.07	5	f_0	0.18	-0.2	0.8
1^-	$B^*\rho$	5.32, 5.93	g	0.019	-0.04	1	V	0.25	0.2	0.9
1^+	$B\rho$	5.78, 5.78	f	0.0055	-0.01	2	A_1	0.11	0.5	4
1^+	$B\rho$	5.78, 5.78	$\mathcal{F}_1$	0.0010	-0.003	0.6	A_2	0.16	-0.1	6
0^-	$B\rho$	5.28, 5.91	$\mathcal{F}_2$	0.022	-0.05	0.5	A_0	0.12	0.3	20

For the $B_c \to D$ transition the form factors are related to each other at the maximum recoil point, so the fit is done simultaneously, and the error covariance

matrix, defined as

$$\left(\mathcal{M}_{f_{+,0}}\right)_{ij} = \mathrm{cov}[\theta_i, \theta_j] \tag{5.18}$$

with vectors in this case being $\vec{\theta} = (b_0^{f_+}, b_1^{f_+}, b_0^{f_0})^T$, is

$$\mathcal{M}_{f_{+,0}^{B_c\to D}} = \begin{bmatrix} 0.000531195 & -0.00492472 & 1.48099 \times 10^{-7} \\ -0.00492472 & 0.0536992 & -0.0000114013 \\ 1.48099 \times 10^{-7} & -0.0000114013 & 0.000313175 \end{bmatrix}, \tag{5.19}$$

where the fourth expansion parameter has been fixed using the fact that $f_+(0) = f_0(0)$ as

$$b_1^{f_0} = \frac{b_0^{f_+} - b_0^{f_0}}{z(0)} + b_1^{f_+}\,. \tag{5.20}$$

In the case of $B_c \to D^*$ transition the form factors aren't related so that the vectors entering the covariance look like $\vec{\theta} = (b_0^{\mathrm{F}}, b_1^{\mathrm{F}})^T$, with $\mathrm{F} = \{V, A_{\{1,2,0\}}\}$, and

$$\begin{aligned} \mathcal{M}_{V^{B_c\to D^*}} &= \begin{bmatrix} 0.0033 & -0.0359 \\ -0.0359 & 0.9093 \end{bmatrix}, \quad \mathcal{M}_{A_1^{B_c\to D^*}} = \begin{bmatrix} 0.0004 & -0.0033 \\ -0.0033 & 0.1650, \end{bmatrix} \\ \mathcal{M}_{A_2^{B_c\to D^*}} &= \begin{bmatrix} 0.0002 & -0.0007 \\ -0.0007 & 0.1006 \end{bmatrix}, \quad \mathcal{M}_{A_0^{B_c\to D^*}} = \begin{bmatrix} 0.0013 & -0.0145 \\ -0.0145 & 0.3363 \end{bmatrix}. \end{aligned} \tag{5.21}$$

In $B_c \to D^{(*)}$ decays, being $b \to u$ transitions, the parameter $|z_{\max}|$ in the form factor q^2-expansion is somewhat larger, and the functions $|\phi_i(z)_{\min}|$ are smaller than in typical $b \to c$ transitions. One would need to go to higher order in z to reduce the truncation error - which would be unusable here, since no high-q^2 points are available to impose bounds on parameters of the fit multiplying higher orders in z. Actually adding higher orders of z to the fit function only marginally changes its central shape, which is mostly witnessed through the central value of $f_+^{\mathrm{fit}}(q^2_{\max})$, which changes at most by $\sim 10\%$ and always stays inside the uncertainties of the linear z fit. Using $f_+(q^2)$ as a benchmark, the difference of the two fitting procedures is made obvious in figure 5.2, where one can see that compensating multiple resonances using a

multipole function $P_i(q^2)$ can be a bit more violent, driving the fit towards higher form factor values.

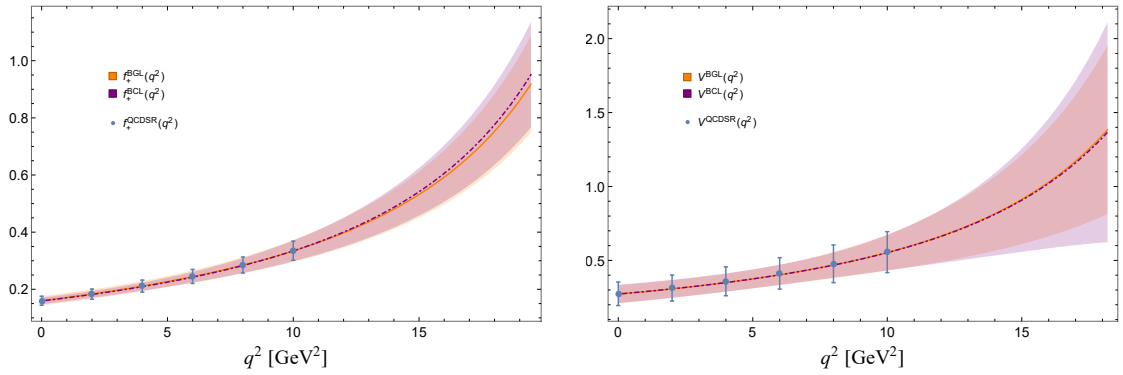

Figure 5.2: The BGL (purple, dot-dashed line) and BCL (orange, full line) fits to the QCDSR values of $f_+(q^2)$ and $V(q^2)$.

Knowing that traditionally (in $B \to \pi$, $B \to D^{(*)}$ decays) sum rules undervalue the form factors' value at zero-recoil, one is tempted to use the fit that reproduces higher values of zero-recoil form factors, even if this is somewhat less faithful to our QCDSR results in terms of χ^2, defined for the $i-$th form factor as

$$\chi_i^2 = \sum_j \frac{[F_i^{\text{fit}}(q_j^2) - F_i^{\text{QCDSR}}(q_j^2)]^2}{[\sigma_{F_i}^2(q_j^2)]^2}. \tag{5.22}$$

In the fits presented here this turns out to be the case when the more simple BCL choice of parametrization is adopted, which is consequently the one used in the following phenomenological analysis from now on. The difference anyways turns out to be almost negligible for all of the form factors.

In figure 5.3 the q^2-dependence of form factors used further in the analysis is presented. One can notice that the $B_c \to D^*$ form factors come with a larger uncertainty, which stems from the fact that the value of f_{D^*} decay constant is more uncertain than that of f_D, in both lattice and our fitted results, see table 5.1. In figure 5.4 a comparison of the QCDSR prediction for $f_+(q^2)$ to two quark models is shown, namely the constituent quark model, CCQM [234] and the light quark model, LFQM [138], where a good agreement among results can be noticed, despite the difference in approaches to their calculation.

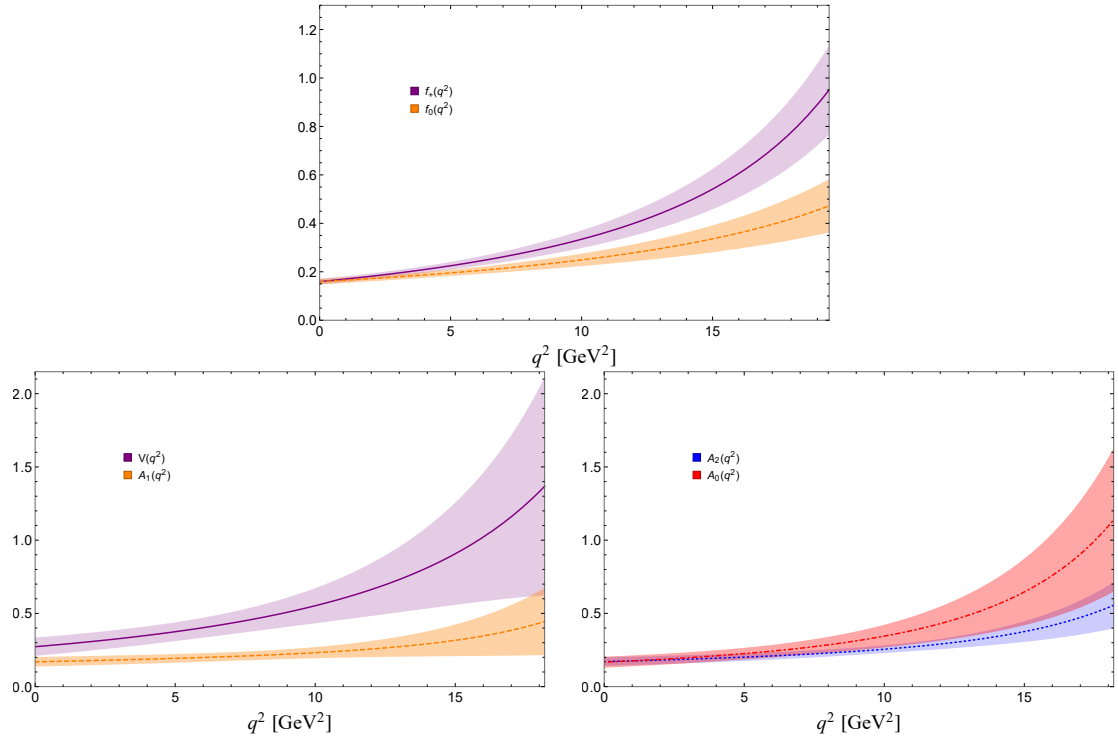

Figure 5.3: Final predictions for $B_c \to D^{(*)}$ form factors obtained by extrapolating 3ptSR results to higher q^2 regions by using the BCL parametrizations.

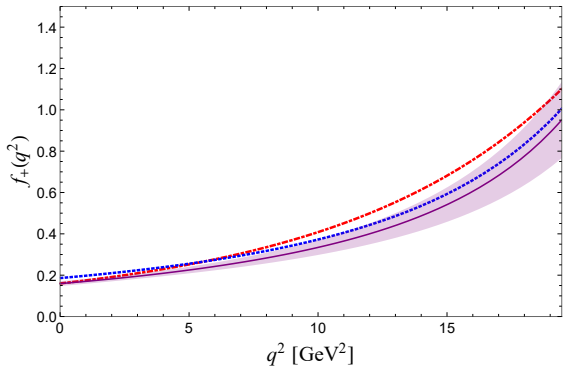

Figure 5.4: The purple solid line and the area represents the QCDSR result from this work for $f_+(q^2)$ form factor with errors; the blue dashed-line is the CCQM prediction [234], while the red dash-dotted one is the LFQM prediction [138].

5.1.3. A comment on correlations between pseudo data points

When minimizing χ^2 in the fitting procedure the pseudo data points were chosen to be uncorrelated. This is a rather strong assumption, and stems from the fact that the correlations are hard to be determined exactly. In order to estimate the effect the correlation might have on the form factor uncertainties and observables, first a

new $\tilde{\chi}^2$ to be minimized is defined, namely,

$$\tilde{\chi}_i^2 \equiv [F_i(q_a^2;\vec{\theta}) - F_i^{\rm QCDSR}(q_a^2)]\big(\Sigma^{-1}\big)_{ab}[F_i(q_b^2;\vec{\theta}) - F_i^{\rm QCDSR}(q_b^2)]. \tag{5.23}$$

For the first estimate of $\tilde{\chi}_i^2$ the points are correlated rather crudely, by introducing the covariance

$$\Sigma_{ij} \equiv (1-x)\cdot s_i s_j \delta_{ij} + x\cdot s_i s_j\,, \tag{5.24}$$

where x describes the correlation, varied between $50\% - 90\%$, while s_i are the errors of the parameters arising from the QCDSR calculation. The effect this arbitrary correlation has on the goodness of fit is that (as expected) $\tilde{\chi}^2$ is now much larger, $\tilde{\chi}^2 \approx [2-10]\cdot\chi^2$. The integrated decay rates remain at the same level of uncertainty. The observables defined as ratios have much smaller uncertainties (as expected, since they cancel to a larger extent in the ratio), while the form factors and differential decay rates have larger uncertainties in the q^2 region below ~ 8 GeV^2, and somewhat smaller uncertainties in the upper q^2 region.

For a more nuanced assesement of the pseudo data correlations the Jacobian $\mathcal{J}$ is numerically estimated for each form factor. It is a 11×6 matrix (11 pseudo data points and 6 parameters), with which a "raw" covariance matrix is calculated by

$$\Sigma = \mathcal{J}^T P \mathcal{J}, \tag{5.25}$$

where P is a 6×6 diagonal matrix containing the errors in the parameters (the parameters themselves are assumed to be uncorrelated). The covariance matrix used when minimizing $\tilde{\chi}^2$ is estimated then by

$$\tilde{\Sigma} = \sigma^T \rho\, \sigma, \tag{5.26}$$

where ρ is the correlation matrix obtained from Σ, and σ is a vector containing the QCDSR errors of the pseudo data points.

Globally, now the $\tilde{\chi}^2$ grows to an even larger value, $\tilde{\chi}^2 \approx 20\cdot\chi^2$. The effect this has on the net uncertainties of the quantities presented in this paper is the same as described above, only to a larger extent. In particular, for the correlated case

the lower q^2 region have now larger uncertainties, while in the upper q^2 region the errors become smaller, as compared with the uncorrelated case, as is witnessed in figure 5.5. This is taken into consideration when the $|V_{ub}|$ determination prospect is

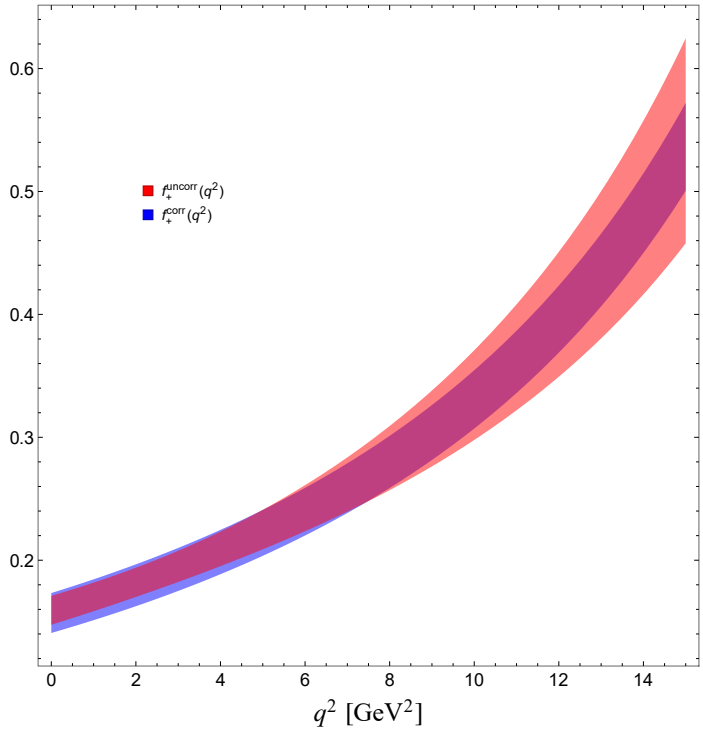

Figure 5.5: Comparison of the uncorrelated fit with the correlated one.

presented.

It should be stressed again that all the central values of the fit parameters remain the same, regardless of the treatment of the correlations between pseudo data.

5.2. Phenomenology

The definition of the two-fold differential decay width is given in eq. (4.51), which reduces to the differential decay width by explicitly integrating over $\cos\theta_\ell$, or, specifically in the case of $B_c \to D^0\ell\bar{\nu}_\ell$,

$$\begin{aligned}\frac{\mathrm{d}\Gamma(B_c \to D^0\ell\bar{\nu}_\ell)}{\mathrm{d}q^2} = \frac{G_F^2|V_{ub}|^2 q^2}{192\pi^3 m_{B_c}^3}\sqrt{\lambda(m_{B_c}^2, m_{D^0}^2, q^2)}\;\left(1-\frac{m_l^2}{q^2}\right)^2\times \\ \left(\times\left[\;1+\frac{m_l^2}{2q^2}\right)|h_0(q^2)|^2 + \frac{3m_l^2}{2q^2}|h_t(q^2)|^2\right],\end{aligned} \tag{5.27}$$

whereas for the case of $B_c \to D^*\ell\bar{\nu}_\ell$

$$\begin{aligned}\frac{\mathrm{d}\Gamma(B_c \to D^*\ell\bar{\nu}_\ell)}{\mathrm{d}q^2} = \frac{G_F^2|V_{ub}|^2 q^2}{192\pi^3 m_{B_c}^3}\sqrt{\lambda(m_{B_c}^2, m_{D^*}^2, q^2)}\;\left(1-\frac{m_l^2}{q^2}\right)^2\times \\ \left(\times\left[\;1+\frac{m_l^2}{2q^2}\right)(|H_+(q^2)|^2 + |H_-(q^2)|^2 + |H_0(q^2)|^2) + \frac{3}{2}\frac{m_l^2}{q^2}|H_t(q^2)|^2\right],\end{aligned} \tag{5.28}$$

with a new set of helicity form factors, defined as

$$h_0(q^2) = \sqrt{\frac{\lambda(m_{B_c}^2, m_{D^0}^2, q^2)}{q^2}}f_+(q^2)\,, \qquad h_t(q^2) = \frac{m_{B_c}^2 - m_{D^0}^2}{\sqrt{q^2}}f_0(q^2), \tag{5.29}$$

and

$$\begin{aligned}H_\pm(q^2) &= -\mathrm{i}\left[\pm\frac{\sqrt{\lambda(m_{B_c}^2, m_{D^*}^2, q^2)}}{m_{B_c}+m_{D^*}}V(q^2) + (m_{B_c}+m_{D^*})A_1(q^2)\right], \\ H_0(q^2) &= -\frac{\mathrm{i}}{2m_{D^*}\sqrt{q^2}}\left[(m_{B_c}+m_{D^*})(m_{B_c}^2 - m_{D^*}^2 - q^2)A_1(q^2)\right. \\ &\qquad\left. - \frac{\lambda(m_{B_c}^2, m_{D^*}^2, q^2)}{m_{B_c}+m_{D^*}}A_2(q^2)\right], \\ H_t(q^2) &= -\mathrm{i}\frac{\sqrt{\lambda(m_{B_c}^2, m_{D^*}^2, q^2)}}{\sqrt{q^2}}A_0(q^2).\end{aligned} \tag{5.30}$$

This set of helicity form factors differs from the one defined in section 4.2.1 only through the choice of basis for the polarization vectors of the final state meson and lepton. The general definitions from appendix D still stand. However, since the helicity form factors relate to the WS basis form factors in a different way, the

relations are written up in this basis.

In both of these cases it is also beneficial to define the differential decay width as a sum of contributions of left and right lepton helicity projections along the z-axis

$$\begin{aligned}
\frac{\mathrm{d}\Gamma^-(B_c \to D^0 l\bar{\nu}_l)}{\mathrm{d}q^2} &= \frac{G_F^2|V_{ub}|^2 q^2}{192\pi^3 m_{B_c}^3}\sqrt{\lambda(m_{B_c}^2, m_{D^0}^2, q^2)}\left(1-\frac{m_l^2}{q^2}\right)^2 |h_0(q^2)|^2\,,\\
\frac{\mathrm{d}\Gamma^+(B_c \to D^0 l\bar{\nu}_l)}{\mathrm{d}q^2} &= \frac{G_F^2|V_{ub}|^2 q^2}{192\pi^3 m_{B_c}^3}\sqrt{\lambda(m_{B_c}^2, m_{D^0}^2, q^2)}\left(1-\frac{m_l^2}{q^2}\right)^2 \frac{m_l^2}{2q^2}\left[|h_0(q^2)|^2 + 3|h_t(q^2)|^2\right],
\end{aligned} \tag{5.31}$$

and

$$\begin{aligned}
\frac{\mathrm{d}\Gamma^-(B_c \to D^* l\bar{\nu}_l)}{\mathrm{d}q^2} &= \frac{G_F^2|V_{ub}|^2 q^2}{192\pi^3 m_{B_c}^3}\sqrt{\lambda(m_{B_c}^2, m_{D^*}^2, q^2)}\left(1-\frac{m_l^2}{q^2}\right)^2 \times\\
&\qquad \times \left[|H_+(q^2)|^2 + |H_-(q^2)|^2 + |H_0(q^2)|^2\right],\\
\frac{\mathrm{d}\Gamma^+(B_c \to D^* l\bar{\nu}_l)}{\mathrm{d}q^2} &= \frac{G_F^2|V_{ub}|^2 q^2}{192\pi^3 m_{B_c}^3}\sqrt{\lambda(m_{B_c}^2, m_{D^*}^2, q^2)}\left(1-\frac{m_l^2}{q^2}\right)^2 \frac{m_l^2}{2q^2}\times\\
&\qquad \times \left[|H_+(q^2)|^2 + |H_-(q^2)|^2 + |H_0(q^2)|^2 + 3|H_t(q^2)|^2\right],
\end{aligned} \tag{5.32}$$

so that it's obvious that $\Gamma = \Gamma^+ + \Gamma^-$. In the case of the D^* in the final state, one can look at both the longitudinal and the transverse D^* polarization contribution,

$$\begin{aligned}
\frac{\mathrm{d}\Gamma_L(B_c \to D^* l\bar{\nu}_l)}{\mathrm{d}q^2} &= \frac{G_F^2|V_{ub}|^2 q^2}{192\pi^3 m_{B_c}^3}\sqrt{\lambda(m_{B_c}^2, m_{D^*}^2, q^2)}\left(1-\frac{m_l^2}{q^2}\right)^2 \times\\
&\qquad \times\left[\left(1+\frac{m_l^2}{2q^2}\right)|H_0(q^2)|^2 + \frac{3}{2}\frac{m_l^2}{q^2}|H_t(q^2)|^2\right],\\
\frac{\mathrm{d}\Gamma_T(B_c \to D^* l\bar{\nu}_l)}{\mathrm{d}q^2} &= \frac{G_F^2|V_{ub}|^2 q^2}{192\pi^3 m_{B_c}^3}\sqrt{\lambda(m_{B_c}^2, m_{D^*}^2, q^2)}\left(1-\frac{m_l^2}{q^2}\right)^2 \times\\
&\qquad \times\left(1+\frac{m_l^2}{2q^2}\right)\left[|H_+(q^2)|^2 + |H_-(q^2)|^2\right],
\end{aligned} \tag{5.33}$$

respectively, where again $\Gamma = \Gamma_L + \Gamma_T$.

Predictions for integrated decay rates of both decays using the QCDSR form factors from section 5.1.2 are given in table 5.5.

Table 5.5: Decay widths of $B_c \to D^{0,*}$ decays, given in 10^{-18} GeV using the PDG average value of $|V_{ub}|$ [4]

Mode	This work	[102]	[132]	[133]	[184]	[138]	[235]	[104]	[134]	[105]	[135]
$\Gamma(B_c \to D^0 l\bar{\nu}_l)$	31 ± 6	51	59	293	43	43	46	19	26	20	49
$\Gamma(B_c \to D^0 \tau\bar{\nu}_\tau)$	21 ± 4	31	32	219	27	30	32	-	-	-	-
$\Gamma(B_c \to D^* l\bar{\nu}_l)$	85 ± 33	56	270	512	78	64	160	110	53	34	192
$\Gamma(B_c \to D^* \tau\bar{\nu}_\tau)$	46 ± 20	32	120	293	44	39	94	-	-	-	-

In Fig.5.6 the partial differential decay rates are given in units of $|V_{ub}|$ GeV^{-1}. It is obvious that one can achieve the satisfactory precision for $B_c \to Dl\bar{\nu}_l$ decays, while the theoretical errors in the $B_c \to D^*$ form factors and uncertainties in the B_c and D^* decay constants drive predictions for $B_c \to D^*\ell\bar{\nu}_\ell$ to be quite uncertain.

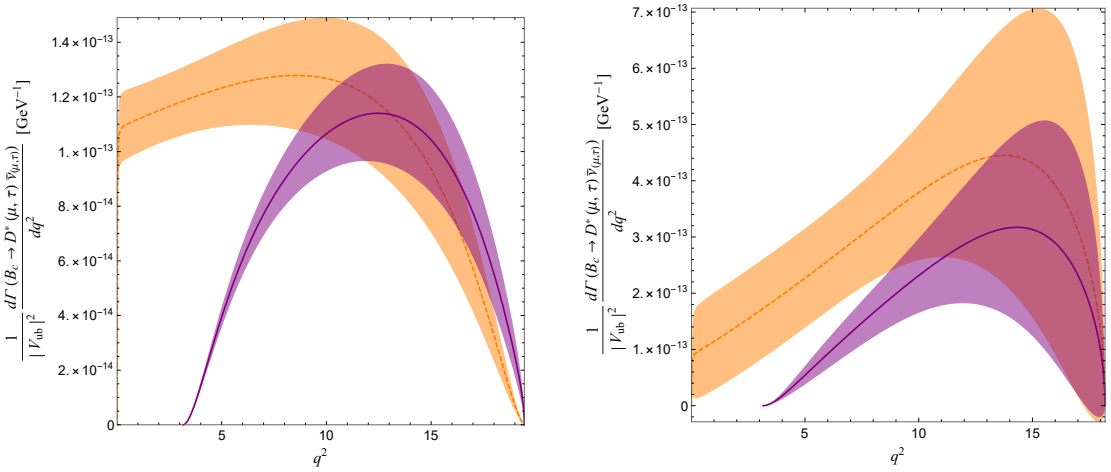

Figure 5.6: Partial differential decay rates with errors of B_c semileptonic transitions to D (left), and to D^* (right), where the orange solid-line/area corresponds to μ in the final state, and the purple dashed-line/area to the case with τ final state.

5.2.1. Lepton flavor universality ratios

Both experimentally and theoretically, due to the cancellations of systematic hadronic uncertainties, it is preferable to extract the ratios

$$\begin{aligned} R_c(D^0) &\equiv \frac{\mathcal{B}(B_c \to D^0 \tau \bar{\nu}_\tau)}{\mathcal{B}(B_c \to D^0 \mu \bar{\nu}_\mu)} = 0.64 \pm 0.05, \\ R_c(D^*) &\equiv \frac{\mathcal{B}(B_c \to D^* \tau \bar{\nu}_\tau)}{\mathcal{B}(B_c \to D^* \mu \bar{\nu}_\mu)} = 0.55 \pm 0.05, \end{aligned} \tag{5.34}$$

that is - ratios of branching fractions of semileptonic decays including a τ lepton in a final state to the branching fractions including a muon in a final state. Once measured, the ratios in eq. (5.34) will serve as an additional test of the lepton flavour universality in B_c decays. Considering this ratio, it can be noticed that although the models discussed in e.g. [133], [132], [102, 184, 234], and [235] apply different approaches in the calculation of the form factors, we agree well with the predictions of [102,184,234,235] for the ratios $R_c(D^0)$ and $R_c(D^*)$, and quite disagree with [132]. One can also notice that, in spite of the huge difference between the form factors presented here and decay width values and the ones reported in [133] the values presented here still agree quite well on the $R_c(D^*)$ value, while the $R_c(D^0)$ from the aforementioned publication seems to be somewhat larger. The main disagreement with the results presented here is visible when it is compared with the previous 3ptSR calculation of [132]. There, the authors accounted for Coulomb interactions which were modeled to be very large and consequently drive the $B_c \to D^{(*)}$ form factors to large values, hardly compatible with any of the models above. The origin of the discrepancy was already discussed, above table 5.3. Here, the reader is reminded that these corrections, aside from enlarging the form factor magnitudes, might also alter their q^2 scaling - which in turn might impact the ratios significantly. Also, the decay constants used in [132] (not precisely known at the time) are significantly smaller, which additionally increased their results.

The q^2 distributions of differential forms of $\mathrm{d}R_c(D^0)$ and $\mathrm{d}R_c(D^*)$ (which are just ratios of partial differential decay rates, as opposed to integrated rates) are shown in figure 5.7.

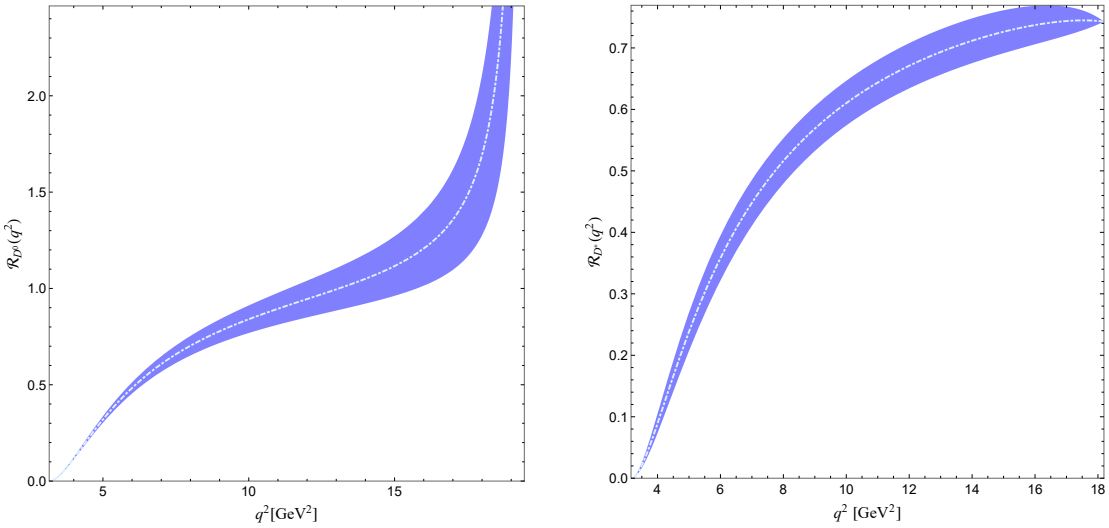

Figure 5.7: Ratios of differential partial decay rates B_c semileptonic transitions to D (left), and to D^* (right) with tau in the final state to the case with muon in the final state.

5.2.2. Angular observables in $B_c \to D^{(*)}\ell\bar{\nu}_\ell$

Further on, three independent angular observables are written up in the helicity basis from eq. (5.29) and (5.30) for the decay $B_c \to D^0\ell\bar{\nu}_\ell$, namely the forward-backward asymmetry $A_{\rm FB}^{D^0,\ell}(q^2)$, the polarization asymmetry of the lepton l, $P^{D^0,\ell}(q^2)$, and the so-called convexity parameter $C_F^{D^0,\ell}(q^2)$ as:

$$\begin{aligned}
\frac{\mathrm{d}}{\mathrm{d}q^2}A_{\rm FB}^{D^0,\ell}(q^2) &= \frac{3m_l^2}{2q^2}\frac{\mathrm{Re}\big[h_0(q^2)h_t^*(q^2)\big]}{\big(1+\frac{m_l^2}{2q^2}\big)|h_0(q^2)|^2+\frac{3m_l^2}{2q^2}|h_t(q^2)|^2},\\
\frac{\mathrm{d}}{\mathrm{d}q^2}P^{D^0,\ell}(q^2) &= \frac{\frac{m_\ell^2}{2q^2}\big[|h_0(q^2)|^2+3|h_t(q^2)|^2\big]-|h_0(q^2)|^2}{\frac{m_\ell^2}{2q^2}\big[|h_0(q^2)|^2+3|h_t(q^2)|^2\big]+|h_0(q^2)|^2},\\
\frac{\mathrm{d}}{\mathrm{d}q^2}C_F^{D^0,\ell}(q^2) &= \frac{3}{2}\frac{|h_0(q^2)|^2\big(\frac{m_\ell^2}{q^2}-1\big)}{\big(1+\frac{m_\ell^2}{2q^2}\big)|h_0(q^2)|^2+\frac{3m_\ell^2}{2q^2}|h_t(q^2)|^2}.
\end{aligned} \tag{5.35}$$

The arbitrary choice of the lepton angle can change the sign of the forward-backward asymmetry, so one should be careful when referring to its definition. In figure 5.8 the above observables are plotted just for the case with the τ lepton in the final state, since the asymmetries with light leptons in the final state are basically constant in the entire q^2 range (with the exception of extreme upper and lower

kinematical limits)

$$\frac{\mathrm{d}}{\mathrm{d}q^2}A_{\mathrm{FB}}^{D^0,\,\mu/e}(q^2) \approx 0\,, \qquad \frac{\mathrm{d}}{\mathrm{d}q^2}P^{D^0,\,\mu/e}(q^2) \approx -1\,, \qquad \frac{\mathrm{d}}{\mathrm{d}q^2}C_F^{D^0,\,\mu}(q^2) \approx -\frac{3}{2}\,. \quad (5.36)$$

For the case of $B_c \to D^*\ell\bar{\nu}_\ell$ we similarly have

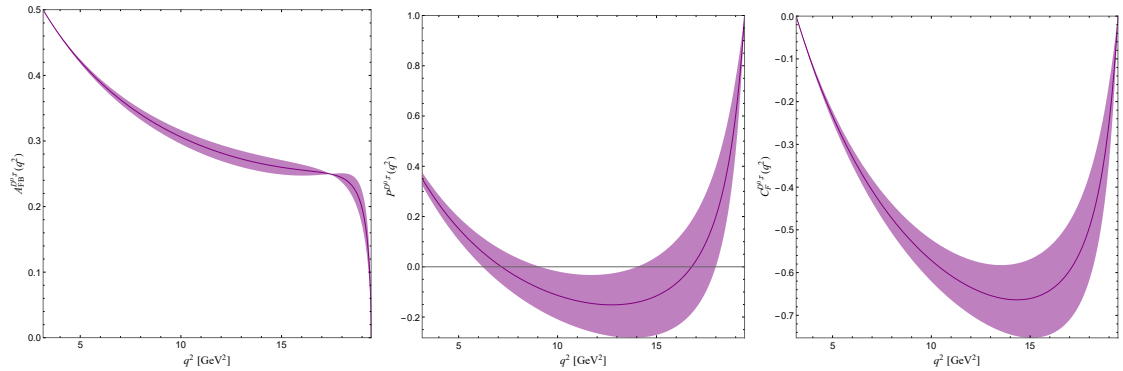

Figure 5.8: Angular observables defined in eq. (5.35) for $B_c \to D^0\tau\bar{\nu}_\tau$.

$$\begin{aligned}
&\frac{\mathrm{d}}{\mathrm{d}q^2}A_{\mathrm{FB}}^{D^*,\,\ell}(q^2) \\
&\quad = -\frac{3}{4}\frac{|H_+(q^2)|^2 - |H_-(q^2)|^2 - 2\frac{m_\ell^2}{q^2}\mathrm{Re}\big[H_0(q^2)H_t^*(q^2)\big]}{(|H_+(q^2)|^2 + |H_-(q^2)|^2 + |H_0(q^2)|^2)\big(1+\frac{m_\ell^2}{2q^2}\big) + \frac{3}{2}\frac{m_\ell^2}{q^2}|H_t(q^2)|^2}\,, \\
&\frac{\mathrm{d}}{\mathrm{d}q^2}P^{D^*,\,\ell}(q^2) \\
&\quad = -1 + \frac{m_\ell^2}{q^2}\frac{|H_+(q^2)|^2 + |H_-(q^2)|^2 + |H_0(q^2)|^2 + 3|H_t(q^2)|^2}{(|H_+(q^2)|^2 + |H_-(q^2)|^2 + |H_0(q^2)|^2)\big(1+\frac{m_\ell^2}{2q^2}\big) + \frac{3}{2}\frac{m_\ell^2}{q^2}|H_t(q^2)|^2}\,, \\
&\frac{\mathrm{d}}{\mathrm{d}q^2}C_F^{D^*,\,\ell}(q^2) \\
&\quad \left(= \frac{3}{4}\;\;1 - \frac{m_\ell^2}{q^2}\right)\frac{|H_+(q^2)|^2 + |H_-(q^2)|^2 - 2|H_0(q^2)|^2}{(|H_+(q^2)|^2 + |H_-(q^2)|^2 + |H_0(q^2)|^2)\big(1+\frac{m_\ell^2}{2q^2}\big) + \frac{3}{2}\frac{m_\ell^2}{q^2}|H_t(q^2)|^2}\,, \\
&\frac{\mathrm{d}}{\mathrm{d}q^2}F_L^{D^*,\,l}(q^2) = \frac{|H_0(q^2)|^2 + 3|H_t(q^2)|^2/(1+\frac{2q^2}{m_\ell^2})}{|H_+(q^2)|^2 + |H_-(q^2)|^2 + |H_0(q^2)|^2 + 3|H_t(q^2)|^2/(1+\frac{2q^2}{m_\ell^2})}\,,
\end{aligned} \quad (5.37)$$

where in addition we compute the longitudinal polarization fraction of D^*, $F_L^{D^*}$, in the decay. The results for these observables are shown in Figure 5.9. Similarly to

the prior case one observable is approximately constant

$$\frac{\mathrm{d}}{\mathrm{d}q^2} P^{D^*,\mu/e}(q^2) \approx -1 \tag{5.38}$$

and it it not shown there. Values of $B_c \to D^*$ angular observables integrated separately in the numerator and the denominator are given in table 5.6. Again, proving that these observables are relatively independent of the hadronic form factors, good agreement with the recent analysis provided in [240], where the LFQM form factors from [138] are used, is found.

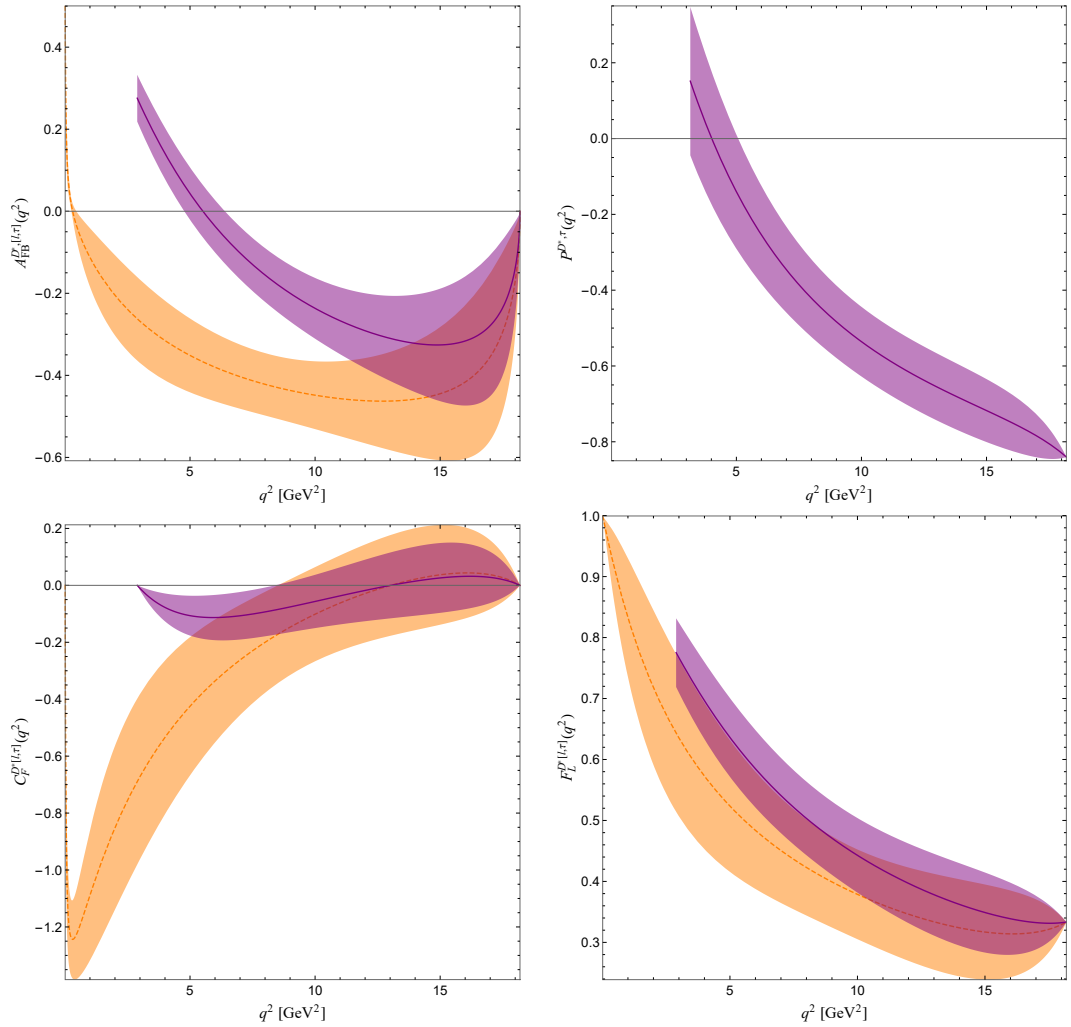

Figure 5.9: Angular observables defined in eq. (5.37) with errors for $B_c \to D^*(l,\tau)\bar{\nu}_{(l,\tau)}$, where now l stands for light leptons, a case depicted by a dashed-line/area in orange, whereas the case with the final τ state is depicted in purple.

Table 5.6: Angular observables integrated over the entire kinematic region.

	$l=\mu$	$l=\tau$		$l=\mu$	$l=\tau$
$A_{\rm FB}^{D^*,l}$	-0.4 ± 0.2	-0.3 ± 0.2	$A_{\rm FB}^{D^0,l}$	≈ 0	0.30 ± 0.06
$P^{D^*,l}$	≈ -1	-0.6 ± 0.4	$P^{D^0,l}$	≈ -1	-0.1 ± 0.1
$C_F^{D^*,l}$	-0.2 ± 0.2	-0.02 ± 0.08	$C_F^{D^0,l}$	$\approx -\frac{3}{2}$	-0.6 ± 0.1
$F_L^{D^*,l}$	0.4 ± 0.2	0.4 ± 0.3	-	-	-

5.3. Exclusive $|V_{ub}|$ determination and the $|V_{ub}|/|V_{cb}|$ ratio

A proposal to determine $|V_{ub}|$ by measuring the decay width of $B_c \to D\mu\bar{\nu}_\mu$ is put forward in this section. An estimate is presented for

$$\zeta_{D^0}|V_{ub}|^2 \equiv \Gamma(B_c \to D^0\mu\bar{\nu}_\mu) \tag{5.39}$$

as

$$\zeta_{D^0} = (2.0 \pm 0.3) \times 10^{-3}\,\text{eV}\,. \tag{5.40}$$

Combining the predictions from table 5.5 with the future experimental data, the $|V_{ub}|$ can be determined from $B_c \to D^0\mu\nu$ with the theoretical uncertainty of $\mathcal{O}(10\%)$. By calculating the same for the semileptonic $B_c \to D^*\mu\nu$ decay,

$$\begin{aligned} \zeta_{D^*}|V_{ub}|^2 &\equiv \Gamma(B_c \to D^*\mu\bar{\nu}_\mu), \\ \zeta_{D^*} &= (5 \pm 2) \times 10^{-3}\,\text{eV}\,, \end{aligned} \tag{5.41}$$

it is obvious that in this case the error is much larger and amounts to $\mathcal{O}(20\%)$, which makes this decay at present less suitable for the $|V_{ub}|$ determination. Gaining a little insight into the size of α_s corrections might prove to justify correlating the QCDSR pseudo data and performing a real Bayesian analysis. This would deem both of these decays very interesting in terms of $|V_{ub}|$ determination.

In figure 5.10 $|V_{ub}|$ dependence on the decay rate is presented using the value of ζ_{D^0} quoted in eq. (5.40). It is clear that if the decay rate can be measured with $10-20\%$ accuracy, as expected in the LHCb Run II [241], then the $B_c \to D^0$ might prove a powerful channel for the exclusive extraction of $|V_{ub}|$.

Also given here is the value for

$$\Delta\zeta_{D^0}(q_1^2, q_2^2) \equiv \frac{1}{|V_{ub}|^2}\int_{q_1^2}^{q_2^2} dq^2 \frac{d\Gamma(B_c \to D^0\mu\bar{\nu}_\mu)}{dq^2}, \tag{5.42}$$

which, employing the predicted QCDSR $B_c \to D^0$ form factor $f^+(q^2)$ from the 3ptSR at $m_{\mu^2} \leq q^2 \leq 10$ GeV^2, figure 5.2, amounts to

$$\Delta\zeta_{D^0}(m_\mu^2, 10\ \text{GeV}^2) = (1.2 \pm 0.1 \pm 0.1) \times 10^{-3}\,\text{eV}\,, \tag{5.43}$$

where an additional 10% uncertainty has been added, which is the error estimate stemming from the correlations between the QCDSR pseudo data points in the low q^2 region. Also presented are the the other bins of $\Delta\zeta_{D^0}(q_1^2, q_2^2)$, which can be used together with future experimental data to determine $|V_{ub}|$ from $B_c \to D^0\mu\bar{\nu}_\mu$ decays in table 5.7.

Table 5.7: Distribution of $\Delta\zeta_{D^0}(q_1^2, q_2^2)$ placed in bins spaced by 2 GeV apart.

$[q_1^2 - q_2^2]$ [GeV^2]	$[m_\mu^2 - 2]$	[2-4]	[4-6]	[6-8]	[8-10]	[10-12]	[12-14]	[14-16]	[16-18]	[18-q^2_{max}]
$\Delta\zeta_{D^0}(q_1^2, q_2^2)$ [10^{-4} eV]	2.2	2.4	2.5	2.5	2.6	2.5	2.3	1.9	1.1	0.21
	±0.2	±0.2	±0.3	±0.3	±0.4	±0.5	±0.5	±0.5	±0.3	±0.06

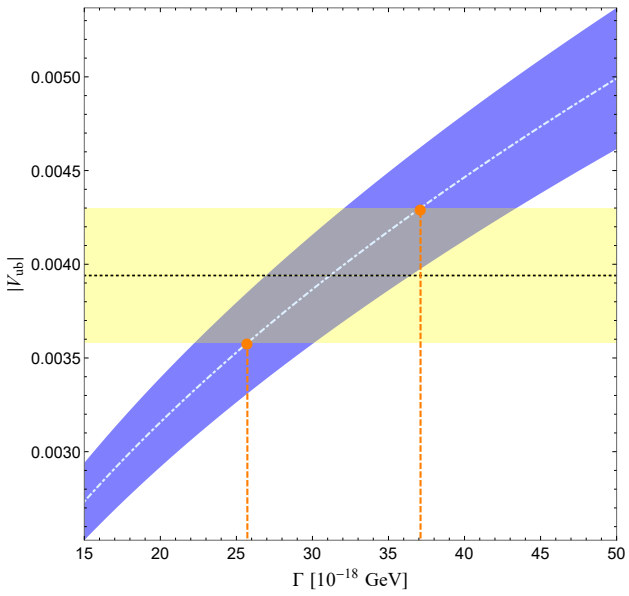

Figure 5.10: The prospect for $|V_{ub}|$ determination from $\Gamma(B_c \to D\mu\bar{\nu}_\mu)$; the yellow band represents the PDG value of $|V_{ub}|$.

5.3.1. The $|V_{ub}|/|V_{cb}|$ ratio

The theoretical error of 7.5% in eq. (5.40) might be improved by explicitly adding the α_s-corrections to the 3ptSR, which would certainly reduce the main systematic theoretical uncertainty of adjusting s_0 sum rule parameter. In order to suppress the unknown systematic uncertainty in the estimation of $|V_{ub}|$ arising from the method itself, here defined is the ratio of branching fractions

$$\mathcal{R}_{D^0 J/\psi} \equiv \frac{\zeta_{D^0}(q^2_{\min_1}, q^2_{\max_1})}{\zeta_{J/\psi}(q^2_{\min_2}, q^2_{\max_2})} = \left(\frac{|V_{ub}|^2}{|V_{cb}|^2}\right)^{-1} \frac{\int_{q^2_{\min_1}}^{q^2_{\max_1}} \frac{\mathrm{d}\Gamma(B_c \to D^0 \mu \bar{\nu}_\mu)}{\mathrm{d}q^2} \mathrm{d}q^2}{\int_{q^2_{\min_2}}^{q^2_{\max_2}} \frac{\mathrm{d}\Gamma(B_c \to J/\psi \mu \bar{\nu}_\mu)}{\mathrm{d}q^2} \mathrm{d}q^2}\,, \tag{5.44}$$

where the form factors entering $\mathrm{d}\Gamma(B_c \to J/\psi \mu \bar{\nu}_\mu)/\mathrm{d}q^2$ are known to some extent from lattice calculation [55, 148], and are reproduced to a satisfactory precision by the QCDSR method. The form factors for $B_c \to J/\psi$ transition were already briefly presented in [3]. Here the used parameters differ a little from ones used there, due to a necessary update. The specific values of parameters used in the calculation are listed in table 5.8, and the form factors are given in figure 5.12. Also experi-

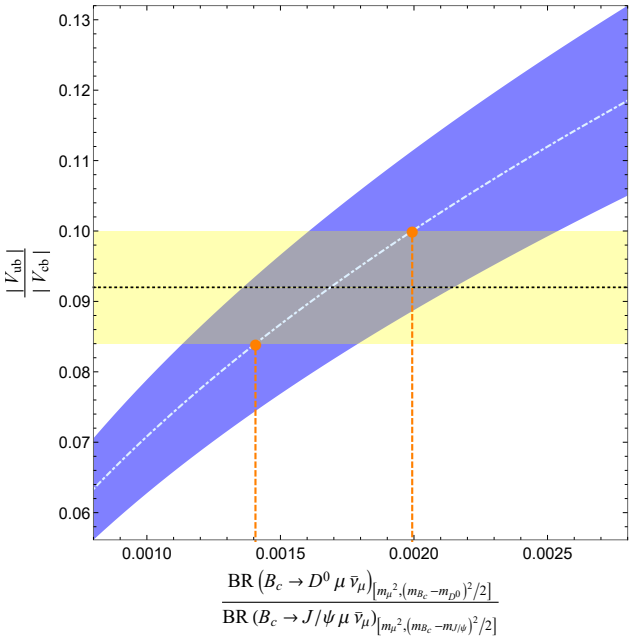

Figure 5.11: The prospect for $|V_{ub}|/|V_{cb}|$ determination from $\mathcal{R}_{D^0 J/\psi}$; the yellow band represents the PDG value of $|V_{ub}|/|V_{cb}|$.

mentally, due to the very short lifespan of the B_c and a huge background stemming

from B decays, measuring the $|V_{ub}|$ quark coupling strength directly is highly challenging [209, 212]. Not surprisingly, it turns out that measuring it through the ratio defined above has some benefits from the experimental standpoint as well (such as canceling the production rate uncertainty). Although challenging, the prospects of using Run 1 + Run 2 data at LHCb are indicating that one could come around 10-20% uncertainties in $|V_{ub}|/|V_{cb}|$ measurement in an analysis looking at the $\mathcal{B}(B_c \to D^0\mu\bar{\nu}_\mu)/\mathcal{B}(B_c \to J/\psi\mu\bar{\nu}_\mu)$ ratio [241]. By combining the predictions presented for $\mathcal{R}_{D^0 J/\psi}$ with future measurements one can achieve the most precise determination of $|V_{ub}|/|V_{cb}|$ in the low-q^2 kinematic region in $B_c \to D^0$ transition and moderate-q^2 region in $B_c \to J/\psi$ transition.

In figure 5.11 this ratio is plotted in the bin defined through $q^2_{\text{min}_1} = q^2_{\text{min}_2} = m^2_\mu$, $q^2_{\text{max}_1} = (m_{B_c} - m_{D^0})^2/2$, and $q^2_{\text{max}_2} = (m_{B_c} - m_{J/\psi})^2/2$, which is approximately the kinematic region in which the QCDSR turn to be most reliable. The current experimental world average of $|V_{ub}|/|V_{cb}|$ is also shown on the plot for comparison of theoretical and future experimental predictions for the ratio of branching fractions directly with the present limit on $|V_{ub}|/|V_{cb}|$.

One should keep in mind that here the differential decay widths are integrated in the lower half of the q^2 region of both decay channels and that the form factors used to produce the plot are the result of fits to uncorrelated pseudo-data points. In line with the estimate of the contribution of the correlation among the points to the error budget discussed in section 5.1.3, one should assign a further 10% uncertainty to $|V_{ub}|/|V_{cb}|$ not shown in the plot.

Table 5.8: Decay constants of mesons with 3ptSR parameters.

Meson	lattice [MeV]	our value [MeV]	s_0^{eff} [GeV^2]	M^2 [GeV^2]
$f_{J/\psi}$	405±6 [165], 399±6 [242]	394 ± 17	16-17	10-15
f_{B_s}	224±5 [222], 229±5 [243]	225±16	37.5-39.5	20-35

When fitting the threshold parameters for the $B_c \to J/\psi$ and $B_c \to B_s$ transitions to those obtained in the calculation of $f_{J/\psi}$ and f_{B_s} decay constants using the same criteria as for $B_c \to D^{(*)}$ explained in section 5.1.1, the values listed in

table 5.8 are obtained, and used in the 3pt correlation function calculations.

As for the Borel mass window in the three-point calculation, the approximate relation from eq. (5.13) holds, and $M^2_{3\text{pt},J/\psi} \approx 20-25$ GeV^2, while $M^2_{3\text{pt},B_s} \approx 30-60$ GeV^2. The plot of the form factors for the $B_c \to J/\psi$ transition obtained using the latter parameters is given in figure 5.12 together with the lattice points given by the HPQCD Collaboration [148]. Once again excellent agreement can be seen between the lattice result and the QCDSR form factors, an agreement which is reproduced in all of the LFQM form factors [138]. The plot of the $B_c \to B_s$ form factors is

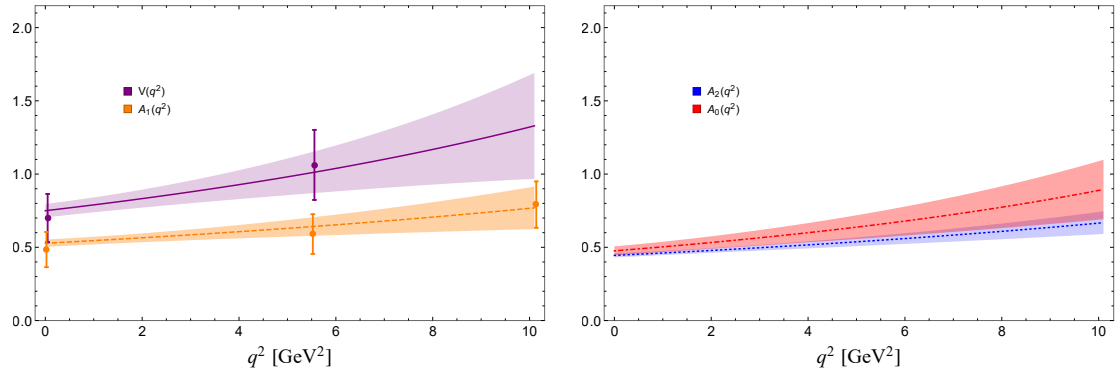

Figure 5.12: Final predictions for $B_c \to J/\psi$ form factors obtained by extrapolating 3ptSR results to higher q^2 regions using the BCL parametrization.

included in figure 5.13. The form factors show a large uncertainty appearing due to the inability of utilizing QCDSR deeper in the high q^2 region. One should also always keep in mind that these uncertainties do not include the truncation error, which is always of the order of 20-30% at q^2_{max} in our calculations, since we extrapolate only linearly in $z(q^2)$.

Finally, the table 5.9 contains the results of these two fits. The unitarity threshold used in each case is listed in the same table under the column "threshold". Note that when fitting the $B_c \to J/\psi$ form factors we exclude two of the poles appearing beneath the B^*D threshold, since numerically their value is very close to the threshold itself. Namely these poles are $M(1P_1) \approx M(1P_1') \approx 7.14$ GeV, and are very close to $\sqrt{t_*} \approx 7.2$ GeV. This is done in order to keep the monotonic behaviour of $A_1(q^2)$ and $A_2(q^2)$ around q^2_{max}, and it does not significantly alter their numerical value. A more nuanced discussion on the impact of near-threshold poles in pole fits one can find in e.g. [94]. The poles for the $B_c \to J/\psi$ case are taken from [187], whereas for

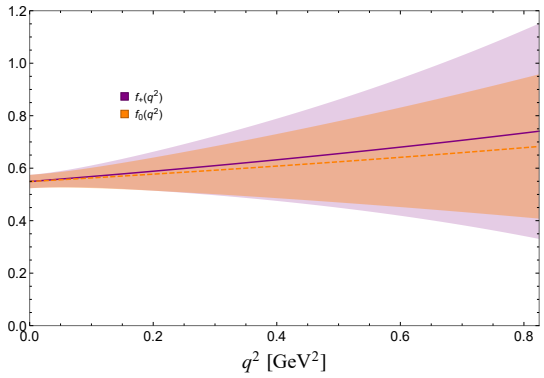

Figure 5.13: Final predictions for $B_c \to B_s$ form factors obtained by extrapolating 3ptSR results to higher q^2 regions using the BCL parametrization.

the $B_c \to B_s$ case the needed pole masses are known from experiments [4].

Table 5.9: Summary of the fits for $B_c \to J/\psi$ and $B_c \to B_s$ form factors.

J^P	threshold	m_R [GeV]	BCL:	b_0	b_1	$\chi^2[10^{-4}]$
1^-	BD	6.34, 6.90, 7.01	$V^{B_c\to J/\psi}$	0.69	2	23
1^+	B^*D	6.73, 6.74	$A_1^{B_c\to J/\psi}$	0.50	1	45
1^+	B^*D	6.73, 6.74	$A_2^{B_c\to J/\psi}$	0.42	1	102
0^-	B^*D	6.28, 6.84	$A_0^{B_c\to J/\psi}$	0.50	-1	13
1^-	$D_s\eta'$	2.11, 2.71, 2.86	$f_+^{B_c\to B_s}$	0.5	3	0.7
0^+	$D_s\eta'$	2.138	$f_0^{B_c\to B_s}$	0.6	-1	0.3

In the time between the writing of this thesis, and publishing the research this section is based upon, both $B_c \to J/\psi$ and $B_c \to B_s$ decays were investigated on the lattice [55, 73]. QCDSR results presented here agree very well with the lattice QCD results, for all of the form factors.

5.3.2. The $|V_{ub}|/|V_{cs}|$ ratio and the HQSS compatibility

In [189] the authors propose to use the differential ratio of $\mathcal{B}(B_c \to D^0\ell\bar{\nu}_\ell)$ and $\mathcal{B}(B_c \to B_s\ell\bar{\nu}_\ell)$ at zero recoil defined as

$$\mathcal{R}^{\max}_{D^0 B_s} = \left(\frac{|V_{ub}|^2}{|V_{cs}|^2}\right)^{-1} \frac{\mathrm{d}\Gamma(B_c^+ \to D^0 e^+\nu_e)/\mathrm{d}q^2|_{q^2\simeq q^2_{\max}}}{\mathrm{d}\Gamma(B_c^+ \to B_s e^+\nu_e)/\mathrm{d}q^2|_{q^2\simeq q^2_{\max}}} \tag{5.45}$$

to determine the $|V_{ub}|/|V_{cs}|$ ratio. Experimentally, to measure the ratio $|V_{ub}|/|V_{cs}|$ would be more challenging than $|V_{ub}|/|V_{cb}|$, since the experimental systematics do not nicely cancel in this ratio [241]. However, this could be as well an interesting possibility in the future, and is examined here. Around the zero hadronic-recoil region HQSS reduces the number of the form factors of these two decays to just one, and the differential decay rate ratio in the limit becomes insensitive to specifics of the B_c wave function, thus becoming proportional just to a ratio of the final meson masses and decay constants. Namely, in HQET the following parametrization is valid:

$$\begin{aligned}
\left\langle D^0(v,q')\right| V_\mu(q^2)\left|B_c(v)\right\rangle &= 2\sqrt{m_{B_c} m_{D^0}}\left[\Sigma_1(a_0 q')v_\mu + a_0\Sigma_2(a_0 q')q'_\mu\right],\\
\left\langle B_s(v,q')\right| V_\mu(q^2)\left|B_c(v)\right\rangle &= 2\sqrt{m_{B_c} m_{B_s}}\left[\Omega_1^s(a_0 q')v_\mu + a_0\Omega_2^s(a_0 q')q'_\mu\right],
\end{aligned} \tag{5.46}$$

where v is the velocity of the B_c meson, and q' is a small residual velocity carried by the final state meson (denoted such as to avoid confusion with q, the momentum carried by the lepton pair system), so that

$$p_{1\mu} = m_{B_c} v_\mu; \quad p_{2\mu} = m_f v_\mu + q'_\mu, \tag{5.47}$$

with $m_f = [m_{D^0}, m_{B_s}]$. The parameter a_0 is connected to the Bohr radius of the B_c meson and is not discussed here. The form factors $\Sigma_2(a_0 q')$ and $\Omega_2^s(a_0 q')$ are irrelevant for this discussion, as they do not contribute around the zero-recoil region ($q'^2 = 0$), so in principle one could deduce the differential branching fractions near zero recoil just from the form factors $\Sigma_1(a_0 q')$ and $\Omega_1^s(a_0 q')$. In [189] it is argued that, owing to this fact, and by considering the heavy-quark spin symmetry for the

remained form factors which one can write as

$$\begin{aligned}\Sigma_1(a_0 q') &= \frac{1}{\sqrt{2}} f_{D^0}\sqrt{m_{D^0}} \int \mathrm{d}^3x\, \mathrm{e}^{\mathrm{i}\vec{q}'\cdot\vec{x}}\Psi(x),\\ \Omega_1^s(a_0 q') &= \frac{1}{\sqrt{2}} f_{B_s}\sqrt{m_{B_s}} \int \mathrm{d}^3x\, \mathrm{e}^{\mathrm{i}\vec{q}'\cdot\vec{x}}\Psi(x),\end{aligned} \tag{5.48}$$

where $\Psi(x)$ is the B_c meson wave function, the ratio at the zero-recoil,

$$R_{\mathrm{FF}} = \frac{\Sigma_1(a_0 q' \approx 0)}{\Omega_1^s(a_0 q' \approx 0)} \tag{5.49}$$

should in principle very weakly depend on the particular shape of the wave function, due to its cancellation, so that in the heavy quark limit

$$R_{\mathrm{FF}}^{\mathrm{HQ}} \approx \frac{f_{D^0}}{f_{B_s}}\sqrt{\frac{m_{D^0}}{m_{B_s}}} \approx 0.53. \tag{5.50}$$

In section 5.3.1 some details on calculation of $B_c \to B_s$ form factors obtained analogously to the ones of the $B_c \to D^0$ transition are presented, and they give

$$R_{\mathrm{FF}}^{\mathrm{our}} = 0.8 \pm 0.3, \tag{5.51}$$

which can also be compared with the result from ref. [191], where the wave functions have been calculated in the framework of a HQET-inspired quark model, explicitly,

$$R_{\mathrm{FF}}^{[191]} = 0.89\,. \tag{5.52}$$

Comparison shows that the heavy quark spin symmetry relations are obeyed in the QCDSR calculation. This also agrees well with values extracted from other quark models [104,105,138]. However, the error in the calculation presented in this section is quite large, since the form factors relevant for the $b \to u$ and $c \to s$ decays are not very correlated. Also, one can reliably use the sum rules for the $B_c \to B_s$ case only very close to the maximum recoil region, as can be noticed from figure 5.13, due to the occurrence of non-Landau singularities. Lattice input might prove to be useful here in order to extrapolate to higher order z terms for both decays and with

more theoretical input the extraction of the $|V_{ub}|/|V_{cs}|$ ratio from eq. (5.45) could be viable.

5.4. Conclusion

For the extraction of $|V_{ub}|$ from the $B_c \to D^0$ semileptonic decay it is important to determine precisely the relevant form factors, since the predictions for the light leptons in the final state come out essentially proportional to $|f_+(q^2)|^2|V_{ub}|^2$. In this section the calculation of the $B_c \to D^0$ form factors $f_+(q^2)$ and $f_0(q^2)$ and the $B_c \to D^*$ form factors $V(q^2), A_1(q^2), A_0(q^2)$ and $A_2(q^2)$ has been presented, using the three-point QCD sum rules. The form factors are then theoretically confined in the region of $q^2 \leq 10\ \text{GeV}^2$. The extrapolation to higher q^2 values is discussed for the BGL and BCL z-series and final predictions are given for the BCL parametrization of form factors, summarized in table 5.4 and figure 5.2 and figure 5.3.

The q^2 differential decay rate distributions (divided by $|V_{ub}|^2$) are also presented for both a light (e or μ) and a τ lepton in the final state. The numerical predictions for various angular observables in the $B_c \to D^{(*)}$ semileptonic transitions are given in figure 5.8 and figure 5.9, which can be useful to further scrutinize the SM predictions for these decays. Those are the forward-backward asymmetry $A_{FB}^\ell(q^2)$, the lepton polarization $P_L^\ell(q^2)$, convexity parameter $C_F^\ell(q^2)$ and the D^* meson longitudinal polarization fraction, $F_L^{D^*}$ in $B_c \to D^*$ decays. In addition, the values of the ratios of branching fractions of the semileptonic decays to a τ lepton to the branching fractions to a muon are calculated, $R_c(D^0) = 0.64 \pm 0.05$ and $R_c(D^*) = 0.55 \pm 0.05$, for testing the lepton favour universality violation in the semileptonic B_c channels, with the q^2 distributions shown in figure 5.7.

The possibility of determining the $|V_{ub}|$ CKM matrix element from $B_c \to D^{(*)}$ decays is carefully studied and the conclusion has been drawn that $|V_{ub}|$ can be determined with the uncertainty of 7.5% from the $B_c \to D^0\mu\bar{\nu}_\mu$ decay. Experimentally there are good prospects for this measurement. The B_c decays will be extensively investigated at LHCb in the Upgrade II [212]. With approximately 30,000 reconstructed $B_c \to D^0\ell\bar{\nu}_\ell$ decays which can be expected with the 300 fb^{-1} Upgrade II dataset, a competitive extraction of $|V_{ub}|$ from $B_c \to D^0$ semileptonic decays can be expected. By normalizing $B_c \to D^0\mu\bar{\nu}_\mu$ to $B_c \to J/\psi\mu\bar{\nu}_\mu$ the ratio $|V_{ub}|/|V_{cb}|$ could be experimentally extracted with $10 - 20\%$ of uncertainty [241].

It was further demonstrated that numerically the QCDSR form factors do obey the behaviour imposed on them by the heavy quark spin symmetry, as dictated by the ratio of $B_c \to D^0$ and $B_c \to B_s$ transitions [189]. Although the precision is still not satisfactory enough, this opens up new possibilities in terms of extraction of the $|V_{ub}|/|V_{cs}|$ ratio, even if experimentally this turns out to be extremely challenging.

6. $|V_{ub}|$ DETERMINATION FROM THE $\bar{B} \to \pi\, \ell \bar{\nu}_\ell$ DECAY

This chapter is based on research accepted for publishing in Journal of High Energy Physics, D. Leljak, B. Melić and D. van Dyk, [arXiv:2102.07233 [hep-ph]] [3].

The world average of the inclusive $|V_{ub}|$ determinations following the BNLP approach [230, 244–247] and the GGOU approach [248, 249] as determined by the HFLAV collaboration reads [42]:

$$\begin{aligned} 10^3 \times |V_{ub}|_{\text{BLNP}} &= 4.44\, {}^{+0.13}_{-0.14}|_{\text{exp.}}\, {}^{+0.21}_{-0.22}|_{\text{theory}} \simeq 4.44^{+0.25}_{-0.26}\,, \\ 10^3 \times |V_{ub}|_{\text{GGOU}} &= 4.32\, \pm 0.12|_{\text{exp.}}\, {}^{+0.12}_{-0.13}|_{\text{theory}} \simeq 4.32^{+0.17}_{-0.18}\,. \end{aligned} \tag{6.1}$$

These results deviate significantly from $|V_{ub}|$ determinations that use the exclusive decays $\bar{B}^0 \to \pi^+ \ell^- \bar{\nu}_\ell$, where $\ell = e, \mu$. The present world average thereof reads [42]:

$$10^3 \times |V_{ub}|^{\bar{B} \to \pi}_{\text{LQCD+LCSR}} = 3.67 \pm 0.09|_{\text{exp.}}\, \pm 0.12|_{\text{theory}} \simeq 3.67 \pm 0.15\,. \tag{6.2}$$

Assuming the inclusive and exclusive results to be uncorrelated and normally distributed with the stated overall uncertainties, these results are mutually incompatible. One finds a deviation of $\approx 2.7\sigma$, depending on which of the inclusive determinations is considered. This long-standing situation is commonly referred to as the "exclusive vs inclusive" puzzle, which continues to be a topic of active research [250].

The most recent inclusive determination by the Belle collaboration [251] finds the tension reduced, with the central value dropping closer to the exclusive one, while simultaneously increasing the uncertainty. The average of the values extracted using

four different theoretical frameworks is reported as:

$$10^3 \times |V_{ub}| = 4.10 \pm 0.09 \pm 0.22 \pm 0.15\,. \tag{6.3}$$

where the uncertainties are of statistical, systematical, and theoretical origin, respectively. Compared to the relative uncertainty of $\approx 4\%$ in the determination from exclusive $\bar{B} \to \pi\ell^-\bar{\nu}_\ell$ decays, the inclusive determination has a much larger relative uncertainty of $\approx 7\%$. The latter is partially dominated by the subtraction of a large $B \to X_c\ell^-\bar{\nu}_\ell$ background, which is one focus of the recent Belle analysis [251]. The smallness of the (theory) uncertainties in the exclusive determination therefore warrant heightened scrutiny.

The description of exclusive semileptonic decays requires knowledge of the hadronic form factors. The set of form factors includes f_+ and f_0, which are relevant to the SM predictions for charged-current semileptonic $\bar{B} \to \pi\ell^-\bar{\nu}_\ell$ decays. Another form factor f_T is needed for SM predictions of rare semileptonic $\bar{B} \to \pi\ell^+\ell^-$ decays and also arises in Beyond the Standard Model (BSM) analyses of the charged-current decay. All three form factors are scalar-valued coefficients defined in section 3.1.1.

Presently, the determination of $|V_{ub}|$ from the exclusive $\bar{B} \to \pi\ell^-\bar{\nu}_\ell$ decays is the most competetive. Other determinations either lack precision on the theoretical side (such as $\bar{B}_c \to D\ell^-\bar{\nu}_\ell$, discussed in section 5) or the experimental side (such as $\bar{B} \to \ell^-\bar{\nu}_\ell$ or $\Lambda_b \to p\mu^-\bar{\nu}_\mu$), with improvements to the precision expected in the future. A more detailed discussion is available in ref. [42]. The increase in precision of the theoretical predictions for and the experimental measurements of $\bar{B} \to \pi\ell^-\bar{\nu}_\ell$ has also made this decay a prime candidate for searches of BSM effects in charged currents. These searches are well motivated in light of recent tensions in $b \to c\ell^-\bar{\nu}_\ell$ processes.

The purpose of this section is three-fold:

1. to revisit light-cone sum rule predictions for the full set of local $\bar{B} \to \pi$ form factors, with focus on the systematic uncertainties that affect this method;

2. to carry out a combined fit with the precise lattice QCD (LQCD) results for the form factors, in order to provide the most up-to-date exclusive determination

of $|V_{ub}|$;

3. to provide up-to-date predictions for $\bar{B} \to \pi\ell^-\bar{\nu}_\ell$ observables that probe lepton-flavour universality and non-standard weak effective couplings.

6.1. LCSR FORM FACTORS

In this section the LCSRs for full set of local $\bar{B} \to \pi$ form factors associated with dimension-three $b \to u$ or $b \to d$ currents is revisited. The LCSRs are constructed with an on-shell pion and an interpolated B meson, and by the use of pion distribution amplitudes, and in the WS basis.

The analytical expressions for the two-point correlation functions that give rise to the sum rules are known to high accuracy. The expansion in light-cone operators uses the twist of an operator as an expansion parameter, as discussed in section 2.2. Operators of higher twist are supressed by power of $\Lambda_{\rm had}/m_b$. The leading contributions at the twist-two level are known at next-to-leading order (NLO) in α_s [95,205]. Next-to-next-to-leading order (NNLO) [252] are partially computed in the large β_0 approximation. In $\bar{B} \to \pi$ transitions, the next-to-leading twist contributions are known to by enhanced by the factor

$$\frac{\mu_\pi}{m_b} = \frac{m_\pi^2}{m_b(m_u + m_d)}\,, \tag{6.4}$$

which is formally power-suppressed but numerically large. Due to this enhancement, the twist-three terms contribute approximately 50% to the correlation function, e.g. [95]. Due to the chiral enhancement it is important to include the twist-three terms also at NLO [95]. Beyond this level, contributions up to twist-six follow the expected pattern of power suppression [122].

In the following sections, the predictions for the three hadronic form factors based on the analytic expressions in ref. [95, 96, 253] are provided. These LCSRs use π-meson distribution amplitudes. They include expressions up to twist-four accuracy at leading order in α_s and expressions up to twist-three accuracy at next-to-leading order in α_s. Expressions beyond twist-four accuracy are numerically

negligible [122]. In the preparation of this work we have identified two typos in the analytic expressions in the literature.[1] These two typos do not significantly impact the form factor values, but have a non-negligible effect on the computation of the B-meson mass predictor, which is used below, in determination of the duality thresholds.

The numerical results for the form factors as presented below differ from previous LCSR studies in the following aspects:

1. Updated input parameters for quark masses, strong coupling and — most importantly — for the two-particle twist-two π LCDA are used. The full set of input parameters is discussed in section section 6.1.1.

2. The duality thresholds are determined for *all three* form factors from three daughter sum rules. The latter are obtained from the derivative of the initial sum rules with respects to the Borel parameter. In this way a predictor for the mass squared of the B meson can be included in a statistical analysis. The method is discussed for the f_+ form factor in ref. [206], and for LCSRs with B-meson LCDAs in ref. [254]. Details of this procedure and practical considerations for this step are discussed in section 6.1.2.

3. Within the threshold-setting procedure, the dependence of the duality thresholds on the momentum transfer q^2 is investigated. Two models of the thresholds are compared, and their difference is used to assign a systematic uncertainty to the final results.

6.1.1. Input parameters

The setup follows the usual approach to calculate both the B-meson decay constant f_B in two-point QCD sum rules and the $\bar{B} \to \pi$ form factors in LCSR within a simultaneous analysis [95, 206, 259]. The rationale for this approach is that perturbative corrections to the correlation functions in both sum rules partially cancel.

[1] First, in eq. (4.12) of ref. [95] the factor 1/2 in front of the $\mathrm{d}^2\phi_{4\pi}/\mathrm{d}u^2$ term should be replaced by a factor 1/4. Second, in the fourth line of eq. (B.35) the plus prescription should extend to the entire term rather than only to the $\rho/(1-\rho)$ factor. The first typo is corrected in subsequent publications, while the second typo is not.

Table 6.1: Input parameters used in the numerical analysis of the two-point sum rules for the f_B decay constant and LCSRs for $\bar{B} \to \pi$ form factors. The full prior distribution is a product of uncorrelated individual priors, which are either uniform or gaussian distributed. gaussian priors cover the intervals at 68% probability, and their central value corresponds to the mode. For practical purpose, variates of the gaussian priors are only sampled inside their respective 99% intervals. The prior intervals of the duality threshold parameters are chosen such that the peaking posterior distribution is fully contained.

Parameter	value/interval	unit	prior	comments/source
quark-gluon coupling and quark masses				
$\alpha_s(m_Z)$	0.1179 ± 0.0010	—	gaussian	[4]
$\overline{m}_b(\overline{m}_b)$	4.18 ± 0.03	GeV	gaussian	[4]
$[m_u + m_d](2\,\text{GeV})$	6.9 ± 1.1	MeV	gaussian	[4]
hadron masses				
m_B	5279.58	MeV	—	[4]
m_π	139.57	MeV	—	[4]
vacuum condensate densities				
$\langle\bar{q}q(2\text{GeV})\rangle$	$-(288^{+17}_{-14})^3$	MeV^3	—	$m_\pi^2 f_\pi^2/2(m_u+m_d)$
$\langle\frac{\alpha_s}{\pi}G^2\rangle$	$[0.000, 0.018]$	GeV^4	uniform	[255]
m_0^2	$[0.6, 1.0]$	GeV^2	uniform	[255]
r_{vac}	$[0.1, 1.0]$	—	uniform	[255]
parameters of the pion DAs				
f_π	130.2 ± 0.8	MeV	gaussian	[256]
$a_{2\pi}(1\text{GeV})$	0.157 ± 0.027	—	gaussian	[257]
$a_{4\pi}(1\text{GeV})$	$[-0.04, 0.16]$	—	uniform	[258]
$\mu_\pi(2\text{GeV})$	$2.8^{+0.6}_{-0.4}$	GeV	—	$m_\pi^2/(m_u+m_d)$
$f_{3\pi}(1\text{GeV})$	$[0.003, 0.006]$	GeV^2	uniform	[119]
$\omega_{3\pi}(1\text{GeV})$	$[-2.2, -0.8]$	—	uniform	[119]
$\delta_\pi^2(1\text{GeV})$	$[0.11, 0.33]$	GeV^2	uniform	(50% sys. unc.) [257]
$\omega_{4\pi}(1\text{GeV})$	$[0.1, 0.3]$	—	uniform	[119]
sum rule parameters and scales				
μ	3.0	GeV	—	[221, 258]
M^2	$[12.0, 20.0]$	GeV^2	uniform	[258]
$s_0^{f_+}$	$[30.0, 42.0]$	GeV^2	uniform	
$s_0'^{f_+}$	$[-1.0, +1.0]$	—	uniform	
$s_0^{f_0}$	$[30.0, 42.0]$	—	uniform	
$s_0'^{f_0}$	$[-1.0, +1.0]$	—	uniform	
$s_0^{f_T}$	$[30.0, 42.0]$	GeV^2	uniform	
$s_0'^{f_T}$	$[-1.0, +1.2]$	—	uniform	
$\overline{M}^2$	5.5 ± 1.0	GeV^2	gaussian	[221]
$\overline{s}_0^B$	$[29.0, 44.0]$	GeV^2	uniform	

As a consequence, the input parameters presented here involve the full set of all, the two-point sum rule and the light-cone sum rule parameters. The parameters are classified as follows:

strong coupling and quark masses These parameters include the strong coupling at $\mu = M_Z$, the bottom quark mass in the $\overline{\text{MS}}$ scheme at the scale m_b, and the sum of the up and down quark masses in the $\overline{\text{MS}}$ scheme at the scale 2 GeV.

hadron masses These parameters include the masses of the initial-state B meson m_B and the final-state pion m_π.

vacuum condensate densities These parameters include the quark condensate evaluated using the GMOR relation at 2 GeV and the gluon condensate, while the mixed quark-gluon condensate is implemented through m_0^2, its ratio with the quark condensate. Lastly, r_{vac} parametrizes factorization in the four-quark condensate density. These parameters are needed exclusively in the two-point sum rule.

parameters of the π LCDAs These parameters include the pion decay constant f_π to which the leading-twist LCDA is normalised. The shape of the leading-twist DA is described by an expansion in Gegenbauer polynomials, which are eigenfunction of the RGE kernel to leading-logarithmic accuracy. Isospin symmetry implies that only even Gegenbauer polynomials contribute, and we retain the first two non-vanishing Gegenbauer coefficients $a_{2\pi}$ and $a_{4\pi}$. Following ref. [119], we normalise the twist-3 two-particle LCDAs to the chiral parameter $\mu_\pi(2\,\text{GeV})$ and twist-three three-particle LCDAs to the decays constants $f_{3\pi}$. The shape of the three-particle LCDAs additional involves the parameter $\omega_{3\pi}$. The twist-four LCDAs are parametrized in terms of δ_π^2 and $\omega_{4\pi}$. If not specified otherwise, all parameter of this class are renormalised at a scale of 1 GeV.

sum rule parameters and scales These parameters include the Borel parameter M^2 and the values and slopes of the duality threshold parameters s_0^F and

$s_0'^F$, where F denotes one of the form factors $\{f_+, f_0, f_T\}$. We discuss the parametrisation of the thresholds in detail below. The perturbative LCSR kernels are evaluated at a renormalisation scale μ. Further parameters are the Borel parameter $\bar{M}^2$ and duality threshold $\bar{s}_0^B$ of the auxilliary two-point sum rule.

All the input parameters are listed and their prior probability density functions (PDFs) are summarized in table 6.1.

The differences between the inputs used in this work and the inputs used in Refs. [206, 259] is briefly discussed:

1. While the input parameters for the light quark masses m_u and m_d change only slightly, this change has a large numerical effect on μ_π^2, which normalises the twist-three two-particle contributions to the sum rules. It also affected the value of $\bar{q}q$ condensate density.

2. A recent lattice QCD analysis [257] of the shape of the leading-twist pion LCDA has provided for the first time a determination of the leading Gegenbauer moment a_2 from first principles. This result is used as a gaussian prior in the following analysis. Note that the RGE to LL are used here to translate the lattice results to the relevant input scale of 1 GeV. The uniform prior PDFs for the parameters a_4 and δ_π^2 are adjusted to match the lattice QCD results for these parameters within their uncertainty intervals.

3. The Borel window for the LCSR to the interval is slightly increased, to $12\,\text{GeV}^2 \leq M^2 \leq 20\,\text{GeV}^2$. Here, the Borel parameter is varied uniformly, rather than with a gaussian prior. This increases the uncertainty due to the Borel parameter in the final numerical results and also fully includes the peaking structure in the posterior PDF.

6.1.2. Setting the duality thresholds and Borel parameters

Each of the duality thresholds s_0^F corresponds to a point at which to artificially split the dispersive integral for its form factor F into two contributions: one corresponding

to the $\bar{B} \to \pi$ form factor, and one corresponding to hadronic transition matrix elements for excited B-mesons and the continuum of b-flavoured states. To obtain the threshold parameters, one commonly uses daughter sum rules obtained by taking a derivative of the form factors' correlation function with respect to $-1/M^2$ and by subsequently normalizing to the correlation function. By using the same input parameters as in the original sum rule, one thereby constrains the duality thresholds parameters. This new daughter sum rule can be cast into a pseudo observable that serves as a predictor of the mass square for the interpolated state, i.e. here the B meson; see e.g. ref. [206]. Schematically,

$$[m_B^2(q^2; F)]_{\text{LCSR}} = \frac{\int_0^{s_0} ds\, s\, \rho^F(s, q^2)\, e^{-s/M^2}}{\int_0^{s_0} ds\, \rho^F(s, q^2)\, e^{-s/M^2}}\,. \tag{6.5}$$

Here F denotes any of the three form factor under consideration, and ρ^F is the OPE result for the form factor's spectral density.

To determine the duality thresholds the procedure used in ref. [206] for the f_+ form factor is followed. A theoretical Gaussian likelihood centered around the experimental results for the B-meson mass is constructed. Further, a theoretical uncertainty of 1% is assigned to the LCSR prediction of the B-meson mass. For each form factor the likelihood challenges the LCSR predictions for the mass in five different q^2 points equally spaced between $-8\,\text{GeV}^2$ to $+8\,\text{GeV}^2$. The parameters listed in table 6.1 are then fitted to this likelihood, using two different models for the duality thresholds, see below. The posteriors for most parameters are in good agreement with the priors, with the exception of the posteriors for the duality threshold parameters and the LCSR Borel parameter, which change from uniform to peaking distributions. This change clearly indicates that we successfully infer the duality thresholds and the Borel parameter from the daughter sum rules.

The procedure carried out in this work is similar but not identical to the one presented in [206], where instead of π-LCDAs, the significantly less precise B-meson LCDAs were appropriated. It differs in the following points:

1. Here, all three transition form factors are determined simultaneously, while in ref. [206] the analysis is constrained to f_+ only. The procedure presented here

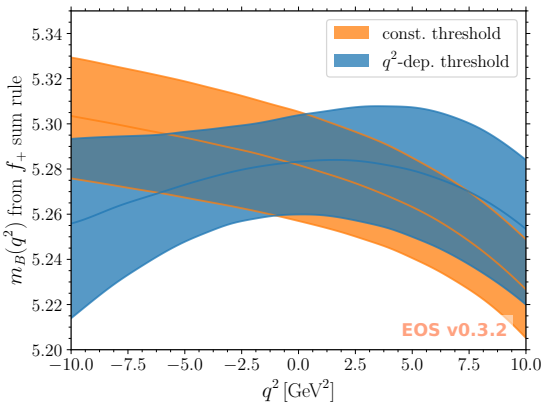

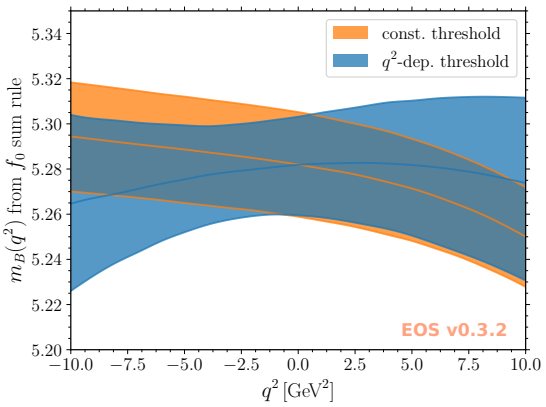

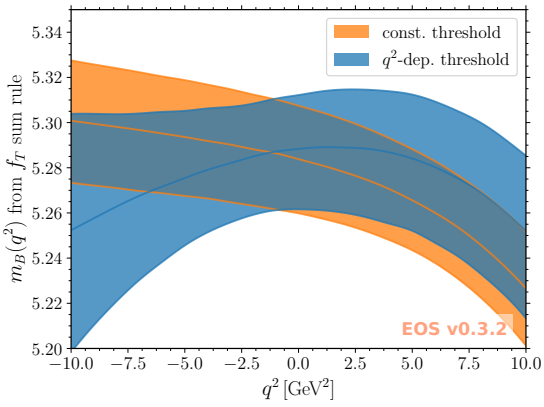

Figure 6.1: The dependence of the B-meson mass predictor $[m_B^2(q^2; F)]_{\text{LCSR}}$ for each of the three form factors $F = \{f_+, f_0, f_T\}$ on the momentum transfer q^2. We show the posterior-prediction for a q^2-invariant threshold (in orange) and a threshold with linear q^2 dependence as in eq. (6.6) (in blue). The shaded areas correspond to the respective 68% probability envelopes.

restricts the possible parameters space more strongly, since all form factors share the same input parameter set except for their respective threshold parameters. The effect is mostly visible in the posterior of the Borel parameter and discussed in detail below.

2. The q^2 derivatives of the form factors (as suggested in ref. [206]) *are not* determined. This decision is based on the following observation. If the predictor for a form factor and for its q^2 derivative share the same threshold parameter, then the mass predictor for the derivative cannot in general be expected to produce a value close to the B meson mass squared. Therefore, new and independent duality threshold parameters would need to be introduced for each derivative. This reduces the usefulness of the derivatives as a similar amount of information can be extracted by increasing the number of q^2 points, which

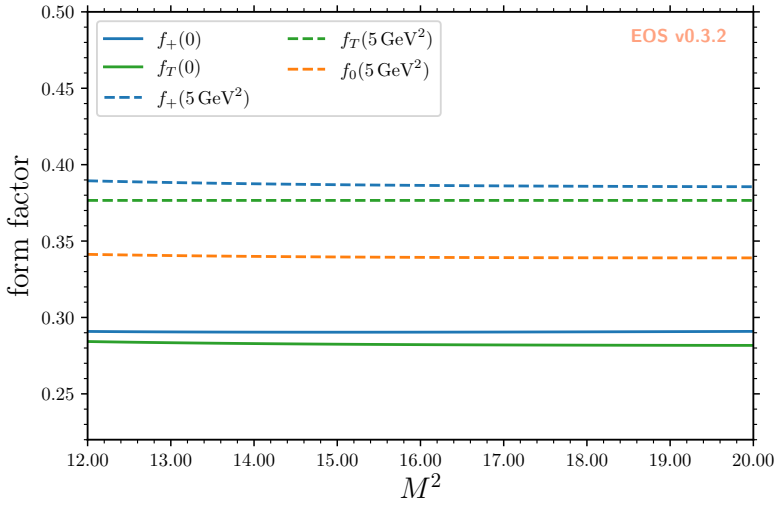

Figure 6.2: The dependence of the form factors f_+ (in blue), f_0 (in orange), and f_T (in green) on the Borel parameter M^2. This dependence is exemplified for two different choices of q^2: $0\,\mathrm{GeV}^2$ (solid lines), and $5\,\mathrm{GeV}^2$ (dashed lines). The form factor f_0 coincides with with f_+ at $q^2 = 0$, and is therefore not depicted at this value.

is computationally easier.

In a first fit the duality thresholds are assumed to be constant with respect to q^2. In a second fit, a linear q^2 dependence of the thresholds is allowed , i.e.,

$$s_0^F(q^2) \equiv s_0^F + q^2\, s_0'^F\,. \tag{6.6}$$

As already disussed in ref. [206], evidence is found for a mild q^2 dependence of the duality thresholds. Here, a reduction of the global χ^2 by ~ 0.5 is evident when allowing for a linear q^2 dependence in all three thresholds. This has to be compared to a decrease of three degrees of freedom. While this result does in no way *require* to impose a q^2 dependence of the thresholds, here it is considered grounds enough to further investigate the q^2 dependence of the B-meson mass predictors. To this end, the median curve and its 68% probability envelope for each mass predictor and for both fit models is computed. The findings are illustrated in figure 6.1. As can be expected due to the three additional parameters, the 68% envelopes of the fit model with q^2-dependent thresholds (blue bands) have a larger uncertainty than the envelopes of the fit model with constant thresholds (orange bands). How-

ever, the former model reproduces the physical B-meson mass on average better than the fit model with constant thresholds in the q^2 interval considered here. The maximal deviation of the B-meson mass predictors from the physical mass is reduced for all three form factors. Therefore, the q^2-dependent ansatz is chosen as a representation for the duality thresholds for the central values of form factor predictions computed here. The difference between the constant and the q^2-dependent threshold parametrizations is used to estimate systematic uncertainties due to the determination of the duality threshold parameters.

The dependence on the Borel parameter M^2 is accounted for by varying this parameter in the prefered window $12\,\mathrm{GeV}^2 \leq M^2 \leq 20\,\mathrm{GeV}^2$. In this way, the residual M^2 dependence of the form factor predictions is accounted for. This procedure was carried out in ref. [206], where a gaussian prior was used. Here, this procedure is applied instead with a uniform prior. Despite the mild dependence of each form factor on the Borel parameter value, its posterior differs strongly from its prior, with a peak at around $15\,\mathrm{GeV}^2$. This can be understood, since each form factor and each q^2 point entering the theoretical likelihood differs slightly in its dependence on the Borel parameter. Only when investigating all form factors and q^2 simultaneously, the posterior of the Borel parameter is found to exhibit a clearly peaking structure. As expected, the overall form factors dependence on the Borel parameter is very weak and is shown in figure 6.2.

6.1.3. Numerical results for the form factors

The form factors are predicted at five equally-distanced q^2 points in the interval $-10\,\mathrm{GeV}^2 \leq q^2 \leq +10\,\mathrm{GeV}^2$. The choice of q^2 points simultaneously maximizes the number of pseudo data points while keeping correlations of neighbouring points below 80% in the combined parametric and systematic uncertainty. Two systematic uncertainties are estimated by the following procedures:

1. For each form factor prediction the renormalization scale is varied by dividing and multiplying it with a factor of 1.25, corresponding to the interval $[2.40\,\mathrm{GeV}, 3.75\,\mathrm{GeV}]$. The maximal one-sided variation of all our predictions

can be found when lowering the renormalization scale. Across all form factors and all q^2 points, this variation evaluates consistently to $\sim 4\%$. For a conservative estimate of this effects, an uncorrelated 4% systematic uncertainty is added to all form factor predictions.

2. For each form factor the difference between the predictions with constant duality thresholds and q^2-dependent duality thresholds is computed. The largest difference occurs for $f_0(q^2 = 10\,\mathrm{GeV}^2)$, corresponding to roughly $\sim 6\%$ of the central value. The differences are added in quadrature to the variances.

The joint posterior predictive distribution for all of the form factors is to excellent approximation a multivariate Gaussian distribution. The mean values and standard deviations are provided in table 6.2. For convenience the mean values and the covariance matrix are attached to the arXiv preprint of the manuscript this section is based no as an ancillary machine-readable file. One can immediately notice the very close numerical values of f_+ and f_T form factors, which is expected as a consequence of the heavy-quark expansion and the large-energy symmetry limit [181]. The $f_0(q^2 = 0)$ pseudo data point is not included, since it coincides with $f_+(q^2 = 0)$ by definition. Uncertainties amount to $\sim 10\%$ across all q^2 points. The parametric covariance matrix for the prrediction exhibits a large degree of correlation. The determinant of ρ, the linear correlation matrix reads

$$\det \rho \Big|_{\text{parametric}} = 4.0 \times 10^{-31}\,. \tag{6.7}$$

Accounting for the systematic uncertainties as discussed above increases the determinant to

$$\det \rho \Big|_{\text{total}} = 3.7 \times 10^{-5}\,, \tag{6.8}$$

thereby reducing the degree of correlation. The largest correlation of 81% occurs amongst $f_0(-5\,\mathrm{GeV}^2)$ and $f_+(-5\,\mathrm{GeV}^2)$. These findings give confidence that the 14 data points can be treated as 14 independent observations in the following studies.

Table 6.2: The LCSR predictions for the form factors in five q^2 points. The value of $f_0(q^2 = 0)$ is not independent, since $f_+(q^2 = 0) = f_0(q^2 = 0)$ by construction.

q^2	$-10\,\mathrm{GeV}^2$	$-5\,\mathrm{GeV}^2$	$0\,\mathrm{GeV}^2$	$+5\,\mathrm{GeV}^2$	$+10\,\mathrm{GeV}^2$
$f_+(q^2)$	0.170 ± 0.022	0.224 ± 0.022	0.297 ± 0.030	0.404 ± 0.044	0.574 ± 0.062
$f_0(q^2)$	0.211 ± 0.029	0.251 ± 0.024	—	0.356 ± 0.040	0.441 ± 0.052
$f_T(q^2)$	0.170 ± 0.021	0.222 ± 0.020	0.293 ± 0.028	0.396 ± 0.039	0.560 ± 0.053

6.1.4. Extrapolation to high q^2

The standard approach to extrapolate the form factors is a fit of a parametrization of the form factors to LCSR pseudo data points. For the extrapolation of our LCSR results to large q^2 here the BCL parametrization [129] is chosen, as it is commonly applied in the literature [78–80]. Details can be again be seen in section 3.3.

A common choice is choice is made $t_* = t_+ \equiv (m_B + m_\pi)^2$. The magnitude of $z(q^2)$ for q^2 within the semileptonic phase space is again minimized by choosing

$$t_0 = t_{0,\mathrm{opt}} = (m_B + m_\pi)(\sqrt{m_B} - \sqrt{m_\pi})^2\,, \tag{6.9}$$

which is also adopted here. As a consequence, $|z| < 0.284$ for semileptonic $\bar{B} \to \pi$ decays. The $\bar{B} \to \pi$ vector and tensor form factors feature a single subthreshold pole, each due to the B^* bound state, which is located outside the semileptonic phase space. The scalar form factor f_0 has no subthreshold pole.

The features of the form factor $f_+(q^2)$ in the BCL parametrization are very well known, but there is some ambiguity as to how the the scalar form factor f_0 should be parametrized, which is not discussed in ref. [129]. Commonly [78, 80] f_0 is parametrized without the use of a pole, due to the absence of a subthreshold bound state. In addition, the behaviour of Disc $f_0 \sim p^{1/2}$ just above the pair production threshold cannot be used to eliminate one of the expansion coefficients. It is therefore ambiguous if f_0 should be expanded to order K or $K-1$ to ensure consistency when simultaneously fitting f_+. In this section, f_0 is expanded to order z^{K-1} to make it compatible with the literature [78, 80].

For the tensor form factor f_T most of the same considerations as for f_+ apply.

BCL parameters ($K = 3$)	
$f_+(0)$	$0.283^{+0.027}_{-0.027}$
b_1^+	$-1.0^{+4.3}_{-4.5}$
b_2^+	$-2.9^{+6.2}_{-5.8}$
b_1^0	$-6.8^{+6.3}_{-6.9}$
b_2^0	4^{+12}_{-12}
$f_T(0)$	$0.282^{+0.026}_{-0.026}$
b_1^T	$-0.7^{+4.3}_{-4.6}$
b_2^T	$-3.0^{+6.3}_{-5.9}$

Table 6.3: The median values and central 68% probability intervals obtained from the one-dimensional marginalized posterior distributions for the parameters of the common BCL parametrization eq. (6.10) for the $K = 3$ fit when fitted to the LCSR pseudo data points. The total χ^2 is 0.017 for 6 degrees of freedom, corresponding to a p value in excess of 99% at the best-fit point.

There is a single subthreshold pole, which corresponds to the B^* bound state. The factor $(1 - q^2/M_{B^*}^2)^{-1}$ accounts simultaneously for the asymptotic behaviours for $q^2 \to \infty$ and the bound state. As for the vector form factor we expand to order z^K. Above the pair production threshold, two units of orbital angular momentum impose that Disc $f_+ \propto p^{5/2}$. Hence, the absence of a $p^{1/2}$ term can again be used to eliminate the expansion coefficient b_K^T in lieu of the coefficients b_n^T with $n < K$.

Based on the above considerations, the common BCL parametrization then reads:

$$
\begin{aligned}
f_+(q^2) &= \frac{f_+(q^2=0)}{1 - q^2/m_{B^*}^2}\left[1 + \sum_{n=1}^{K-1} b_n^+ \left(\bar{z}_n - (-1)^{n-K}\frac{n}{K}\bar{z}_K\right)\right], \\
f_0(q^2) &= f_+(q^2=0)\left[1 + \sum_{n=1}^{K-1} b_n^0 \bar{z}_n\right], \\
f_T(q^2) &= \frac{f_T(q^2=0)}{1 - q^2/m_{B^*}^2}\left[1 + \sum_{n=1}^{K-1} b_n^T \left(\bar{z}_n - (-1)^{n-K}\frac{n}{K}\bar{z}_K\right)\right],
\end{aligned}
\tag{6.10}
$$

with $\bar{z}_n \equiv z^n - z_0^n$, $z \equiv z(q^2; t_+, t_0)$, and $z_0 = z(0; t_+, t_0)$. Here the kinematical constraint $f_+(0) = f_0(0)$ is manifestly fulfilled, which reduces the overall number of free parameters by one.

In the following a fit to the common BCL parametrization eq. (6.10) to the 14 LCSR pseudo data points and their correlated uncertainties is presented. As discussed in that section, the correlated pseudo data points can be counted as 14 independent observations. Adding further data points is unlikely to increase the

amount of information, due to the already large degree of correlation among the data points. In the fit to the LCSR prediction, the number of fit parameters is therefore limited to be smaller than 14, corresponding to a maximal order $K = 4$ in the z expansion, which has eleven independent parameters.

Two fits are carried out: one with $K = 3$, and one with $K = 4$. Already for $K = 3$ a good fit is obtained, with $\chi^2/\text{d.o.f.} \sim 0.017/6$ and a p value in excess of 99%. The goodness of fit therefore gives no indication that higher orders of z are required in the fit model. Nevertheless, a fit is carried out with $K = 4$ to obtain a handle on the systematic extrapolation error inherent to the form factor parametrization. Medians and central 68% probability intervals of the marginalized one-dimensional posterior distributions are shown for each of the BCL parameters for the $K = 3$ fit in table 6.3. Corresponding results in the $K = 4$ fit are compatible with the results of the $K = 3$ fit at the 1σ level. This is not surprising, since the uncertainty intervals for the shape parameters in the $K = 4$ fit are an order of magnitude larger than those in the $K = 3$ fit, while the goodness of fit cannot be improved further. Therefore, the $K = 3$ fit is used as our default for numerical values and illustrations in this section. Note that the unitarity bounds that have been formulated for exclusive $b \to u$ transitions form factors [129, 260] are not used here.

Fit results in relation to the LCSR pseudo data points are shown in figure 6.3. This figure also indicates that this extrapolation to large q^2 has sizable uncertainties. Within these uncertainties, results are compatible with the available lattice QCD results [78–80] for the $\bar{B} \to \pi$ form factors. The latter are not part of the analyses in this section and are merely shown for an illustrative purpose. In both the $K = 3$ and the $K = 4$ fit the bands of posterior-predictions at 68% probability do not correspond to the 68% uncertainty regions of the data points. Empirically, it is found that this effect is caused by the large correlations among q^2-neighbouring data points and between the predictions for f_+ and f_0. The effect causes the BCL fit's uncertainty bands to trail slightly below the form factor pseudo data points.

The extrapolations of the LCSR results can be challenged in several ways.

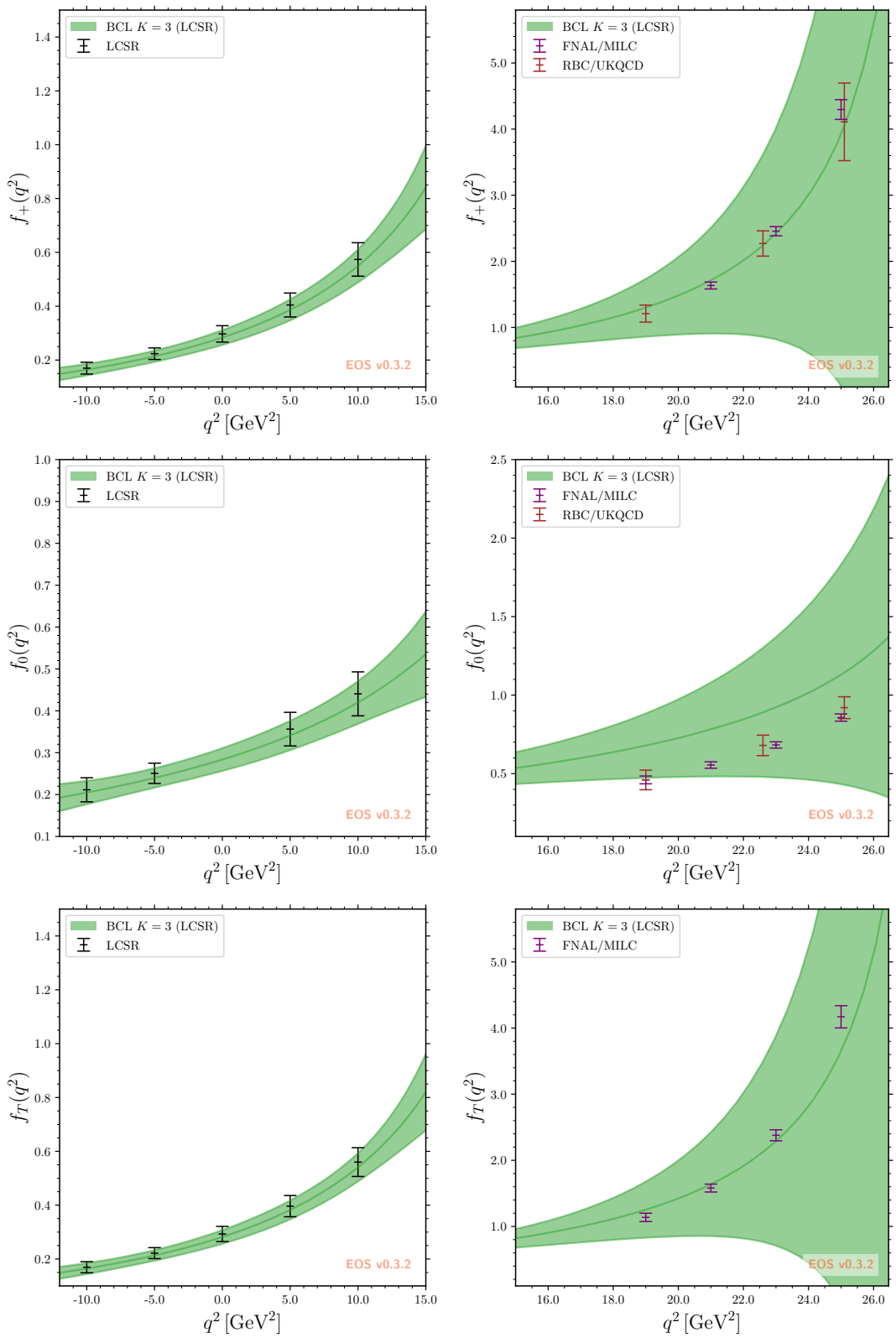

Figure 6.3: Posterior-predictions for the form factors f_+ (top), f_0 (center), and f_T (bottom) obtained from the fits of the common BCL parametrization (6.10) to *only* the LCSR pseudo data points discussed in section 6.1.3. Lattice QCD points are merely shown for illustrative purpose. The bands correspond to the envelope at 68% probability.

First, a dispersive representation of $f_+(q^2)$ implies that:

$$\text{Res}_{q^2 \to m_{B^*}^2} f_+(q^2) = \frac{1}{2} f_{B^*} m_{B^*} g_{B^* B\pi} = 14.6 \pm 1.3\,\text{GeV}^2\,, \tag{6.11}$$

for which $f_B = 190 \pm 1.3\,\text{MeV}$ from a lattice calculation is used, $f_B^*/f_B = 0.958 \pm 0.022$ [226] and $g_{B^*B\pi} = 30.1^{+2.6}_{-2.4}$ from a recent QCD light-cone sum rule calculation [261]. Since the common BCL parametrization for f_+ includes a pole for the B^*, an analytical formula for the residue can be obtained. From the fit described above

$$\text{Res}_{q^2 \to m_{B^*}^2}\, f_+(q^2) = 12 \pm 29\,\text{GeV}^2\,, \tag{6.12}$$

which is in agreement with eq. (6.11) within its sizable uncertainties. The uncertainties presented are of parametric origin only. Systematic uncertainties due to higher orders in the z expansion are not taken into account, and could be sizable due to the magnitude of $z(q^2 = m_{B^*}^2)$. The residue is therefore not immediately useful to check the validity of our extrapolation to large q^2.

Second, the soft-pion theorem relates the form factor f_0 to the B-meson and pion decay constants [70, 71, 262–264] as

$$f_0(t_-) + f_0(t_+) = \frac{2 f_B}{f_\pi} \left[1 - \frac{m_u + m_d}{m_d + m_b}\right] = 2.914 \pm 0.092\,. \tag{6.13}$$

The relation holds even at next-to-leading order in $1/m_b$, and including short-distance corrections [265]. Here the same numerical inputs are used as above and additionally $f_\pi = 130.2 \pm 0.8\text{MeV}$ [4]. From the fit described above

$$f_0(t_-) + f_0(t_+)\Big|_{\text{LCSR only}} = 5.1 \pm 6.3\,. \tag{6.14}$$

Although our results are consistent with the expectation in eq. (6.13), the uncertainties are so large that we cannot use the above relations to carry out a meaningful test of the validity of our extrapolation.

Third, in the large-energy symmetry limit the form factors f_+ and f_0 are related

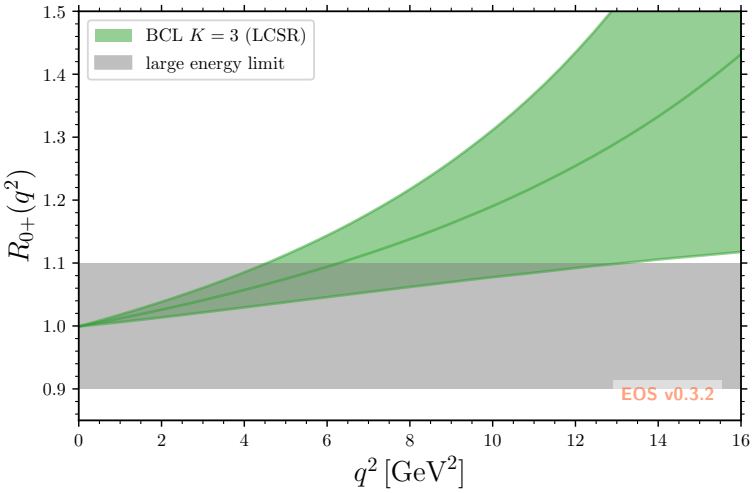

Figure 6.4: The ratio of form factors $R_{0+}(q^2)$ as defined in the text. We extrapolation is based on the fit to LCSR pseudo data and compared with the symmetry limit (6.15), which is valid for large π energy in the B-meson rest frame or equivalently at small q^2.

via [181]:

$$f_0(q^2) = \frac{m_B^2 + m_\pi^2 - q^2}{m_B^2} f_+(q^2) \left(1 + \mathcal{O}\left(\frac{\Lambda_\text{had}}{E_\pi}, \frac{\Lambda_\text{had}}{m_B}\right)\right). \tag{6.15}$$

Here E_π is the energy of the π in the B rest frame. A useful measure of compatibility can therefore be obtained through the ratio

$$R_{0+}(q^2) = \frac{m_B^2}{m_B^2 + m_\pi^2 - q^2} \frac{f_0(q^2)}{f_+(q^2)}. \tag{6.16}$$

This ratio is shown in figure 6.4 based on an extrapolation of the LCSR form factors. The LCSR results are consistent with the large-energy limit within $\sim 10\%$ uncertainty up to $\simeq 13\,\text{GeV}^2$, *i.e.* within the whole region of applicability of the LCSRs.

In the next section form factor extractions are performed in a combined fit to LCSR and lattice QCD inputs. This procedure further constrains the form factors at high q^2 and reduces the uncertainties appreciably.

6.2. Interpolation between LCSR and lattice QCD form factors

In this section the LCSR results obtained in section section 6.1.3 is interpolated with precise results for the $\bar{B} \to \pi$ form factors obtained from lattice QCD simulations. These lattice QCD results exhibit very small uncertainties for $19\,\text{GeV}^2 \lesssim q^2 \lesssim 25\,\text{GeV}^2$, outside the reach of the light-cone sum rules. In this section two independent sets of lattice QCD results are used. The first set is provided by the FNAL/MILC collaboration [78, 79] based on $N_f = 2 + 1$ gauge ensembles and a staggered-quark action. The second set is provided by the RBC/UKQCD collaboration [80] based on $N_f = 2 + 1$ gauge ensembles with domain wall fermions.

Information from an older analysis by the HPQCD collaboration [266] isn't appropriated here for two reasons: first, it shares some of the $N_f = 2 + 1$ ensembles with the results published by FNAL/MILC [78]; second, it does not provide correlations between the f_+ and f_0 results. A more recent HPQCD analysis [267] providing a single, very precise value for f_0 at zero-recoil is also bypassed. Again, some of the $N_f = 2{+}1$ ensembles are shared with the FNAL/MILC analysis, and the correlations between the HPQCD and the FNAL/MILC results cannot be accounted for.

The usage of RBC/UKCQCD data is straightforward, since ref. [80] provides both the f_+ and the f_0 form factor in three different q^2 points including their correlations. These data are therefore used in the likelihood as a multivariate gaussian constraint.

The usage of the FNAL/MILC data is more involved, since refs. [78, 79] do not provide data points for any of the form factors. Instead, these references provide the outcome of a BCL fit to the data points. As discussed below, a need to modify the BCL parametrization is present, making it impossible to use the BCL results of FNAL/MILC collaboration as is. Instead, the BCL results are used to produce pseudo data points of the form factors. Three such points are produced for f_+ and four points both for f_0 and for f_T. The points are chosen in the range $19\,\text{GeV}^2 \leq q^2 \leq 25\,\text{GeV}^2$. Based on information provided in ref. [78, 79], this range of q^2 was

Table 6.4: A complete list of the data points for the 3 transition form factors used in the combined fit.

form factor	# of points	q^2 values (in GeV^2)	type	source
f_+	5	-10.0, -5.0, 0.0, 5.0, 10.0	LCSR	this work
	3	21.0, 23.0, 25.0	LQCD	FNAL/MILC [78]
	3	19.0, 22.6, 25.1	LQCD	RBC/UKQCD [80]
f_0	4	-10.0, -5.0, 5.0, 10.0	LCSR	this work
	4	19.0, 21.0, 23.0, 25.0	LQCD	FNAL/MILC [78]
	3	19.0, 22.6, 25.1	LQCD	RBC/UKQCD [80]
f_T	5	-10.0, -5.0, 0.0, 5.0, 10.0	LCSR	this work
	4	19.0, 21.0, 23.0, 25.0	LQCD	FNAL/MILC [79]

chosen to minimize the total uncertainty. The smaller number of points for f_+ is due to a peculiarity in the BCL fit results. The covariance matrix provided in ref. [78] is singular. This can be understood, since in that work the identity $f_+(0) = f_0(0)$ is not manifestly fulfilled by the parametrization. Based on the authors' suggestions [268], the coefficient b_3^+ (in their notation) is replaced by a linear combination of the remaining coefficients, such that the identity $f_+(0) = f_0(0)$ is manifestly fulfilled. This replacements requires the removal of the row and column associated with b_3^+ from the correlation matrix, reducing the number of free parameters to three. Hence, the maximal number of independent pseudo data points from FNAL/MILC is now also limited to three.

An overview of the data points used is provided in table 6.4.

With the likelihood for the lattice QCD results at hand, a simultaneous fit of the common BCL parametrization is carried out in eq. (6.10) to both the LCSR pseudo data points and the lattice QCD data points. For $K = 3$ the fit yields a minimal $\chi^2 \simeq 154$. Given 23 degrees of freedom in the fit, this corresponds to a p value considerably smaller than the a-priori threshold of choice amounting to 3%. Therefore, this fit is rejected. Investigating the BCL paramatrization with $K = 4$, Better agreement, with a minimal $\chi^2 = 27.5$ for 20 degrees of freedom, is found. The corresponding p value of 12% is acceptable. For both cases, a visual comparison of the extrapolation of the LCSR results for f_+ and f_T with the lattice data as shown in figure 6.3 does not give any reason to expect a bad fit. However, the same figure illustrates that the extrapolation of f_0 is not easily compatible with the

lattice points. Therefore, the goodness of fit of the overall analysis hinges crucially on the correlations between f_0 and the other form factors.

The surprising result for the fit with the common BCL parametrization implies an investigation of alternative fit models is needed. The parametrization of the f_0 form factor is thus modified by including a pole above the $B\pi$ pair production threshold, corresponding to a scalar $B\pi$ resonance. Since no such resonance has been observed yet, its mass has to be estimated. To this end, the heavy-quark limit is employed, which yields:

$$m_{B_{s,0}} - m_{B_s^*} = m_{B_0} - m_{B^*} \simeq 215\,\text{MeV} \tag{6.17}$$

Here $B_{s,0}$ and B_0 denote the lowest-lying scalar BK and $B\pi$ resonances, respectively, with valence quark contents $(\bar{b}s)$ and $(\bar{b}d)$. Using the known masses of the $B^*_{(s)}$, $m_{B^*} = 5.325\,\text{GeV}$ $m_{B_s^*} = 5.415\,\text{GeV}$ [4], the value $m_{B_0} = 5.540\,\text{GeV}$ arises. This value is meant as rough estimate only, and slight variations of the value can and will be accommodated by the parameters of the modified BCL parametrization. The modified BCL parametrization then reads:

$$\begin{gathered} f_0(q^2) = \frac{f_+(z_0)}{1 - q(z)^2/m_{B_0}^2}\left[1 + \sum_{n=1}^{K} b_n^0 \bar{z}_n\right], \\ f_+(q^2),\, f_T(q^2) : \text{unchanged with respect to eq. (6.10)}\,, \end{gathered} \tag{6.18}$$

where the maximal order of the z expansion for the f_0 form factor has also been increased. In this way the same number of shape parameters for each form factor is used. (Note that for f_+ and f_T one shape parameter is fixed as discussed in section 6.1.4.) The stated modification does not allow to apply the unitarity bounds for the f_0 form factor as is. However, alternative parametrizations such as the BGL parametrization can account for above-threshold poles in the formulation of the unitarity bounds [269], which are not considered here. The fits are repeated with the modified BCL parametrization in eq. (6.18) with $K = 3$ and $K = 4$. In both cases acceptable to good fits are obtained, with p values of 52% and 54%

respectively.[2] Effectively, the pole modifies the shape parameters and implicitly allows for more flexibility of the fit. Explicitly expanding the B^* pole factor in z around $q^2 = 0$ yields:

$$\frac{1}{1 - q(z)^2/m_{B^*}^2} \approx \frac{1}{1 - \frac{t_0}{m_{B^*}^2}} + 4\frac{m_{B^*}^2(t_0 - t_+)}{(m_{B^*}^2 - t_0)^2} z + \mathcal{O}\left(z^2\right) . \tag{6.19}$$

This illustrates that additional powers of z are now available to relieve the apparent tension between the LCSR and LQCD data of f_0.

The median values and central 68% probability intervals for each marginalized one-dimension posteriors are provided in table 6.5. The covariance matrix is provided as an ancillary file together with the arXiv preprint of the publication this section is based upon. The fit parameter values for $K = 4$ are consistent with the ones for $K = 3$ within uncertainties. Investigating the $K = 5$ case, the p value increases insignificantly compared to the $K = 4$ case. Although the $K = 3$ fit is also acceptable, the $K = 4$ fit is presented here as the main result. The reason is that at $K = 4$ the fit can account for an additional systematic uncertainty due higher orders in the z expansion.

Plots of the posterior predictions for each form factor are provided in figure 6.5. A cursory glance at the $f_+(0)$ plot suggest a $\sim 1.4\sigma$ deviation between the fit to the LCSR results only and the fit to the combined LCSR+LQCD likelihood. This naive interpretation *is not useful*, due to strong correlation between the normalization and the shape parameters. As a consequence, the compatibility in this point cannot be accurately computed, and the overall goodness-of-fit diagnostics of our fits, such as the p value, must suffice.

The fits to LCSR data only shown in this section are carried out with the modified BCL parametrization as given in eq. (6.18) and therefore differ slightly to those obtained in section 6.1.4.

The precision of the extrapolation of the form factors significantly improves by combining the LCSR and LQCD inputs, especially in the large q^2 region, as expected.

[2] The inclusion of the scalar resonance makes up for the majority of the p value improvement. Keeping only the pole and fixing the additional shape parameter to zero yields p values of 7% and 60%, respectively.

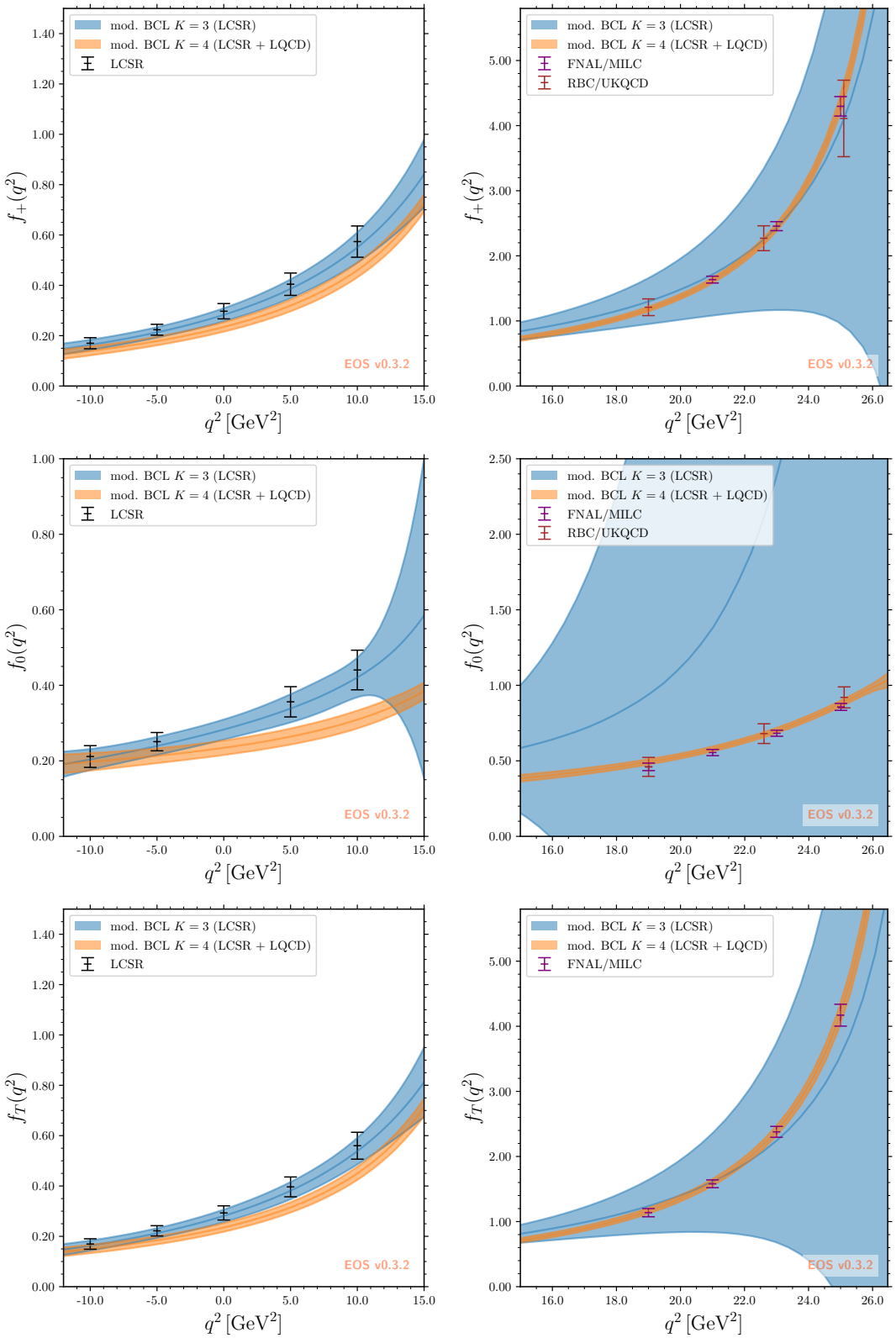

Figure 6.5: Posterior-predictions for the form factors f_+ (top), f_0 (center), and f_T (bottom) obtained from the fits of the modified BCL parametrization (6.18) to the LCSR pseudo data points only (blue bands), and both the LCSR and lattice QCD inputs (orange bands). The bands correspond to the envelope at 68% probability.

Table 6.5: The median values and central 68% probability intervals for the parameters of the modified BCL parametrisation from eq. (6.18) when fitted to the LQCD and LCSR pseudo data.

scenario / param.	LCSR+LQCD		LCSR
	$K = 3$	$K = 4$	$K = 3$
$f_+(0)$	$0.237^{+0.017}_{-0.017}$	$0.235^{+0.019}_{-0.019}$	$0.283^{+0.027}_{-0.027}$
b_1^+	$-2.38^{+0.33}_{-0.38}$	$-2.45^{+0.49}_{-0.54}$	$-1.0^{+3.5}_{-3.6}$
b_2^+	$-0.82^{+0.76}_{-0.81}$	$-0.2^{+1.1}_{-1.2}$	$-2.8^{+4.9}_{-4.7}$
b_3^+	—	$-0.9^{+4.2}_{-4.0}$	—
b_1^0	$0.48^{+0.07}_{-0.07}$	$0.40^{+0.18}_{-0.20}$	-5^{+52}_{-51}
b_2^0	$0.14^{+0.39}_{-0.44}$	$0.1^{+1.1}_{-1.2}$	22^{+200}_{-200}
b_3^0	$2.79^{+0.71}_{-0.77}$	$3.7^{+1.6}_{-1.6}$	-32^{+240}_{-240}
b_4^0	—	1^{+14}_{-13}	—
$f_T(0)$	$0.240^{+0.016}_{-0.016}$	$0.235^{+0.017}_{-0.017}$	$0.281^{+0.025}_{-0.025}$
b_1^T	$-2.05^{+0.32}_{-0.36}$	$-2.45^{+0.45}_{-0.50}$	$-0.6^{+4.2}_{-4.4}$
b_2^T	$-1.45^{+0.63}_{-0.66}$	$-1.08^{+0.68}_{-0.71}$	$-3.2^{+5.9}_{-5.8}$
b_3^T	—	$2.6^{+2.1}_{-2.0}$	—
p value	$\sim 52\%$	$\sim 54\%$	$\sim 100\%$
χ^2/d.o.f	$\sim 21.01/22$	$\sim 17.75/19$	$\sim 0.0278/5$

Now, eq. (6.11) is revisited in order to extract the strong coupling constant from the combined fit. We obtain:

$$g_{B^*B\pi} = 39.8 \pm 1.1\,, \tag{6.20}$$

where the uncertainties are of parametric origin only. Systematic uncertainties due to higher orders in the z expansion are not taken into account, and could be sizable due to the magnitude of $z(q^2 = m_{B^*}^2)$. The result eq. (6.20) agrees well with the lattice determination $g_{B^*B\pi} = 45.3 \pm 6.0$ by the RBC/UKQCD collaboration [270], but it shows a tension with respect to the recent direct LCSR determination $g_{B^*B\pi} = 30.1^{+2.6}_{-2.4}$ [261] at the level of $3.4\,\sigma$.[3]

However, the extrapolation becomes unstable for $q^2 \geq t_-$, *i.e.*, outside the

[3]Note that it was already observed in [261] that a significantly larger result arises when using eq. (6.11) than when calculating this quantity directly.

Table 6.6: Comparison of the results for the form factor normalizations with other QCD-based results in the literature. The result of ref. [254] is included for completeness, although the authors caution that the threshold setting procedure employed in that work fails for the $\bar{B} \to \pi$ form factors.

Source	$f_+(0) = f_0(0)$	$f_T(0)$
Lattice QCD		
Fermilab/MILC [78, 79]	0.2 ± 0.2	0.2 ± 0.2
RBC/UKQCD [80]	0.24 ± 0.08	—
combination w/ Pade approx. [207]	$0.265 \pm 0.010 \pm 0.002$	—
Light-cone sum rules		
Duplancic et al. [95]	$0.26^{+0.04}_{-0.03}$	0.255 ± 0.035
Imsong et al. [206]	0.31 ± 0.02	—
Bharucha [252]	$0.261^{+0.020}_{-0.023}$	—
Khodjamirian/Rusov [259]	0.301 ± 0.023	0.273 ± 0.021
Gubernari et al. (B LCDA) [254]	0.21 ± 0.07	0.19 ± 0.06
this work	0.283 ± 0.027	0.282 ± 0.026
Light-cone sum rules + Lattice QCD combination		
this work	0.235 ± 0.019	0.235 ± 0.017

semileptonic phase space: the 68% probability region for the f_0 form factor starts to cover both positive and negative values, and the central value turns negative just below $q^2 = t_+$. This finding of negative form factors is inconsistent with a dispersive representation of the form factor. The behaviour is suspected to be an artifact of the fit model. Hence, no meaningful way is obvious to compare these results to the expectation from the Callan-Treiman type relation in eq. (6.14).

In figure 6.6 a plot of $R_{0+}(q^2)$ for the form factors interpolating the LCSR and LQCD data is provided. The results appear to be consistent with the large-energy limit from eq. (6.15). Compared to the LCSR-only result, the range in which the large-energy symmetry limit holds has expanded up to $\simeq 15\,\mathrm{GeV}^2$.

A comparison of form factor values computed here and those in the literature is compiled in table 6.6.

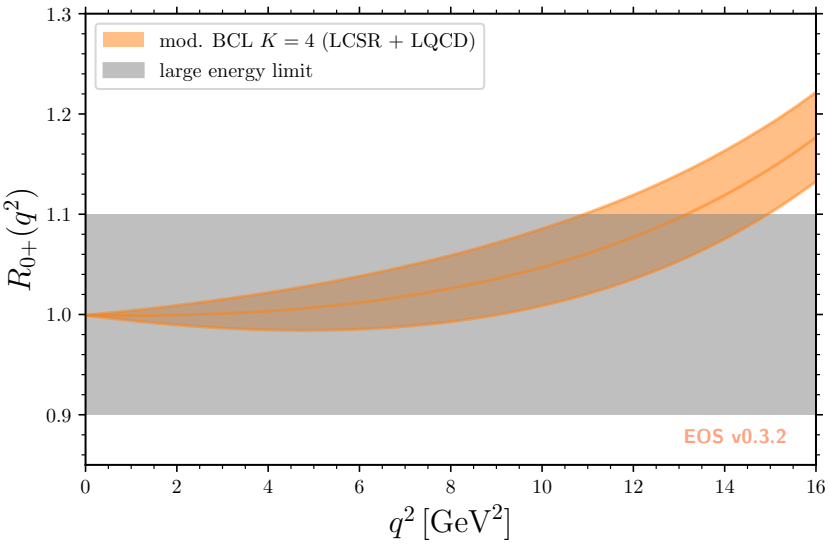

Figure 6.6: The form factor ratio $R_{0+}(q^2)$ interpolated between LCSR and LQCD data and compared to the large-energy symmetry limit in the low q^2 region.

6.3. Phenomenology

6.3.1. Exclusive $|V_{ub}|$ determination

Following the determination of the form factors from LCSRs and lattice QCD input, the extraction of the magnitude of the CKM matrix element $|V_{ub}|$ is now possible from measurements of the $\bar{B} \to \pi \ell^- \bar{\nu}_\ell$ branching ratio.

To this end, the world average of the branching ratio as provided by the HFLAV collaboration [42] is used. This average is based on individual measurements by the BaBar [271, 272] and Belle [273, 274] collaborations. The world average is provided in terms of 13 bins of the squared momentum transfer q^2, with identical bin sizes. Within the averaging process, HFLAV accounts for shared systematic correlations among the individual measurements.

A visual representation of this data, which is provided in figure 6.7, shows that the highest relative experimental precision is achieved in for intermediate q^2, *i.e.*, in a region that is not reliably accessible with LCSRs and not yet accessible with lattice QCD simulations. Consequently, the efforts presented in teh section above – to obtain high-precision determinations of the form factors at intermediate q^2 through interpolation of the respective theory results is of high importance to the $|V_{ub}|$ determination. This is nicely illustrated in Fig. 3 of ref. [130].

The $|V_{ub}|$ extraction analysis is set up in the same way as in section 6.2. This means that the fit using the modified BCL parametrization is exclusively employed in this section. As the only modification with respect to section 6.2, the HFLAV average is included as part of the likelihood. The theory prediction for the $\bar{B} \to \pi \ell^- \bar{\nu}_\ell$ branching ratio does not depend on the form factor f_T in the SM, which is assumed for the following fit. For $\ell = e, \mu$ the branching ratio is only very weakly dependent on the form factor f_0, which contributes measurably only for $q^2 \lesssim 1\,\text{GeV}^2$. Additionally, the predictions for f_0 are affected by interaction between the experimental constraint on f_+ and the theoretical correlations between f_+ and f_0. As a consequence, the results are presented as one-dimensional marginalized posterior distributions only for $|V_{ub}|$ and the parameters describing the f_+ form

Table 6.7: Results from the three fits to combinations of fit models and data sets as described in the text. The median values and central intervals ar provided at 68% probability for the one-dimensional marginalized posterior distributions.

param. \ method	LCSR+LQCD		LCSR only
	$K = 3$	$K = 4$	$K = 3$
$10^{-3} \times \lvert V_{ub}\rvert$	$3.80^{+0.14}_{-0.14}$	$3.77^{+0.15}_{-0.15}$	$3.28^{+0.33}_{-0.28}$
$f_+(0)$	$0.248^{+0.009}_{-0.009}$	$0.246^{+0.009}_{-0.009}$	$0.284^{+0.025}_{-0.025}$
b_1^+	$-2.13^{+0.19}_{-0.19}$	$-2.10^{+0.22}_{-0.21}$	$-1.91^{+0.31}_{-0.30}$
b_2^+	$-0.82^{+0.54}_{-0.55}$	$0.23^{+0.87}_{-0.87}$	$-1.42^{+0.85}_{-0.89}$
b_3^+	—	$-3.0^{+2.8}_{-2.8}$	—
χ^2/d.o.f	$\sim 32.33/34$	$\sim 29.30/31$	$\sim 10.72/17$
p value	$\sim 55\%$	$\sim 55\%$	$\sim 87\%$

factor. Fits are carried out to the LCSR pseudo data only in the $K = 3$ fit model as well as combined fits to the LCSR + lattice QCD inputs in the $K = 3$ and $K = 4$ models. In all cases a good fit is found, with p values in excess of 55%. While the $K = 4$ fit model to LCSR + lattice QCD inputs does not provide a significantly improved goodness of fit, it is still adopted it as the nominal fit model here. The reasoning is that this model can account for additional systematic uncertainties inherent to the extrapolation process, which slightly increases the uncertainty of the $|V_{ub}|$ extraction. The smallness of the difference in the $K = 3$ and $K = 4$ uncertainties seems to indicate that systematic uncertainties are under reasonable control. Summaries of the one-dimension marginalized posteriors in terms of their median values and central 68% probability intervals are provided in table 6.7.

The LCSR-only fit yields a $|V_{ub}|$ result that is slightly smaller than the LCSR + lattice LQCD results by approximately more than one sigma. The latter results for $K = 3$ and $K = 4$ are in mutual agreement. This is not surprising, given the shift in $f_+(0)$ between these two scenarios, which is already discussed in section 6.2. The results for $K = 3$ and $K = 4$ for fit to LCSR + lattice LQCD results are perfectly compatible with each other. The nominal result is obtained from the fit to LCSR

Table 6.8: Comparison of the $|V_{ub}|$ CKM matrix element determinations from the $\bar{B} \to \pi\ell^-\bar{\nu}_\ell$ decays, using QCD-based form factor predictions.

Source	$10^{-3} \times \lvert V_{ub}\rvert$
LQCD	
Fermilab/MILC [78, 79]	3.72 ± 0.16
RBC/UKQCD [80]	3.61 ± 0.32
combination w/ Pade approx. [207]	$3.53 \pm 0.08_{\text{stat}} \pm 0.06_{\text{syst}}$
HFLAV [42]	$3.70 \pm 0.10_{\text{stat}} \pm 0.12_{\text{syst}}$
LCSR	
Duplancic et al. [95]	$3.5 \pm 0.4 \pm 0.2 \pm 0.1$
Imsong et al. [206]	$3.32^{+0.26}_{-0.22}$
this work	$3.28^{+0.33}_{-0.28}$
LCSR + LQCD	
HFLAV [42]	$3.67 \pm 0.09_{\text{stat}} \pm 0.12_{\text{syst}}$
this work	3.77 ± 0.15

+ lattice QCD input with $K = 4$, and reads

$$|V_{ub}|^{\bar{B}\to\pi}_{\text{LCSR+LQCD}} = (3.77 \pm 0.15) \cdot 10^{-3}. \tag{6.21}$$

The apparent slight tension between $f_+(0)$ obtained from the fit to LCSR data only and the fit to LCSR+LQCD data, as previously discussed in section 6.2, persists here as well. It translates to a reasonable agreement between the determinations of $|V_{ub}|$ at the $1.4\,\sigma$ level. A very good fit is found using the combined LCSR and LQCD data, with $\chi^2/\text{d.o.f.} \sim 1$, and a p value of $\sim 55\%$ at the best-fit point. Adding information on the form factor shape through the HFLAV average of the experimental data does not affect the results for the BCL parameters compared to results of the theory-only fit in section 6.2. This result exhibits a slight tension with the BLNP and GGOU determinations from eq. (6.1), in both cases at the $\approx 2\,\sigma$ level. However, it is in very good agreement with the recent method-averaged result by the Belle collaboration as given in eq. (6.3). Here the tension reduces to $\approx 1\,\sigma$ only.

The nominal results for $|V_{ub}|$ is compared with other methods in table 6.8 and in figure 6.8 the Standard Model prediction is presented for the differential decay rate of $\bar{B} \to \pi\ell^-\nu_\ell$ divided by $|V_{ub}|$ for the electron and tau lepton final states.

The normalized branching ratios obtained with the use of the theory-only form factors from section 6.2 yield

$$\begin{aligned} \mathcal{B}(\bar{B} \to \pi\mu^-\bar{\nu}_\mu) &= \left(9.6^{+1.0}_{-1.0}\right) \times |V_{ub}|^2\,, \\ \mathcal{B}(\bar{B} \to \pi\tau^-\bar{\nu}_\tau) &= \left(6.7^{+0.6}_{-0.5}\right) \times |V_{ub}|^2\,. \end{aligned} \tag{6.22}$$

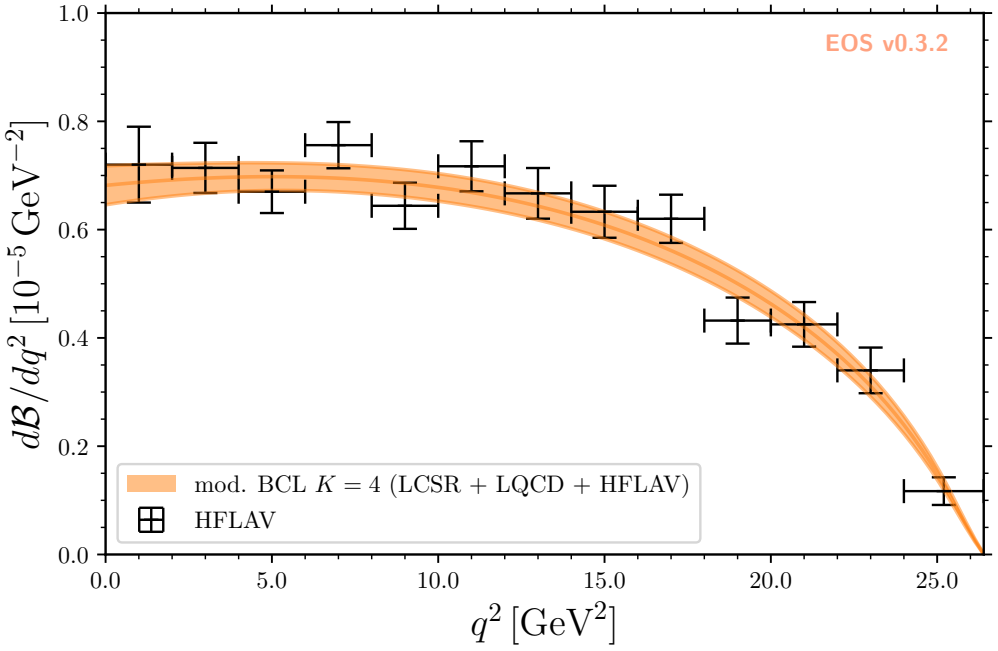

Figure 6.7: Differential branching ratio for $\bar{B}^0 \to \pi^+\ell^-\bar{\nu}_\ell$ decay as obtained from the combined fit to LCSR and lattice QCD inputs and experimental data, compared to the HFLAV average of the experimental data.

6.3.2. Lepton flavour universality ratio

Next, predictions are made for the SM observables for the $\bar{B} \to \pi\ell^-\bar{\nu}_\ell$ decay results as obtained in section 6.2.

In light of hints for LFU violating effects in $\bar{B} \to D^{(*)}\ell^-\bar{\nu}_\ell$ decays [42, 275], the

LFU-probing observable for $\bar{B} \to \pi\ell^-\bar{\nu}_\ell$ decays is investigated, as

$$R_\pi = \frac{\Gamma(\bar{B} \to \pi\tau^-\bar{\nu}_\tau)}{\Gamma(\bar{B} \to \pi\ell^-\bar{\nu}_\ell)} = \frac{\int_{m_\tau^2}^{q^2_{\rm max}} d\Gamma(\bar{B} \to \pi\tau^-\bar{\nu}_\tau)/dq^2}{\int_{m_\ell^2}^{q^2_{\rm max}} d\Gamma(\bar{B} \to \pi\ell^-\bar{\nu}_\ell)/dq^2}, \qquad (\ell = e, \mu)\,. \tag{6.23}$$

In the SM, predictions for R_π involve only two out of three form factors, f_+ and f_0. Using the results from the form factor fit with $K = 4$ as obtained in section 6.2 it is found that

$$R_\pi\big|_{\rm LCSR+LQCD} = 0.699^{+0.022}_{-0.020}\,. \tag{6.24}$$

The central values for R_π as predicted from the $K = 3$ and $K = 5$ fits fall entirely within the above uncertainties. Also shown are the differential branching ratios for the tauonic and light-lepton modes individually in figure 6.8.

It is important to stress that for a precise determination of R_π knowledge of the scalar form factor $f_0(q^2)$ is key. To demonstrate this, the contributions to the tauonic decay width stemming from each of the form factors is disentangled

$$R_\pi \equiv R_\pi^+ + R_\pi^0\,, \tag{6.25}$$

corresponding to the $|f_+|^2$ and $|f_0|^2$ contributions, respectively. Numerically

$$R_\pi^+\big|_{\rm LCSR+LQCD} = 0.476^{+0.014}_{-0.013}\,, \quad R_\pi^0\big|_{\rm LCSR+LQCD} = 0.224^{+0.014}_{-0.013}\,. \tag{6.26}$$

Although the f_0 contribution is half the size of the f_+ contribution, its relative uncertainty is about two times as large as the one of the f_+ term. This illustrates the importance of accurately predicting both of the form factors for this LFU probe.

In table 6.9 a comparison of the nominal results presented in previous sections with the available determinations of R_π in the literature is provided. The prediction presented in this section is in very good agreement at or below the $1\,\sigma$ level with the previous determinations provided in refs. [80, 276]. A minor exception is the prediction of ref. [277], which is in slight tension with results presented here at the $2\,\sigma$ level.

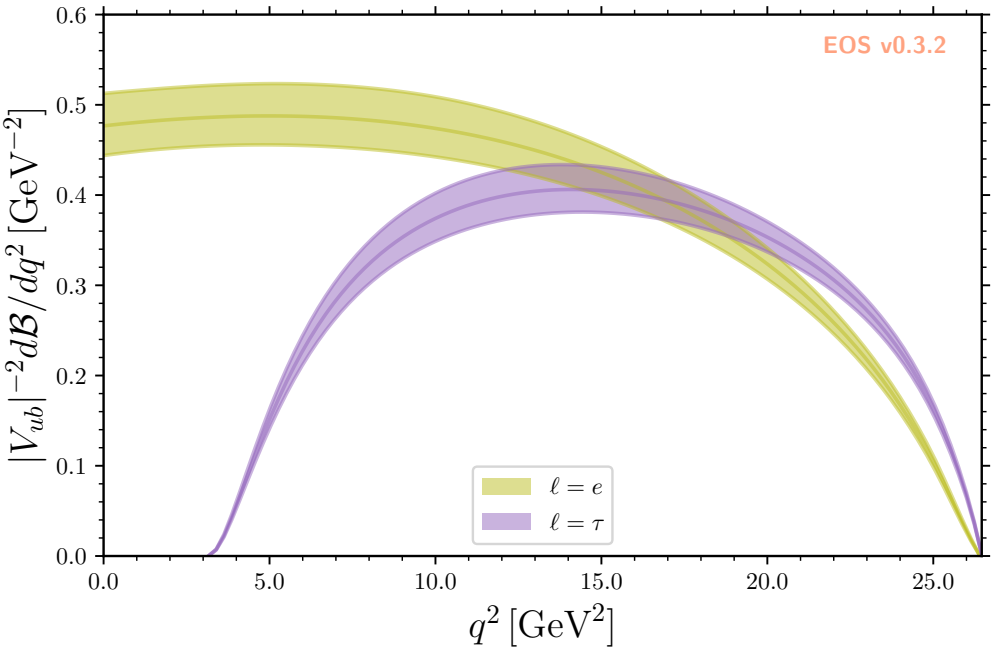

Figure 6.8: Our Standard Model prediction of the differential decay rate of $\bar{B} \to \pi\ell^-\bar{\nu}_\ell$ divided by $|V_{ub}|$ for the electron and tau final states. The form factors are obtained from a fit to both LCSR and LQCD inputs using modified BCL parametrization in the $K = 4$ fit model.

Although the LFU ratio R_π is $|V_{ub}|$-independent, it could, on the other hand, be sensitive to potential new physics effects in $\bar{B} \to \pi\tau^-\bar{\nu}_\tau$ decay due to the presence of new scalar currents and/or electroweak symmetry breaking effects associated with the large mass of the τ lepton. Hence, R_π is a very interesting candidate for future measurements. To date, there is a single experimental result by the Belle collaboration [278]. It is obtained from an upper limit on the branching ratio of $\bar{B} \to \pi\tau^-\bar{\nu}_\tau$, which has not yet been observed. This result reads:

$$R_\pi\big|_{\text{Belle}} = 1.05 \pm 0.51\,, \tag{6.27}$$

which, again, agrees with the predicition using form factors from section 6.2.

Table 6.9: Comparison of theory results for the LFU ratio R_π in the literature.

Th. only	source	RBC/UKQCD [80]	Bečirević et al. [276]	this work
	R_π	0.69±0.19	0.78±0.10	0.699±0.022
Th. + Exp.	source	Bernlochner [277]	Bečirević et al. [276]	this work
	R_π	0.641±0.016	0.66±0.02	0.688±0.014

6.3.3. Angular observables and polarizations in $\bar{B} \to \pi\ell^-\bar{\nu}_\ell$

Now the form factor results can be used to predict the two angular observables in the two-fold differential decay rate of $\bar{B} \to \pi\ell^-\bar{\nu}_\ell$ as well as the lepton polarization in these decays, as defined in appendix D.

Firstly, there is the forward-backward asymmetry in the Standard model. The integrated normalized forward-backward asymmetry is defined as

$$A_{\rm FB}^\ell = \frac{1}{\Gamma(\bar{B} \to \pi\ell^-\bar{\nu}_\ell)} \int_{m_\ell^2}^{q^2_{\rm max}} dq^2 \left[\int_{-1}^{0} - \int_{0}^{-1}\right] d\cos\theta_\ell \frac{d\Gamma^2(\bar{B} \to \pi\ell^-\bar{\nu}_\ell)}{dq^2 d\cos\theta_\ell}. \tag{6.28}$$

The forward-backward asymmetry arises from interference of the timelike polarization with the longitudinal polarization of the dilepton final state. The asymmetry is proportional to the mass of the charged lepton. Hence, $A_{\rm FB}$ is small for the $\ell = e, \mu$, which makes it very sensitive to BSM effects that could lift the helicity suppression. With the results for the form factors from section 6.2 in the SM

$$\begin{aligned} A_{\rm FB}^\mu &= -0.0048 \pm 0.0003\,, \\ A_{\rm FB}^\tau &= -0.259 \pm 0.004\,. \end{aligned} \tag{6.29}$$

The SM prediction for the electron mode is not provided, since it is indistinguishable from zero. The results are in reasonable agreement with the RBC/UKQCD results [80], but are more precise.[4]

The flat term F_H [279, 280] is another observables that arises in the normalized angular distribution. In the SM it is proportional to the lepton mass and therefore small. This makes it an appropriate candidate for a BSM probe, too. It can be

[4]Note that the convention for lepton helicity angle in ref. [80] differs from the one used in this section by a sign, which is also affecting the overall sign of $A_{\rm FB}$.

defined as

$$F_H^\ell = 1 + \frac{2}{3} \frac{1}{\Gamma(\bar{B} \to \pi \ell^- \bar{\nu}_\ell)} \frac{d^2}{d(\cos\theta)^2} \left[\frac{d\Gamma(\bar{B} \to \pi \ell^- \bar{\nu}_\ell)}{d\cos\theta} \right] = 1 + \frac{2}{3} C_F^\ell \,, \tag{6.30}$$

and is therefore related to the convexity parameter C_F^ℓ. With the results for the form factors from section 6.2 in the SM

$$F_H^\mu = 0.0024 \pm 0.0001; \qquad F_H^\tau = 0.134 \pm 0.003 \,. \tag{6.31}$$

The SM prediction for the electron mode is not provided, since it is indistinguishable from zero.

As a final BSM probe the integrated normalized τ polarization asymmetry is investigated, which can be expressed as

$$P^\tau = \frac{\Gamma(\bar{B} \to \pi \tau_\uparrow^- \bar{\nu}_\tau) - \Gamma(\bar{B} \to \pi \tau_\downarrow^- \bar{\nu}_\tau)}{\Gamma(\bar{B} \to \pi \tau^- \bar{\nu}_\tau)} \,, \tag{6.32}$$

where $\tau_{\uparrow,\downarrow}$ denotes the tau helicities $\lambda_\tau = \pm 1/2$. With the results for the form factors from section 6.2, in the SM

$$P^\tau = -0.21 \pm 0.02. \tag{6.33}$$

6.4. Conclusion

In this section, the $\bar{B} \to \pi$ form factors are studied and use their numerical results from QCD-based methods to update the exclusive determination of $|V_{ub}|$ from $\bar{B} \to \pi$ semileptonic decays and the SM predictions of a number of phenomenologically interesting observables.

The determination of the form factors using light-cone sum rules with π distribution amplitudes is revisited. The analysis presented in this section includes the full set of local $\bar{B} \to \pi$ form factors of dimension-three currents. For the first time, a threshold setting procedure based on Bayesian inference to the full set of these form factors is applied. Beside the thresholds, a value for the (unphysical) Borel parameter that is mutually compatible among all three form factors can be inferred.

The results for the form factors, obtained at small momentum transfer q^2, are then extrapolated to large q^2 by applying a standard BCL parametrization. This extrapolation agrees well with precise lattice QCD results for the form factor f_+ and f_T. However, in order to ensure good agreement also for the form factor f_0, its parametrization needs to be modified. For precise and consistent predictions the correct treatment of the correlations in the pseudo data points is crucial, especially between f_+ and f_0; this is sometimes overlooked in the literature. Correlated results are provided for the normalization and shape parameters of all form factors, including their correlations through ancillary machine-readable data files.

The predictions for the form factors agree very well with measurements of the q^2 spectrum of the semileptonic decay $\bar{B}^0 \to \pi^+ \ell^- \bar{\nu}_\ell$. Using its current world average the value $|V_{ub}| = (3.77 \pm 0.15) \cdot 10^{-3}$ is deduced. This result is in good agreement with the most recent inclusive determination by Belle at the $1\,\sigma$ level, which removes the long-standing tension between inclusive and exclusive $|V_{ub}|$ determinations.

The form factors at hand, SM predictions are also computed for a number of phenomenologically interesting observables, such as the lepton-flavour universality ratio R_π, the leptonic forward-backward asymmetry A_{FB}, the flat term F_H and the τ polarization P_τ. Based on the precise and correlated results for the form factors very precise predictions are obtained of the aforementioned observables. Their relative

uncertainties range from $\approx 10\%$ for the branching ratios to about 4% for some of the normalized observables. Precision measurements of these observables by the Belle experiment will further constrain the form factors and probe the SM at a precision level.

Conclusions

In this thesis several exclusive semileptonic channels of b-flavored mesonic decays were reviewed and proposed as tests of the SM. Form factor determinations were performed in the sum rule approaches coupled with HQET/HQSS/NRQCD consistency checks. The results are in each case extrapolated to a fit model inspired by dispersive relations and considerations of the correlations functions' analytical structure. For each decay, a specific phenomenological investigation is executed. In summary:

1. In $B_c \to (J/\psi, \eta_c)\ell\bar{\nu}_\ell$ decays:

   (a) A full set of $B_c \to J/\psi, \eta_c$ form factors computed using LCSR accompanied with gaussian NRQCD-inspired wave functions is presented. Form factors were found to satisfy the HQSS/NRQCD constraints.

   (b) Values of $R_{J/\psi,\eta_c}$ using the latter form factors are in line with what was obtained in similar QCD based approaches. Specifically,

$$R_{\eta_c}|_{\rm SM} \equiv \frac{\Gamma(B_c \to \eta_c \tau \bar{\nu}_\tau)}{\Gamma(B_c \to \eta_c \mu \bar{\nu}_\mu)} = 0.32 \pm 0.02\,, \tag{6.34}$$

$$R_{J/\psi}|_{\rm SM} \equiv \frac{\Gamma(B_c \to J/\psi \tau \bar{\nu}_\tau)}{\Gamma(B_c \to J/\psi \mu \bar{\nu}_\mu)} = 0.24 \pm 0.02\,. \tag{6.35}$$

   (c) Concerning the discrepancy between $R_{J/\psi}$ in the SM and the one measured on the LHCb experiment, it was found that no NP operator considered in the study can alleviate the tension significantly.

   (d) For the first time, four-fold angular decay distribution expressions are obtained for the $B_c \to J/\psi(\to \mu^+\mu^-)\ell\bar{\nu}_\ell$ decay, including the contribu-

tions from NP operators. Several observables potentially measurable are predicted.

2. In $B_c \to D^{(*)}\ell\bar{\nu}_\ell$ decays:

   (a) A proposal is made to measure the $|V_{ub}|$ CKM matrix element in the $B_c \to D^{(*)}\ell\bar{\nu}_\ell$ decay, for which the form factors were calculated using the QCDSR method. The form factors satisfy HQET relations.

   (b) Possible non-locality of the condensates is considered as a contribution to the $B_c \to D^{(*)}$ correlation functions. Non-local effects are completely negligible in the Borel-window relevat for the form factors, but help to constraint its lower bounds.

   (c) For the LFU ratios it was found that

$$\begin{aligned} R_c(D^0) &\equiv \frac{\mathcal{B}(B_c \to D^0\tau\bar{\nu}_\tau)}{\mathcal{B}(B_c \to D^0\mu\bar{\nu}_\mu)} = 0.64 \pm 0.05, \\ R_c(D^*) &\equiv \frac{\mathcal{B}(B_c \to D^*\tau\bar{\nu}_\tau)}{\mathcal{B}(B_c \to D^*\mu\bar{\nu}_\mu)} = 0.55 \pm 0.05, \end{aligned} \tag{6.36}$$

   where correlating the form factors appropriately would serve to reduce the uncertainties without changing the central values. Several angular observables are predicted as well, to be tested experimentally.

3. In $\bar{B} \to \pi\ell\bar{\nu}_\ell$ decays:

   (a) The full set of $\bar{B} \to \pi$ LCSR form factors is updated in a Bayesian analysis using the latest available hadronic parameters. Form factors values at different q^2 are shown to be very correlated, which serves to further constraint the predictions.

   (b) All of the available lattice QCD pseudo data on $\bar{B} \to \pi$ form factors is incorporated in a Bayesian fit in order to scrutinize the predictions as much as possible.

   (c) The LFU ratio using the LCSR + lattice QCD $\bar{B} \to \pi$ form factors is predicted as

$$R_\pi = 0.699 \pm 0.22, \tag{6.37}$$

which agrees with similar QCD-based determinations, but is more precise.

(d) Using the most recent HFLAV experimental data average, the exclusive value

$$|V_{ub}| = (3.77 \pm 0.15) \cdot 10^{-3} \tag{6.38}$$

is obtained. This result is in good agreement with the most recent inclusive determination, which removes the long-standing tension between inclusive and exclusive $|V_{ub}|$ determinations.

These results serve as a further motivation to explore the possibilities of testing the SM on particle colliders such as LHCb or Belle II. In order to get a definitive answer on the prospects of NP effects, more involved computations will have to be performed in the future on the theoretical side, and on the experimental side more precise data will have to be collected. It is clear that in the years to come a lot of work is to be done in the sector of flavour physics in hopes that more sophisticated insight can be gained in the non-perturbative effects of weak hadronic transitions.

Appendices

A. QCDSR expressions

A.1. Correlation function calculation

A.1.1. Perturbative terms

- $B_c \to D$

By evaluating the first line in (3.20) up to first order in propagator expansion one obtains what is referred to as the perturbative part of the amplitude, which is the quantity that would have been obtained if one just squeezed the product of the currents between free vacua.

$$
\begin{aligned}
\Pi_P^{(0)\mu}(p_{1_c}, p_P) &= -\mathrm{i}^2 \iint \mathrm{d}^4x\, \mathrm{d}^4y\, \mathrm{e}^{-i(p_{1_c}x - p_P y)} \times \\
&\times \langle\Omega|{:}\, \overbrace{\bar{c}_i^y \big(\gamma_5\big)_{ij} u_j^{\overbrace{y}} \bar{u}_k^0 \big(\gamma^\mu\big)_{kl} \big(1-\gamma_5\big)_{lm} b_m^{\overbrace{0}} \bar{b}_n^x \big(\gamma_5\big)_{np} c_p^x}\, {:}|\Omega\rangle \\
&= \mathrm{i}^5 \iint \mathrm{d}^4x\, \mathrm{d}^4y\, \mathrm{e}^{-i(p_{1_c}x - p_P y)} \times \\
&\times \langle\Omega|{:} S_c(x,y)_{pi} \big(\gamma_5\big)_{ij} S_u(y,0)_{jk} \big(\gamma^\mu\big)_{kl} \big(1-\gamma_5\big)_{lm} S_b(0,x)_{mn} \big(\gamma_5\big)_{np} {:}|\Omega\rangle \\
&= -12\,\mathrm{i}^3 \int \frac{\mathrm{d}^4k}{(2\pi)^4} \Bigg[\frac{(m_b m_c + m_u m_c - m_b m_u - k^2 + p_1{\cdot}p_2) k^\mu}{(k^2 - m_c^2)((k+p_1)^2 - m_b^2)((k+p_2)^2 - m_u^2)} \\
&+ \frac{(m_u m_c - k^2 - k{\cdot}p_2) p_1^\mu + (m_b m_c - k^2 - k{\cdot}p_1) p_2^\mu}{(k^2 - m_c^2)((k+p_1)^2 - m_b^2)((k+p_2)^2 - m_u^2)} \Bigg]
\end{aligned}
\tag{A.1}
$$

The integral is solved by imposing the Cutkosky rules

$$\begin{aligned}\frac{1}{(p_1+k)^2-m_1^2+\mathrm{i}\varepsilon} &\to -2\pi\mathrm{i}\delta((p_1+k)^2-m_1^2)\theta(k^0+p_1^0)\\ \frac{1}{(p_2+k)^2-m_2^2+\mathrm{i}\varepsilon} &\to -2\pi\mathrm{i}\delta((p_2+k)^2-m_2^2)\theta(k^0+p_2^0)\\ \frac{1}{k^2-m_3^2+\mathrm{i}\varepsilon} &\to -2\pi\mathrm{i}\delta(k^2-m_3^2)\theta(-k^0)\end{aligned} \tag{A.2}$$

using the integrals from appendix A.2.1 which gives the discontinuity of the amplitude in the p_1^2 and the p_2^2 channel, and then using the double dispersion relation

$$\Pi_{P,i}^{(0)}(p_1^2,p_2^2,q^2) = -\frac{1}{(2\pi)^2}\iint\frac{\mathcal{D}[\Pi_{P,i}^{(0)}(s_1,s_2,q^2)]}{(s_1-p_1^2)(s_2-p_2^2)}\mathrm{d}s_1\mathrm{d}s_2 \tag{A.3}$$

where $\mathcal{D}$ is a symbolic way of writing down the discontinuity of the amplitude, the perturbative contribution is obtained. The integration is performed after the Borel transformation

$$\mathcal{B}_{-p_1^2}(M_1^2)\mathcal{B}_{-p_2^2}(M_2^2) \to -\frac{M_1^{-2}M_2^{-2}}{(2\pi)^2}\iint\mathcal{D}[\Pi_{P,i}^{(0)}(s_1,s_2,q^2)]\mathrm{e}^{-\frac{s_1}{M_1^2}-\frac{s_2}{M_2^2}}\mathrm{d}s_1\mathrm{d}s_2 \tag{A.4}$$

over a phase space up until some effective thresholds s_1^0 and s_2^0, which come as phenomenological parameters in the calcuation. Here they are evaluated by requiring that the decay constants reproduce the lattice results, which are known, in the QCD sum rules approach. The final expressions are

$$\begin{aligned}\mathcal{D}[\Pi_{P,1}^{(0)}] \Big\{ &\frac{3}{\lambda^{\frac{3}{2}}}\Big(m_c(m_u-m_c)+\frac{s_2+m_c^2-m_u^2}{2}\Big)\lambda\\ &+\mathcal{M}(s_1,s_2,q^2)\big(2s_2(s_1+m_c^2-m_b^2)-(s_2+m_c^2-m_u^2)(s_1+s_2-q^2)\big)\Big)\\ \mathcal{D}[\Pi_{P,2}^{(0)}] \Big\{ &\frac{3}{\lambda^{\frac{3}{2}}}\Big(m_c(m_b-m_c)+\frac{s_1+m_c^2-m_b^2}{2}\Big)\lambda\\ &+\mathcal{M}(s_1,s_2,q^2)\big(2s_1(s_2+m_c^2-m_u^2)-(s_1+m_c^2-m_b^2)(s_1+s_2-q^2)\big)\Big)\end{aligned} \tag{A.5}$$

where additional shorthand notation has been introduced,

$$\lambda \equiv \lambda(s_1,s_2,q^2) = (s_1+s_2+q^2)^2-4s_1s_2. \tag{A.6}$$

- $B_c \to D^*$

Since in the $B_c \to D^*$ case the procedure is the same as in the case of the decay to pseudoscalar meson, here only the densities are given

$$
\begin{aligned}
&\mathcal{D}\big[\Pi_{V,0}\big] \\
&= 3\Big\{(m_b - m_c)\frac{m_c^2\lambda(s_1,s_2,q^2) + s_1\Delta_2^2 + s_2\Delta_1^2 - \Delta_1\Delta_2 u}{\big[\lambda(s_1,p_2^2,q^2)\big]^{\frac{3}{2}}} \\
&+ \frac{m_c^2}{\big[\lambda(s_1,p_2^2,q^2)\big]^{\frac{1}{2}}}(m_c - m_u - m_b) + \frac{m_c}{\big[\lambda(s_1,p_2^2,q^2)\big]^{\frac{1}{2}}}\big(\frac{u}{2} + m_b m_2\big) \\
&- (m_c - m_u)\frac{\Delta_1}{2\big[\lambda(s_1,s_2,q^2)\big]^{\frac{1}{2}}} - (m_c - m_b)\frac{\Delta_2}{2\big[\lambda(s_1,s_2,q^2)\big]^{\frac{1}{2}}}\Big\}, \\
&\mathcal{D}\big[\Pi_V\big] \\
&= 3\big\{(m_c - m_b)\frac{2s_2\Delta_1 - \Delta_2 u}{\big[\lambda(s_1,s_2,q^2)\big]^{\frac{3}{2}}} + (m_c - m_u)\frac{2s_1\Delta_2 - \Delta_2 u}{\big[\lambda(s_1,s_2,q^2)\big]^{\frac{3}{2}}} + \frac{m_c}{\big[\lambda(s_1,s_2,q^2)\big]^{\frac{1}{2}}}\big\}, \\
&\mathcal{D}\big[\frac{1}{2}(\Pi_1^A + \Pi_2^A)\big] \\
&= \frac{3}{2\big[\lambda(s_1,s_2,q^2)\big]^{\frac{5}{2}}}\Big\{\big[(m_u - m_c)\big(2s_1\Delta_2 - \Delta_1 u\big) + (m_b - m_c)\big(2s_2\Delta_1 - \Delta_2 u - \\
&- 2m_c^2(u - 2s_2)\big) - 2m_c(2s_2\Delta_1 - \Delta_2 u)\big]\lambda(s_1,s_2,q^2) + \\
&+ 2(m_b - m_c)\big[\Delta_1\Delta_2(2u^2 + 4s_1s_2 - 6s_2u) - 3u(s_1\Delta_2^2 + s_2\Delta_1^2) + 6s_2^2\Delta_1^2 + \\
&+ 2s_1s_2\Delta_2^2 + \Delta_2^2u^2\big] - m_c\big[\lambda(s_1,s_2,q^2)\big]^2\Big\}, \\
&\mathcal{D}\big[\frac{1}{2}(\Pi_1^A - \Pi_2^A)\big] \\
&= \frac{3}{2\big[\lambda(s_1,s_2,q^2)\big]^{\frac{5}{2}}}\Big\{\big[(m_u - m_c)\big(2s_1\Delta_2 - \Delta_1 u\big) + (m_b - m_c)\big(2s_2\Delta_1 - \Delta 2u - \\
&- 2m_c^2(u + 2s_2)\big) + 2m_c(2s_2\Delta_1 - \Delta_2 u)\big]\lambda(s_1,s_2,q^2) + \\
&+ 2(m_b - m_c)\big[\Delta_1\Delta_2(2u^2 + 4s_1s_2 + 6s_2u) - 3u(s_1\Delta_2^2 + s_2\Delta_1^2) - 6s_2^2\Delta_1^2 - \\
&- 2s_1s_2\Delta_2^2 - \Delta_2^2u^2\big] - m_c\big[\lambda(s_1,s_2,q^2)\big]^2\Big\}.
\end{aligned}
\tag{A.7}
$$

where some shorthand notation is introduced

$$\begin{aligned} \Delta_1 &\equiv s_1 + m_c^2 - m_b^2, \\ \Delta_2 &\equiv s_2 + m_c^2 - m_u^2, \\ u &\equiv s_1 + s_2 - q^2. \end{aligned} \tag{A.8}$$

A.1.2. Nonlocal quark and quark-gluon condensate terms

- $B_c \to D$

The quark condensate contribution to the $B_c \to P$ correlation function is

$$\Pi_P^{(3)\mu}(p_1, p_2) = -\frac{3\,\mathrm{i}^4}{12} \iint \mathrm{d}^4x\, \mathrm{d}^4y\, \mathrm{e}^{-\mathrm{i}(p_1 x - p_2 y)} \langle \bar{u}_a(0) u_a(y) \rangle \mathrm{Tr}\big[S_c(x,y) \gamma_5 \gamma^\mu (1-\gamma_5) S_b(0,x) \gamma_5 \big], \tag{A.9}$$

where the color trace has been taken. By expanding the $\bar{q}q$ operator one gets

$$\langle \bar{q}(0) q(y) \rangle \approx \langle \bar{q}q \rangle - g\frac{y^2}{16} \langle \bar{q} \sigma^{\mu\nu} G_{\mu\nu} q \rangle + \ldots, \tag{A.10}$$

which, in order to model the nonlocal effects is then substituted with

$$\langle \bar{q}(0) \exp\left\{ \mathrm{i}g \int_0^\infty dy_\mu A^\mu(y) \right\} q(y) \rangle = \langle \bar{q}q \rangle f(y^2). \tag{A.11}$$

After the Fourier transforming of propagators and evaluating the trace we obtain

$$\Pi_P^{(3)\mu}(p_1, p_2) = \langle \bar{q}q \rangle \int \frac{d^4k}{(2\pi)^4} \frac{(m_b - m_c)k^\mu - m_c p_1^\mu}{(k^2 - m_c^2)((k+p_1)^2 - m_b^2)} \tilde{f}(k + p_2), \tag{A.12}$$

where $\tilde{f}(k+p_2)$ is the Fourier transform of the chosen model function in coordinate space $f(y^2)$. Then it's easy to express the Borel-transformed contribution to the

form factors as

$$\begin{aligned}
&\mathcal{B}_{-p_1^2}(M_1^2)\mathcal{B}_{-p_2^2}(M_2^2)\Pi^{(3)}_{P,1}(q^2) = \\
&\quad 4\pi^2\,\mathrm{i}\langle\bar{q}q\rangle\left(\frac{4}{m_0^2}\right)^2\Big[m_c I_0(M_1^2,M_2^2,q^2;1,1)+(m_c-m_b)I_1(M_1^2,M_2^2,q^2;1,1)\Big],\\
&\mathcal{B}_{-p_1^2}(M_1^2)\mathcal{B}_{-p_2^2}(M_2^2)\Pi^{(3)}_{P,2}(q^2) = \\
&\quad 4\pi^2\,\mathrm{i}\langle\bar{q}q\rangle\left(\frac{4}{m_0^2}\right)^2\Big[(m_c-m_b)I_2(M_1^2,M_2^2,q^2;1,1)\Big].
\end{aligned} \tag{A.13}$$

The mixed quark-gluon condensate contribution amounts to

$$\begin{aligned}
\Pi_P^{(5)\mu}(p_1,p_2) = -\mathrm{i}^4\frac{g}{2\cdot 192}\iint \mathrm{d}^4x\,\mathrm{d}^4y\,\mathrm{d}^4z\,\mathrm{e}^{-\mathrm{i}(p_1x-p_2y)}z^\alpha\\
\langle\bar{u}(0)(\sigma\cdot G)u(y)\rangle\mathrm{Tr}_c\Big[t^ct^c\Big]\;\;\mathrm{Tr}\Big[S_c(x,z)\gamma^\beta S_c(z,y)\gamma_5\sigma_{\alpha\beta}\gamma^\mu(1-\gamma_5)S_b(0,x)\gamma_5\Big]\\
+\mathrm{Tr}\Big[S_c(x,y)\gamma_5\sigma_{\alpha\beta}\gamma^\mu(1-\gamma_5)S_b(0,z)\gamma^\beta S_b(z,x)\gamma_5\Big]\Big).
\end{aligned} \tag{A.14}$$

The quark-gluon condensate can be approximated in terms of the quark condensate as [213]

$$g\langle\bar{q}(0)(\sigma\cdot G)q(y)\rangle \approx m_0^2\langle\bar{q}(0)q(y)\rangle. \tag{A.15}$$

After the Fourier transformation the amplitude becomes

$$\begin{aligned}
&\Pi_P^{(5)\mu}(p_1,p_2) = \mathrm{i}m_0^2\frac{\langle\bar{q}q\rangle}{96}\int\frac{d^4k}{(2\pi)^4}\frac{\partial}{\partial q_\alpha}\\
&\Big\{\mathrm{Tr}\Big[\frac{\not k+\not q+m_c}{(k+q)^2-m_c^2}\gamma^\beta\frac{\not k+m_c}{k^2-m_c^2}\gamma_5\sigma_{\alpha\beta}\gamma^\mu(1-\gamma_5)\frac{\not k+\not q+\not p_1+m_b}{(k+q+p_1)^2-m_b^2}\gamma_5\Big]\\
&+\mathrm{Tr}\Big[\frac{\not k+\not q+\not p_1+m_b}{(k+q+p_1)^2-m_b^2}\gamma^\beta\frac{\not k+\not p_1+m_b}{(k+p_1)^2-m_b^2}\gamma_5\frac{\not k+m_c}{k^2-m_c^2}\gamma_5\sigma_{\alpha\beta}\gamma^\mu(1-\gamma_5)\Big]\Big\}_{q=0}\cdot\tilde{f}(k+p_2),
\end{aligned} \tag{A.16}$$

or, after differentiating

$$\Pi_P^{(5)\mu}(p_1,p_2) = -\mathrm{i}\, m_0^2 \frac{\langle\bar{q}q\rangle}{96}\int\frac{d^4k}{(2\pi)^4}\tilde{f}(k+p_2)$$
$$\Big\{\mathrm{Tr}\big[\frac{\not k+m_c}{k^2-m_c^2}\gamma^\alpha\frac{\not k+m_c}{k^2-m_c^2}\gamma^\beta\frac{\not k+m_c}{k^2-m_c^2}\gamma_5\sigma_{\alpha\beta}\gamma^\mu(1-\gamma_5)\frac{\not k+\not p_1+m_b}{(k+p_1)^2-m_b^2}\gamma_5\big]$$
$$+\mathrm{Tr}\big[\frac{\not k+m_c}{k^2-m_c^2}\gamma^\beta\frac{\not k+m_c}{k^2-m_c^2}\gamma_5\sigma_{\alpha\beta}\gamma^\mu(1-\gamma_5)\frac{\not k+\not p_1+m_b}{(k+p_1)^2-m_b^2}\gamma^\alpha\frac{\not k+\not p_1+m_b}{(k+p_1)^2-m_b^2}\gamma_5\big]$$
$$+\mathrm{Tr}\big[\frac{\not k+\not p_1+m_b}{(k+p_1)^2-m_b^2}\gamma^\alpha\frac{\not k+\not p_1+m_b}{(k+p_1)^2-m_b^2}\gamma^\beta\frac{\not k+\not p_1+m_b}{(k+p_1)^2-m_b^2}\gamma_5\frac{\not k+m_c}{k^2-m_c^2}\gamma_5\sigma_{\alpha\beta}\gamma^\mu(1-\gamma_5)\big]\Big\}. \tag{A.17}$$

The integrals are done with complete analogy to the previous case, with one difference. Now, due to the differentiation, additional powers of squares of external momenta are present in the trace, so one needs to Borel-transform according to the rule

$$I_{[\mathrm{in}]}^{(m)}(M_1^2,M_2^2,q^2;a,b) \equiv \mathcal{B}_{-p^2}(M^2)\big[(-p^2)^m\tilde{I}_{[\mathrm{in}]}(p_1^2,p_2^2,q^2;a,b)\big]$$
$$= (M^2)^m\left(\frac{\partial}{\partial M^2}\right)^m[(M^2)^m\mathcal{B}_{-p^2}(M^2)\,I_{[\mathrm{in}]}(M_1^2,M_2^2,q^2;a,b)], \tag{A.18}$$

where again, "[in]" stands for any of the indices of the integrals in Eq. (A.54), so that finally, for the Borel-transformed quark-gluon contribution to the correlation

function we have

$$
\begin{aligned}
&\mathcal{B}_{-p_1^2}(M_1^2)\mathcal{B}_{-p_2^2}(M_2^2)\Pi_{P,1}^{(5)}(q^2) = \\
&\quad \frac{\mathrm{i}\pi^2}{6}\Big(\langle\bar{q}q\rangle \quad \frac{4}{m_0^2}\Big)\Big\{ -40m_c I_0(M_1^2,M_2^2,q^2;2,1) + 32(m_b-m_c)I_1(M_1^2,M_2^2,q^2;2,1) \\
&\quad + 8(m_b-2m_c)I_0(M_1^2,M_2^2,q^2;1,2) + 16(m_b-m_c)I_1(M_1^2,M_2^2,q^2;1,2) \\
&\quad + 8m_c\big(m_b-m_c\big)^2 I_0(M_1^2,M_2^2,q^2;2,2) \\
&\quad + 8\big[(m_b+m_c)^3 - 4m_b m_c(m_b+m_c)\big] I_1(M_1^2,M_2^2,q^2;2,2) \\
&\quad - 8m_c I_0^{(1)}(M_1^2,M_2^2,q^2;2,2) - 8(m_b+m_c)I_1^{(1)}(M_1^2,M_2^2,q^2;2,2)\Big\}, \\
&\mathcal{B}_{-p_1^2}(M_1^2)\mathcal{B}_{-p_2^2}(M_2^2)\Pi_{P,2}^{(5)}(q^2) = \\
&\quad \frac{\mathrm{i}\pi^2}{6}\Big(\langle\bar{q}q\rangle \quad \frac{4}{m_0^2}\Big)\Big\{32(m_b-m_c)I_2(M_1^2,M_2^2,q^2;2,1) + 16(m_b-m_c)I_2(M_1^2,M_2^2,q^2;1,2) \\
&\quad + 8\big[(m_b+m_c)^3 - 4m_b m_c(m_b+m_c)\big] I_2(M_1^2,M_2^2,q^2;2,2) \\
&\quad - 8(m_b+m_c)I_2^{(1)}(M_1^2,M_2^2,q^2;2,2)\Big\}.
\end{aligned}
\tag{A.19}
$$

- $B_c \to D^*$

The quark condensate contribution to the $B_c \to V$ correlation function is

$$
\Pi_V^{(3)\mu\nu}(p_1,p_2) = \frac{3\,\mathrm{i}^5}{12}\iint \mathrm{d}^4x\,\mathrm{d}^4y\,\mathrm{e}^{-\mathrm{i}(p_1x-p_2y)}\langle\bar{u}_a(0)u_a(y)\rangle \mathrm{Tr}\big[S_c(x,y)\gamma^\nu\gamma^\mu(1-\gamma_5)S_b(0,x)\gamma_5\big],
\tag{A.20}
$$

so that, after Fourier transforming the propagators, and evaluating the trace we obtain

$$
\begin{aligned}
&\Pi_V^{(3)\mu\nu}(p_1,p_2) = \\
&\quad \mathrm{i}\langle\bar{q}q\rangle\int\frac{d^4k}{(2\pi)^4}\frac{\big(k^2+(k\cdot p_1)-m_b m_c\big)g^{\mu\nu}+k^\nu p_1^\mu - p_1^\nu k^\mu + \mathrm{i}\epsilon^{\mu\nu\alpha\beta}k_\alpha p_{1\beta}}{(k^2-m_c^2)((k+p_1)^2-m_b^2)}\tilde{f}(k+p_2).
\end{aligned}
\tag{A.21}
$$

Then it's easy to express the Borel-transformed contribution to the form factors as

$$\begin{aligned}
&\mathcal{B}_{-p_1^2}(M_1^2)\mathcal{B}_{-p_2^2}(M_2^2)\Pi_{V,0}^{(3)}(q^2) = \\
&\quad 4\pi^2\,\mathrm{i}\Big(\langle\bar{q}q\rangle \quad \frac{4}{m_0^2}\Big)^2\Big[m_b(m_b-m_c)I_0(M_1^2,M_2^2,q^2;1,1) - I_0^{(1)}(M_1^2,M_2^2,q^2;1,1)\Big], \\
&\mathcal{B}_{-p_1^2}(M_1^2)\mathcal{B}_{-p_2^2}(M_2^2)\Pi_{V,1}^{(3)}(q^2) = -4\pi^2\,\mathrm{i}\Big(\langle\bar{q}q\rangle \quad \frac{4}{m_0^2}\Big)^2 I_2(M_1^2,M_2^2,q^2;1,1), \\
&\mathcal{B}_{-p_1^2}(M_1^2)\mathcal{B}_{-p_2^2}(M_2^2)\Pi_{V,2}^{(3)}(q^2) = 0, \\
&\mathcal{B}_{-p_1^2}(M_1^2)\mathcal{B}_{-p_2^2}(M_2^2)\Pi_{V,v}^{(3)}(q^2) = 4\pi^2\,\mathrm{i}\Big(\langle\bar{q}q\rangle \quad \frac{4}{m_0^2}\Big)^2 I_2(M_1^2,M_2^2,q^2;1,1).
\end{aligned}$$

The mixed quark-gluon condensate contribution amounts to

$$\begin{aligned}
&\Pi_V^{(5)\mu\nu}(p_1,p_2) = \mathrm{i}^5\frac{g}{2\cdot 192}\iint \mathrm{d}^4x\,\mathrm{d}^4y\,\mathrm{d}^4z\,\mathrm{e}^{-\mathrm{i}(p_1x-p_2y)}z^\alpha \\
&\langle\bar{u}(0)(\sigma\cdot G)u(y)\rangle\mathrm{Tr}_c\Big[t^ct^c\Big] \quad \mathrm{Tr}\big[S_c(x,z)\gamma^\beta S_c(z,y)\gamma^\nu\sigma_{\alpha\beta}\gamma^\mu(1-\gamma_5)S_b(0,x)\gamma_5\big] \\
&\qquad\qquad + \mathrm{Tr}\big[S_c(x,y)\gamma^\nu\sigma_{\alpha\beta}\gamma^\mu(1-\gamma_5)S_b(0,z)\gamma^\beta S_b(z,x)\gamma_5\big]\Big).
\end{aligned} \tag{A.22}$$

Or, completely analogously to the previous case, by differentiating we get

$$\begin{aligned}
&\Pi_V^{(5)\mu\nu}(p_1,p_2) = -\,m_0^2\frac{\langle\bar{q}q\rangle}{96}\int\frac{d^4k}{(2\pi)^4}\tilde{f}(k+p_2) \\
&\Big\{\mathrm{Tr}\big[\frac{\not{k}+m_c}{k^2-m_c^2}\gamma^\alpha\frac{\not{k}+m_c}{k^2-m_c^2}\gamma^\beta\frac{\not{k}+m_c}{k^2-m_c^2}\gamma^\nu\sigma_{\alpha\beta}\gamma^\mu(1-\gamma_5)\frac{\not{k}+\not{p}_1+m_b}{(k+p_1)^2-m_b^2}\gamma_5\big] \\
&+\mathrm{Tr}\big[\frac{\not{k}+m_c}{k^2-m_c^2}\gamma^\beta\frac{\not{k}+m_c}{k^2-m_c^2}\gamma^\nu\sigma_{\alpha\beta}\gamma^\mu(1-\gamma_5)\frac{\not{k}+\not{p}_1+m_b}{(k+p_1)^2-m_b^2}\gamma^\alpha\frac{\not{k}+\not{p}_1+m_b}{(k+p_1)^2-m_b^2}\gamma_5\big] \\
&+\mathrm{Tr}\big[\frac{\not{k}+\not{p}_1+m_b}{(k+p_1)^2-m_b^2}\gamma^\alpha\frac{\not{k}+\not{p}_1+m_b}{(k+p_1)^2-m_b^2}\gamma^\beta\frac{\not{k}+\not{p}_1+m_b}{(k+p_1)^2-m_b^2}\gamma_5\frac{\not{k}+m_c}{k^2-m_c^2}\gamma^\nu\sigma_{\alpha\beta}\gamma^\mu(1-\gamma_5)\big]\Big\}.
\end{aligned} \tag{A.23}$$

The final contributions are then

$$\mathcal{B}_{-p_1^2}(M_1^2)\mathcal{B}_{-p_2^2}(M_2^2)\Pi_{V,0}^{(5)}(q^2) =$$
$$\frac{4\mathrm{i}\pi^2}{3}\begin{pmatrix}\langle\bar{q}q\rangle & \frac{4}{m_0^2}\end{pmatrix}\Big\{I_0(M_1^2,M_2^2,q^2;1,1)+\frac{1}{2}(m_b^2-m_c^2)^2 I_0(M_1^2,M_2^2,q^2;2,2)$$
$$-(m_b^2+m_c^2)I_0^{(1)}(M_1^2,M_2^2,q^2;2,2)+\frac{1}{2}I_0^{(2)}(M_1^2,M_2^2,q^2;2,2)\Big\},$$

$$\mathcal{B}_{-p_1^2}(M_1^2)\mathcal{B}_{-p_2^2}(M_2^2)\Pi_{V,1}^{(5)}(q^2) =$$
$$\frac{4\mathrm{i}\pi^2}{3}\begin{pmatrix}\langle\bar{q}q\rangle & \frac{4}{m_0^2}\end{pmatrix}\Big\{\big[4m_c^2-(m_b+m_c)^2\big]I_2(M_1^2,M_2^2,q^2;2,2)+I_2^{(1)}(M_1^2,M_2^2,q^2;2,2)$$
$$+4I_{21}^{(1)}(M_1^2,M_2^2,q^2;2,2)\Big\},$$

$$\mathcal{B}_{-p_1^2}(M_1^2)\mathcal{B}_{-p_2^2}(M_2^2)\Pi_{V,2}^{(5)}(q^2) =$$
$$\frac{16\mathrm{i}\pi^2}{3}\begin{pmatrix}\langle\bar{q}q\rangle & \frac{4}{m_0^2}\end{pmatrix}\Big\{\big(m_c^2-m_b^2\big)I_1(M_1^2,M_2^2,q^2;2,2)+I_1^{(1)}(M_1^2,M_2^2,q^2;2,2)$$
$$+I_{11}^{(1)}(M_1^2,M_2^2,q^2;2,2)\Big\},$$

$$\mathcal{B}_{-p_1^2}(M_1^2)\mathcal{B}_{-p_2^2}(M_2^2)\Pi_{V,v}^{(5)}(q^2) =$$
$$\frac{4\mathrm{i}\pi^2}{3}\begin{pmatrix}\langle\bar{q}q\rangle & \frac{4}{m_0^2}\end{pmatrix}\Big\{\big(m_b-m_c\big)^2 I_2(M_1^2,M_2^2,q^2;2,2)-I_2^{(1)}(M_1^2,M_2^2,q^2;2,2)\Big\}.$$

A.1.3. Gluon condensate terms

The gluon condensate $\left\langle\frac{\alpha_s}{\pi}G^{a\,\mu\nu}G^a_{\mu\nu}\right\rangle \equiv \left\langle\frac{\alpha_s}{\pi}G^2\right\rangle$ contributions are computed in the Fock-Schwinger gauge. Since, due to translational non-invariance, this is not technically a gauge, one should be careful when applying it - it can be shown that gauge-invariant quantities should recover translational invariance. Usually the origin $x_0 = 0$ is chosen as the fixed point, and then the contributing diagrams are calculated in that gauge. Then, the gluon field can be written just using $G^a_{\mu\nu}$ and its covariant derivative, becoming (to first order in momentum space):

$$A_\mu(k) = -\mathrm{i}\frac{(2\pi)^4}{2}G_{\alpha\mu}(0)\frac{\partial}{\partial k_\alpha}\delta^{(4)}(k)+\ldots \tag{A.24}$$

It is obvious that, if one wants to correct the perturbative part of the correlation function with the operator $\langle G^2\rangle$, the corrections will come from inserting the external

field twice (in the Feynman diagram sense), associating i-th gluon line with the factor of

$$\mathrm{i}\not{A}(k_i)\frac{\mathrm{d}^4k_i}{(2\pi)^4}, \tag{A.25}$$

and then integrating over the momenta k_i. Since gluon field is proportional to derivative of delta function with respect to k_i, effectively one needs just to differentiate the amplitude resulting from expanded quark propagators and inserted vertices with respect to the momenta of inserted external fields, and then say that all external momenta are zero, $k_i \to 0$. After using the fact that

$$\left\langle G^a_{\mu\nu}(0)G^b_{\alpha\beta}(0)\right\rangle = \frac{1}{96}\delta^{ab}(g_{\mu\alpha}g_{\nu\beta} - g_{\mu\beta}g_{\nu\alpha})\left\langle G^{c\,\rho\sigma}G^c_{\rho\sigma}\right\rangle, \tag{A.26}$$

the tensor reduction of the loop integral to D-dimensional scalar integrals of the type

$$I_0^D(a,b,c) = \int \frac{\mathrm{d}^Dk}{(2\pi)^D}\frac{1}{\left[k^2-m_3^2\right]^a\left[(k+p_1)^2-m_1^2\right]^b\left[(k+p_2)^2-m_2^2\right]^c}, \tag{A.27}$$

can be done automatically, using the ROLI package [281] (implemented in Wolfram's Mathematica). In order to Borel-transform the correlation function it was found that

$$\begin{aligned} B_{p_1^2}(M_1^2)B_{p_2^2}(M_2^2)\,I_0^D(a,b,c) = {} & \frac{\mathrm{i}}{(4\pi)^{D/2}}\frac{(-)^{a+b+c}}{\Gamma(a)\Gamma(b)\Gamma(c)}(M_1^2)^{D/2-a-c}(M_2^2)^{D/2-a-b} \\ & \times\int_0^\infty \mathrm{d}y(y+M_1^2+M_2^2)^{a+b+c-D}y^{D/2-1-b-c}\exp\left\{-\frac{B_-}{y}-B_0-B_+y\right\}, \end{aligned} \tag{A.28}$$

where additional functions are defined as

$$\begin{aligned} B_- &= \frac{m_2^2M_1^4+m_1^2M_2^4+M_1^2M_2^2(m_1^2+m_2^2-Q^2)}{M_1^2M_2^2}, \\ B_0 &= \frac{M_1^2(m_2^3+m_2^2)+M_2^2(m_1^2+m_3^2)}{M_1^2M_2^2},\ B_+ = \frac{m_3^2}{M_1^2M_2^2}, \end{aligned} \tag{A.29}$$

and also

$$B_{p_1^2}(M_1^2)B_{p_2^2}(M_2^2)\,(p_1^2)^{m_1}(p_2^2)^{m_2}I_0^D(a,b,c) = (M_1^2)^{m_1}(M_2^2)^{m_2} \\ \times \frac{\mathrm{d}^{m_1}}{\mathrm{d}(M_1^2)^{m_1}}\frac{\mathrm{d}^{m_2}}{\mathrm{d}(M_2^2)^{m_2}}\Big[(M_1^2)^{m_1}(M_2^2)^{m_2}B_{p_1^2}(M_1^2)B_{p_2^2}(M_2^2)\,I_0^D(a,b,c)\Big], \tag{A.30}$$

so that the gluonic contribution to the correlation function is

$$\Pi_{\mu\nu}^{\mathrm{nonpert}} = \left\langle \frac{\alpha_s}{\pi}\,G^2 \right\rangle \frac{1}{96}(g_{\rho\alpha}g_{\sigma\beta} - g_{\rho\beta}g_{\sigma\alpha}) \sum_i (2\pi)^2 \big[I_0^D(a,b,c)\big]_i \big[\Gamma_{\mu\nu}^{\alpha\beta\rho\sigma}\big]_i. \tag{A.31}$$

A.2. Master integrals

The perturbative loop integrals are most easily evaluated in the B_c meson rest frame defined through

$$p_1^\mu \equiv \begin{bmatrix} \sqrt{s} \\ \vec{0} \end{bmatrix} \; ; \; p_2^\mu \equiv \begin{bmatrix} p_2^0 \\ -\vec{p_2} \end{bmatrix} \; ; \; q^2 \equiv (p_1 - p_2)^2. \tag{A.32}$$

The delta functions are integrated over first over k_0, then $\left|\vec{k}\right|$, and lastly $\cos\theta$, where θ is the angle between $\vec{p}_2$ and $\vec{k}$. Therefore

$$\begin{aligned} \delta(k^2 - m_3^2) = \delta(k_0^2 - |\vec{k}|^2 - m_3^2) &= \frac{\delta(k_0 + \sqrt{|\vec{k}|^2 + m_3^2}\,)}{2\sqrt{|\vec{k}|^2 + m_3^2}} \\ \delta((p_1{+}k)^2 - m_1^2) \to \delta(s - 2\sqrt{s}\sqrt{|\vec{k}|^2 + m_3^2} + m_3^2 - m_1^2) &= \frac{\delta(|\vec{k}| - \frac{\sqrt{\lambda(s,m_3^2,m_1^2)}}{2\sqrt{s}})}{2\sqrt{s}\frac{\sqrt{\lambda(s,m_3^2,m_1^2)}}{s+m_3^2-m_1^2}}, \end{aligned} \tag{A.33}$$

where the arrow implies the form the δ-functions take after integrating over k_0. After integrating over $\left|\vec{k}\right|$ the first delta function looks like

$$\delta(k^2 - m_3^2) \to \frac{\delta(k_0 + \frac{s+m_3^2-m_1^2}{2\sqrt{s}})}{2(\frac{s+m_3^2-m_1^2}{2\sqrt{s}})}, \tag{A.34}$$

and

$$\begin{aligned} \delta((p_2{+}k)^2 - m_2^2) &\to \delta(p_2^2 - 2p_2^0\sqrt{|\vec{k}|^2 + m_3^2} - 2|\vec{k}||\vec{p_2}|\cos\theta + m_3^2 - m_2^2) \\ &\to 4s\frac{\delta(\cos\theta - \cos\theta_0)}{2\sqrt{\lambda(s,m_3^2,m_1^2)}\sqrt{\lambda(s,p_2^2,q^2)}}. \end{aligned} \tag{A.35}$$

In the last expression the first arrow implies integration over k_0, and the second one integration over $\left|\vec{k}\right|$. In the B meson rest frame $|\vec{p_2}| = (2\sqrt{s})^{-1}\sqrt{\lambda(s,p_2^2,q^2)}$, and

$$\begin{aligned}\cos\theta_0 &\equiv 4s\frac{-2p_2^0\sqrt{|\vec{k}|^2+m_3^2}+p_2^2+m_3^2-m_2^2}{2|\vec{k}||\vec{p_2}|}\\ &\to \frac{-(s+p_2^2-q^2)(s+m_3^2-m_1^2)+2s(p_2^2+m_3^2-m_2^2)}{\sqrt{\lambda(s,m_3^2,m_1^2)}\sqrt{\lambda(s,p_2^2,q^2)}}.\end{aligned} \tag{A.36}$$

Since the cosine always gives values between $-1 \leq \cos\theta_0 \leq 1$, this constrains the range of integration.

A.2.1. Perturbative master integrals

Rank 0 integral

It is instructive to firstly integrate just the phase space integral containing the phase space Φ_k,

$$\begin{aligned}I_{(0)} = 3\int\frac{\mathrm{d}^4k}{(2\pi)^4}\Phi_k = \frac{3s}{\lambda(s,m_3^2,m_2^2)\sqrt{\lambda(s,p_2^2,q^2)}}\int\mathrm{d}k_0\iint|\vec{k}|^2\mathrm{d}|\vec{k}|\mathrm{d}(\cos\theta)\times\\ \times\ \delta(k_0+\sqrt{|\vec{k}|^2+m_3^2})\delta(|\vec{k}|-\frac{\sqrt{\lambda(s,m_3^2,m_1^2)}}{2\sqrt{s}})\delta(\cos\theta-\cos\theta_0) = \frac{3}{4}\big[\lambda(s,p_2^2,q^2)\big]^{-\frac{1}{2}},\end{aligned} \tag{A.37}$$

where Φ_k is

$$\begin{aligned}\frac{\Phi_k}{(2\pi)^3} &\equiv \delta((p_1+k)^2-m_1^2)\delta(k^2-m_3^2)\delta((p_2+k)^2-m_2^2)\\ &\to s\frac{\delta(k_0+\sqrt{|\vec{k}|^2+m_3^2})}{\lambda(s,m_3^2,m_2^2)\sqrt{\lambda(s,p_2^2,q^2)}}\delta(|\vec{k}|-\frac{\sqrt{\lambda(s,m_3^2,m_1^2)}}{2\sqrt{s}})\delta(\cos\theta-\cos\theta_0).\end{aligned} \tag{A.38}$$

Rank 1 integral

Now the following integral is evaluated

$$I^{\mu}_{(1)} = 3\int\frac{\mathrm{d}^4k}{(2\pi)^4}\Phi_k k^{\mu} \tag{A.39}$$

Considering the Lorentz structure, the integral can be decomposed as

$$I^{\mu}_{(1)} = C_1 p_1^{\mu} + C_2 p_2^{\mu}, \tag{A.40}$$

where C_1 and C_2 are functions of Lorentz invariants. The left-hand side and the right-hand side are then multiplied by each momenta, after which the system of equations is easily solvable.

$$\begin{aligned} I^{\mu}_{(1)} p_{1\mu} &= C_1 s + \frac{C_2}{2}(s + p_2^2 - q^2) \\ I^{\mu}_{(1)} p_{2\mu} &= \frac{C_1}{2}(s + p_2^2 - q^2) + C_2 p_2^2 \end{aligned} \tag{A.41}$$

1. $I^{\mu}_{(1)} p_{1\mu}$:

$$\begin{aligned} I^{\mu}_{(1)} p_{1\mu} &= 3\int \frac{\mathrm{d}^4 k}{(2\pi)^4}\Phi_k(k\cdot p_1) = 3\int \frac{\mathrm{d}^4 k}{(2\pi)^4}\Phi_k(\sqrt{s}k_0) \\ &= \frac{3s\sqrt{s}}{\lambda(s,m_3^2,m_2^2)\sqrt{\lambda(s,p_2^2,q^2)}}\int \mathrm{d}k_0 \iint |\vec{k}|^2 \mathrm{d}|\vec{k}|\mathrm{d}(\cos\theta)\times \\ &\times\ k_0\delta(k_0 + \sqrt{|\vec{k}|^2 + m_3^2})\delta(|\vec{k}| - \frac{\sqrt{\lambda(s,m_3^2,m_1^2)}}{2\sqrt{s}})\delta(\cos\theta - \cos\theta_0) \\ &= -3\,\frac{s + m_3^2 - m_1^2}{8\sqrt{\lambda(s,p_2^2,q^2)}}. \end{aligned} \tag{A.42}$$

2. $I^{\mu}_{(1)} p_{2\mu}$:

$$\begin{aligned} I^{\mu}_{(1)} p_{2\mu} &= 3\int \frac{\mathrm{d}^4 k}{(2\pi)^4}\Phi_k(k\cdot p_2) = 3\int \frac{\mathrm{d}^4 k}{(2\pi)^4}\Phi_k(p_2^0 k_0 - |\vec{k}||\vec{p_2}|\cos\theta) \\ &= -3\,\frac{p_2^2 + m_3^2 - m_2^2}{8\sqrt{\lambda(s,p_2^2,q^2)}}. \end{aligned} \tag{A.43}$$

The coefficients are then

$$\begin{aligned} C_1 &= 3\,\frac{2p_2^2(s + m_3^2 - m_1^2) - (p_2^2 + m_3^2 - m_2^2)(s + p_2^2 - q^2)}{4\big[\lambda(s,p_2^2,q^2)\big]^{\frac{3}{2}}} \\ C_2 &= 3\,\frac{2s(p_2^2 + m_3^2 - m_2^2) - (s + m_3^2 - m_1^2)(s + p_2^2 - q^2)}{4\big[\lambda(s,p_2^2,q^2)\big]^{\frac{3}{2}}} \end{aligned} \tag{A.44}$$

Rank two integrals

For the following integral

$$I^{\mu\nu}_{(2)} = 3\int \frac{\mathrm{d}^4k}{(2\pi)^4}\Phi_k k^\mu k^\nu, \tag{A.45}$$

the decomposition goes as

$$I^{\mu\nu}_{(2)} = D_1 g^{\mu\nu} + D_2 p_1^\mu p_1^\nu + D_3 p_2^\mu p_2^\nu + D_4(p_1^\mu p_2^\nu + p_2^\mu p_1^\nu) \tag{A.46}$$

where D_{1-4} are functions of Lorentz invariants. Contracting the integral with, repectively, $g_{\mu\nu}, p_{1\mu}p_{1\nu}, p_{2\mu}p_{2\nu}$ ans $p_{1\mu}p_{2\nu}$ a system of equations is acquired

$$\begin{aligned}
I^{\mu\nu}_{(2)} g_{\mu\nu} &= 4D_1 + sD_2 + p_2^2 D_3 + (s + p_2^2 - q^2)D_4, \\
I^{\mu\nu}_{(2)} p_{1\mu}p_{1\nu} &= sD_1 + s^2 D_2 + (s + p_2^2 - q^2)^2 \frac{D_3}{4} + s(s + p_2^2 - q^2)D_4, \\
I^{\mu\nu}_{(2)} p_{2\mu}p_{2\nu} &= p_2^2 D_1 + (s + p_2^2 - q^2)^2 \frac{D_2}{4} + p_2^4 D_3 + p_2^2(s + p_2^2 - q^2)D_4, \\
I^{\mu\nu}_{(2)} p_{1\mu}p_{2\nu} &= (s + p_2^2 - q^2)\frac{D_1}{2} + s(s + p_2^2 - q^2)\frac{D_2}{2} + p_2^2(s + p_2^2 - q^2)\frac{D_3}{2}, \\
&\qquad + \big[\frac{1}{4}(s + p_2^2 - q^2)^2 + sp_2^2\big]D_4
\end{aligned} \tag{A.47}$$

1. $I^{\mu\nu}_{(2)} g_{\mu\nu}$:

$$I^{\mu\nu}_{(2)} g_{\mu\nu} = 3\int \frac{\mathrm{d}^4k}{(2\pi)^4}\Phi_k k^2 = 3\,\frac{m_3^2}{4\sqrt{\lambda(s, p_2, q^2)}} \tag{A.48}$$

2. $I^{\mu\nu}_{(2)} p_{1\mu}p_{1\nu}$:

$$I^{\mu\nu}_{(2)} p_{1\mu}p_{1\nu} = 3\int \frac{\mathrm{d}^4k}{(2\pi)^4}\Phi_k (sk_0^2) = 3\,\frac{(s + m_3^2 - m_1^2)^2}{16\sqrt{\lambda(s, p_2^2, q^2)}} \tag{A.49}$$

3. $I^{\mu\nu}_{(2)} p_{2\mu}p_{2\nu}$:

$$I^{\mu\nu}_{(2)} p_{2\mu}p_{2\nu} = 3\int \frac{\mathrm{d}^4k}{(2\pi)^4}\Phi_k (p_2^0 k_0 - |\vec{p_2}||\vec{k}|\cos\theta)^2 = 3\,\frac{(p_2^2 + m_3^2 - m_2^2)^2}{16\sqrt{\lambda(s, p_2^2, q^2)}} \tag{A.50}$$

4. $I^{\mu\nu}_{(2)} p_{1\mu}p_{2\nu}$:

$$I^{\mu\nu}_{(2)} p_{1\mu}p_{2\nu} = 3\int \frac{\mathrm{d}^4k}{(2\pi)^4}\Phi_k (\sqrt{s}k_0)(p_2^0 k_0 - |\vec{p_2}||\vec{k}|\cos\theta) = 3\,\frac{(s + m_3^2 - m_1^2)(p_2^2 + m_3^2 - m_2^2)}{16\sqrt{\lambda(s, p_2^2, q^2)}} \tag{A.51}$$

So that the coefficients are:

$$
\begin{aligned}
D_1 &= \frac{3}{8}\frac{m_3^2\lambda(s,p_2^2,q^2)+s\Delta_{\Psi 32}^2+p_2^2\Delta_{\mathrm{B}31}^2-\Delta_{\Psi 32}\Delta_{\mathrm{B}31}u}{\left[\lambda(s,p_2^2,q^2)\right]^{\frac{3}{2}}},\\
D_2 &= \frac{3}{4}\frac{2m_3^2p_2^2\lambda(s,p_2^2,q^2)+6p_2^4\Delta_{\mathrm{B}31}^2+2sp_2^2\Delta_{\Psi 32}^2+\Delta_{\Psi 32}^2u^2-6p_2^2u\Delta_{\mathrm{B}31}\Delta_{\Psi 32}}{\left[\lambda(s,p_2^2,q^2)\right]^{\frac{5}{2}}},\\
D_3 &= \frac{3}{4}\frac{2m_3^2s\lambda(s,p_2^2,q^2)+6s^2\Delta_{\Psi 32}^2+2sp_2^2\Delta_{\mathrm{B}31}^2+\Delta_{\mathrm{B}31}^2u^2-6su\Delta_{\mathrm{B}31}\Delta_{\Psi 32}}{\left[\lambda(s,p_2^2,q^2)\right]^{\frac{5}{2}}},\\
D_4 &= -\frac{3}{4}\frac{m_3^2u\lambda(s,p_2^2,q^2)-4sp_2^2\Delta_{\Psi 32}\Delta_{\mathrm{B}31}+3u(s\Delta_{\Psi 32}^2+p_2^2\Delta_{\mathrm{B}31}^2)-2u^2\Delta_{\mathrm{B}31}\Delta_{\Psi 32}}{\left[\lambda(s,p_2^2,q^2)\right]^{\frac{5}{2}}},
\end{aligned}
\tag{A.52}
$$

where a shorthand notation has been introduced

$$
\begin{aligned}
\Delta_{\mathrm{B}31} &\equiv s+m_3^2-m_1^2,\\
\Delta_{\Psi 32} &\equiv p_2^2+m_3^2-m_2^2,\\
u &\equiv s+p_2^2-q^2.
\end{aligned}
\tag{A.53}
$$

A.2.2. Non-perturbative master integrals

The master integrals used in the calculation of nonlocal condesate contributions to correlation function are

$$
\begin{aligned}
I_0'(p_1^2,p_2^2,q^2;a,b) &= \int\frac{\mathrm{d}^4k}{(2\pi)^4}\frac{1}{[k^2-m_c^2]^a[(k+p_1)^2-m_b^2]^b}\mathrm{e}^{A(k+p_2)^2}\\
&= \tilde{I}_0(p_1^2,p_2^2,q^2;a,b)\,,\\
I_1'^{\mu}(p_1^2,p_2^2,q^2;a,b) &= \int\frac{\mathrm{d}^4k}{(2\pi)^4}\frac{k^\mu}{[k^2-m_c^2]^a[(k+p_1)^2-m_b^2]^b}\mathrm{e}^{A(k+p_2)^2}\\
&= \tilde{I}_1(p_1^2,p_2^2,q^2;a,b)\,p_1^\mu+\tilde{I}_2(p_1^2,p_2^2,q^2;a,b)\,p_2^\mu\,,\\
I_2'^{\mu\nu}(p_1^2,p_2^2,q^2;a,b) &= \int\frac{\mathrm{d}^4k}{(2\pi)^4}\frac{k^\mu k^\nu}{[k^2-m_c^2]^a[(k+p_1)^2-m_b^2]^b}\mathrm{e}^{A(k+p_2)^2}\\
&= \tilde{I}_{00}(p_1^2,p_2^2,q^2;a,b)g^{\mu\nu}+\tilde{I}_{11}(p_1^2,p_2^2,q^2;a,b)p_1^\mu p_1^\nu\\
&+\tilde{I}_{12}(p_1^2,p_2^2,q^2;a,b)p_1^\mu p_2^\nu+\tilde{I}_{21}(p_1^2,p_2^2,q^2;a,b)p_2^\mu p_1^\nu\\
&+\tilde{I}_{22}(p_1^2,p_2^2,q^2;a,b)p_2^\mu p_2^\nu\,,
\end{aligned}
\tag{A.54}
$$

where, for brevity $A = 4/m_0^2$. After symbolically denoting the operation of Borel transformation of independent tensor structures by the letter $\mathcal{B}$, we can write

$$\mathcal{B}_{-p_1^2}(M_1^2)\mathcal{B}_{-p_2^2}(M_2^2)\tilde{I}_{[\text{in}]}(p_1^2, p_2^2, q^2; a, b) = I_{[\text{in}]}(M_1^2, M_2^2, q^2; a, b)\,, \tag{A.55}$$

where "[in]" stands for any of the indices from Eq. (A.54), and

$$\begin{aligned}
&I_0(M_1^2, M_2^2, q^2; a, b)\\
&\quad = \frac{(-1)^{a+b}}{(a-1)!(b-1)!}\frac{\mathrm{i}}{(4\pi)^2}\left(\frac{1}{M_1^2}\quad\frac{A(M_1^2+M_2^2)}{M_1^2(AM_2^2-1)}\right)^{a-2}\quad A\frac{M_2^2}{M_1^2}\Bigg)^{b-1}\mathcal{F}(M_1^2, M_2^2; q^2),\\
&I_1(M_1^2, M_2^2, q^2; a, b) = \frac{M_2^2}{M_1^2}I_2(M_1^2, M_2^2, q^2; a, b)\\
&\quad = \frac{(-1)^{a+b+1}}{(a-1)!(b-1)!}\frac{\mathrm{i}}{(4\pi)^2}\left(\frac{1}{M_1^4}\quad\frac{A(M_1^2+M_2^2)}{M_1^2(AM_2^2-1)}\right)^{a-3}\quad A\frac{M_2^2}{M_1^2}\Bigg)^{b-1}\mathcal{F}(M_1^2, M_2^2; q^2),\\
&I_{00}(M_1^2, M_2^2, q^2; a, b)\\
&\quad = \frac{(-1)^{a+b+1}}{(a-1)!(b-1)!}\frac{\mathrm{i}}{(4\pi)^2}\left(\frac{1}{2M_1^4}\quad\frac{A(M_1^2+M_2^2)}{M_1^2(AM_2^2-1)}\right)^{a-3}\quad A\frac{M_2^2}{M_1^2}\Bigg)^{b-2}\mathcal{F}(M_1^2, M_2^2; q^2),\\
&I_{11}(M_1^2, M_2^2, q^2; a, b)\\
&\quad = \frac{(-1)^{a+b}}{(a-1)!(b-1)!}\frac{\mathrm{i}}{(4\pi)^2}\left(\frac{1}{M_1^6}\quad\frac{A(M_1^2+M_2^2)}{M_1^2(AM_2^2-1)}\right)^{a-2}\quad A\frac{M_2^2}{M_1^2}\Bigg)^{b-3}\mathcal{F}(M_1^2, M_2^2; q^2),\\
&I_{12}(M_1^2, M_2^2, q^2; a, b) = I_{21}(M_1^2, M_2^2, q^2; a, b)\\
&\quad = \frac{(-1)^{a+b}}{(a-1)!(b-1)!}\frac{\mathrm{i}}{(4\pi)^2}\left(\frac{1}{M_1^4M_2^2}\quad\frac{A(M_1^2+M_2^2)}{M_1^2(AM_2^2-1)}\right)^{a-3}\quad A\frac{M_2^2}{M_1^2}\Bigg)^{b-2}\mathcal{F}(M_1^2, M_2^2; q^2),\\
&I_{22}(M_1^2, M_2^2, q^2; a, b)\\
&\quad = \frac{(-1)^{a+b}}{(a-1)!(b-1)!}\frac{\mathrm{i}}{(4\pi)^2}\left(\frac{1}{M_1^2M_2^4}\quad\frac{A(M_1^2+M_2^2)}{M_1^2(AM_2^2-1)}\right)^{a-4}\quad A\frac{M_2^2}{M_1^2}\Bigg)^{b-1}\mathcal{F}(M_1^2, M_2^2; q^2)
\end{aligned} \tag{A.56}$$

and

$$\mathcal{F}(M_1^2, M_2^2; q^2) \equiv \frac{1}{AM_2^2-1}\exp\Big[-A\frac{M_1^2+M_2^2}{M_1^2(AM_2^2-1)}m_c^2 - A\frac{M_2^2}{M_1^2}m_b^2 + \frac{AM_2^2-1}{M_1^2+M_2^2}q^2\Big]. \tag{A.57}$$

B. LCSR HIGHER-TWIST EXPRESSIONS

The twist-three LCSR parameters relevant for symmetric wave functions (explored in this thesis) are defined through

$$\begin{aligned} z_\mu z^\nu \langle\Omega|\, \bar{q}\sigma^{\mu\omega}\gamma_5 g_s G_{\nu\omega} q\,|M_f\rangle &= 2\mathrm{i} f_{3M_f}(p\cdot z)^2, \\ z_\mu z^\nu \left(\langle\Omega|\, \bar{q} \quad \sigma^{\mu\omega}\gamma_5[\mathrm{i}D_\nu, g_s G_{\nu\omega}] - \frac{3}{7}\mathrm{i}z^\lambda \overleftarrow{\partial_\lambda}\sigma^{\mu\omega}\gamma_5 g_s G_{\nu\omega}\right) q\,|M_f\rangle &= \frac{3}{14}\mathrm{i} f_{3M_f}\omega_{3M_f}(p\cdot z)^3, \end{aligned} \tag{B.1}$$

with the momentum definitions from section 2.2, while the twist-four parameters are

$$\begin{aligned} \langle\Omega|\, \bar{q}\gamma^\alpha g_s \tilde{G}_{\mu\alpha} q\,|M_f(p_f)\rangle &= \mathrm{i} p_{f\mu} f_{M_f}\delta^2_{M_f}, \\ \left(\langle\Omega|\, \bar{q} \quad [\mathrm{i}D_\mu, g_s G_{\nu\omega}] - \frac{4}{9}\mathrm{i}\overleftarrow{\partial_\mu} g_s \tilde{G}_{\nu\omega}\right)\gamma^\omega q\,|M_f(p_f)\rangle &= f_{M_f}\delta^2_{M_f}\begin{pmatrix} \omega_{4M_f} & p_{f\mu}p_{f\nu} - \frac{1}{4}m^2_{M_f} g_{\mu\nu}\end{pmatrix}. \end{aligned} \tag{B.2}$$

All of the parameters renormalize [119]. The parameters enter the twist-three wave functions like

$$\begin{aligned} \phi^p_{3;M_f}(u;\mu^2) &= 1 + 30\frac{f_{3M_f}}{\mu_{M_f} f_{M_f}} C_2^{1/2}(2u-1) - 3\frac{f_{3M_f}\omega_{3M_f}}{\mu_{M_f} f_{M_f}} C_4^{1/2}(2u-1), \\ \phi^\sigma_{3;M_f}(u;\mu^2) &= 6u(1-u)\left(1 + 5\frac{f_{3M_f}}{\mu_{M_f} f_{M_f}}(1 - \frac{\omega_{3M_f}}{10}) C_2^{3/2}(2u-1)\right), \\ \Phi_{3;M_f}(\alpha_{\{1,2,3\}};\mu^2) &= 360\alpha_1\alpha_2\alpha_3^2\left[1 + \frac{\omega_{3M_f}}{2}(7\alpha_3 - 3)\right], \end{aligned} \tag{B.3}$$

and the twist-four wave functions like

$$
\begin{aligned}
\Phi_{4;M_f}(\alpha_{\{1,2,3\}};\mu^2) &= 120\delta^2_{M_f}(-\frac{8}{21}\omega_{4M_f})(\alpha_1-\alpha_2)\alpha_1\alpha_2\alpha_3,\\
\Psi_{4;M_f}(\alpha_{\{1,2,3\}};\mu^2) &= 30\delta^2_{M_f}(\alpha_1-\alpha_2)\alpha_3^2[\frac{1}{3}+2(-\frac{8}{21}\omega_{4M_f})(1-2\alpha_3)],\\
\tilde{\Phi}_{4;M_f}(\alpha_{\{1,2,3\}};\mu^2) &= -120\delta^2_{M_f}\alpha_1\alpha_2\alpha_3[\frac{1}{3}+(-\frac{8}{21}\omega_{4M_f})(1-3\alpha_3)],\\
\tilde{\Psi}_{4;M_f}(\alpha_{\{1,2,3\}};\mu^2) &= 30\delta^2_{M_f}\alpha_3^2(1-\alpha_3)[\frac{1}{3}+2(-\frac{8}{21}\omega_{4M_f})(1-2\alpha_3)].
\end{aligned}
\tag{B.4}
$$

C. Effective theory of weak interactions

The WET Lagrangian describing $b \to q$ (where $q = c, u$) transition, after integrating all the degrees of freedom above the weak scale $\mu \approx m_{W^\pm}$, can be written as [282]

$$\mathcal{L}^{\text{WET}} = -\frac{G_F V_{qb}}{\sqrt{2}} \left[(1 + V_L)\mathcal{O}_{V_L} + V_R \mathcal{O}_{V_R} + S_L \mathcal{O}_{S_L} + S_R \mathcal{O}_{S_R} + T_L \mathcal{O}_{T_L} \right].$$

The operators, including possible NP degrees of freedom are

$$\begin{aligned}
\mathcal{O}_{V_L} &= (\bar{q}\gamma^\mu(1-\gamma_5)b)\left(\bar{\ell}\gamma_\mu(1-\gamma_5)\nu_\ell\right), & \mathcal{O}_{V_R} &= (\bar{q}\gamma^\mu(1+\gamma_5)b)\left(\bar{\ell}\gamma_\mu(1-\gamma_5)\nu_\ell\right), \\
\mathcal{O}_{S_L} &= (\bar{q}(1-\gamma_5)b)\left(\bar{\ell}(1-\gamma_5)\nu_\ell\right), & \mathcal{O}_{S_R} &= (\bar{q}(1+\gamma_5)b)\left(\bar{\ell}(1-\gamma_5)\nu_\ell\right), \\
\mathcal{O}_{T_L} &= (\bar{q}\sigma^{\mu\nu}(1-\gamma_5)b)\left(\bar{\ell}\sigma_{\mu\nu}(1-\gamma_5)\nu_\ell\right).
\end{aligned}$$

In the SM, the couplings $V_{L,R}, S_{L,R}$ and T_L are all exactly zero, and the only operator contributing is $\mathcal{O}_{V_L}$. Of course, the Lagrangian can be written in a different operator basis [283] reproducing the same physics, so that

$$\tilde{\mathcal{L}}^{\text{WET}} = \frac{4 V_{ub} G_F}{\sqrt{2}} \mathcal{J}_\mu^{\text{had}}(x) \left[\bar{\ell}(x)\gamma^\mu P_L \nu_\ell(x)\right], \tag{C.1}$$

where $\mathcal{J}_\mu^{\text{had}}(x)$ contains all the relevant quark field operators and couplings, and $P_L = (1-\gamma_5)/2$ is the left-handed projector. This is convenient when defining the helicity form factor basis in a unified way, as made obvious in appendix D.1.

D. Angular observables

D.1. Helicity form factors

For a generic $B_q \to M_f \ell \bar{\nu}_\ell$ semileptonic decay, a set of helicity form factors can be defined [284] that simplify expressions and differentiate between specific helicity contributions to the semileptonic decay width. For a pseudoscalar meson $M_f = P_f$ in the final state this means

$$h_{0,t}(q^2) = \tilde{\epsilon}^\mu_{0,t}(q) \langle P_f(p_2)| \mathcal{J}^{\text{had}}_\mu(0) |B_q(p_1)\rangle \,, \tag{D.1}$$

where $\tilde{\epsilon}^\mu_{0,t}(q)$ represents the polarization of the charged $W^\pm$ boson. Since the mesonic transition is of the type $0^- \to 0^-$, the only polarizations of the $W^\pm$ contributing are the longitudinal component $\tilde{\epsilon}^\mu_0(q)$, and the timelike component $\tilde{\epsilon}^\mu_t(q)$. Equivalently, for a vector meson $M_f = V_f$ in the final state

$$\begin{aligned} H_\pm(q^2) &= \tilde{\epsilon}^\mu_\pm(q) \langle V_f(p_2;\epsilon_\pm)| \mathcal{J}^{\text{had}}_\mu(0) |B_q(p_1)\rangle \,, \\ H_{0,t}(q^2) &= \tilde{\epsilon}^\mu_{0,t}(q) \langle V_f(p_2;\epsilon_0)| \mathcal{J}^{\text{had}}_\mu(0) |B_q(p_1)\rangle \,, \end{aligned} \tag{D.2}$$

where now transverse components $\tilde{\epsilon}^\mu_\pm(q)$ of the $W^\pm$ boson have been introduced, and the amplitudes now contain helicity contributions from the V_f polarization. Since V_f is produced on-shell, it has only three physical polarizations, unlike $W^\pm$ which is produced off-shell, so also the timelike polarization is available.

The helicity form factors can be written up using the usual WS form factors, but the exact expressions depend on the polarization bases. In section 5.2 the basis from [284] is used in a SM analysis, so $\mathcal{J}^{\text{had}}_\mu(0) = \bar{u}(0)\gamma_\mu(1-\gamma_5)b(0)$, and the virtual

boson polarization in the B_c rest frame is taken as

$$\tilde{\epsilon}_{\pm\mu} = \frac{1}{\sqrt{2}} \begin{pmatrix} 0 \\ \pm 1 \\ -\mathrm{i} \\ 0 \end{pmatrix}, \qquad \tilde{\epsilon}_{0\mu} = \frac{1}{\sqrt{q^2}} \begin{pmatrix} |\vec{q}| \\ 0 \\ 0 \\ -q_0 \end{pmatrix}, \qquad \tilde{\epsilon}_{t\mu} = \frac{1}{\sqrt{q^2}} \begin{pmatrix} q_0 \\ 0 \\ 0 \\ -|\vec{q}| \end{pmatrix}, \tag{D.3}$$

which amounts to quantizing along the $z-$axis. Additionaly, for the V_f meson the polarizations are

$$\epsilon_{\pm\mu} = \frac{1}{\sqrt{2}} \begin{pmatrix} 0 \\ \mp 1 \\ -\mathrm{i} \\ 0 \end{pmatrix}, \qquad \epsilon_{0\mu} = \frac{1}{m_{D^*}} \begin{pmatrix} |\vec{q}| \\ 0 \\ 0 \\ E_{D^*} \end{pmatrix}. \tag{D.4}$$

The B_c rest frame is actually defined by the momenta of the particles being

$$p_{1\mu} = \begin{pmatrix} m_{B_c} \\ 0 \\ 0 \\ 0 \end{pmatrix}, \qquad p_{2\mu} = \begin{pmatrix} E_{D^{(*)}} \\ 0 \\ 0 \\ |\vec{q}| \end{pmatrix}, \qquad q_\mu = \begin{pmatrix} q_0 \\ 0 \\ 0 \\ -|\vec{q}| \end{pmatrix}. \tag{D.5}$$

where it was chosen that the z-axis is aligned with the direction of $D^{(*)}$, and with the indices being made explicit in order to stress the covariant nature of our definitions. The energy of the W boson, and the $D^{(*)}$ in this frame amount respectively to

$$q_0 = \frac{m_{B_c}^2 - m_{D^{(*)}}^2 + q^2}{2m_{B_c}}, \qquad E_{D^{(*)}} = \frac{m_{B_c}^2 + m_{D^{(*)}}^2 - q^2}{2m_{B_c}}. \tag{D.6}$$

In section 4.2 a different basis is used, equivalent to the one in Ref. [285]. Also, the NP couplings have been pulled out of the helicity form factor definitions. Therefore, the helicity form factors and the decay width expressions look differently, but reproduce the same physics. A further difference between the two sections is the complex phase between the helicity form factor definitions. This is a convention

choice, in order to make the helicity form factors real in section 4.2.

D.2. Angular observables

The general expressions for the two-fold differential distributions in $B_q \to M_f \ell \bar{\nu}_\ell$ semileptonic decays can be given as

$$\frac{\mathrm{d}^2\Gamma(B_q \to M_f \ell \bar{\nu}_\ell)}{\mathrm{d}q^2 \mathrm{d}\cos\theta_\ell} = a_{\theta_\ell}^{M_f}(q^2) + b_{\theta_\ell}^{M_f}(q^2)\cos\theta_\ell + c_{\theta_\ell}^{M_f}(q^2)\cos^2\theta_\ell\,, \tag{D.7}$$

where θ_l is the angle between the lepton and the final state meson in the center-of-momentum frame of the leptonic pair.

Two kinematical variables - q^2 and θ_ℓ

The following angular observable definitions are often appropriated in SM tests when the lepton angle is considered additional to the momentum transfer

1. The forward-backward asymmetry

$$A_{\mathrm{FB}}^{\ell}(q^2) = \frac{\left(\int_0^1 - \int_{-1}^0\right)\mathrm{d}\cos\theta \frac{\mathrm{d}^2\Gamma(B_1 \to M_f \ell \bar{\nu}_\ell)}{\mathrm{d}q^2\,\mathrm{d}\cos\theta}}{\frac{\mathrm{d}\Gamma(B_q \to M_f \ell \bar{\nu}_\ell)}{\mathrm{d}q^2}} \left(= \frac{b_{\theta_\ell}^{M_f}(q^2)}{2\;\; a_{\theta_\ell}^{M_f}(q^2) + c_{\theta_\ell}^{M_f}(q^2)/3}\right), \tag{D.8}$$

   which measures the asymmetry in the angle at which the momenta of the produced lepton propagates (with respect to the z-axis).

2. The convexity parameter

$$C_F^{\ell}(q^2) = \frac{1}{\frac{\mathrm{d}\Gamma(B_q \to M_f \ell \bar{\nu}_\ell)}{\mathrm{d}q^2}} \frac{\mathrm{d}^2}{\mathrm{d}(\cos\theta)^2}\left[\frac{\mathrm{d}^2\Gamma(B_q \to M_f \ell \bar{\nu}_\ell)}{\mathrm{d}q^2\,\mathrm{d}\cos\theta}\right] = \frac{c_{\theta_\ell}^{M_f}(q^2)}{a_{\theta_\ell}^{M_f}(q^2) + c_{\theta_\ell}^{M_f}(q^2)/3}, \tag{D.9}$$

   which is connected to the so-called "flat term"

$$F_H^{\ell} = 1 + \frac{2}{3} C_F^{\ell}\,. \tag{D.10}$$

   In the SM both F_H^{ℓ} and A_{FB}^{ℓ} are small for $\ell = e, \mu$, since they are proportional to the lepton mass. This makes them appropriate SM tests.

3. The lepton polarization

$$P^{\ell}(q^2) = \frac{\frac{\mathrm{d}\Gamma^{+}(B_q\to M_f\ell\bar{\nu}_\ell)}{\mathrm{d}q^2} - \frac{\mathrm{d}\Gamma^{-}(B_q\to M_f\ell\bar{\nu}_\ell)}{\mathrm{d}q^2}}{\frac{\mathrm{d}\Gamma(B_q\to M_f\ell\bar{\nu}_\ell)}{\mathrm{d}q^2}}, \tag{D.11}$$

where the differential decay width is considered as a sum of contributions of left and right lepton helicity projections along the z-axis, Γ^{-} and Γ^{+} respectively.

4. If there is a vector meson $M_f = V_f$ in the final state, a longitudinal polarization fraction can also be investigated, as

$$F_L^{V_f,\ell}(q^2) = \frac{\mathrm{d}\Gamma_L(B_q\to V_f\ell\bar{\nu}_\ell)}{\mathrm{d}q^2}\Big/\frac{\mathrm{d}\Gamma(B_q\to V_f\ell\bar{\nu}_\ell)}{\mathrm{d}q^2}. \tag{D.12}$$

Four kinematical variables - q^2, θ_ℓ, θ_V, χ

If, additionally to the lepton angle and the momentum transfer, two other variables are considered, describing the angle θ_V between the leptonic decay products of the final state vector meson decay, and the angle χ between the planes of leptonic decay, additional angular observables can be constructed, where in the case of $B_c \to (J/\psi \to \mu^+\mu^-)\ell\bar{\nu}_\ell$ they have been defined using (section 4.2)

$$\begin{aligned}
\mathcal{T}_{V_L} &= \sin^2\theta_V\Big(2H_{00}^2(\sin^2\theta_\ell + 2\delta_\tau\cos^2\theta_\ell) + 4\delta_\tau H_{t0}^2\Big) \\
&+ 8H_{++}^2\sin^2\frac{\theta_\ell}{2}\sin^4\frac{\theta_V}{2}\Big(2\delta_\tau\cos^2\frac{\theta_\ell}{2} + \sin^2\frac{\theta_\ell}{2}\Big) \\
&+ 8H_{--}^2\cos^2\frac{\theta_\ell}{2}\cos^4\frac{\theta_V}{2}\Big(2\delta_\tau\sin^2\frac{\theta_\ell}{2} + \cos^2\frac{\theta_\ell}{2}\Big) \\
&+ H_{++}H_{--}\sin^2\theta_\ell\sin^2\theta_V\cos 2\chi(1-2\delta_\tau) \\
&- 8\sin\theta_\ell\sin\theta_V\cos\chi H_{00}\times \\
&\qquad\times\Big(H_{++}\sin^2\frac{\theta_V}{2}(\sin^2\frac{\theta_\ell}{2} + \delta_\tau\cos\theta_\ell) + H_{--}\cos^2\frac{\theta_V}{2}(\cos^2\frac{\theta_\ell}{2} - \delta_\tau\cos\theta_\ell)\Big) \\
&+ 8\delta_\tau\sin\theta_\ell\sin\theta_V\cos\chi H_{t0}\Big(H_{++}\sin^2\frac{\theta_V}{2} - H_{--}\cos^2\frac{\theta_V}{2}\Big) \\
&- 8\sin\theta_V^2\cos\theta_\ell\delta_\tau H_{t0}H_{00},
\end{aligned} \tag{D.13}$$

$$
\begin{aligned}
\mathcal{T}_{|V_R|^2} = & \sin^2\theta_V\Big(2H_{00}^2(\sin^2\theta_\ell + 2\delta_\tau\cos^2\theta_\ell) + 4\delta_\tau H_{t0}^2\Big) \\
& + 8H_{--}^2\sin^2\frac{\theta_\ell}{2}\sin^4\frac{\theta_V}{2}\Big(2\delta_\tau\cos^2\frac{\theta_\ell}{2} + \sin^2\frac{\theta_\ell}{2}\Big) \\
& + 8H_{++}^2\cos^2\frac{\theta_\ell}{2}\cos^4\frac{\theta_V}{2}\Big(2\delta_\tau\sin^2\frac{\theta_\ell}{2} + \cos^2\frac{\theta_\ell}{2}\Big) \\
& + H_{++}H_{--}\sin^2\theta_\ell\sin^2\theta_V\cos 2\chi(1-2\delta_\tau) \\
& - 8\sin\theta_\ell\sin\theta_V\cos\chi H_{00}\times \\
& \quad\times\Big(H_{--}\sin^2\frac{\theta_V}{2}(\sin^2\frac{\theta_\ell}{2} + \delta_\tau\cos\theta_\ell) + H_{++}\cos^2\frac{\theta_V}{2}(\cos^2\frac{\theta_\ell}{2} - \delta_\tau\cos\theta_\ell)\Big) \\
& + 8\delta_\tau\sin\theta_\ell\sin\theta_V\cos\chi H_{t0}\Big(H_{--}\sin^2\frac{\theta_V}{2} - H_{++}\cos^2\frac{\theta_V}{2}\Big) \\
& - 8\sin\theta_V^2\cos\theta_\ell\delta_\tau H_{t0}H_{00},
\end{aligned}
\tag{D.14}
$$

$$
\begin{aligned}
\mathcal{T}_{V_R^{int}} = & -2\mathrm{Re}V_R\sin^2\theta_V\Big(2H_{00}^2(\sin^2\theta_\ell + 2\delta_\tau\cos^2\theta_\ell) + 4\delta_\tau H_{t0}^2\Big) \\
& - \sin^2\theta_\ell\sin^2\theta_V(1-2\delta_\tau)\times \\
& \quad\times\Big[H_{++}^2(\mathrm{Re}V_R\cos 2\chi + \mathrm{Im}V_R\sin 2\chi) + H_{--}^2(\mathrm{Re}V_R\cos 2\chi - \mathrm{Im}V_R\sin 2\chi)\Big] \\
& - 2\mathrm{Re}V_R H_{++}H_{--}\Big[(1+\cos^2\theta_V)\Big(1+\cos^2\theta_\ell + 2\delta_\tau\sin^2\theta_\ell\Big) + 4\cos\theta_V\cos\theta_\ell\Big] \\
& + 16\mathrm{Re}V_R\cos\theta_\ell\sin^2\theta_V H_{00}H_{t0} \\
& + \Big(4\sin\theta_V\cos\theta_\ell - \sin 2\theta_V\sin 2\theta_\ell(2\delta_\tau - 1)\Big)H_{00}\times \\
& \quad\times\Big(H_{++}(\mathrm{Re}V_R\cos\chi + \mathrm{Im}V_R\sin\chi) + H_{--}(\mathrm{Re}V_R\cos\chi - \mathrm{Im}V_R\sin\chi)\Big) \\
& + 4\delta_\tau\sin\theta_\ell\sin 2\theta_V H_{t0}\times \\
& \quad\times\Big[H_{++}(\mathrm{Re}V_R\cos\chi + \mathrm{Im}V_R\sin\chi) + H_{--}(\mathrm{Re}V_R\cos\chi - \mathrm{Im}V_R\sin\chi)\Big],
\end{aligned}
\tag{D.15}
$$

$$
\begin{aligned}
\mathcal{T}_{P^{int}} = & 4\sqrt{2\delta_\tau}H_S^V\Big[\mathrm{Re}P\sin^2\theta_V\Big(H_{t0} - H_{00}\cos\theta_\ell\Big) + \sin\theta_V\sin\theta_\ell\Big\{H_{++}\sin^2\frac{\theta_V}{2}\times \\
& \times\Big(\mathrm{Re}P\cos\chi + \mathrm{Im}P)\sin\chi\Big) - H_{--}\cos^2\frac{\theta_V}{2}\Big(\mathrm{Re}P\cos\chi - \mathrm{Im}P\sin\chi\Big)\Big\}\Big],
\end{aligned}
\tag{D.16}
$$

$$\begin{aligned}\mathcal{T}_{|T_L|^2} = 16|T_L|^2\Big\{&2|H_T^0|^2\sin^2\theta_V(\cos^2\theta_\ell + 2\delta_\tau\sin^2\theta_\ell)\\ &+ 8|H_T^+|^2\sin^2\frac{\theta_\ell}{2}\sin^4\frac{\theta_V}{2}\Big(2\delta_\tau\sin^2\frac{\theta_\ell}{2} + \cos^2\frac{\theta_\ell}{2}\Big)\\ &+ 8|H_T^-|^2\cos^2\frac{\theta_\ell}{2}\cos^4\frac{\theta_V}{2}\Big(2\delta_\tau\cos^2\frac{\theta_\ell}{2} + \sin^2\frac{\theta_\ell}{2}\Big)\\ &- H_T^+H_T^-\sin^2\theta_\ell\sin^2\theta_V\cos 2\chi(1-2\delta_\tau) - 4\sin\theta_\ell\sin\theta_V\cos\chi H_T^0\times\\ &\times\Big[H_T^+\sin^2\frac{\theta_V}{2}\Big(2\delta_\tau\sin^2\frac{\theta_\ell}{2} + \cos\theta_\ell\Big)\\ &\quad + H_T^-\cos^2\frac{\theta_V}{2}\Big(2\delta_\tau\cos^2\frac{\theta_\ell}{2} - \cos\theta_\ell\Big)\Big]\Big\},\end{aligned} \tag{D.17}$$

$$\begin{aligned}\mathcal{T}_{T_L^{int}} = 16\sqrt{2\delta_\tau}\Big\{&H_T^0\Big[\mathrm{Re}T_L\sin^2\theta_V\Big(H_{t0}\cos\theta_\ell - H_{00}\Big)\\ &\quad + \sin\theta_\ell\sin\theta_V\Big(H_{++}\sin^2\frac{\theta_V}{2}(\mathrm{Re}T_L\cos\chi + \mathrm{Im}T_L\sin\chi)\\ &\qquad + H_{--}\cos^2\frac{\theta_V}{2}(\mathrm{Re}T_L\cos\chi - \mathrm{Im}T_L\sin\chi)\Big)\Big]\\ &+ H_T^+\Big[\sin\theta_\ell\sin\theta_V\Big(\mathrm{Re}T_L\cos\chi - \mathrm{Im}T_L\sin\chi\Big)(H_{00} - H_{t0})\sin^2\frac{\theta_V}{2}\\ &\quad - 4\mathrm{Re}T_L\sin^2\frac{\theta_\ell}{2}\sin^4\frac{\theta_V}{2}H_{++}\Big]\\ &+ H_T^-\Big[\sin\theta_\ell\sin\theta_V\Big(\mathrm{Re}T_L\cos\chi + \mathrm{Im}T_L\sin\chi\Big)(H_{00} + H_{t0})\cos^2\frac{\theta_V}{2}\\ &\quad - 4\mathrm{Re}T_L\cos^2\frac{\theta_\ell}{2}\cos^4\frac{\theta_V}{2}H_{--}\Big]\Big\}.\end{aligned} \tag{D.18}$$

E. Bayesian analysis using EOS

EOS [286] is a software framework for use in high energy physics, specifically quark flavor physics. With the source code written in C++14 and an interface in Python 3, EOS is very well equipped to deal with Bayesian analyses of both theoretical and experimental data sets. To demonstrate how the uncertainty inferred from model parameters propagates to physical observables, here the B meson mass estimation from eq. (6.5) is presented in detail.

The initial probability distributions followed by the parameters are presented in table 6.1. An initial distribution is called the prior, and each parameter is assumed to follow a prior distribution independently of the other variables, i.e. in an uncorrelated way. The posterior parameter distributions are obtained from Bayes' theorem

$$p\left(\vec{\theta}\,\middle|\,\vec{m}_B^2\right) = \frac{p\left(\vec{m}_B^2\,\middle|\,\vec{\theta}\right) p\left(\vec{\theta}\right)}{N}, \tag{E.1}$$

where $\vec{\theta}$ and $\vec{m}_B^2$ are vectors containing model parameters, and the B meson mass, respectively. The probabilities $p\left(x \,\middle|\, y\right)$ are read "the probability of x given y". On the left-hand side is the target distribution, called the posterior distribution, while on the right-hand side $p\left(\vec{m}_B^2\,\middle|\,\vec{\theta}\right)$ is the probability of obtaining $\vec{m}_B^2$ given $\vec{\theta}$ (often called the likelihood) multiplied by the prior $p\left(\vec{\theta}\right)$. The normalization is given by

$$N = p\left(\vec{m}_B^2\right) = \int \mathrm{d}\vec{\theta}\, p\left(\vec{m}_B^2\,\middle|\,\vec{\theta}\right) p\left(\vec{\theta}\right). \tag{E.2}$$

For the likelihood, the d-dimesional multivariate gaussian distribution is chosen

$$\begin{aligned}\Big(p\ \vec{m}_B^2 \,\Big|\, \vec{\theta}\Big) &\equiv \mathcal{N}\ \vec{m}_B^2 \,\Big|\, \vec{\theta}\Big) \\ &= \frac{1}{(2\pi)^{d/2}} |\underline{\Sigma}|^{-1/2} \exp\left[-\frac{1}{2}(\vec{m}_B^2 - [\vec{m}_B^2]_{\text{LCSR}})^{\text{T}} \underline{\Sigma}^{-1} (\vec{m}_B^2 - [\vec{m}_B^2]_{\text{LCSR}})\right],\end{aligned} \tag{E.3}$$

centered around $\vec{m}_B^2$ with the covariance matrix $\underline{\Sigma}$, and $[\vec{m}_B^2]_{\text{LCSR}}$ is defined in eq. (6.5). Since the denominator doesn't depend on $\vec{\theta}$, the Bayesian estimator is obtained by maximizing the numerator of the right-hand side of eq. (E.1), as explained below.

In the next step the adaptive Metropolis-Hastings algorithm for Markov-Chain Monte Carlo (MCMC) random walks is employed. The process is iterative, and k chains are run in parallel in the following way:

1. For the 0-th iteration of k-th chain, a random point is sampled from the proposal. The proposal is given by a multivariate gaussian, $q(\vec{\theta}' \,|\, \vec{\theta}) \equiv \mathcal{N}(\vec{\theta}' \,|\, \vec{\theta})$, initially with a diagonal covariance containing parameter variances from the prior on the diagonal.

2. The proposed point is accepted with a probability

$$\Big(\alpha\ \vec{\theta}, \vec{\theta}'\Big) = \min\left(1, \frac{p(\vec{\theta}')p(\vec{m}_B^2 \,|\, \vec{\theta}')q(\vec{\theta} \,|\, \vec{\theta}')}{p(\vec{\theta})p(\vec{m}_B^2 \,|\, \vec{\theta})q(\vec{\theta}' \,|\, \vec{\theta})}\right), \tag{E.4}$$

   which comes from Bayes' theorem. Otherwise, it is discarded. This is done for $\bar{N}$ iterations.

3. For the $(\bar{N}+1)$-th iteration the proposal covariance matrix is slightly perturbed for the first time, according to the rule

$$\underline{\Sigma}^t = (1 - a^t)\underline{\Sigma}^{t-1} + a^t \underline{S}^t, \tag{E.5}$$

   where $t = 1$ for the first perturbation (after $\bar{N}$ iterations), $t = 2$ for the second perturbation (after $2\bar{N}$ iterations), and so on, $a^t = 1/t^\lambda,\ \lambda \in [0, 1]$ is a weight

chosen to make for a smooth transition from the initial guess to the target covariance, and

$$[\underline{S}^t]_{mn} = \frac{1}{\bar{N}-1} \sum_{i=\bar{N}(t-1)}^{\bar{N}t} \left((\vec{\theta}^i)_m - E_P[\vec{\theta}_m]\right) \left((\vec{\theta}^i)_n - E_P[\vec{\theta}_n]\right), \tag{E.6}$$

where i goes over iterations. The estimator for m-th parameter $E_P[\vec{\theta}_m]$, is introduced as

$$E_P[\vec{\theta}_m] = \frac{1}{\bar{N}} \sum_i \vec{\theta^i}_m. \tag{E.7}$$

In summary, every $\bar{N}$ iterations, the covariance is perturbed according to the samples accepted in the prior chunk of iterations.

4. After the first perturbation, the proposal is different from the prior, and the process is repeated for the next chunk of $\bar{N}$ iterations with the new covariance matrix, after which it is perturbed again. This iterative process is repeated until convergence is declared in all chains if the sample acceptance rate satisfies a criteria set beforehand.

5. After all k chains are run, the main chain is run, in which the covariance matrix is set to the one the random walk converged to. This samples the posterior.

After a posterior for the parameters is sampled, and a set of chains is ran, the procedure is updated with the so-called Population Monte-Carlo (PMC) method [287], which isn't explained here. The parametric uncertainties are easily propagated to the LCSR form factors by evaluating the form factors at each parameter point drawn according to the posterior.

In EOS, a large set of (pseudo-)observables, parameters and constraints relevant for flavour physics and QCD is readily available for statistical analysis. The observables range from decay widths and angular observables to form factors. Parameters encompass for example the CKM matrix elements, decay constants and hadronic spectra. Constraints are stored as dictionary classes, and include relevant information on the likelihood distribution the specific constraint follows.

Also offered are numerical tools required for the analysis. This might include a

simple evaluation of a parameter or an observable based on a set of parameters, but more complicated multivariate analyses, such as the one explained in this appendix section, are also very conveniently handled.

Curriculum Vitae

Domagoj Leljak was born on December 16 1990, in Zagreb, Croatia. After moving to Biograd, Croatia, in 1996, he graduated from the primary school "Biograd" in 2005. Moving back to Zagreb for his secondary school education, he graduated from "The Fifth Gymnasium" in 2009, and enrolled at the Physics Department of the Faculty of Science, University of Zagreb. In 2010, he also graduated from the "Popular and jazz music high school", and gained the title of musician/guitarist. Under the supervision of dr.sc. Davor Horvatić, he obtained his master's degree in 2016, with the thesis titled "Finite temperature effective model of gluonic matter". Since February 2017 he has been employed as a research assistant at the Ruđer Bošković Institute, on the "Young researchers' career development" (DOK-10-2015) project. Under the supervision of dr.rer.nat. Blaženka Melić, the research work performed within the project was compiled in a doctoral thesis titled "Testing the Standard Model in heavy quark decays".

He has attended five different theoretical physics schools in Croatia, Italy, France, Germany and Russia, and was invited to two research visits, one in Paris, France, at Laboratoire de Physique Théorique d'Orsay in 2017, to collaborate with dr.sc. Damir Bećirević on a research project regarding lepton flavour universality in the decays of B_c meson, and one in Munich, Germany, at Technische Universität München in 2019, to collaborate with dr.sc. Danny van Dyk on a research project regarding form factors and CKM matrix element relevant for $\bar{B} \to \pi$ transitions. He has also participated in many conferences, giving a talk at the "Getting to Grips with QCD" conference at Campus des Cordeliers in Paris, France in 2018, and presenting a poster at the Humboldt conference at Croatian Academy of Sciences and Arts in Zagreb, Croatia in 2019. In 2020 he was awarded with the "Ruđer Bošković" yearly

reward for scientific research. He is a coauthor of 3 published research papers.

The list of his scientific publications consists of:

1. D. Leljak, B. Melic and M. Patra, "*On lepton flavour universality in semileptonic $B_c \to \eta_c, J/\psi$ decays*," JHEP **05** (2019), 094, doi:10.1007/JHEP05(2019)094, [arXiv:1901.08368 [hep-ph]],

2. D. Leljak and B. Melic, "*$|V_{ub}|$ determination and testing of lepton flavour universality in semileptonic $B_c \to D^{(*)}$ decays*," JHEP **02** (2020), 171, doi:10.1007/JHEP02(2020)171, [arXiv:1909.01213 [hep-ph]],

3. D. Leljak, B. Melić and D. van Dyk, "*The $\bar{B} \to \pi$ form factors from QCD and their impact on $|V_{ub}|$*," JHEP **07** (2021), 036, doi:10.1007/JHEP07(2021)036, [arXiv:2102.07233 [hep-ph]].

Bibliography

[1] D. Leljak, B. Melic and M. Patra, *On lepton flavour universality in semileptonic $B_c \to \eta_c, J/\psi$ decays*, *JHEP* **05** (2019) 094, [1901.08368]. ↑ vi, 2, 67.

[2] D. Leljak and B. Melic, *$|V_{ub}|$ determination and testing of lepton flavour universality in semileptonic $B_c \to D^{(*)}$ decays*, *JHEP* **02** (2020) 171, [1909.01213]. ↑ vii, 2, 107.

[3] D. Leljak, D. van Dyk and B. Melić, *The $\bar{B} \to \pi$ form factors from QCD and their impact on $|V_{ub}|$*, 2102.07233. ↑ vii, 2, 107, 133, 142.

[4] Particle Data Group collaboration, P. A. Zyla et al., *Review of Particle Physics*, *PTEP* **2020** (2020) 083C01. ↑ 4, 22, 24, 125, 136, 146, 158, 162.

[5] T. Nakano and K. Nishijima, *Charge Independence for V-particles*, *Prog. Theor. Phys.* **10** (1953) 581–582. ↑ 7.

[6] M. Gell-Mann, *The interpretation of the new particles as displaced charge multiplets*, *Nuovo Cim.* **4** (1956) 848–866. ↑ 7.

[7] M. Gell-Mann, *The Eightfold Way: A Theory of strong interaction symmetry*, . ↑ 7.

[8] O. W. Greenberg, *Spin and Unitary Spin Independence in a Paraquark Model of Baryons and Mesons*, *Phys. Rev. Lett.* **13** (1964) 598–602. ↑ 7.

[9] M. Y. Han and Y. Nambu, *Three Triplet Model with Double SU(3) Symmetry*, *Phys. Rev.* **139** (1965) B1006–B1010. ↑ 7.

[10] H. Fritzsch, M. Gell-Mann and H. Leutwyler, *Advantages of the Color Octet Gluon Picture*, *Phys. Lett. B* **47** (1973) 365–368. ↑ 7.

[11] M. Gell-Mann, *Symmetries of baryons and mesons*, *Phys. Rev.* **125** (1962) 1067–1084. ↑ 8, 29.

[12] D. J. Gross and F. Wilczek, *Ultraviolet Behavior of Nonabelian Gauge Theories*, *Phys. Rev. Lett.* **30** (1973) 1343–1346. ↑ 8.

[13] H. D. Politzer, *Reliable Perturbative Results for Strong Interactions?*, *Phys. Rev. Lett.* **30** (1973) 1346–1349. ↑ 8.

[14] A. Deur, S. J. Brodsky and G. F. de Teramond, *The QCD Running Coupling*, *Nucl. Phys.* **90** (2016) 1, [1604.08082]. ↑ 9.

[15] J. Greensite, *The Confinement problem in lattice gauge theory*, *Prog. Part. Nucl. Phys.* **51** (2003) 1, [hep-lat/0301023]. ↑ 10.

[16] H.-X. Chen, W. Chen, X. Liu, Y.-R. Liu and S.-L. Zhu, *A review of the open charm and open bottom systems*, *Rept. Prog. Phys.* **80** (2017) 076201, [1609.08928]. ↑ 10.

[17] T. Regge, *Introduction to complex orbital momenta*, *Nuovo Cim.* **14** (1959) 951. ↑ 10.

[18] V. N. Gribov, *Partial waves with complex orbital angular momenta and the asymptotic behavior of the scattering amplitude*, *Zh. Eksp. Teor. Fiz.* **41** (1961) 1962. ↑ 10.

[19] O. Aharony, *The NonAdS / nonCFT correspondence, or three different paths to QCD*, in *NATO Advanced Study Institute and EC Summer School on Progress in String, Field and Particle Theory*, 12, 2002, hep-th/0212193. ↑ 10.

[20] S. J. Brodsky, H.-C. Pauli and S. S. Pinsky, *Quantum chromodynamics and other field theories on the light cone*, *Phys. Rept.* **301** (1998) 299–486, [hep-ph/9705477]. ↑ 11.

[21] M. Neubert, *Lectures on the theory of nonleptonic B decays*, in *Theoretical Advanced Study Institute in Elementary Particle Physics (TASI 2000): Flavor Physics for the Millennium*, 6, 2000, hep-ph/0012204, DOI. ↑ 11, 75.

[22] P. W. Higgs, *Broken Symmetries and the Masses of Gauge Bosons*, *Phys. Rev. Lett.* **13** (1964) 508–509. ↑ 13.

[23] P. W. Higgs, *Spontaneous Symmetry Breakdown without Massless Bosons*, *Phys. Rev.* **145** (1966) 1156–1163. ↑ 13.

[24] T. W. B. Kibble, *Symmetry breaking in non-Abelian gauge theories*, *Phys. Rev.* **155** (1967) 1554–1561. ↑ 13.

[25] I. Low and A. V. Manohar, *Spontaneously broken space-time symmetries and Goldstone's theorem*, *Phys. Rev. Lett.* **88** (2002) 101602, [hep-th/0110285]. ↑ 15.

[26] N. Cabibbo, *Unitary Symmetry and Leptonic Decays*, *Phys. Rev. Lett.* **10** (1963) 531–533. ↑ 16.

[27] M. Kobayashi and T. Maskawa, *CP Violation in the Renormalizable Theory of Weak Interaction*, *Prog. Theor. Phys.* **49** (1973) 652–657. ↑ 16.

[28] L. Wolfenstein, *Parametrization of the Kobayashi-Maskawa Matrix*, *Phys. Rev. Lett.* **51** (1983) 1945. ↑ 16.

[29] G. 't Hooft, *Symmetry Breaking Through Bell-Jackiw Anomalies*, *Phys. Rev. Lett.* **37** (1976) 8–11. ↑ 17.

[30] C. Jarlskog, *Commutator of the Quark Mass Matrices in the Standard Electroweak Model and a Measure of Maximal CP Violation*, *Phys. Rev. Lett.* **55** (1985) 1039. ↑ 18.

[31] J. H. Christenson, J. W. Cronin, V. L. Fitch and R. Turlay, *Evidence for the* 2π *Decay of the* K_2^0 *Meson*, *Phys. Rev. Lett.* **13** (1964) 138–140. ↑ 18.

[32] BaBar collaboration, B. Aubert et al., *Observation of CP violation in the B^0 meson system*, *Phys. Rev. Lett.* **87** (2001) 091801, [hep-ex/0107013]. ↑ 18.

[33] KTeV collaboration, A. Alavi-Harati et al., *Observation of direct CP violation in $K_{S,L} \to \pi\pi$ decays*, *Phys. Rev. Lett.* **83** (1999) 22–27, [hep-ex/9905060]. ↑ 18.

[34] LHCb collaboration, R. Aaij et al., *Observation of CP Violation in Charm Decays*, *Phys. Rev. Lett.* **122** (2019) 211803, [1903.08726]. ↑ 18.

[35] BaBar collaboration, B. Aubert et al., *Observation of direct CP violation in $B^0 \to K^+\pi^-$ decays*, *Phys. Rev. Lett.* **93** (2004) 131801, [hep-ex/0407057]. ↑ 18.

[36] J. M. Flynn and L. Randall, *The Electromagnetic Penguin Contribution to Epsilon-prime / Epsilon for Large Top Quark Mass*, *Phys. Lett. B* **224** (1989) 221. ↑ 18.

[37] S. M. Faber and R. E. Jackson, *Velocity dispersions and mass to light ratios for elliptical galaxies*, *Astrophys. J.* **204** (1976) 668. ↑ 20.

[38] E. Corbelli and P. Salucci, *The Extended Rotation Curve and the Dark Matter Halo of M33*, *Mon. Not. Roy. Astron. Soc.* **311** (2000) 441–447, [astro-ph/9909252]. ↑ 20.

[39] G. L. Fogli, E. Lisi, A. Marrone, D. Montanino, A. Palazzo and A. M. Rotunno, *Global analysis of neutrino masses, mixings and phases: entering the era of leptonic CP violation searches*, *Phys. Rev. D* **86** (2012) 013012, [1205.5254]. ↑ 21.

[40] R. N. Mohapatra and A. Y. Smirnov, *Neutrino Mass and New Physics*, *Ann. Rev. Nucl. Part. Sci.* **56** (2006) 569–628, [hep-ph/0603118]. ↑ 21.

[41] L. Canetti, M. Drewes and M. Shaposhnikov, *Matter and Antimatter in the Universe*, *New J. Phys.* **14** (2012) 095012, [1204.4186]. ↑ 21.

[42] HFLAV collaboration, Y. S. Amhis et al., *Averages of b-hadron, c-hadron, and τ-lepton properties as of 2018*, *Eur. Phys. J. C* **81** (2021) 226, [1909.12524]. ↑ 22, 25, 108, 142, 143, 168, 170, 171.

[43] BaBar collaboration, J. P. Lees et al., *Evidence for an excess of $\bar{B} \to D^{(*)}\tau^-\bar{\nu}_\tau$ decays*, *Phys. Rev. Lett.* **109** (2012) 101802, [1205.5442]. ↑ 25.

[44] BaBar collaboration, J. P. Lees et al., *Measurement of an Excess of $\bar{B} \to D^{(*)}\tau^-\bar{\nu}_\tau$ Decays and Implications for Charged Higgs Bosons*, *Phys. Rev. D* **88** (2013) 072012, [1303.0571]. ↑ 25.

[45] Belle collaboration, M. Huschle et al., *Measurement of the branching ratio of $\bar{B} \to D^{(*)}\tau^-\bar{\nu}_\tau$ relative to $\bar{B} \to D^{(*)}\ell^-\bar{\nu}_\ell$ decays with hadronic tagging at Belle*, *Phys. Rev. D* **92** (2015) 072014, [1507.03233]. ↑ 25.

[46] LHCb collaboration, R. Aaij et al., *Measurement of the ratio of branching fractions $\mathcal{B}(\bar{B}^0 \to D^{*+}\tau^-\bar{\nu}_\tau)/\mathcal{B}(\bar{B}^0 \to D^{*+}\mu^-\bar{\nu}_\mu)$*, *Phys. Rev. Lett.* **115** (2015) 111803, [1506.08614]. ↑ 25.

[47] Belle collaboration, S. Hirose et al., *Measurement of the τ lepton polarization and $R(D^*)$ in the decay $\bar{B} \to D^*\tau^-\bar{\nu}_\tau$*, *Phys. Rev. Lett.* **118** (2017) 211801, [1612.00529]. ↑ 25.

[48] LHCb collaboration, R. Aaij et al., *Measurement of the ratio of the $B^0 \to D^{*-}\tau^+\nu_\tau$ and $B^0 \to D^{*-}\mu^+\nu_\mu$ branching fractions using three-prong τ-lepton decays*, *Phys. Rev. Lett.* **120** (2018) 171802, [1708.08856]. ↑ 25.

[49] LHCb collaboration, R. Aaij et al., *Test of Lepton Flavor Universality by the measurement of the $B^0 \to D^{*-}\tau^+\nu_\tau$ branching fraction using three-prong τ decays*, *Phys. Rev. D* **97** (2018) 072013, [1711.02505]. ↑ 25.

[50] Belle collaboration, A. Abdesselam et al., *Measurement of $\mathcal{R}(D)$ and $\mathcal{R}(D^*)$ with a semileptonic tagging method*, 1904.08794. ↑ 25.

[51] D. Bigi and P. Gambino, *Revisiting $B \to D\ell\nu$*, *Phys. Rev. D* **94** (2016) 094008, [1606.08030]. ↑ 25.

[52] S. Fajfer, J. F. Kamenik and I. Nisandzic, *On the $B \to D^* \tau \bar{\nu}_\tau$ Sensitivity to New Physics*, *Phys. Rev. D* **85** (2012) 094025, [1203.2654]. ↑ 25.

[53] LHCb collaboration, R. Aaij et al., *Measurement of the ratio of branching fractions $\mathcal{B}(B_c^+ \to J/\psi \tau^+ \nu_\tau)/\mathcal{B}(B_c^+ \to J/\psi \mu^+ \nu_\mu)$*, *Phys. Rev. Lett.* **120** (2018) 121801, [1711.05623]. ↑ 26, 67.

[54] LATTICE-HPQCD collaboration, J. Harrison, C. T. H. Davies and A. Lytle, *$R(J/\psi)$ and $B_c^- \to J/\psi \ell^- \bar{\nu}_\ell$ Lepton Flavor Universality Violating Observables from Lattice QCD*, *Phys. Rev. Lett.* **125** (2020) 222003, [2007.06956]. ↑ 26, 69.

[55] HPQCD collaboration, J. Harrison, C. T. H. Davies and A. Lytle, *$B_c \to J/\psi$ form factors for the full q^2 range from lattice QCD*, *Phys. Rev. D* **102** (2020) 094518, [2007.06957]. ↑ 26, 31, 69, 133, 136.

[56] S. Descotes-Genon, L. Hofer, J. Matias and J. Virto, *Global analysis of $b \to s\ell\ell$ anomalies*, *JHEP* **06** (2016) 092, [1510.04239]. ↑ 27.

[57] N. Serra, R. Silva Coutinho and D. van Dyk, *Measuring the breaking of lepton flavor universality in $B \to K^* \ell^+ \ell^-$*, *Phys. Rev. D* **95** (2017) 035029, [1610.08761]. ↑ 27.

[58] LHCb collaboration, R. Aaij et al., *Test of lepton universality in beauty-quark decays*, 2103.11769. ↑ 27.

[59] LHCb collaboration, R. Aaij et al., *Test of lepton universality with $B^0 \to K^{*0} \ell^+ \ell^-$ decays*, *JHEP* **08** (2017) 055, [1705.05802]. ↑ 27.

[60] BaBar collaboration, J. P. Lees et al., *Measurement of Branching Fractions and Rate Asymmetries in the Rare Decays $B \to K^{(*)} l^+ l^-$*, *Phys. Rev. D* **86** (2012) 032012, [1204.3933]. ↑ 27.

[61] BELLE collaboration, S. Choudhury et al., *Test of lepton flavor universality and search for lepton flavor violation in $B \to K\ell\ell$ decays*, *JHEP* **03** (2021) 105, [1908.01848]. ↑ 27.

[62] H. Georgi, *An Effective Field Theory for Heavy Quarks at Low-energies*, *Phys. Lett. B* **240** (1990) 447–450. ↑ 28.

[63] E. Eichten and B. R. Hill, *An Effective Field Theory for the Calculation of Matrix Elements Involving Heavy Quarks*, *Phys. Lett. B* **234** (1990) 511–516. ↑ 28.

[64] M. E. Luke and A. V. Manohar, *Reparametrization invariance constraints on heavy particle effective field theories*, *Phys. Lett. B* **286** (1992) 348–354, [hep-ph/9205228]. ↑ 28.

[65] B. A. Thacker and G. P. Lepage, *Heavy quark bound states in lattice QCD*, *Phys. Rev. D* **43** (1991) 196–208. ↑ 29.

[66] G. P. Lepage, L. Magnea, C. Nakhleh, U. Magnea and K. Hornbostel, *Improved nonrelativistic QCD for heavy quark physics*, *Phys. Rev. D* **46** (1992) 4052–4067, [hep-lat/9205007]. ↑ 29.

[67] S. R. Coleman, J. Wess and B. Zumino, *Structure of phenomenological Lagrangians. 1.*, *Phys. Rev.* **177** (1969) 2239–2247. ↑ 29.

[68] C. G. Callan, Jr., S. R. Coleman, J. Wess and B. Zumino, *Structure of phenomenological Lagrangians. 2.*, *Phys. Rev.* **177** (1969) 2247–2250. ↑ 29.

[69] S. Gasiorowicz and D. A. Geffen, *Effective Lagrangians and field algebras with chiral symmetry*, *Rev. Mod. Phys.* **41** (1969) 531–573. ↑ 29.

[70] G. Burdman and J. F. Donoghue, *Union of chiral and heavy quark symmetries*, *Phys. Lett. B* **280** (1992) 287–291. ↑ 30, 158.

[71] M. B. Wise, *Chiral perturbation theory for hadrons containing a heavy quark*, *Phys. Rev. D* **45** (1992) R2188. ↑ 30, 158.

[72] HPQCD, UKQCD collaboration, E. Follana, Q. Mason, C. Davies, K. Hornbostel, G. P. Lepage, J. Shigemitsu et al., *Highly improved staggered quarks on the lattice, with applications to charm physics*, *Phys. Rev. D* **75** (2007) 054502, [hep-lat/0610092]. ↑ 31.

[73] HPQCD collaboration, L. J. Cooper, C. T. H. Davies, J. Harrison, J. Komijani and M. Wingate, *$B_c \to B_{s(d)}$ form factors from lattice QCD*, *Phys. Rev. D* **102** (2020) 014513, [2003.00914]. ↑ 31, 136.

[74] MILC collaboration, J. A. Bailey et al., *$B \to D\ell\nu$ form factors at nonzero recoil and $-V_{cb}-$ from 2+1-flavor lattice QCD*, *Phys. Rev. D* **92** (2015) 034506, [1503.07237]. ↑ 31.

[75] HPQCD collaboration, H. Na, C. M. Bouchard, G. P. Lepage, C. Monahan and J. Shigemitsu, *$B \to Dl\nu$ form factors at nonzero recoil and extraction of $|V_{cb}|$*, *Phys. Rev. D* **92** (2015) 054510, [1505.03925]. ↑ 31.

[76] Fermilab Lattice, MILC collaboration, J. A. Bailey et al., *Update of $|V_{cb}|$ from the $\bar{B} \to D^* \ell \bar{\nu}$ form factor at zero recoil with three-flavor lattice QCD*, *Phys. Rev. D* **89** (2014) 114504, [1403.0635]. ↑ 31.

[77] HPQCD collaboration, J. Harrison, C. Davies and M. Wingate, *Lattice QCD calculation of the $B_{(s)} \to D^*_{(s)} \ell\nu$ form factors at zero recoil and implications for $|V_{cb}|$*, *Phys. Rev. D* **97** (2018) 054502, [1711.11013]. ↑ 31.

[78] Fermilab Lattice, MILC collaboration, J. A. Bailey et al., *$|V_{ub}|$ from $B \to \pi\ell\nu$ decays and (2+1)-flavor lattice QCD*, *Phys. Rev. D* **92** (2015) 014024, [1503.07839]. ↑ 31, 107, 154, 156, 160, 161, 166, 170.

[79] Fermilab Lattice, MILC collaboration, J. A. Bailey et al., *$B \to \pi\ell\ell$ form factors for new-physics searches from lattice QCD*, *Phys. Rev. Lett.* **115** (2015) 152002, [1507.01618]. ↑ 31, 154, 156, 160, 161, 166, 170.

[80] J. M. Flynn, T. Izubuchi, T. Kawanai, C. Lehner, A. Soni, R. S. Van de Water et al., *$B \to \pi\ell\nu$ and $B_s \to K\ell\nu$ form factors and $|V_{ub}|$ from 2+1-flavor lattice QCD with domain-wall light quarks and relativistic heavy quarks*, *Phys. Rev. D* **91** (2015) 074510, [1501.05373]. ↑ 31, 107, 154, 156, 160, 161, 166, 170, 172, 174.

[81] M. A. Shifman, A. I. Vainshtein and V. I. Zakharov, *QCD and Resonance Physics. Theoretical Foundations*, *Nucl. Phys. B* **147** (1979) 385–447. ↑ 32, 108.

[82] M. A. Shifman, A. I. Vainshtein and V. I. Zakharov, *QCD and Resonance Physics: Applications*, *Nucl. Phys. B* **147** (1979) 448–518. ↑ 32, 108.

[83] V. A. Novikov, M. A. Shifman, A. I. Vainshtein and V. I. Zakharov, *Calculations in External Fields in Quantum Chromodynamics. Technical Review*, *Fortsch. Phys.* **32** (1984) 585. ↑ 32, 58, 108.

[84] K. G. Wilson, *Nonlagrangian models of current algebra*, *Phys. Rev.* **179** (1969) 1499–1512. ↑ 32.

[85] C. Becchi, S. Narison, E. de Rafael and F. J. Yndurain, *Light Quark Masses in Quantum Chromodynamics and Chiral Symmetry Breaking*, *Z. Phys. C* **8** (1981) 335. ↑ 32.

[86] S. Narison, *Heavy Quark Mass in the MS Scheme: Revisited*, *Phys. Lett. B* **197** (1987) 405–408. ↑ 32.

[87] L. J. Reinders, H. R. Rubinstein and S. Yazaki, *Masses of Lowest Lying Heavy Mesons in QCD*, *Phys. Lett. B* **95** (1980) 103–106. ↑ 32.

[88] B. L. Ioffe, *Calculation of Baryon Masses in Quantum Chromodynamics*, *Nucl. Phys. B* **188** (1981) 317–341. ↑ 32.

[89] E. Bagan, M. Chabab, H. G. Dosch and S. Narison, *Spectra of heavy baryons from QCD spectral sum rules*, *Phys. Lett. B* **287** (1992) 176–178. ↑ 32.

[90] V. M. Braun and I. E. Filyanov, *QCD Sum Rules in Exclusive Kinematics and Pion Wave Function*, *Z. Phys. C* **44** (1989) 157. ↑ 33.

[91] I. I. Balitsky, V. M. Braun and A. V. Kolesnichenko, *Radiative Decay $\sigma^+ \to p\gamma$ in Quantum Chromodynamics*, *Nucl. Phys. B* **312** (1989) 509–550. ↑ 33, 34.

[92] V. L. Chernyak and I. R. Zhitnitsky, *B meson exclusive decays into baryons*, *Nucl. Phys. B* **345** (1990) 137–172. ↑ 33.

[93] P. Ball, $B \to \pi$ *and* $B \to K$ *transitions from QCD sum rules on the light cone*, *JHEP* **09** (1998) 005, [hep-ph/9802394]. ↑ 33.

[94] P. Ball and R. Zwicky, $B_{d,s} \to \rho, \omega, K^*, \phi$ *decay form-factors from light-cone sum rules revisited*, *Phys. Rev. D* **71** (2005) 014029, [hep-ph/0412079]. ↑ 33, 69, 77, 135.

[95] G. Duplancic, A. Khodjamirian, T. Mannel, B. Melic and N. Offen, *Light-cone sum rules for* $B \to \pi$ *form factors revisited*, *JHEP* **04** (2008) 014, [0801.1796]. ↑ 33, 69, 107, 144, 145, 166, 170.

[96] G. Duplancic and B. Melic, *B, B(s) —> K form factors: An Update of light-cone sum rule results*, *Phys. Rev. D* **78** (2008) 054015, [0805.4170]. ↑ 33, 69, 144.

[97] G. Duplancic and B. Melic, *Form factors of* $B, B_s \to \eta^{(\prime)}$ *and* $D, D_s \to \eta^{(\prime)}$ *transitions from QCD light-cone sum rules*, *JHEP* **11** (2015) 138, [1508.05287]. ↑ 33, 69.

[98] A. Ali, V. M. Braun and H. Simma, *Exclusive radiative B decays in the light cone QCD sum rule approach*, *Z. Phys. C* **63** (1994) 437–454, [hep-ph/9401277]. ↑ 34.

[99] P. Ball, V. M. Braun and H. G. Dosch, *Form-factors of semileptonic D decays from QCD sum rules*, *Phys. Rev. D* **44** (1991) 3567–3581. ↑ 34, 46, 69, 113.

[100] T. M. Aliev, A. Ozpineci and M. Savci, *Rare* $B \to K^* \ell^+ \ell^-$ *decay in light cone QCD*, *Phys. Rev. D* **56** (1997) 4260–4267, [hep-ph/9612480]. ↑ 34.

[101] M. A. Ivanov, V. E. Lyubovitskij, J. G. Korner and P. Kroll, *Heavy baryon transitions in a relativistic three quark model*, *Phys. Rev. D* **56** (1997) 348–364, [hep-ph/9612463]. ↑ 34.

[102] M. A. Ivanov, J. G. Korner and P. Santorelli, *Exclusive semileptonic and nonleptonic decays of the B_c meson*, *Phys. Rev. D* **73** (2006) 054024, [hep-ph/0602050]. ↑ 34, 67, 68, 90, 125, 126.

[103] D. Ebert, R. N. Faustov and V. O. Galkin, *Properties of heavy quarkonia and B_c mesons in the relativistic quark model*, *Phys. Rev. D* **67** (2003) 014027, [hep-ph/0210381]. ↑ 34.

[104] D. Ebert, R. N. Faustov and V. O. Galkin, *Weak decays of the B_c meson to charmonium and D mesons in the relativistic quark model*, *Phys. Rev. D* **68** (2003) 094020, [hep-ph/0306306]. ↑ 34, 67, 68, 78, 90, 115, 125, 138.

[105] M. A. Nobes and R. M. Woloshyn, *Decays of the B_c meson in a relativistic quark meson model*, *J. Phys. G* **26** (2000) 1079–1094, [hep-ph/0005056]. ↑ 34, 67, 68, 78, 90, 115, 125, 138.

[106] E. E. Salpeter and H. A. Bethe, *A Relativistic equation for bound state problems*, *Phys. Rev.* **84** (1951) 1232–1242. ↑ 34.

[107] Y. Nambu, *Force potentials in quantum field theory*, *Prog. Theor. Phys.* **5** (1950) 614–633. ↑ 34.

[108] I. C. Cloet and C. D. Roberts, *Explanation and Prediction of Observables using Continuum Strong QCD*, *Prog. Part. Nucl. Phys.* **77** (2014) 1–69, [1310.2651]. ↑ 34.

[109] G. Eichmann, H. Sanchis-Alepuz, R. Williams, R. Alkofer and C. S. Fischer, *Baryons as relativistic three-quark bound states*, *Prog. Part. Nucl. Phys.* **91** (2016) 1–100, [1606.09602]. ↑ 34.

[110] M. Q. Huber, *Nonperturbative properties of Yang–Mills theories*, *Phys. Rept.* **879** (2020) 1–92, [1808.05227]. ↑ 34.

[111] H. Sanchis-Alepuz and R. Williams, *Recent developments in bound-state calculations using the Dyson–Schwinger and Bethe–Salpeter equations*, *Comput. Phys. Commun.* **232** (2018) 1–21, [1710.04903]. ↑ 34.

[112] P. Colangelo and A. Khodjamirian, *QCD sum rules, a modern perspective*, hep-ph/0010175. ↑ 35.

[113] R. Zwicky, *A brief Introduction to Dispersion Relations and Analyticity*, in *Quantum Field Theory at the Limits: from Strong Fields to Heavy Quarks*, 10, 2016, 1610.06090, DOI. ↑ 42.

[114] M. Dimou, J. Lyon and R. Zwicky, *Exclusive Chromomagnetism in heavy-to-light FCNCs*, *Phys. Rev. D* **87** (2013) 074008, [1212.2242]. ↑ 42.

[115] V. M. Braun, *Light cone sum rules*, in *4th International Workshop on Progress in Heavy Quark Physics*, 9, 1997, hep-ph/9801222. ↑ 46.

[116] V. A. Nesterenko and A. V. Radyushkin, *Pion Form-factor and QCD Sum Rules*, *JETP Lett.* **35** (1982) 488–492. ↑ 46.

[117] V. A. Nesterenko and A. V. Radyushkin, *Sum Rules and Pion Form-Factor in QCD*, *Phys. Lett. B* **115** (1982) 410. ↑ 46.

[118] D. J. Gross and S. B. Treiman, *Light cone structure of current commutators in the gluon quark model*, *Phys. Rev. D* **4** (1971) 1059–1072. ↑ 46.

[119] P. Ball, V. M. Braun and A. Lenz, *Higher-twist distribution amplitudes of the K meson in QCD*, *JHEP* **05** (2006) 004, [hep-ph/0603063]. ↑ 47, 75, 146, 147, 199.

[120] P. Ball, V. M. Braun, Y. Koike and K. Tanaka, *Higher twist distribution amplitudes of vector mesons in QCD: Formalism and twist - three distributions*, *Nucl. Phys. B* **529** (1998) 323–382, [hep-ph/9802299]. ↑ 49, 76.

[121] A. Bharucha, D. M. Straub and R. Zwicky, $B \to V\ell^+\ell^-$ *in the Standard Model from light-cone sum rules*, *JHEP* **08** (2016) 098, [1503.05534]. ↑ 49, 73.

[122] A. V. Rusov, *Higher-twist effects in light-cone sum rule for the* $B \to \pi$ *form factor*, *Eur. Phys. J. C* **77** (2017) 442, [1705.01929]. ↑ 49, 144, 145.

[123] M. Wirbel, B. Stech and M. Bauer, *Exclusive Semileptonic Decays of Heavy Mesons*, *Z. Phys. C* **29** (1985) 637. ↑ 52.

[124] N. N. Meiman, *The causality principle and the asymptotic behavior of the scattering amplitude*, *Zh. Eksp. Teor. Fiz.* **47** (1964) 1966–1983. ↑ 61.

[125] C. Bourrely, B. Machet and E. de Rafael, *Semileptonic Decays of Pseudoscalar Particles ($M \to M' \ell \nu_\ell$) and Short Distance Behavior of Quantum Chromodynamics*, *Nucl. Phys. B* **189** (1981) 157–181. ↑ 61.

[126] C. G. Boyd, B. Grinstein and R. F. Lebed, *Constraints on form-factors for exclusive semileptonic heavy to light meson decays*, *Phys. Rev. Lett.* **74** (1995) 4603–4606, [hep-ph/9412324]. ↑ 61.

[127] C. G. Boyd, B. Grinstein and R. F. Lebed, *Model independent determinations of $\bar{B} \to D \ell \bar{\nu}, D^* \ell \bar{\nu}$ form-factors*, *Nucl. Phys. B* **461** (1996) 493–511, [hep-ph/9508211]. ↑ 64, 79, 115.

[128] C. G. Boyd, B. Grinstein and R. F. Lebed, *Precision corrections to dispersive bounds on form-factors*, *Phys. Rev. D* **56** (1997) 6895–6911, [hep-ph/9705252]. ↑ 64, 115, 117.

[129] C. Bourrely, I. Caprini and L. Lellouch, *Model-independent description of $B \to \pi \ell \nu u$ decays and a determination of $|V_{ub}|$*, *Phys. Rev. D* **79** (2009) 013008, [0807.2722]. ↑ 64, 115, 154, 156.

[130] T. Becher and R. J. Hill, *Comment on form-factor shape and extraction of $|V_{ub}|$ from $B \to \pi \ell \nu$*, *Phys. Lett. B* **633** (2006) 61–69, [hep-ph/0509090]. ↑ 66, 168.

[131] W.-F. Wang, Y.-Y. Fan and Z.-J. Xiao, *Semileptonic decays $B_c \to (\eta_c, J/\Psi) l \nu$ in the perturbative QCD approach*, *Chin. Phys. C* **37** (2013) 093102, [1212.5903]. ↑ 67, 68, 78, 90.

[132] V. V. Kiselev, *Exclusive decays and lifetime of B_c meson in QCD sum rules*, hep-ph/0211021. ↑ 67, 68, 78, 90, 115, 125, 126.

[133] T. Huang and F. Zuo, *Semileptonic B_c decays and charmonium distribution amplitude*, *Eur. Phys. J. C* **51** (2007) 833–839, [hep-ph/0702147]. ↑ 67, 68, 78, 90, 109, 115, 125, 126.

[134] D. Scora and N. Isgur, *Semileptonic meson decays in the quark model: An update*, *Phys. Rev. D* **52** (1995) 2783–2812, [hep-ph/9503486]. ↑ 67, 68, 90, 125.

[135] A. Abd El-Hady, J. H. Munoz and J. P. Vary, *Semileptonic and nonleptonic B(c) decays*, *Phys. Rev. D* **62** (2000) 014019, [hep-ph/9909406]. ↑ 67, 68, 90, 125.

[136] E. Hernandez, J. Nieves and J. M. Verde-Velasco, *Study of exclusive semileptonic and non-leptonic decays of B_c - in a nonrelativistic quark model*, *Phys. Rev. D* **74** (2006) 074008, [hep-ph/0607150]. ↑ 67, 68.

[137] C.-F. Qiao and R.-L. Zhu, *Estimation of semileptonic decays of B_c meson to S-wave charmonia with nonrelativistic QCD*, *Phys. Rev. D* **87** (2013) 014009, [1208.5916]. ↑ 67, 68.

[138] W. Wang, Y.-L. Shen and C.-D. Lu, *Covariant Light-Front Approach for B_c transition form factors*, *Phys. Rev. D* **79** (2009) 054012, [0811.3748]. ↑ 67, 68, 78, 90, 115, 119, 120, 125, 129, 135, 138.

[139] A. Y. Anisimov, I. M. Narodetsky, C. Semay and B. Silvestre-Brac, *The B_c meson lifetime in the light front constituent quark model*, *Phys. Lett. B* **452** (1999) 129–136, [hep-ph/9812514]. ↑ 67, 68.

[140] R. Watanabe, *New Physics effect on $B_c \to J/\psi\tau\bar{\nu}$ in relation to the $R_{D^{(*)}}$ anomaly*, *Phys. Lett. B* **776** (2018) 5–9, [1709.08644]. ↑ 69.

[141] R. Dutta and A. Bhol, *$B_c \to (J/\psi, \eta_c)\tau\nu$ semileptonic decays within the standard model and beyond*, *Phys. Rev. D* **96** (2017) 076001, [1701.08598]. ↑ 69.

[142] T. D. Cohen, H. Lamm and R. F. Lebed, *Model-independent bounds on $R(J/\psi)$*, *JHEP* **09** (2018) 168, [1807.02730]. ↑ 69, 83, 84, 90, 116, 117.

[143] A. Berns and H. Lamm, *Model-Independent Prediction of $R(\eta_c)$*, *JHEP* **12** (2018) 114, [1808.07360]. ↑ 69, 83, 84, 90.

[144] C. W. Murphy and A. Soni, *Model-Independent Determination of $B_c^+ \to \eta_c \ell^+ \nu$ Form Factors*, *Phys. Rev. D* **98** (2018) 094026, [1808.05932]. ↑ 69, 83, 84, 90.

[145] C.-T. Tran, M. A. Ivanov, J. G. Körner and P. Santorelli, *Implications of new physics in the decays $B_c \to (J/\psi, \eta_c)\tau\nu$*, *Phys. Rev. D* **97** (2018) 054014, [1801.06927]. ↑ 69, 78, 90.

[146] A. Khodjamirian, C. Klein, T. Mannel and Y. M. Wang, *Form Factors and Strong Couplings of Heavy Baryons from QCD Light-Cone Sum Rules*, *JHEP* **09** (2011) 106, [1108.2971]. ↑ 69.

[147] G. Bell, T. Feldmann, Y.-M. Wang and M. W. Y. Yip, *Light-Cone Distribution Amplitudes for Heavy-Quark Hadrons*, *JHEP* **11** (2013) 191, [1308.6114]. ↑ 69.

[148] HPQCD collaboration, B. Colquhoun, C. Davies, J. Koponen, A. Lytle and C. McNeile, *B_c decays from highly improved staggered quarks and NRQCD*, *PoS* **LATTICE2016** (2016) 281, [1611.01987]. ↑ 69, 78, 80, 133, 135.

[149] B. Chauhan and B. Kindra, *Invoking Chiral Vector Leptoquark to explain LFU violation in B Decays*, 1709.09989. ↑ 69.

[150] X.-G. He and G. Valencia, *Lepton universality violation and right-handed currents in $b \to c\tau\nu$*, *Phys. Lett. B* **779** (2018) 52–57, [1711.09525]. ↑ 69.

[151] J. Zhu, B. Wei, J.-H. Sheng, R.-M. Wang, Y. Gao and G.-R. Lu, *Probing the R-parity violating supersymmetric effects in $B_c \to J/\psi \ell^- \bar{\nu}_\ell, \eta_c \ell^- \bar{\nu}_\ell$ and $\Lambda_b \to \Lambda_c \ell^- \bar{\nu}_\ell$ decays*, *Nucl. Phys. B* **934** (2018) 380–395, [1801.00917]. ↑ 69.

[152] A. Biswas, D. K. Ghosh, S. K. Patra and A. Shaw, *$b \to c\ell\nu$ anomalies in light of extended scalar sectors*, *Int. J. Mod. Phys. A* **34** (2019) 1950112, [1801.03375]. ↑ 69.

[153] R. Dutta, *Exploring R_D, R_{D^*} and $R_{J/\Psi}$ anomalies*, 1710.00351. ↑ 69.

[154] Z.-R. Huang, Y. Li, C.-D. Lu, M. A. Paracha and C. Wang, *Footprints of New Physics in $b \to c\tau\nu$ Transitions*, *Phys. Rev. D* **98** (2018) 095018, [1808.03565]. ↑ 69.

[155] Y. Li and C.-D. Lü, *Recent Anomalies in B Physics*, *Sci. Bull.* **63** (2018) 267–269, [1808.02990]. ↑ 69.

[156] R. Alonso, A. Kobach and J. Martin Camalich, *New physics in the kinematic distributions of $\bar{B} \to D^{(*)}\tau^-(\to \ell^-\bar{\nu}_\ell\nu_\tau)\bar{\nu}_\tau$*, *Phys. Rev. D* **94** (2016) 094021, [1602.07671]. ↑ 70.

[157] A. Greljo, J. Martin Camalich and J. D. Ruiz-Álvarez, *Mono-τ Signatures at the LHC Constrain Explanations of B-decay Anomalies*, *Phys. Rev. Lett.* **122** (2019) 131803, [1811.07920]. ↑ 70.

[158] M. Blanke, A. Crivellin, S. de Boer, T. Kitahara, M. Moscati, U. Nierste et al., *Impact of polarization observables and $B_c \to \tau\nu$ on new physics explanations of the $b \to c\tau\nu$ anomaly*, *Phys. Rev. D* **99** (2019) 075006, [1811.09603]. ↑ 70, 85, 87, 92, 103, 106.

[159] F. Feruglio, P. Paradisi and O. Sumensari, *Implications of scalar and tensor explanations of $R_{D^{(*)}}$*, *JHEP* **11** (2018) 191, [1806.10155]. ↑ 70.

[160] A. K. Alok, D. Kumar, J. Kumar, S. Kumbhakar and S. U. Sankar, *New physics solutions for R_D and R_{D^*}*, *JHEP* **09** (2018) 152, [1710.04127]. ↑ 70.

[161] A. K. Alok, D. Kumar, S. Kumbhakar and S. Uma Sankar, *Resolution of R_D/R_{D^*} puzzle*, *Phys. Lett. B* **784** (2018) 16–20, [1804.08078]. ↑ 70.

[162] V. L. Chernyak and A. R. Zhitnitsky, *Asymptotic Behavior of Exclusive Processes in QCD*, *Phys. Rept.* **112** (1984) 173. ↑ 73.

[163] C. McNeile, C. T. H. Davies, E. Follana, K. Hornbostel and G. P. Lepage, *High-Precision c and b Masses, and QCD Coupling from Current-Current*

Correlators in Lattice and Continuum QCD, *Phys. Rev. D* **82** (2010) 034512, [1004.4285]. ↑ 74.

[164] C. McNeile, C. T. H. Davies, E. Follana, K. Hornbostel and G. P. Lepage, *Heavy meson masses and decay constants from relativistic heavy quarks in full lattice QCD*, *Phys. Rev. D* **86** (2012) 074503, [1207.0994]. ↑ 74, 112.

[165] G. C. Donald, C. T. H. Davies, R. J. Dowdall, E. Follana, K. Hornbostel, J. Koponen et al., *Precision tests of the J/ψ from full lattice QCD: mass, leptonic width and radiative decay rate to η_c*, *Phys. Rev. D* **86** (2012) 094501, [1208.2855]. ↑ 74, 134.

[166] C. T. H. Davies, C. McNeile, E. Follana, G. P. Lepage, H. Na and J. Shigemitsu, *Update: Precision D_s decay constant from full lattice QCD using very fine lattices*, *Phys. Rev. D* **82** (2010) 114504, [1008.4018]. ↑ 74.

[167] D. Bečirević, G. Duplančić, B. Klajn, B. Melić and F. Sanfilippo, *Lattice QCD and QCD sum rule determination of the decay constants of η_c, J/ψ and h_c states*, *Nucl. Phys. B* **883** (2014) 306–327, [1312.2858]. ↑ 74.

[168] G. T. Bodwin, E. Braaten and G. P. Lepage, *Rigorous QCD analysis of inclusive annihilation and production of heavy quarkonium*, *Phys. Rev. D* **51** (1995) 1125–1171, [hep-ph/9407339]. ↑ 74.

[169] V. V. Braguta, A. K. Likhoded and A. V. Luchinsky, *The Study of leading twist light cone wave function of η_c meson*, *Phys. Lett. B* **646** (2007) 80–90, [hep-ph/0611021]. ↑ 74, 75.

[170] V. V. Braguta, *The study of leading twist light cone wave functions of J/ψ meson*, *Phys. Rev. D* **75** (2007) 094016, [hep-ph/0701234]. ↑ 74, 75.

[171] Y. Grossman, M. König and M. Neubert, *Exclusive Radiative Decays of W and Z Bosons in QCD Factorization*, *JHEP* **04** (2015) 101, [1501.06569]. ↑ 75.

[172] G. T. Bodwin, H. S. Chung, D. Kang, J. Lee and C. Yu, *Improved determination of color-singlet nonrelativistic QCD matrix elements for S-wave charmonium*, *Phys. Rev. D* **77** (2008) 094017, [0710.0994]. ↑ 75.

[173] X.-P. Wang and D. Yang, *The leading twist light-cone distribution amplitudes for the S-wave and P-wave quarkonia and their applications in single quarkonium exclusive productions*, *JHEP* **06** (2014) 121, [1401.0122]. ↑ 75.

[174] W. Wang, J. Xu, D. Yang and S. Zhao, *Relativistic corrections to light-cone distribution amplitudes of S-wave B_c mesons and heavy quarkonia*, *JHEP* **12** (2017) 012, [1706.06241]. ↑ 75.

[175] A. Czarnecki and K. Melnikov, *Two loop QCD corrections to the heavy quark pair production cross-section in e^+e^- annihilation near the threshold*, *Phys. Rev. Lett.* **80** (1998) 2531–2534, [hep-ph/9712222]. ↑ 75.

[176] M. Beneke, A. Signer and V. A. Smirnov, *Two loop correction to the leptonic decay of quarkonium*, *Phys. Rev. Lett.* **80** (1998) 2535–2538, [hep-ph/9712302]. ↑ 75.

[177] M. Beneke, Y. Kiyo, P. Marquard, A. Penin, J. Piclum, D. Seidel et al., *Leptonic decay of the $\Upsilon(1S)$ meson at third order in QCD*, *Phys. Rev. Lett.* **112** (2014) 151801, [1401.3005]. ↑ 75.

[178] H. S. Chung, J. Lee and C. Yu, *NRQCD matrix elements for S-wave bottomonia and $\Gamma[\eta_b(nS) \to \gamma\gamma]$ with relativistic corrections*, *Phys. Lett. B* **697** (2011) 48–51, [1011.1554]. ↑ 75.

[179] G. T. Bodwin, H. S. Chung, J.-H. Ee, J. Lee and F. Petriello, *Relativistic corrections to Higgs boson decays to quarkonia*, *Phys. Rev. D* **90** (2014) 113010, [1407.6695]. ↑ 75.

[180] P. Ball and V. M. Braun, *Handbook of higher twist distribution amplitudes of vector mesons in QCD*, in *3rd Workshop on Continuous Advances in QCD (QCD 98)*, 4, 1998, hep-ph/9808229. ↑ 76.

[181] M. Beneke and T. Feldmann, *Symmetry breaking corrections to heavy to light B meson form-factors at large recoil*, *Nucl. Phys. B* **592** (2001) 3–34, [hep-ph/0008255]. ↑ 76, 153, 159.

[182] P. Ball, V. M. Braun and A. Lenz, *Twist-4 distribution amplitudes of the K* and phi mesons in QCD*, *JHEP* **08** (2007) 090, [0707.1201]. ↑ 76.

[183] D. Bećirević, D. Leljak and B. Melić, $B_c \to J/\psi$ *form factors and lepton flavor universality violation in* $R(J/\psi)$, https://indico.cern.ch/event/685400/contributions/2947713/attachments/1627828/2592987/QCDgrips2018.pdf, (Paris, France), 2018. ↑ 78, 113.

[184] A. Issadykov, M. A. Ivanov and G. Nurbakova, *Semileptonic decays of* B_c *mesons into charmonium states*, *EPJ Web Conf.* **158** (2017) 03002, [1907.13210]. ↑ 78, 90, 115, 125, 126.

[185] ATLAS collaboration, G. Aad et al., *Observation of an Excited* $B_c^{\pm}$ *Meson State with the ATLAS Detector*, *Phys. Rev. Lett.* **113** (2014) 212004, [1407.1032]. ↑ 79.

[186] LHCb collaboration, R. Aaij et al., *Observation of* $B_c^+ \to J/\psi D^{(*)} K^{(*)}$ *decays*, *Phys. Rev. D* **95** (2017) 032005, [1612.07421]. ↑ 79.

[187] E. J. Eichten and C. Quigg, *Mesons with beauty and charm: Spectroscopy*, *Phys. Rev. D* **49** (1994) 5845–5856, [hep-ph/9402210]. ↑ 79, 135.

[188] S. Godfrey, *Spectroscopy of* B_c *mesons in the relativized quark model*, *Phys. Rev. D* **70** (2004) 054017, [hep-ph/0406228]. ↑ 79.

[189] E. E. Jenkins, M. E. Luke, A. V. Manohar and M. J. Savage, *Semileptonic* B_c *decay and heavy quark spin symmetry*, *Nucl. Phys. B* **390** (1993) 463–473, [hep-ph/9204238]. ↑ 81, 137, 141.

[190] V. V. Kiselev, A. K. Likhoded and A. I. Onishchenko, *Semileptonic* B_c *meson decays in sum rules of QCD and NRQCD*, *Nucl. Phys. B* **569** (2000) 473–504, [hep-ph/9905359]. ↑ 81, 82, 112.

[191] P. Colangelo and F. De Fazio, *Using heavy quark spin symmetry in semileptonic B_c decays*, *Phys. Rev. D* **61** (2000) 034012, [hep-ph/9909423]. ↑ 81, 82, 108, 138.

[192] Particle Data Group collaboration, M. Tanabashi et al., *Review of Particle Physics*, *Phys. Rev. D* **98** (2018) 030001. ↑ 85, 90.

[193] M. Beneke and G. Buchalla, *The B_c Meson Lifetime*, *Phys. Rev. D* **53** (1996) 4991–5000, [hep-ph/9601249]. ↑ 85.

[194] R. Alonso, B. Grinstein and J. Martin Camalich, *Lepton universality violation and lepton flavor conservation in B-meson decays*, *JHEP* **10** (2015) 184, [1505.05164]. ↑ 86.

[195] M. Tanaka and R. Watanabe, *New physics in the weak interaction of $\bar{B} \to D^{(*)}\tau\bar{\nu}$*, *Phys. Rev. D* **87** (2013) 034028, [1212.1878]. ↑ 86.

[196] X.-G. He and G. Valencia, *B decays with τ leptons in nonuniversal left-right models*, *Phys. Rev. D* **87** (2013) 014014, [1211.0348]. ↑ 86.

[197] J. Kalinowski, *Semileptonic Decays of B Mesons into $\tau\nu_\tau$ in a Two Higgs Doublet Model*, *Phys. Lett. B* **245** (1990) 201–206. ↑ 86.

[198] N. Kosnik, *Model independent constraints on leptoquarks from $b \to s\ell^+\ell^-$ processes*, *Phys. Rev. D* **86** (2012) 055004, [1206.2970]. ↑ 86.

[199] A. Crivellin, C. Greub and A. Kokulu, *Explaining $B \to D\tau\nu$, $B \to D^*\tau\nu$ and $B \to \tau\nu$ in a 2HDM of type III*, *Phys. Rev. D* **86** (2012) 054014, [1206.2634]. ↑ 86.

[200] D. Bečirević, S. Fajfer, N. Košnik and O. Sumensari, *Leptoquark model to explain the B-physics anomalies, R_K and R_D*, *Phys. Rev. D* **94** (2016) 115021, [1608.08501]. ↑ 86.

[201] D. Bečirević, I. Doršner, S. Fajfer, N. Košnik, D. A. Faroughy and O. Sumensari, *Scalar leptoquarks from grand unified theories to accommodate*

the B-physics anomalies, *Phys. Rev. D* **98** (2018) 055003, [1806.05689]. ↑ 87.

[202] A. Faessler, T. Gutsche, M. A. Ivanov, J. G. Korner and V. E. Lyubovitskij, *The Exclusive rare decays $B \to K(K^*)\, \bar{\ell}\ell$ and $B_c \to D(D^*)\, \bar{\ell}\ell$ in a relativistic quark model*, *Eur. Phys. J. direct* **4** (2002) 18, [hep-ph/0205287]. ↑ 94.

[203] T. Gutsche, M. A. Ivanov, J. G. Körner, V. E. Lyubovitskij and P. Santorelli, *Polarization effects in the cascade decay $\Lambda_b \to \Lambda(\to p\pi^-) + J/\psi(\to \ell^+\ell^-)$ in the covariant confined quark model*, *Phys. Rev. D* **88** (2013) 114018, [1309.7879]. ↑ 94.

[204] T. Gutsche, M. A. Ivanov, J. G. Körner, V. E. Lyubovitskij, P. Santorelli and N. Habyl, *Semileptonic decay $\Lambda_b \to \Lambda_c + \tau^- + \bar{\nu_\tau}$ in the covariant confined quark model*, *Phys. Rev. D* **91** (2015) 074001, [1502.04864]. ↑ 94.

[205] P. Ball and R. Zwicky, *New results on $B \to \pi, K, \eta$ decay formfactors from light-cone sum rules*, *Phys. Rev. D* **71** (2005) 014015, [hep-ph/0406232]. ↑ 107, 144.

[206] I. Sentitemsu Imsong, A. Khodjamirian, T. Mannel and D. van Dyk, *Extrapolation and unitarity bounds for the $B \to \pi$ form factor*, *JHEP* **02** (2015) 126, [1409.7816]. ↑ 107, 145, 148, 149, 150, 151, 152, 166, 170.

[207] S. Gonzàlez-Solís and P. Masjuan, *Study of $B \to \pi\ell\nu_\ell$ and $B^+ \to \eta^{(\prime)}\ell^+\nu_\ell$ decays and determination of $|V_{ub}|$*, *Phys. Rev. D* **98** (2018) 034027, [1805.11262]. ↑ 107, 166, 170.

[208] A. Biswas, S. Nandi, S. K. Patra and I. Ray, *A closer look at the extraction of $|V_{ub}|$ from $B \to \pi l\nu$*, 2103.01809. ↑ 107.

[209] LHCb collaboration, R. Aaij et al., *Determination of the quark coupling strength $|V_{ub}|$ using baryonic decays*, *Nature Phys.* **11** (2015) 743–747, [1504.01568]. ↑ 107, 134.

[210] W. Detmold, C. Lehner and S. Meinel, $\Lambda_b \to p\ell^-\bar{\nu}_\ell$ *and* $\Lambda_b \to \Lambda_c\ell^-\bar{\nu}_\ell$ *form factors from lattice QCD with relativistic heavy quarks*, *Phys. Rev. D* **92** (2015) 034503, [1503.01421]. ↑ 108.

[211] A. Cerri et al., *Report from Working Group 4: Opportunities in Flavour Physics at the HL-LHC and HE-LHC*, *CERN Yellow Rep. Monogr.* **7** (2019) 867–1158, [1812.07638]. ↑ 108.

[212] LHCb collaboration, R. Aaij et al., *Physics case for an LHCb Upgrade II - Opportunities in flavour physics, and beyond, in the HL-LHC era*, 1808.08865. ↑ 108, 134, 140.

[213] A. I. Vainshtein, M. B. Voloshin, V. I. Zakharov, V. A. Novikov, L. B. Okun and M. A. Shifman, *Sum Rules for Light Quarks in Quantum Chromodynamics*, *Sov. J. Nucl. Phys.* **27** (1978) 274. ↑ 108, 186.

[214] S. J. Brodsky, T. Huang and G. P. Lepage, *Hadronic wave functions and high momentum transfer interactions in quantum chromodynamics*, *Conf. Proc. C* **810816** (1981) 143–199. ↑ 109.

[215] S. V. Mikhailov and A. V. Radyushkin, *Quark Condensate Nonlocality and Pion Wave Function in QCD: General Formalism*, *Yad. Fiz.* **49** (1988) 794. ↑ 110.

[216] A. V. Radyushkin, *Pion wave function from QCD sum rules with nonlocal condensates*, in *Workshop on Continuous Advances in QCD*, 2, 1994, hep-ph/9406237. ↑ 110.

[217] V. M. Braun, P. Gornicki, L. Mankiewicz and A. Schafer, *Gluon form-factor of the proton from QCD sum rules*, *Phys. Lett. B* **302** (1993) 291–298. ↑ 111.

[218] S. V. Mikhailov and A. V. Radyushkin, *The Pion wave function and QCD sum rules with nonlocal condensates*, *Phys. Rev. D* **45** (1992) 1754–1759. ↑ 111.

[219] V. Braun, P. Gornicki and L. Mankiewicz, *Ioffe - time distributions instead of parton momentum distributions in description of deep inelastic scattering*, *Phys. Rev. D* **51** (1995) 6036–6051, [hep-ph/9410318]. ↑ 111.

[220] V. M. Braun, D. Y. Ivanov and G. P. Korchemsky, *The B meson distribution amplitude in QCD*, *Phys. Rev. D* **69** (2004) 034014, [hep-ph/0309330]. ↑ 111.

[221] P. Gelhausen, A. Khodjamirian, A. A. Pivovarov and D. Rosenthal, *Decay constants of heavy-light vector mesons from QCD sum rules*, *Phys. Rev. D* **88** (2013) 014015, [1305.5432]. ↑ 112, 146.

[222] HPQCD collaboration, B. Colquhoun, C. T. H. Davies, R. J. Dowdall, J. Kettle, J. Koponen, G. P. Lepage et al., *B-meson decay constants: a more complete picture from full lattice QCD*, *Phys. Rev. D* **91** (2015) 114509, [1503.05762]. ↑ 112, 134.

[223] Fermilab Lattice, MILC collaboration, A. Bazavov et al., *Charmed and Light Pseudoscalar Meson Decay Constants from Four-Flavor Lattice QCD with Physical Light Quarks*, *Phys. Rev. D* **90** (2014) 074509, [1407.3772]. ↑ 112.

[224] N. Carrasco et al., *Leptonic decay constants f_K, f_D, and f_{D_s} with $N_f = 2 + 1 + 1$ twisted-mass lattice QCD*, *Phys. Rev. D* **91** (2015) 054507, [1411.7908]. ↑ 112.

[225] D. Becirevic, V. Lubicz, F. Sanfilippo, S. Simula and C. Tarantino, *D-meson decay constants and a check of factorization in non-leptonic B-decays*, *JHEP* **02** (2012) 042, [1201.4039]. ↑ 112.

[226] ETM collaboration, V. Lubicz, A. Melis and S. Simula, *Masses and decay constants of $D^*_{(s)}$ and $B^*_{(s)}$ mesons with $N_f = 2 + 1 + 1$ twisted mass fermions*, *Phys. Rev. D* **96** (2017) 034524, [1707.04529]. ↑ 112, 158.

[227] M. Beneke, *A Quark mass definition adequate for threshold problems*, *Phys. Lett. B* **434** (1998) 115–125, [hep-ph/9804241]. ↑ 113.

[228] A. H. Hoang, *Bottom quark mass from Upsilon mesons*, *Phys. Rev. D* **59** (1999) 014039, [hep-ph/9803454]. ↑ 113.

[229] I. I. Y. Bigi, M. A. Shifman, N. Uraltsev and A. I. Vainshtein, *High power n of m_b in beauty widths and $n = 5 \to \infty$ limit*, *Phys. Rev. D* **56** (1997) 4017–4030, [hep-ph/9704245]. ↑ 113.

[230] M. Neubert, *Two-loop relations for heavy-quark parameters in the shape-function scheme*, *Phys. Lett. B* **612** (2005) 13–20, [hep-ph/0412241]. ↑ 113, 142.

[231] S. Aoki et al., *Review of lattice results concerning low-energy particle physics*, *Eur. Phys. J. C* **77** (2017) 112, [1607.00299]. ↑ 113.

[232] Fermilab Lattice, MILC, TUMQCD collaboration, A. Bazavov et al., *Up-, down-, strange-, charm-, and bottom-quark masses from four-flavor lattice QCD*, *Phys. Rev. D* **98** (2018) 054517, [1802.04248]. ↑ 113.

[233] B. L. Ioffe and K. N. Zyablyuk, *Gluon condensate in charmonium sum rules with three loop corrections*, *Eur. Phys. J. C* **27** (2003) 229–241, [hep-ph/0207183]. ↑ 114.

[234] S. Dubnicka, A. Z. Dubnickova, A. Issadykov, M. A. Ivanov and A. Liptaj, *Study of B_c decays into charmonia and D mesons*, *Phys. Rev. D* **96** (2017) 076017, [1708.09607]. ↑ 115, 119, 120, 126.

[235] W.-F. Wang, X. Yu, C.-D. Lü and Z.-J. Xiao, *Semileptonic decays $B_c^+ \to D_{(s)}^{(*)}(\ell^+\nu_\ell, \ell^+\ell^-, \nu\bar{\nu})$ in the perturbative QCD approach*, *Phys. Rev. D* **90** (2014) 094018, [1401.0391]. ↑ 115, 125, 126.

[236] D.-s. Du and Z. Wang, *Predictions of the Standard Model for $B_c^\pm$ Weak Decays*, *Phys. Rev. D* **39** (1989) 1342. ↑ 115.

[237] P. Colangelo, G. Nardulli and N. Paver, *QCD sum rules calculation of B_c decays*, *Z. Phys. C* **57** (1993) 43–50. ↑ 115.

[238] R. Dhir and R. C. Verma, *B_c Meson Form-factors and $B_c \to PV$ Decays Involving Flavor Dependence of Transverse Quark Momentum*, *Phys. Rev. D* **79** (2009) 034004, [0810.4284]. ↑ 115.

[239] S. Godfrey, K. Moats and E. S. Swanson, *B and B_s Meson Spectroscopy*, *Phys. Rev. D* **94** (2016) 054025, [1607.02169]. ↑ 117.

[240] R. Dutta, *Predictions of $B_c \to (D, D^*)\tau\,\nu$ decay observables in the standard model*, *J. Phys. G* **46** (2019) 035008, [1809.08561]. ↑ 129.

[241] M. Calvi and M. William Kenzie. personal communication. ↑ 131, 134, 137, 140.

[242] G. Bailas, B. Blossier and V. Morénas, *Some hadronic parameters of charmonia in $\boldsymbol{N_f = 2}$ lattice QCD*, *Eur. Phys. J. C* **78** (2018) 1018, [1803.09673]. ↑ 134.

[243] ETM collaboration, A. Bussone et al., *Mass of the b quark and B -meson decay constants from N_f=2+1+1 twisted-mass lattice QCD*, *Phys. Rev. D* **93** (2016) 114505, [1603.04306]. ↑ 134.

[244] S. W. Bosch, B. O. Lange, M. Neubert and G. Paz, *Factorization and shape function effects in inclusive B meson decays*, *Nucl. Phys. B* **699** (2004) 335–386, [hep-ph/0402094]. ↑ 142.

[245] S. W. Bosch, M. Neubert and G. Paz, *Subleading shape functions in inclusive B decays*, *JHEP* **11** (2004) 073, [hep-ph/0409115]. ↑ 142.

[246] B. O. Lange, M. Neubert and G. Paz, *Theory of charmless inclusive B decays and the extraction of V_{ub}*, *Phys. Rev. D* **72** (2005) 073006, [hep-ph/0504071]. ↑ 142.

[247] M. Neubert, *Advanced predictions for moments of the $\bar{B} \to X_s\gamma$ photon spectrum*, *Phys. Rev. D* **72** (2005) 074025, [hep-ph/0506245]. ↑ 142.

[248] P. Gambino, P. Giordano, G. Ossola and N. Uraltsev, *Inclusive semileptonic B decays and the determination of $|V_{ub}|$*, *JHEP* **10** (2007) 058, [0707.2493]. ↑ 142.

[249] P. Gambino, *B semileptonic moments at NNLO*, *JHEP* **09** (2011) 055, [1107.3100]. ↑ 142.

[250] P. Gambino et al., *Challenges in semileptonic B decays*, *Eur. Phys. J. C* **80** (2020) 966, [2006.07287]. ↑ 142.

[251] Belle collaboration, L. Cao et al., *Measurements of Partial Branching Fractions of Inclusive $B \to X_u \ell^+ \nu_\ell$ Decays with Hadronic Tagging*, 2102.00020. ↑ 142, 143.

[252] A. Bharucha, *Two-loop Corrections to the Btoπ Form Factor from QCD Sum Rules on the Light-Cone and $|V_{ub}|$*, *JHEP* **05** (2012) 092, [1203.1359]. ↑ 144, 166.

[253] A. Khodjamirian, C. Klein, T. Mannel and N. Offen, *Semileptonic charm decays $D \to \pi \ell \nu_\ell$ and $D \to K \ell \nu_\ell$ from QCD Light-Cone Sum Rules*, *Phys. Rev. D* **80** (2009) 114005, [0907.2842]. ↑ 144.

[254] N. Gubernari, A. Kokulu and D. van Dyk, *$B \to P$ and $B \to V$ Form Factors from B-Meson Light-Cone Sum Rules beyond Leading Twist*, *JHEP* **01** (2019) 150, [1811.00983]. ↑ 145, 166.

[255] B. L. Ioffe, *Condensates in quantum chromodynamics*, *Phys. Atom. Nucl.* **66** (2003) 30–43, [hep-ph/0207191]. ↑ 146.

[256] Flavour Lattice Averaging Group collaboration, S. Aoki et al., *FLAG Review 2019: Flavour Lattice Averaging Group (FLAG)*, *Eur. Phys. J. C* **80** (2020) 113, [1902.08191]. ↑ 146.

[257] RQCD collaboration, G. S. Bali, V. M. Braun, S. Bürger, M. Göckeler, M. Gruber, F. Hutzler et al., *Light-cone distribution amplitudes of pseudoscalar mesons from lattice QCD*, *JHEP* **08** (2019) 065, [1903.08038]. ↑ 146, 148.

[258] A. Khodjamirian, T. Mannel, N. Offen and Y. M. Wang, *$B \to \pi \ell \nu_l$ Width and $|V_{ub}|$ from QCD Light-Cone Sum Rules*, *Phys. Rev. D* **83** (2011) 094031, [1103.2655]. ↑ 146.

[259] A. Khodjamirian and A. V. Rusov, *$B_s \to K \ell \nu_\ell$ and $B_{(s)} \to \pi(K) \ell^+ \ell^-$ decays at large recoil and CKM matrix elements*, *JHEP* **08** (2017) 112, [1703.04765]. ↑ 145, 148, 166.

[260] A. Bharucha, T. Feldmann and M. Wick, *Theoretical and Phenomenological Constraints on Form Factors for Radiative and Semi-Leptonic B-Meson Decays*, *JHEP* **09** (2010) 090, [1004.3249]. ↑ 156.

[261] A. Khodjamirian, B. Melić, Y.-M. Wang and Y.-B. Wei, *The $D^* D\pi$ and $B^* B\pi$ couplings from light-cone sum rules*, *JHEP* **03** (2021) 016, [2011.11275]. ↑ 158, 165.

[262] N. Isgur and M. B. Wise, *Influence of the B^* Resonance on $\bar{B} \to \pi e \bar{\nu}_e$*, *Phys. Rev. D* **41** (1990) 151. ↑ 158.

[263] C. A. Dominguez, J. G. Korner and K. Schilcher, *The scalar form-factor in the exclusive semileptonic decay of $B \to \pi \tau \nu_\tau$*, *Phys. Lett. B* **248** (1990) 399–405. ↑ 158.

[264] L. Wolfenstein, *General results for the decays $D \to \pi \ell \nu$ and $B \to \pi \ell \nu$*, *Phys. Lett. B* **291** (1992) 177–179. ↑ 158.

[265] G. Burdman, Z. Ligeti, M. Neubert and Y. Nir, *The Decay $B \to \pi \ell \nu$ in heavy quark effective theory*, *Phys. Rev. D* **49** (1994) 2331–2345, [hep-ph/9309272]. ↑ 158.

[266] E. Dalgic, A. Gray, M. Wingate, C. T. H. Davies, G. P. Lepage and J. Shigemitsu, *B meson semileptonic form-factors from unquenched lattice QCD*, *Phys. Rev. D* **73** (2006) 074502, [hep-lat/0601021]. ↑ 160.

[267] B. Colquhoun, R. J. Dowdall, J. Koponen, C. T. H. Davies and G. P. Lepage, *$B \to \pi \ell \nu$ at zero recoil from lattice QCD with physical u/d quarks*, *Phys. Rev. D* **93** (2016) 034502, [1510.07446]. ↑ 160.

[268] Fermilab Lattice, MILC collaboration, A. Bazavov et al., *$B_s \to K\ell\nu$ decay from lattice QCD*, *Phys. Rev. D* **100** (2019) 034501, [1901.02561]. ↑ 161.

[269] I. Caprini, B. Grinstein and R. F. Lebed, *Model-independent constraints on hadronic form factors with above-threshold poles*, *Phys. Rev. D* **96** (2017) 036015, [1705.02368]. ↑ 162.

[270] RBC, UKQCD collaboration, J. M. Flynn, P. Fritzsch, T. Kawanai, C. Lehner, B. Samways, C. T. Sachrajda et al., *The $B^*B\pi$ Coupling Using Relativistic Heavy Quarks*, *Phys. Rev. D* **93** (2016) 014510, [1506.06413]. ↑ 165.

[271] BaBar collaboration, P. del Amo Sanchez et al., *Study of $B \to \pi\ell\nu$ and $B \to \rho\ell\nu$ Decays and Determination of $|V_{ub}|$*, *Phys. Rev. D* **83** (2011) 032007, [1005.3288]. ↑ 168.

[272] BaBar collaboration, J. P. Lees et al., *Branching fraction and form-factor shape measurements of exclusive charmless semileptonic B decays, and determination of $|V_{ub}|$*, *Phys. Rev. D* **86** (2012) 092004, [1208.1253]. ↑ 168.

[273] Belle collaboration, H. Ha et al., *Measurement of the decay $B^0 \to \pi^-\ell^+\nu$ and determination of $|V_{ub}|$*, *Phys. Rev. D* **83** (2011) 071101, [1012.0090]. ↑ 168.

[274] Belle collaboration, A. Sibidanov et al., *Study of Exclusive $B \to X_u\ell\nu$ Decays and Extraction of $\|V_{ub}\|$ using Full Reconstruction Tagging at the Belle Experiment*, *Phys. Rev. D* **88** (2013) 032005, [1306.2781]. ↑ 168.

[275] F. U. Bernlochner, M. F. Sevilla, D. J. Robinson and G. Wormser, *Semitauonic b-hadron decays: A lepton flavor universality laboratory*, 2101.08326. ↑ 171.

[276] D. Bečirević, F. Jaffredo, A. Peñuelas and O. Sumensari, *New Physics effects in leptonic and semileptonic decays*, 2012.09872. ↑ 172, 174.

[277] F. U. Bernlochner, *$B \to \pi\tau\overline{\nu}_\tau$ decay in the context of type II 2HDM*, *Phys. Rev. D* **92** (2015) 115019, [1509.06938]. ↑ 172, 174.

[278] Belle collaboration, P. Hamer et al., *Search for $B^0 \to \pi^-\tau^+\nu_\tau$ with hadronic tagging at Belle*, *Phys. Rev. D* **93** (2016) 032007, [1509.06521]. ↑ 173.

[279] C. Bobeth, G. Hiller and G. Piranishvili, *Angular distributions of $\bar{B} \to \bar{K}\ell^+\ell^-$ decays*, *JHEP* **12** (2007) 040, [0709.4174]. ↑ 174.

[280] HPQCD collaboration, C. Bouchard, G. P. Lepage, C. Monahan, H. Na and J. Shigemitsu, *Standard Model Predictions for $B \to K\ell^+\ell^-$ with Form Factors from Lattice QCD*, *Phys. Rev. Lett.* **111** (2013) 162002, [1306.0434]. ↑ 174.

[281] G. Duplancic and B. Nizic, *Reduction method for dimensionally regulated one-loop N-point Feynman integrals*, *Eur. Phys. J. C* **35** (2004) 105–118, [hep-ph/0303184]. ↑ 191.

[282] M. Jung and D. M. Straub, *Constraining new physics in $b \to c\ell\nu$ transitions*, *JHEP* **01** (2019) 009, [1801.01112]. ↑ 201.

[283] B. Dassinger, R. Feger and T. Mannel, *Complete Michel Parameter Analysis of inclusive semileptonic $b \to c$ transition*, *Phys. Rev. D* **79** (2009) 075015, [0803.3561]. ↑ 201.

[284] J. G. Korner and G. A. Schuler, *Exclusive Semileptonic Heavy Meson Decays Including Lepton Mass Effects*, *Z. Phys. C* **46** (1990) 93. ↑ 202.

[285] M. A. Ivanov, J. G. Körner and C. T. Tran, *Exclusive decays $B \to \ell^-\bar{\nu}$ and $B \to D^{(*)}\ell^-\bar{\nu}$ in the covariant quark model*, *Phys. Rev. D* **92** (2015) 114022, [1508.02678]. ↑ 203.

[286] D. van Dyk et al., *EOS — A HEP program for Flavor Observables*, 2016. ↑ 209.

[287] F. Beaujean, *A Bayesian analysis of rare B decays with advanced Monte Carlo methods*, Ph.D. thesis, Munich, Max Planck Inst., 2012. ↑ 211.